THE MECHANICAL AND WEAR BEHAVIOUR OF B(SiC) FIBRE-REINFORCED COMPOSITE MATERIALS

YUSUF SAHIN

Doctor of Philosophy

THE UNIVERSITY OF ASTON IN BIRMINGHAM

December 1994

THE UNIVERSITY OF ASTON IN BIRMINGHAM

THE MECHANICAL AND FRICTION, WEAR BEHAVIOUR OF B(SiC) FIBRE REINFORCED COMPOSITE MATERIALS

YUSUF SAHIN

A thesis submitted for the Degree of Doctor of Philosophy 1994

SUMMARY

The mechanical properties and wear behaviour of B(SiC) fibre-reinforced metal matrix composites (MMCs) and aluminium alloy (2014) produced by metal infiltration technique were determined. Tensile tests were performed at different conditions on both the alloy matrix and its composite, and the tensile fracture surfaces were also examined by Scanning Electron Microscopy (SEM). Dry wear of the composite materials sliding on hardened steel was studied using a pin-on-disc type machine. The effect of fibre orientation on wear rate was studied to provide wear resistance engineering data on the MMCs. Tests were carried out with the wear surface sliding direction set normal, parallel and anti-parallel to the fibre axis. Experiments were performed for sliding speeds of 0.6, 1.0 and 1.6 m/s for a load range from 12 N to 60 N. A number of sensitive techniques were used to examine worn surface and debris, i.e: Scanning Electron Microscopy (SEM), Backscattered Electron Microscopy (BSEM) and X-ray Photoelectron Spectroscopy (XPS). Finally, the effect of fibre orientation on the wear rate of the Borsic-reinforced plastic matrix composites (PMCs) produced by hot pressing technique was also investigated under identical test conditions.

It was found that the composite had a markedly increased tensile strength compared with the matrix. The wear results also showed that the composite exhibited extremely low wear rates compared to the matrix material and the wear rate increased with increasing sliding speed and normal load. The effect of fibre orientation was marked, the lowest wear rates were obtained by arranging the fibre perpendicular to the sliding surface, while the highest wear was obtained for the parallel orientation. The coefficient of friction was found to be lowest in the parallel orientation than the others. Wear of PMCs were influenced to the greatest extent by these test parameters although similar findings were obtained for both composites. Based on the results of analyses using SEM, BSED and XPS, possible wear mechanisms are suggested to explain the wear of these materials.

Key Words: Boron-reinforced metal matrix composite (MMC), plastic matrix composite (PMC), dry wear, fibre orientation, wear mechanism, mechanical properties, metallography.

DEDICATION

To my dear wife Fatma

and

My children Sule, Fatih and Hakan

ACKNOWLEDGEMENTS

The research described in this dissertation was carried out in the Department of Mechanical and Electrical Engineering at the University of Aston in Birmingham.

First of all, I am greatly indebted to my supervisor Dr. Sam Murphy, for his continued guidance and encouragement, and enthusiastic support throughout this project. My gratitude also extends to Dr. J. Penny, head of the department.

I wish to thank Dr K. Swalha for his friendly and advise. I would like also to thank the Dr. Faith Carter and Ms. Bingshu, and Dr. Nasir.

I wish to thank the academic and technical staff of the Mechanical and Electrical Engineering Department of Aston University, for their advise and help. In particular my thanks are due to members of technical staff : R. Howell, P.Pizer, V. Keith, J. Jeffs, J. Folden, A. Evitts and Messrs. D.Farmer, and K. Harrison.

My gratitude is extended to Dr. J. L. Sullivan and Dr. S. Saied.of the Electronic and Physics Department of Aston University, for use of their surface analysis techniques and time.

I would like to thank the University of Gazi-Ankara for its sponsorship. Also my gratitude is extended to Prof. Dr. S. Saritas of Gazi University for his encouragement during my study and M. Emin Tuna of General Director of Tuna A.S. A special mention must go to my brother Nadir.

Finally, I would like to express my thanks and love to my wife Fatma without whose sacrifice, patience and support my work would not have been possible. My love and thanks also to my children Hakan, Fatih and Sule.

CONTENTS

CHAPTER FOUR

4.0 EXPERIMENTAL RESULTS

4.1 MECHANICAL PROPERTIES AND WEAR OF BORSIC-REINFORCED METAL MATRIX COMPOSITES

4.2 WEAR OF BORSIC-REINFORCED PLASTIC MATRIX COMPOSITES

CHAPTER FIVE

CHAPTER SIX

LIST OF FIGURES

LIST OF TABLES

ABBREVIATIONS AND SYMBOLS

MMCs	:	Metal Matrix Composite Materials
PMCs	:	Plastic Matrix Composite Materials
CMC	:	Ceramic Matrix Composite
SEM	:	Scanning Electron Microscopy
BSEM	:	Backscattered Electron Microscopy
XPS	:	X-ray Photoelectron Spectroscopy
ROM	:	Rule of Mixtures
SEN	:	Single Edge Notch
LT	:	Longitudinal notch filament configuration
TT	:	Transverse notch filament configuration
TL	:	Transverse longitudinal filament configuration
Type I	:	High Modulus Graphite Fibre
Type II	:	High Strength Graphite Fibre
Al	:	2014-Aluminium Alloy Matrix
HDPE	:	High Density Polyethylene Polymer Matrix
EDM	:	Electrical Discharge Machining
CLA	:	Centre-line-Average
LVDT	:	Linear Variable Displacement Transducers
En 31	:	Hardened Bearing Steel
B16	:	16 % Volume fraction of fibre
B21	:	21 % Volume fraction of fibre
B32	:	32 % Volume fraction of fibre
FP	:	α– Alumina Fibre
SF	:	δ–Alumina Fibre (Saffil)
E_c	:	Elastic Modulus of the Composite

E_m	:	Elastic Modulus of the Matrix
E_f	:	Elastic Modules of the Fibre
V_f	:	Volume fraction of fibre
V_m	:	Volume fraction of matrix
N	:	Normal Orientation
P	:	Parallel Orientation
AP	:	Anti-parallel Orientation
σ	:	Normal Stress
ε	:	Normal Strain
σ_c	:	Tensile Strength of the Composite
σ_m	:	Tensile Strength of the Matrix
σ_f	:	Tensile Strength of the Fibre
L_c	:	Critical Fibre Length
d	:	Fibre diameter
ρ	:	Bulk Density of the Materials
τ_m	:	Shear Yield Strength of the Matrix
τ	:	Interfacial Shear Strength
α	:	Constant Coefficient
ϕ	:	Fibre Preform Alignment Angle
L	:	Applied Load (N)
V	:	Sliding Speed (m/s)
μ	:	Coefficient of friction

CHAPTER ONE

1.0 INTRODUCTION

Materials have always been an integral part of human culture and civilization, but today's advanced technologies require even more sophisticated materials. Tomorrow' s and even today's technology needs new materials with extraordinary properties like high stiffness, strength, and also wear resistance. An effective solution to today's growing materials problems lies in the synthesis of existing materials, that is, in composites. Metal matrix composite materials are one of the most promising recent candidates for use in high strength and stiffness, particularly at elevated temperatures, and for wear resistance applications.

Metal matrix composite materials (MMCs) can be basically classified into five groups, according to the type of reinforcement : (1) a particulate based material formed by the addition of small particles into a binder that generally derives an increase in stiffness, (2) whisker reinforcement that realizes a greater proportion of the whisker strength due to its higher aspect ratio, and hence a greater ability to transfer load; (3) a short fibre-discontinuous fibre that due to broken fibre in nature, yields lower strength and modulus; but (4) if the short fibre may be randomly or planar-random orientated, it is possible to obtain nearly equal mechanical and physical properties in all direction in the plane of the lamina; (5) a continuous fibre that due to fibre continuity, derives the full properties of the high performance fibre (strength and stiffness). The last case of the composite allows the development to the full of the potential high performance because of fibre continuity.

There are various metal matrix composites commercially available today that conform to the five types of composites discussed above. The mechanical properties of these different systems vary significantly and the greatest interest has been focused on those that incorporate the reinforcement in the form of very thin fibres such as glass,

carbon, boron, silicon carbide and alumina. These fibres have high specific strength and cause a considerable increase in the strength of the composite. For the MMCs, aluminium alloys are the most common metal matrix as structural materials in their own right and hence suggest better mechanical properties. They also provide high electrical and thermal conductivity. Thus, recent demands for materials of high specific strength and stiffness for use in aerospace applications have prompted the development of MMCs.

The first metal matrix composite materials using boron fibre and aluminium alloy were developed in the mid-1970 s, with the realisation that boron fibre reinforcement can be competitive with the glass fibre reinforced material from the standpoints of higher mechanical properties and used in the aerospace industry. However the rapid reaction of boron fibre with molten alloy caused severe fibre degradation and precluded its use both for high temperature applications and fabrication. These drawbacks led to the development of silicon carbide coated boron fibres B(SiC) which inhibits reaction between the fibres and matrix, prevents the loss of fibre strength and hence permits the use of high temperature, low pressure bonding. Commercial varieties of this type of fibre are Borsic and Sicarbo. It was the development of composites reinforced with continuous Borsic fibres that show promise as MMCs for high strength and high temperature capability and light weight applications. In particular, turbo engine fan blades, aircraft wing skins, spars for aircraft struts and aircraft structure have been made besides sport goods. The consideration of metal matrix composites using Borsic fibres for use in engineering structure has motivated the determination of the mechanical and tribological properties of these composites produced by a melt infiltration technique.

A survey of literature indicated that there were limited data available for some mechanical properties such as tensile and compressive strength, and creep and fatigue behaviour of B(SiC)-reinforced aluminium composite. However, no research work had been conducted on the wear and friction properties of B(SiC)/reinforced aluminium matrix composite. The mechanical properties of B(SiC)/MMCs are known to depend on

the properties of the constituent materials, of the interface between fibre and matrix, and on the fibre volume fraction as well as production technique. Obviously, the wear and friction properties of the B(SiC)/MMCs are also expected to depend, at least to some extent on the same variables. The wear and friction resistance are not intrinsic material properties, but are complex functions of a large number of external parameters (such as sliding speed, normal load, temperature, sliding distance, environment, etc.) and of the physical and mechanical properties of the wearing and counterface materials, and on the relative orientation of the unidirectional fibres with respect to the sliding directions. Therefore, experiments were conducted to characterise the composite materials and determine the effect of most of the above parameters on the wear and friction values of the unreinforced and B(SiC) fibre reinforced metal and plastic composites to provide the wear resistive engineering data of these composites. For certain requirements, the coefficient of friction is of importance, but largely it is the mechanical load bearing capacity and the wear life of the components that determine their acceptability in industrial applications. Usually, wear is undesirable not only because it makes necessary frequent inspection and replacement of parts, but it will also leads to deterioration of accuracy (e.g.of machine parts). It can induce vibrations, fatigue and consequently failure by rupture.

Apart from that, a detailed understanding of the micromechanisms of wear is also necessary to set design guidelines for the manufacturing of materials with optimum tribological properties along with mechanical properties. Therefore metallographic investigations of the worn surfaces and subsurfaces, and debris were carried out to delineate the operative mechanisms of wear under different experimental conditions. It is also desirable to correlate the basic knowledge with test results and investigate the changes in structure and composition of solid surface layers due to friction, from both microscopic and macroscopic point of view. For the microscopic observation, it is very important to use a proper combination of tools such as scanning electron microscopy

(SEM) and back-scattered electron microscopy (BSE) and X-ray photoelectron spectroscopy (XPS).

In view of the above, the objective of this current research study, therefore, was to provide an understanding of the sliding wear behaviour of Al alloy reinforced with B(SiC) fibre and HDPE matrix reinforced with B(SiC) fibre composites against a rotating steel disc. The base Al alloy and HDPE polymer matrix were also subjected to similar tests in order to observe the effect of the presence of B(SiC) fibre in the matrices on their tribological characteristics. Nevertheless, tensile properties of the B(SiC)/MMCs were also studied to obtain additional data and examined the fracture surface.

Basically, this research programme consisted of the following stages:

(1). To examine the microstructure of Borsic-reinforced aluminium matrix composite produced by metal infiltration technique, and determine the mechanical properties of the composite and examine the fracture surface of the composite.

(2). To provide wear resistant engineering data on the MMCs at varying normal pressures and sliding speeds and determine the effect of fibre orientation on wear and friction, including normal, parallel and anti-parallel sliding directions.

(3). To examine the worn surfaces of the composites and clarify the operative wear mechanisms.

(4). To determine the effect of the matrix on wear by comparing B(SiC)-reinforced plastic (HDPE) matrix composites produced by hot pressing with the MMC materials.

The mechanical, wear and friction properties of the composites are also discussed based on fibre orientation, volume fraction, matrix properties, and microscopic observations of the worn surfaces, and a detailed consideration of mechanisms of wear and the effect of sliding conditions is made.

CHAPTER TWO

2.0 LITERATURE SURVEY

The survey given in this chapter can be divided into four general areas. First of all, metal matrix composites (MMCs), types of MMCs, and reinforcements and matrices for MMCs and available methods for preparation of variety of MMC materials, and mechanics of MMCs are briefly introduced. Secondly, mechanical behaviour of metal matrix composites using a B(SiC) fibre are reviewed. Thirdly, tribological systems are reviewed and a general description given of friction and wear mechanisms of composites. Finally, the friction and wear behaviour of aluminium alloys containing continuous and particulate additions are also reviewed with a brief concluding summary.

2.1 Metal Matrix Composites (MMCs)

In general, the term of composite usually signifies that two or more different phases of materials are combined in a certain configuration on a macroscopic scale to form a new material that produces synergistic mechanical and physical properties over that of base elements. One of the phases is a reinforcement, which can be a variety of ceramic materials and can take several morphologies including whiskers, particles, short and continuous fibres. The main function of the reinforcement in a composite is to provide an increase in stiffness and strength of the matrix and to reduce the density of the composites. In addition, the presence of stiff fibres or particles improves elevated temperature properties and therefore extends the range of temperatures over which the light alloys can be used, but the primary function of the fibres is to carry the majority of the load. The reinforcements can be divided broadly into five categories : Continuous, discontinuous, particulate, planar-random and whiskers. For example, the composites

which is produced by these fibres are called continuous, particulate reinforced composites.

The other major constituent in the composite, the matrix, serves several critical functions beyond simply holding the reinforcements in place. For example, since many reinforcements tend to be brittle, the matrix protects their surface against abrasion or environmental attack both which initiate fracture. More importantly, the matrix distributes the load borne longitudinally by the reinforcements. In order to accomplish this transfer of loads, and also reduce the chance of failure in the matrix, adhesion to fibres or other reinforcements must be coupled with sufficient matrix shear strength to sustain these loads. The matrix separates the fibres, and by virtue of its relative softness and plasticity, prevents the propagation of brittle cracks from the fibre, which could result in catastrophic failure. Also a matrix which plastically deforms serves to deflect cracks parallel to fibres, preventing the failure of fibres all in one plane. Thus, for a crack to extend through ductile matrix materials, it is necessary for the fibres to pull-out of the matrix, as they break, which absorbs a significant amount of energy. In other words, the matrix phase serves as a barrier to crack propagation. The matrix must perform these functions across the anticipated application temperature range, as well as resist expected chemical and environmental stresses. For this reason, several matrix materials are considered for a composite in many high performance applications. The second phase is a matrix material which can be chosen depending on the type of the composites. Composite materials, thus, may also be grouped into three categories : Metal matrix composites (MMCs), polymer matrix composites (PMCs) and ceramic matrix composites (CMCs).

Recently metal matrix composite studies became an important branch in materials research area due to having several advantages for their use as structural materials. These advantages include a combination of the following properties. [1, 2]

(1). High stiffness,

(2). High strength,

(3). High temperature capability,

(4). High toughness and impact properties,

(5). High surface durability and high wear resistance.

Obviously, all of these properties are not expected to improve simultaneously and there is no requirement to do so in any one application, but these properties can be attained with the proper choice of the matrix and reinforcement, production technique and considering other factors. The choice of the reinforcement is also depend on the following factors such as the compatibility and bonding strength between the reinforcement and the matrix since the ultimate strength of the composite depends to a large degree of the magnitude of this bond.

2.1.1 Matrix Metals and Reinforcements

2.1.1.1 Matrix Metals

For MMCs, metals such as aluminium, magnesium, titanium, copper and their alloys are used as a matrix material. But the most common matrix is aluminium and its alloys although considerable interest is also being shown in magnesium and titanium and their alloys. The concentration of effort on aluminium stems from its unique combination of good corrosion resistance, low density and excellent mechanical properties. Such a metal with good ductility and strength is combined with fibres which have low ductility, high stiffness and lower density. For the matrix, selection criteria such as density, strength and ductility/toughness are important considerations beside that not only desired properties but also which material is best suited for fabrication of the composites. Thus, recently aluminium-lithium alloy has been attracting the attention of researchers due to its good wettability characteristics.[3] However, for the reinforcement, characteristics such as the chemistry, morphology, microstructure, mechanical and physical properties and cost also have been considered.

2.1.1.2 *Reinforcements*

The reinforcements are the principal constituent in a MMC because they share the major portion of the load on a composite structure. Proper selection of the type, amount, and orientation of reinforcement is very important since it influences the mechanical and physical characteristics of a composite. As stated previously, the reinforcement for MMCs can be continuous fibre, discontinuous fibre, whiskers, particulate and planar-random forms. A wide range of ceramic fibres is available for incorporation in the metal matrix composites. A summary of most important reinforcing filaments and their properties of the some ceramic reinforcements are presented in Table 1.[4, 5, 116] The table shows the multifilament family which includes carbon, silicon carbide and alumina fibres while the monofilament family is based on boron only.

Boron fibres are produced by chemical vapour deposition of boron from boron-trichloride gas on tungsten or carbon filament which had about 15 μm in diameter. The resulting boron fibres are usually around 100-140 μm in diameter and are particularly useful where high compressive forces are encountered.[6] Such a thick fibres are too stiff to weave into fabric. Therefore, these fibres are collimated and impregnated with epoxy to form preimpregnated unidirectional tape or parallel filaments held together by thin titanium wires. Boron fibres react with aluminium and titanium at a rapid rate, [7] at the temperatures used for the manufacture of composites with these metals. Thus it is important to have a diffusion barrier layer on the boron fibre, so as to permit the use of high temperature in the manufacturing of aluminium matrix composites. Two versions of the fibre coating are commercially available for use with boron, silicon carbide (Borsic) and boron carbide (B_4C) which prevents degradation of the boron by interaction with the metal matrix during hot pressing. The first coating of silicon carbide which the thickness of it was nearly 2.5 μm.

The structure of the boron is either amorphous or microcrystalline. The high strength amorphous structure can be obtained when the temperature of the tungsten wire is kept below 1250 °C, while crystalline boron is produced at about 1400 °C.[2] This

results in a considerably lower strength. Moreover, the fibres have a very high residual compressive stress state on the surface, which makes the fibre insensitive to surface damage and microscratches even more than glass fibres. In other words, these stress forces reflects in a surface structure that has a nodular or corn-cob appearance.

Silicon carbide fibre is also produced in a CVD process similar to that used for boron. The silicon carbide has a much larger crystal structure but has a smoother surface than boron. These fibres are intended primarily for MMCs applications since the high temperature properties of the SiC on carbon filaments are superior. Thus, SiC does not react as readily with the carbon. The another advantage of the SiC fibre is its potentially low cost. [8]

Carbon or graphite fibre reinforcement is also more common. The carbon fibre consist of two low allotropes turbostratic graphite and mesophase. Both of which have strong covalent bonding between the carbon atoms. Graphite is made of hexagonal layer planes of carbon atoms which are stacked on top of each other in a regular sequence and strong covalent bonds are formed between atoms within the layers, but very weak bonds are produced between the layer. This results in highly anistropic physical and mechanical properties for the fibres. In turbostratic graphite fibre there is no regular stacking for the layer planes. Carbon fibres have also the c-direction orientated normal to the fibre axis, and the layer planes are badly stacked and folded with many defects and misalignments so that modulus is much reduced. The actual properties of the carbon fibre depend on the method of production and conditions.[9]

Carbon fibres are produced by carbonisation of organic precursors such as polyacrylonitrile (PAN) or petroleum pitch and rayon, but the most common textile precursor used is PAN which is wet spun and stretched to orientate the polymer chains, then treated to produce the sheets of turbostratic graphite. The strength and modulus depends on the final heat treatment temperature through its effect on the degree of crystalline perfection and size. The PAN carbon fibres are also known as Type I , High Modulus (HM) and Type II, High Strength (HS) in commercial grade.

As for the case of mesophase form of allotrope, carbon fibre from pitch precursor is produced by melt-spinning process.[10] As a result of this, the required degree of alignment in the filament direction is achieved from the mesophase pitch molecules. But both the PAN and Pitch-based products must be stabilized by thermosetting (crosslinking) so that the polymers do not melt in subsequent processing steps.[8] The PAN-based carbon fibres have a thin highly orientated onion skin surface layer planes and a core with random crystallisers.[9] In contrast, some mesophase pitch-based fibres exhibits radially orientated layer structures, and this also show that radial structure depends substantially on the precursor type and processing.

Ceramic fibres are also available for MMC materials. For example, continuous α-alumina fibres are being the most promising because of their greater inertness. Alumina fibre may exists two types of allotropic forms. One of the form is α-alumina, FP grade, which is produced by Du Pont Company, and which is composed of 99 % α alumina, in a continuous slurry spinning process of alumina particles.[4, 11] The spun fibres is dried at a low temperature and then fried to form dense, high temperature staple α–alumina with a purity in Al_2O_3 content.

The fibre is polycrystalline with a grain size of 0.5 μm in size, and it is available as continuous fibre with a 20 μm average diameter. It has a high purity and has also rough surface. The principal feature of these fibres is their excellent strength and modulus. Therefore, the first application of the fibres was MMCs and CMCs. The filament is comparable with those of boron and carbon. However, FP fibres still have the disadvantage of being costly. Thus, ICI Mond Divison has introduced a new grade of a other form of the alumina, known as " Saffil " RF grade which is only produced in the form of short fibres. It consists of polycrystalline structure in which the predominant phase is δ–alumina. [12, 13]

TABLE 1

TYPICAL PROPERTIES OF FIBRES FOR METAL MATRIX COMPOSITES. (4, 5, 108)

Types of fibres	Diameter (μm)	Density (kg/m^3)	Young's Modulus (GPa)	Tensile Strength (GPa)
Saffil δ Alumina	3	3300	300	2.0
FP α-Alumina	20	3900	380	1.7
Silicon Carbide	13	2500	390	2.0
Boron	100-140	2600	390	3.4
SiC-Coated Boron	100-200	2600	400	2.9
H.Modulus Carbon	8	1950	358	2.2
H.Strength Carbon	6.8	1800	235	2.6

Saffil also contains about 3 to 4 wt % SiO_2 which serves to stablize to the δ–structure and improves the bond with the aluminium alloy matrices besides that its main constituents are 96-97 % Al_2O_3. These fibres are rather fine, with a mean diameter around 3 μm and for the purpose of the MMCs fabrication, they are chopped, milled and sized to give an average length of about 500 μm. It has outstanding high temperature properties due to being a ceramic material, and Saffil has also higher tensile strength than the continuous filament of alumina.

2.1.1 Types of MMCs

MMCs encompasses a broad class of materials which may be classified into five groups according to the type of the reinforcement. These include :

(1). Particle reinforced MMCs,

(2). Continuous reinforced MMCs,

(3). Short fibre reinforced MMCs,

(4). Planar-random orientated MMCs,

(5). Dispersion-strengthened MMCs,

They posses unique combinations of properties which are not achievable in metal alloys and ceramic materials. Each type of the composites is described in the following section.

2.1.1.1 Particle Reinforced MMCs

In these composites, the reinforcement is incorporated in the form of particles which are greater than about 1 μm in diameter.[1] The most widely used particles are alumina and silicon carbide which are produced for grinding media. The volume fraction of reinforcement is limited by practical difficulties in manufacture due to an increase in viscosity in cast composites or mixing difficulties in powder processing when the particles are added. It is practically about 25 vol %. In general, strength increases linearly with increasing volume fraction of particles as the distribution of particles is homogeneous throughout the structure.

The strength of the composites depends on the size of the particles and the interparticle spacing, matrix properties and the strength properties also increase due to effective interaction of particles with dislocation. In general, the strength and ductility of a cast composite is lower than that of a composite produced by powder metallurgy.[14] This is attributed to the difference in microstructure in which the distribution of particles and grain size plays an important role. These composites also show isotropic properties, although the particle reinforcements are not homogeneous in most cases. A number of particulate reinforced composites have been in use industrially for many years, these including cermets, used in electronics industry for the tracks of precision variable resistors and tungsten carbide in cobalt for high speed tool tips. Apart from that, SiC particulate-reinforced aluminium composite also showed that they had a good potential for use as wear resistant materials.[15, 16]

2.1.1.2. Continuous Fibre Reinforced MMCs

In these composites, the continuous fibres are either in the form of mono-filaments or multi-filament yarn or tows. They are produced by chemical or a physical vapour deposition process which involves coating, and the reinforcements used are generally either large diameter >100 μm or smaller diameter <20 μm) and the volume fractions range from 10% to 70% in different orientation. Examples of the former are those based on boron or silicon carbide whereas the multifilament family includes fibres based on carbon, silicon carbide and alumina. Monofilaments tend to be used in unidirectional arrays either as monotape ' prepregs ' for subsequent laying up into multiple arrays with or without cross plies or as multilayer arrays completely or selectively reinforcing a simple component shape. Multifilaments are available in the form of single yarns or two or three dimensional weaves and some as wires and tapes of multifilament preimpregnated with matrix metal.

The most common way of incorporating multifilament family reinforcement into MMCs is by melt infiltration. Silicon carbide coated continuous boron B(SiC) was one

of the first fibres to be produced for MMCs and was produced by Avco Corporation as Borsic. Unidirectional composites provide the highest strength along the fibre direction but the transverse properties are poor since the matrix and the weak matrix/fibre interface are dominant. To overcome this problem, sheets of unidirectional composite, called laminae, are stacked together with the fibres at pre-determined angles to each other in successive sheets. When fully bonded, these laminated composites make the most effective use of their intermediate strength and stiffness.

2.1.1.3. Discontinuous (Short Fibre) Reinforced Composites

The short or discontinuous fibres are available at 3 to 5 μm in diameter and in a range of lengths which lies between 0.5 to 6 mm in length.[5] Short fibre composites can be manufactured either by incorporation of the reinforcement material into the melt or the production of a fibre preform which can then be infiltrated with molten aluminium, as in squeeze casting and the liquid pressure forming process. In the melt mixing the level of reinforcement is restricted in the liquid metal by the increase in viscosity. In the infiltration of preforms, it is also limited as a result of the inability of randomly orientated fibres to achieve a packing density higher than 35 vol %. Squeeze casting is the most effective process for manufacturing discontinuous fibre composites. For example, *Saffil* [17] alumina based short fibre reinforced aluminium composites were produced by squeeze casting technique and, are being used for piston crowns. The use of short fibres to reinforce these areas of the piston has been shown to enhance elevated and thermal fatigue properties.

Other manufacturing process that are used for discontinuous reinforcement include powder metallurgy and plasma cospray deposition. Both have some drawbacks. The mechanical forces involved during powder processing result in considerable fibre damage and the plasma co-spray deposition has a low productivity and is severely limited by shape and size consideration.

The basic advantage of short fibre over continuous reinforcements is being rapid, low cost beside that the ability to mould intricate component configurations that can not be fabricated using continuous fibre. In addition to the use of automobile engine components, short fibre reinforced composites are used mainly for refactory insulation purpose due to their low strength compared with others.

2.1.1.4 Planar-Random Reinforced MMCs

The planar-random composites are also consisted of short fibres, but the fibres are in a random or two dimensional randomly orientated in the matrix. Such fibres are converted to solid preforms by suspension in an aqueous medium, which includes a binder such as sodium silicate, compacted by infiltration and pressing or centrifuging followed by drying and firing.[18] The fibres in the preforms are usually 2D and random in orientation, although more sophisticated aligned preforms are possible. These preforms can be precisely located within a die cavity prior to infiltration to allow for selective reinforcement in specific areas and so minimise the cost of the reinforcement.

A net shape fabrication route such as liquid metal infiltration is attractive, compared with other techniques but the degree of orientation depends on the flow field, process conditions besides that fibre length, V_f and shapes of the mould.[8] The more random distribution of fibres gives lower values of Vf in these materials and large matrix rich areas may occur. This might be due to less efficient packing of the fibres and limitations in the moulding process. With random orientation of fibres in these composites, it is possible to provide more or less equal mechanical properties in all directions.

2.1.1.5 Dispersion-Strengthened MMCs

These composites are characterized either in the form of precipitates in the matrix or ceramics which have a 0.01-0.1 μm diameter and with a length of 50-200 μm. The volume fraction of ceramics range from 1 to 15 %. In general, whiskers are evenly

dispersed into the matrix in a random manner by mechanical alloying or powder processing. However, partial orientation of reinforcement can be obtained during the secondary processing, in particular, extrusion of production technique. The whiskers usually have very low intrinsic defects due to their small diameters. Therefore, higher strength is achieved than with other types of discontinuous reinforcements. The beneficial interactions of the dispersed phases with dislocations leads to an increase in yield strength and creep resistance of the matrix.

The properties of these composites are also isotropic. Recently SiC whisker-reinforced aluminium composite has been used widely in aerospace vehicles beside that engine components and pistons are made of SiCw/Al composites.[3, 19]

2.1. 2 Fabrication Techniques

Fibre-reinforced metal matrix composites can be produced in a variety of ways. These can be broadly divided into two categories :

1. Liquid state fabrication technique,
2. Solid state fabrication technique,

The fabrication method employed to make MMCs depend on the choice of fibre, matrix and the application of component. The main purpose of fabricating MMCs is to enhance the properties of a conventional metal alloy matrix, obtaining enough bonding between the reinforcement and matrix so as to transfer load from the matrix to the reinforcement. Thus, great attention is given to achieve minimum fibre degradation by filament/matrix reaction, reduce fibre breakage, and thus achieve maximum filament loading. Several fabrication techniques were developed for producing MMCs. Recently, more attention has been given to the liquid state processes, although some production difficulties exits.

2.1.2.1 Liquid State Fabrication Technique

Liquid state fabrication methods have been used effectively to produce MMCs due to the ease and rapidity of the process. The most common methods of liquid state processing

include liquid metal infiltration, squeeze casting, melt stirring, compo-casting and plasma spraying. These techniques are described briefly here in the way in which they are used currently.

Liquid Metal Infiltration

The liquid metal infiltration is one of the common liquid state fabrication route applied to produce MMCs. The procedure for fabricating by this technique is as follows : As the first step, a preform is made to the desired shape, orientation and fibre volume loading, usually using a binder, which is then inserted into a casting mould of steel, then the mould is infiltrated with molten metal and allowed to solidify. The infiltration process can be done under atmosphere pressure, in inert gas pressure and/or in vacuum. Among them vacuum infiltration is the best way of producing the composite because of the high surface activity of fibres.[20] However, the application of this process is limited due to the wettability problem of reinforcement with some matrix materials. Most reinforcement materials do not wet properly in molten metals and sometimes it is difficult to produce composites by infiltration. Therefore, fibre surface coating may be necessary.

In the case of squeeze casting technique, the molten metal will be force-infiltrated into the fibre bundles (preform), expelling all absorbed and trapped gases. Since the solidification times become very short when using a pressure of about (70-100 MPa) for squeezing the liquid metal, the composites produced are of good quality, and high and reliable strength is attainable by carefully controlling the process parameters.[21] Hence giving a void-free and high strength composite. It is generally applicable to produce MMCs using all types of reinforcements. For example, Al_2O_3/Al, C/Mg, SiC_w/Al composites were fabricated successfully by this method.[22, 23] However, the major limitation of the method is the size of parts that may be cast due to the high pressure requirements.

Melt Stirring

The simplest and cheapest fabrication route for MMCs. The required amount of reinforcements in the form of particles, whiskers or platelets are added to the liquid matrix alloy and then stirring applied to maintain a homogeneous dispersion of reinforcement. The melt is then cast into the die. Due to difficulties in injection of particles into the melt, more sophisticated techniques have been developed recently.[24] These involved mechanical introduction of particles in the melt just before casting. However, the castings generally suffer from high porosity due to air entrapment and gas absorption in the process.

Compocasting Process

The compocasting or rheocasting process, is similar to the melt stirring route, but instead of stirring the particulate into a fully liquid melt it is stirred into one in which the melt is cooled to a semi-solid or slurry state, when whiskers, particles or chopped fibres are added. Stirring makes the solid particles round so that the semi-solid alloy is not rigid, but thixotropic and prevents ceramic based reinforcements from settling, floating or agglomerating [25] and the solid particles make the slurry viscous and stirring disperses the fibres or particles in the alloy. The particles may interact with liquid metal to form interface bonding with increasing stirring time. However, too long a mixing time can cause some problems such as intermetallic compound formation, a thick interface layer, or degradation of the reinforcement.

Co-Spray Deposition

This process consists of atomising molten metal and particles and collecting the semi-solid droplets with reinforcement on a substrate. Depending on the form of the substrate collector system, a variety of shapes including sheet, tube can be produced by this process. For example, plasma spraying has been used with aluminium/boron fibre composites [26] and aluminium/SiC particulate composite.[76] The advantage of this

technique is the short contact time between the reinforcement and molten metal droplets. However, a secondary processing step is required to achieve full density.

2.1.2. 2 *Solid State Fabrication Techniques*

There are several fabrication techniques available to produce MMCs by using solid state materials, but among them powder metallurgy, diffusion bonding and hot pressing methods are used widely.

Powder Metallurgy

The technique of powder metallurgy involves the compacting of solid materials in the form of powders. The powder process has been used for ceramic as well as metallic materials. In this process, powders of ceramic and matrix materials are blended, then fed into a mould of desired shape. Pressure is then applied to further compact the powder (Cold Pressing), but in order to facilitate the bonding between the powder particles, the compact is then heated to a temperature that is below the melting point (Sintering) and the consolidated product is then used as a MMCs.

This process may be more economical than many other methods since no melting, casting is involved at lower temperature.[28] This resulted in less interaction between the matrix and fibre, hence, leading to improved mechanical properties. However, it has also some drawbacks, the blending step is a time consuming, expensive. The use of powders also requires a high level of cleanness, otherwise inclusions will be caused of a deleterious effect on fracture toughness and fatigue life.[29]

Diffusion Bonding

The diffusion bonding process is also one of the practical solid state fabrication technique, normally used to produce MMCs in the form of sheets or foils. The technique is simply to place foil and mono-filament fibres together layer by layer in predetermined orientation and desired content of reinforcements. The lay-up is encased in a metal can which is sealed and evacuated. The whole assembly is then heated well below the

melting temperature and pressed. For this process, oxide-free and clean surfaces are very important for foil and fibre, so as to allow diffusion, since the strength of the composite depends on the effectiveness of interdiffusion between fibre and matrix. In order to achieve this, fibre surfaces can be coated by plasma spraying, ion plating etc.

With this process, fibre degradation is not such a problem as in liquid casting because of lower temperatures used. Diffusion bonding under vacuum was found to be more effective than under gas or air.[30] Boron, silicon carbide and stainless steel have been used with matrices such as aluminium, titanium and their alloys. However, the limitation of the process is the size of the component and the net shape, and it is also the most expensive of the fabrication route.

Hot pressing and hot isostatic pressing are also commonly utilised to produce fully dense MMCs in a similar route. In current research work, B(SiC) fibre-reinforced plastic matrix composite has also been produced by a hot pressing technique and the resulting composites show good filament to matrix bonding, density and good distribution of fibres in the matrix. The detail description of the method is given in a later section 3. 2.

As discussed above, different fabrication techniques have been used for producing MMC materials by incorporation of various ceramic reinforcements into metal or alloy matrices. For instance, by reinforcing aluminium with B(SiC) fibres, it has been possible to develop composites whose mechanical properties compare favourably with those of the unreinforced matrix, yet exhibits exceptional wear behaviour. (See Table 4 and Appendix 1, 2).

2.1.3 Mechanics of Fibre-Reinforced MMCs

In fibre-reinforced MMCs, the high modulus fibres carry almost all of the load while the matrix serves to transfer the load to fibres and is useful in protecting the fibres from damage. It would thus be preferable to have good bonding between the fibre and matrix which is usually the case with the MMCs. In order to describe the principles of fibre reinforced composites, it is simpler to consider a composite containing unidirectional

orientated fibres lying parallel to the stress axis. Under uniaxial tensile loading, the stress/strain curve consists of four stages as shown in Figure 2.1. In the initial stage, both matrix and fibres undergo the same elastic deformation if there is no slipping at the interface. The elastic modulus of the composite material can be determined by the rule of mixtures.[31]

$$E_c = E_f \ V_f + E_m \ V_m \qquad (2.1)$$

where V_f, V_m are the volume fractions of the fibre and matrix while E_f, E_m are the Young's modulus of the fibre and matrix respectively. If the composite is loaded so that the yield stress of the matrix is exceeded, then E_m is no longer the relevant term in the above expression. This is stage 2, where the matrix deforms plastically and the fibre is still elastic. In this case, the elastic modulus is given by :

$$E_c = E_f V_f + \left(\frac{d\,\sigma_m}{d\,\varepsilon_m}\right) \varepsilon_f V_m \qquad (2.2)$$

Where $\left(\frac{d\,\sigma_m}{d\,\varepsilon_m}\right) \varepsilon_f$ is the slope of the matrix stress/strain curve under these conditions at a given value of the fibre strain. In this stage, the fibres return to the original length when the composite is unloaded, but the matrix is elastically deformed in compression. On further straining of a composite with ductile fibres, the fibres themselves deform plastically in stage 3. However, since most high modulus, high strength fibres are brittle, they fracture on commencing stage 3, effectively by-passing it. In this final stage of deformation, the fibres fracture and the composite as a whole then fractures rapidly.

The ultimate tensile strength (σ_c) of the composite loaded in the uniaxial direction is given by :

$$\sigma_c = \sigma_f v_f + \sigma_m v_m \qquad (2.3)$$

Where σ_c , σ_f are the tensile strength of the composite and fibre respectively and $\sigma_{m'}$ is the tensile stress in the matrix when the fibres are strained to their tensile strength. Since

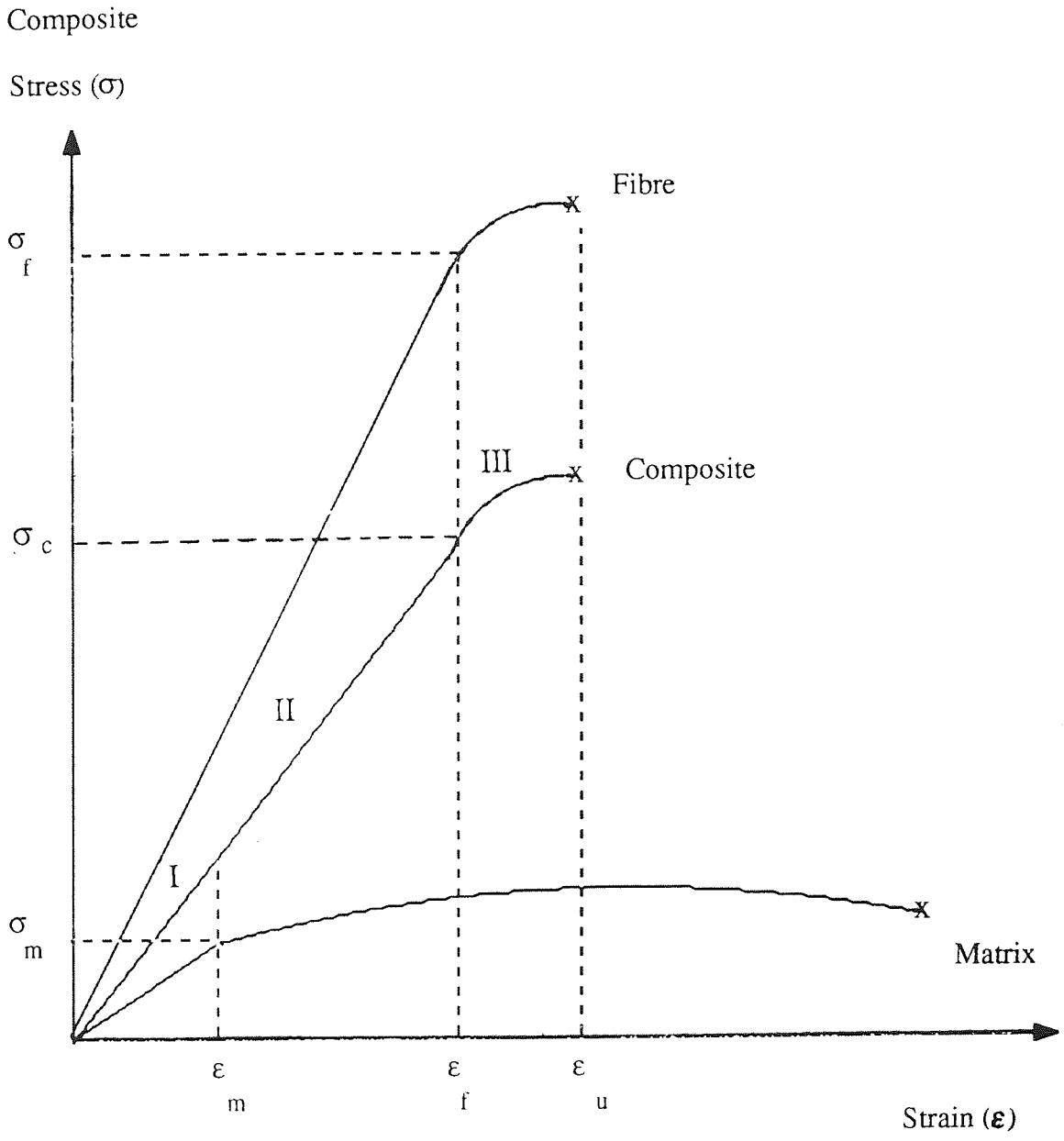

Figure 2.1. Stress/strain behaviour of fibre-reinforced metal matrix composites.

very strong fibres will have little ductility, the strain at which $\sigma_{m'}$ is evaluated is low and $\sigma_{m'} << \sigma_f$.

A critical fibre volume fraction (Vcri) has to be exceeded for fibre strengthening to occur :

$$V_{crit} = \frac{\sigma_u - \sigma'_m}{\sigma_f - \sigma'_m} \qquad (2.4)$$

Where σ_u is the strength of the strain hardened matrix. It is assumed that this critical fibre volume fraction has been exceeded for the metal matrix composites under investigation. So far all of the equations quoted in this section apply to continuous fibres. The condition becomes more complex in the case of discontinuous fibres, since the fibres in a composite are loaded through interfacial shear stress, the end portions of discontinuous fibres are under lower tensile stress than the central portion. But the higher shear stresses at the ends of the fibre mean that a metal matrix will flow plastically above some critical value. To utilise fully the high strength of the fibres, it is thus necessary that the plastic zone in the matrix does not extend from the fibre ends to its midlength before the strain in the fibre reaches its failure strain.

A critical fibre length (L_c) can be derived for a given fibre diameter (d) below which the fibre is not fully loaded by the interfacial shear stresses and reinforcement is inefficient

$$L_c = \frac{\sigma_f . d}{2 . \tau_o} \qquad (2.5)$$

Where τ_o is the shear yield stress of the matrix. The longer the fibre (L), the more the stress/strain behaviour approximates to that of continuous fibre composites. For discontinuous composite materials of length, the tensile strength is given by :

$$\sigma_c = \sigma_f v_f \left(1 - (1 - \beta)\frac{L_c}{L}\right) + \sigma_m V_m \qquad (2.6)$$

Where β is a constant which is equal to 0.5. It can be seen that the reinforcement provided with discontinuous fibres is less than that obtained with continuous fibres. The difference is neglible if Lc/L is small.

A unidirectional fibre orientation in a matrix gives highly anistropic behaviour. If the parallel fibres are orientated at an angle to the load axis then a rapid reduction in strength results as the angle increases. The failure mode changes with increased loading angle, from flow parallel to the fibres to failure (σ_c) by shear in the matrix or at the fibre matrix interface (τ), to failure of the composite in normal direction to the fibres (σ_s). The effect of these three failure modes can be seen in Figure 2.2. The transverse strength (σ_s) of a fibre reinforced composite is dependent upon the properties of interface matrix and the fibre volume fraction. The reduction in strength is usually compensated for in practice by using a laminated sheets in which the fibres have a different orientation in each layer under these conditions. The minimum strength of a laminated composite in any direction should exceed one third of the unidirectional strength.

As far as the random fibre orientated composites are concerned, the same principles are relevant as those applied to unidirectional composites. A modified form of the rule of mixtures law has been used to express the strength properties of planar-random fibre orientated composites. [32]

$$\sigma_c = \alpha \ \sigma_f v_f + \sigma_m v_m \qquad (2.7)$$

Where α is a coefficient which takes into account of changes in fibre orientation, fibre matrix bonding etc.

The ultimate tensile strength in B(SiC) fibre-reinforced aluminium composites show improvements or a decrease from fibre reinforcement, depending on the matrix alloy, orientation of fibre used. Fibre matrix interface strength and matrix ductility also seem to be major factors in dictating ultimate tensile strength. [33]

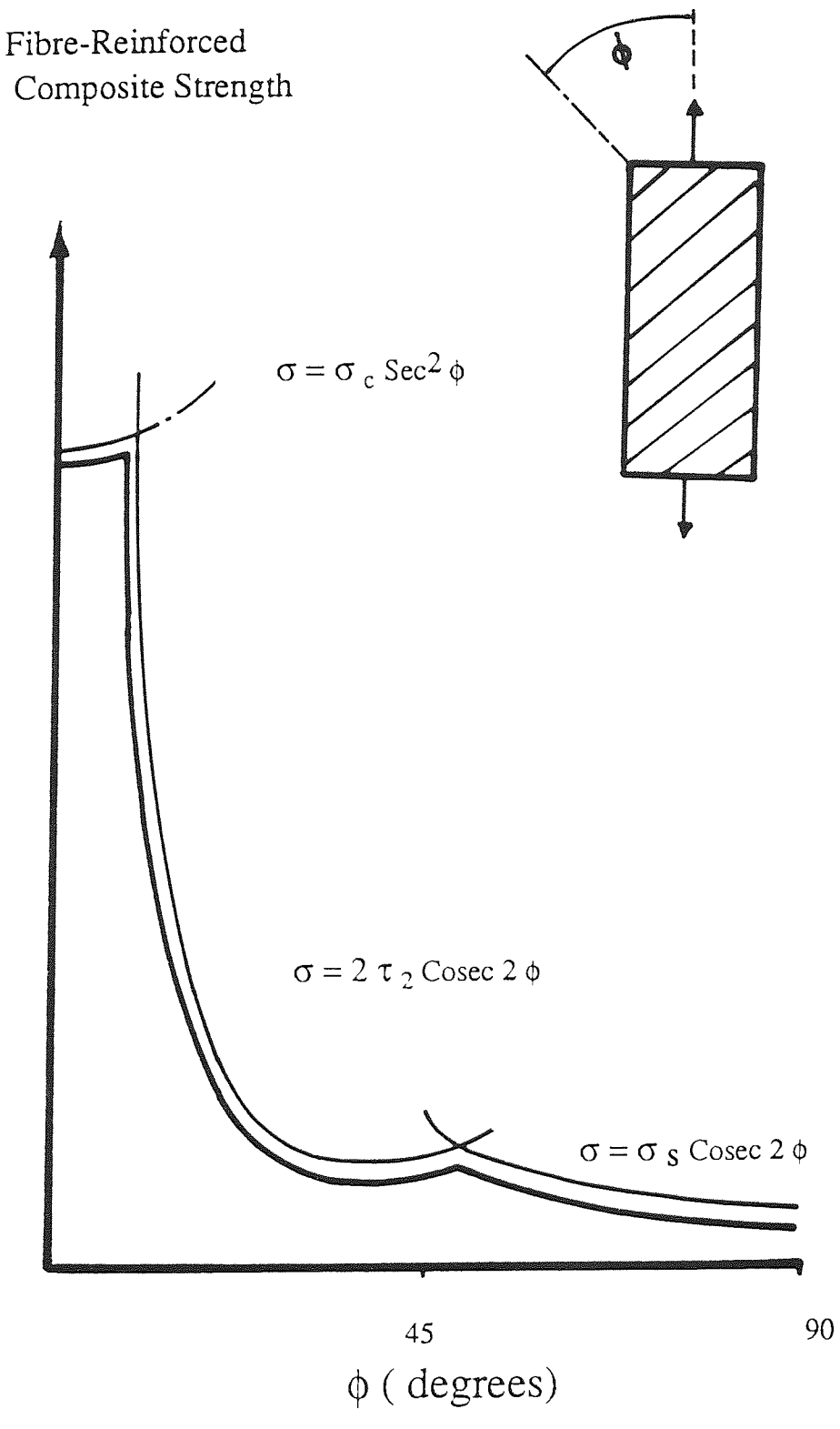

Figure 2.2. Effect of fibre orientation on strength of fibre-reinforced composite materials.

2.2 Mechanical Behaviour of Metal Matrix Composite Using B(SiC) fibre

Some research and development has been carried out on metal matrix composite using Borsic fibre, especially with respect to their mechanical behaviour.

The following is merely a brief overview of the work reported in the literature.

Herokovich et al [36] investigated the mechanical behaviour of Borsic/Al matrix composites including tensile and compressive testing. The composite laminates (up to % 49) were made from 160 μm diameter silicon carbide coated boron fibres with 6061 aluminium matrix. Monolayer tapes were made using a plasma spraying process and consolidated into laminates by diffusion bonding technique.The composites were tested in tension and compression for monotonically increasing load and also for variable loading cycles. The result showed that significant strain hardening and corresponding increases in yield strength were obtained. For matrix dominated laminates, the yield stress was identical to previous maximum stress, unloading was found linear with large permanent strains after unloading. However, for the fibre reinforced laminates, the yield stress increased with increase in previous maximum stress. But the increase in yield stress could not keep pace with the previous max. stress and the fibre dominated laminates indicated that smaller nonlinear strains was reversed nonlinear behaviour during unloading. It was also found that the sandwich beam specimens exhibited higher values for modulus, yield stress and strength than the flat coupons used for the compressive test.

Lynch et al [37] studied the tensile properties of unidirectional B/Al and B/Ti composites, tested parallel and perpendicular to the direction of reinforcement. For 50 vol % B/Al composites, ultimate tensile strength was about 1138 MPa while ultimate strength for 90° was around 103 MPa. In the case of B/Ti composites, ultimate tensile strength of about 1069 MPa and 307 MPa for 0° and 90° respectively was measured. Similar work was carried out by the others [38, 39] but fibre contents were about from 10 to 70% in their work. They reported that the values of the tensile strength and modulus

were in a good agreement with rule of mixture predictions. The explanation for low transverse strength of the boron was reported due to the transverse strength of the boron filament. If filaments split in transverse tensile tests of the composites at these same low stress levels, the load carrying cross section was sharply reduced and severe stress concentrations were introduced.

Examination of transverse tensile fracture surface showed the degrading influence of filament splitting. For well bonded composites with strong matrices, examination of fracture surface showed that nearly all of the filaments were longitudinally split. For a weak matrix interface transverse failure was controlled by the matrix strength and failure took place predominantly through the matrix. Improvement of the transverse properties of the B/Al composite could be accomplished by development of improved filaments by third phase addition or by heat treatment of the matrix. For example, the transverse strength of the annealed specimen was found to be independent of boron content and had strengths of approximately 80% of that of annealed 6061 Al matrix. The transverse strength was also found to be a fairly sensitive function of boron content if the filament splitting controlled the composite failure. Similarly Kreider et al [40] also employed heat treating of Borsic/2024 Al composites to increase matrix strength while producing a residual compressive strengths on the fibre to inhibit splitting. They substantially increased the observed strengths. Hot pressing conditions were varied and their effect on Borsic composites with 6061, 5052 Al determined. The transverse modulus increased at pressures of 14 MPa to 69 MPa and at temperature from 420°C to 565°C for both composites. The maximum increases from one to three times the low values and the curves tended to flatten under the more rigourous conditions. The transverse strengths were found to be less sensitive to hot pressing conditions and for 2024 Al a temperature of 490 °C was found to degrade the strength with increasing pressure.

Jones et al [41] also carried out longitudinal tension tests on a of Boron/Al matrix composite produced by diffusion bonding process, and examined the fracture surface of

the composite. The same matrix alloy (6061) was reinforced with 25 and 50 vol% unidirectional and cross-ply fibre respectively. It was observed that severe debonding of diffusion bond planes was observed at the fracture surface in both unidirectionally and cross-ply reinforced materials. However, in cross-ply composite, incomplete bonding was observed on a large scale between fibres and matrix and there were also voids, cracks and gaps between fibres and matrix. They showed that composite failure strain was found to be in the range of 0.3 to 0.6 percent. A striking difference between 0^o and the 90^o test properties of these composite was also reported. The ultimate compressive strength of composites was also found to equal their ultimate tensile strength.

Unidirectionally reinforced 50 vol% Borsic/Al composites parallel and perpendicular to the filament were tested in compression [42] and resulted in a compressive strength of 2048 MPa with failure occuring as a result of the brooming of one end of the specimen. In comparison, a similar sized specimen tested at 90^o to the filaments, resulted in an ultimate compressive strength of 255 MPa. Failure of this specimen was caused by a matrix shear failure at roughly 45^o to the load axis. A similar specimen was tested at 315°C, resulted in a 66 MPa ultimate compressive strength with the same type of the matrix shear failure. They also showed that the compressive strength of B/Al composites increased with increasing boron content. Moreover, the variation of compressive strength with filament-load angle was conducted for 25% and 50% B/Al composites. They reported that the 0^o compressive strength was very much more sensitive to boron content than the 90^o strength, the transverse compressive strength, being determined primarily by the shear strength of the matrix.

Shaefer et al [39] also investigated the variation of transverse strength and elastic modulus with test temperature of 25, 37 and 50% B/Al composites. The results showed that the temperature dependence of the transverse strength of these composites was independent of the reinforcement content. The transverse strength decreased with increases in filament content at all temperatures. In addition, the variation of elastic modulus with test temperature and boron content exhibited that the longitudinal modulus

increased with increasing boron content. The maximum at 300°C was most likely associated with relaxation of residual stresses both in the matrix and filament. This maximum value was not consistent with the other investigators. [31] In contrast, they found a continuous drop in longitudinal modulus with increasing test temperature. At 315 °C, the room temperature modulus had been reduced 20 to 30% while the transverse modulus was found to be less sensitive to boron content, decreasing with increasing test temperature.

The effect of the test temperature on the tensile strength of unidirectional B/Al composites was also studied [38, 39, 43] and compared with 6061 Al alloy matrix. The composite tensile strength was found to be exceptionally good up to about 315°C and decreased sharply thereafter, and at 315°C the composite tensile strengths were still 10 to 30 times higher than that of the Al matrix. Furthermore, the variation of ultimate tensile strength of cross-ply and angle-ply B/Al composite was also conducted and compared with the unidirectional composite. They reported that 0° to 90° cross-ply composites had the same temperature dependence as the unidirectional composites, while the 30° angle-ply composites reflected to decreasing matrix strengths above 149°C because composites were tested parallel to one half of their filaments. In comparison, extensive load transfer through the matrix was required for 30° angle-ply composites which was reflected in their stronger temperature dependence. Apart from that, the temperature dependence of boron fibre strength was reported by other researchers, [42] but the strength reductions of 20 to 40% were found from room temperature to 400°C for filament, with a room temperature tensile strength of approximately 3448 MPa. The observed composite strengths at 400°C were less than rule of mixtures predictions even if a 40% filament strength reduction was assumed. The synergistic influences of residual stress and matrix constraint were less pronounced at the higher temperature than at the room temperature.

Meyn et al [44] studied the effect of temperature and strain rate on the tensile properties of B/Al matrix composites produced by a hot pressing method (45 Wt %). Three approximate strain rates were chosen : $8 \times 10^{-5}\ s^{-1}$, $0.065\ s^{-1}$ and $0.4\ s^{-1}$

corresponding to test durations 60, 0.1 s, and 0.02 s respectively. The B/Al composite was tested at temperatures up to 260°C. The study showed that the longitudinal properties of the aluminium-based composite were not very sensitive to strain rate. The longitudinal strength of B/Al composite remained high from room temperature to 260°C at low strain and up to 372°C at the high strain. Transverse strength reduced rapidly with temperature and was not affected by high strain rates at low temperatures in particular and was not increased considerably at high temperature in aluminium composites. They also reported that the elastic modulus of B/Al composite at high strain rate was 30 % higher than at low strain rate at all temperatures. In their work, they also used 46 % silicon carbide-coated boron with aluminium alloy (6061).

The effect of test temperature on a B/Al matrix composite (20 Wt %) produced by powder technique was also studied by Akechi et al. [45] They found that a sound fibre interface without a heavy reaction was formed. Consequently, high mechanical strength was obtained for these composites. However this process was found to be inferior to that made by plasma spraying or diffusion bonding.

Toth et al [46] investigated the tensile and fatigue strengths of Borsic-reinforced Aluminium and Titanium matrix composites fabricated by a vacuum diffusion bonding technique. They reported that Al matrix composites tested parallel to the fibre directions were slightly stronger than Ti matrix composites up to a temperature of about 314°C. A Ti matrix composite reinforced with Borsic showed significantly better off-axis strength even at room temperature and a five-fold advantage in transverse strength was obtained over a Boron/Al matrix composite at a test temperature of 260°C. The results clearly showed that 0 degree strengths of Boron/Al and Borsic/Al was slightly affected by the temperature, but transverse strengths were much more affected by the temperature. It was reported that the transverse strength of a Borsic/Ti composite at 427°C was ten times better than that of Borsic/Al at 302°C. In addition, the high-cycle fatigue strength in the 0 degree orientation for the Al composite was significantly higher than that of a

comparable Ti matrix composite. On the other hand, the low cycle fatigue strength of the Ti composite was superior to that of a comparable Al matrix composite.

The creep resistance of unidirectionally reinforced composites loaded parallel to the filament was found to be outstanding primarily because of the creep resistance of the filament. For example, the creep of B/Al composites was studied by Antony et al [43] and found to be relatively insensitive to test temperature unlike homogeneous alloy. For 22 vol% B/Al composites tested from 93°C to 315°C under constant stress of 345 MPa. There was about a tenfold increase in the unidirectional creep rate and a tenfold increase in creep strain. Creep behaviour of 25 vol% B/Al composites also tested at 204°C under varying initial stresses [38, 47] and initial stress level on the unidirectional composites tested parallel to the filaments was found to be much larger than that the initial stress for the orientations. However, at filament-load angles, the creep resistance of the composites became dependent upon the creep properties of the matrix as evidenced by increasing creep strains and minimum creep rate was as the filament-load angle increased. They also observed that minimum creep rate for the 45° cross-ply composites was lower than the minimum creep rate for the 45° unidirectional composites in the case of 45°cross-ply. The examination of the fracture surface for the 45° unidirectional specimen also showed that failure occurred by a matrix shear controlled process parallel to the filaments. In comparison, for the 45° cross-ply composites, extensive shear in the matrix parallel to one set of filaments was impeded by the second set resulting in a lower minimum creep rate. The effect of stress on the min creep rate of 25 vol% B/Al composites, at 204 °C and 315°C for several orientations and showed the stronger dependence for the +45° cross-ply and -45° unidirectional composites compared with the 0° unidirectional composites. This reflected the requirement for extensive load transferred through the matrix and consequently, a greater sensitivity to matrix properties in the +45° and -45° composites.

The stress rupture properties of fibre reinforced composites had been found to be excellent, especially when loaded parallel to the filaments. Breinan et al [48] studied the

stress rupture behaviour of 50 vol% Borsic/Al composites at 300°C and 500°C and compared with the stress rupture behaviour of titanium 6Al-4V at 500°C. The result indicated that the improved performance of the composites became particularly significant for temperature greater than 400°C while the strength of the Ti matrix dropped sharply. Moreover, a comparison of the stress rupture behaviour of 50 vol% Borsic and boron reinforced Al composites at 400°C showed that a substantially lower stress dependence of the rupture time was found for the Borsic filament due to the chemical stability. It was also reported that the rupture stress decreased as the filament load increased.

Hoover et al [49] studied the effect of crack length and bond strength on the delamination process in Borsic/Al composites. The unidirectional composites were produced by diffusion bonding monolayer tapes of plasma-sprayed 1100 aluminium alloy and 140 μm diameter Borsic fibres. The normal volume fraction of Borsic was 0.36. Different diffusion conditions were used to vary the fibre matrix bond strength and transverse tensile strength of the composites. The composite plates were machined into single edge notch (SEN) test pieces. The crack length-to-width ratio was kept constant for specimens used in bond strength studies. To determine the effect of crack length, the ratios of crack length-to-width ranged from 0.20 to 0.50. The study showed that the net section stress at delamination was observed to decrease with increasing crack length in composites with weak fibre-matrix bonds. Variations in crack length, however, did not considerable alter the basic fracture mechanism in which the delamination process led to notch insensitivity. They found that the increase in fibre-matrix bond strength also resulted in a marked increase in the net sections at the delamination, but did not change the general delamination process while for cross-plied composites the transverse strength was raised and delamination was suppressed. This caused a notch-sensitive fracture behaviour and a substantial decrease was obtained in the fracture toughness. Poisson's ratio as a function of tensile strain was examined by the same authors [50] for four volume fraction (up to 54 %) of unidirectional Borsic/Al composites. The result showed that a

linear relationship was found between poisson's ratio and fibre volume fraction for elastic fibre-elastic-matrix stage and elastic fibre plastic matrix stage deformation. These results also confirmed that a rule of mixture calculation can be used to predict elastic and plastic composite poisson's ratios. They also reported that a considerable increase in the poison's ratios of the matrix upon yielding caused a sudden rise in the slope of the composite poisson's ratios versus longitudinal strain curve. This abrupt increase could be used as an accurate method of determining matrix yield in fibre-reinforced composites.

Prewo et al [51] investigated the interface strength of Borsic/Al composites produced by plasma spraying technique (50%) and fracture surfaces were examined by SEM, while the internal composite structure was determined by TEM. It was shown that for fully consolidated composites, well bonded specimens did not exhibit fibre-matrix interface failure as a primary fracture mode, but this mode of failure was predominant only when the composite bonding conditions were lowered from their optimum values. As a result of this, no loss of strength occurred for the composite. In contrast, uncoated boron fibres would have undergone considerable loss of strength under the same fabrication conditions. Examination of the interface by TEM revealed that the boron fibre was amorphous at the magnification used, while the silicon carbide which was deposited as a barrier layer was not .

The impact behaviour of Borsic/Al composites containing of 50 Wt % fibre was also investigated to determine the effect of three types of orientation. [40] The study showed that the LT type of notch configuration gave the highest impact energy and demonstrated an increase in energy absorption capacity with increasing boron content. This was explained to be due to deflection of cracks parallel to the filaments along the filament matrix interface, hence, increasing the composite energy absorption capacity. But the other two configurations indicated a much lower energy absorption, and appeared to be insensitive to boron content.

Fatigue behaviour of unidirectional and angle-ply 25 vol% B/6061 Al composites was investigated by Toth and et al. [47] The ratio of minimum to maximum stress in these

tests was 0.2 in their work. The fatigue strength at 10^7 cycles was approximately 80% of the tensile strength in all cases. The fatigue strength of T-O 6061 Al tested under similar condition was about 110 MPa at 10^7 cycles. The ratio of fatigue strength to tensile strength for the 6061 Al matrix was about 0.73. This suggested that composite fatigue failure may be controlled by the matrix.

Combined stress (tension-bending) fatigue tests were also performed on 22 vol% boron composites contained in a matrix which was 55% 1100 and 45% 2024 Al. [52] The ratio of the alternating stress to mean axial tensile stress was maintained at 0.95. The fatigue strength at 10^7 cycles both at room temperatures and at 260°C was found to be approximately 317 MPa. The ratio of the fatigue strength at 10^7 cycles to ultimate tensile strength was found to be about 0.50 at both temperatures. In comparison, for 0° reverse bending flexure fatigue of 42 vol% B/2024 Al composites the fatigue strength was found to be temperature insensitive up to 121°C (738 MPa), while at 260°C the fatigue strength was found to be reduced 42%. [53] Reversed bending failure fatigue at 260°C seemed to be matrix controlled.

Axial-tension-tension fatigue tests were carried out on B/6061 Al composites with similar boron contents, but different 0° ultimate tensile strengths using a ratio of alternating stress to mean stress of 0.8. [54] The fatigue strengths for these composites were found to be 621 MPa and 586 MPa respectively. Despite a substantial difference in tensile strength, the fatigue strengths were very similar. This suggested that the difference most likely were the different failure mechanisms in tension and fatigue. The fatigue strength for 45° angle-plied composites tested at 45° to the composite axis of symmetry was about 57% of the 0° unidirectional fatigue strength.[31, 41] However, in the case of the 45° angle-plied composites tested parallel to the axis of symmetry, a relatively poor fatigue was obtained to equal to the matrix fatigue strength. The 90° fatigue strength for 25 and 50 vol% B/Al composites with a ratio of 0.1 were found to be poor and showed 56 MPa and 28 MPa respectively. The reason of these low 90° fatigue strengths was explained to relate to pre-existing or stress-induced defects.

Baker et al [55] also studied the reversed bending fatigue strength of B/Al composites which was produced by a hot pressing technique. The superior fatigue resistance of the boron composite appeared partly from the use of the 6061 alloy matrix, but mainly from the manufacture of the composite. They reported that some evidence was found for induced fibre failure in the composites under high stress/low cycle conditions, but matrix fatigue was the primary type of fatigue damage sustained by the composites. Mechanisms of fatigue damage on the same composites has been also investigated by Johnson and Gounda et al [56, 57] recently.

From the literature review conducted above, the presence of continuous boron or Borsic fibre has been shown to give good the mechanical properties in these composites. However this is also concerned with characterizing and understanding the friction and wear properties of composites in order to develop a good bearing material. For certain applications the friction coefficient is of highest importance, but largely it is the mechanical loading carrying capacity and the wear rates of the materials that determine their acceptability in an industrial application. The kind of wear loading can be very different in different applications, and thus the structure of the composite materials used for various applications must also be different in order to fulfil the particular requirements. This may be because wear is not a simple material property, but depends strongly on the system in which surface functions. Because of this a tribological approach towards to friction and wear has been introduced in the following section.

2.3 Tribological Systems

A tribological system is defined as an entity whose functional behaviour is connected with interacting surfaces in relative motion.[58] The behaviour of the interacting materials can be characterised by its friction and wear performance. Friction and wear are interrelated in an intricate manner. By no means can friction and wear be considered as intrinsic material properties nor can they be solely a function of other material properties or parameters, but they must also take into consideration parameters of the system in

which they function. Thus a systems approach towards the friction and wear behaviour of tribological system is needed to create a logical framework in which present tribological knowledge can be organized.

The tribological system can be simply presented as in Figure 2. 3. Four basic aspects are considered, namely ;

(1). Technical function,

(2). Operating variables,

(3). Structure of the tribological system,

(4). Tribological characteristics.

The technical function of a tribological system is to convert given inputs, such as motion or materials, into output for technical usage. These can be generalized such as transmission of motion and work, generation of information, transformation and forming of materials.

The basic operating variables are the following quantities :

(1) Load, (2) Sliding speed, (3) Temperature, (4) Operating duration, (5) Sliding distance, (6) Type of the motion, and (7) Atmosphere etc.

The structure of the tribological system can be discussed in terms of the system's elements and their properties. The system can be simplified into four main elements as illustrated above, namely, two tribo-elements (tribo-element and counterpart) the interfacial medium and the surrounding element or environment. Many properties of the system elements influence the behaviour a material operating in a tribological system.

The pertinent properties of the tribo-element are basically inclusive of microstructural factors, geometrical factors and material properties. Microstructurally, the fibre volume fraction, the fibre/matrix bond and the geometry of the fibre are important. Geometrically, the size and shape of the tribo-element are considered, while hardness, elastic modulus, strength and fracture energy are very important material properties. The properties of the

environment which may have direct effect on the performance of the tribological system are the chemical composition, temperature, pressure and relative humidity. The interfacial layer is concerned when lubricant properties come into play.[59] It is the important to note that the element properties are all interrelated to each other.

Finally, as shown in Figure 2.3, the material components and substances directly participate into the friction and wear processes. These components are part of the structure of the tribological system. In addition to the structural elements, the operating variables have to be identified. (See in the upper part of Fig. 2.3). Through the action of operating variables on the structural elements of the system, tribological interactions occur which may lead to tribo-induced changes of properties of the system components as well as to friction induced energy loses and wear induced material losses. On the other hand, friction and wear behaviour is a function of the operating variables and the structure of the system. A fairly general misconception exists that friction and wear, which must be related in some way since they both arise from the interaction of surfaces, are simply related such that high friction means high wear. That this is not the case is clearly shown in Table 4,5 and 6 for MMCs. In almost all industrial situations the wear effects are more important than the frictional losses because they tend to have the greater economic consequences. Both of these mechanisms will also be discussed in the following section.

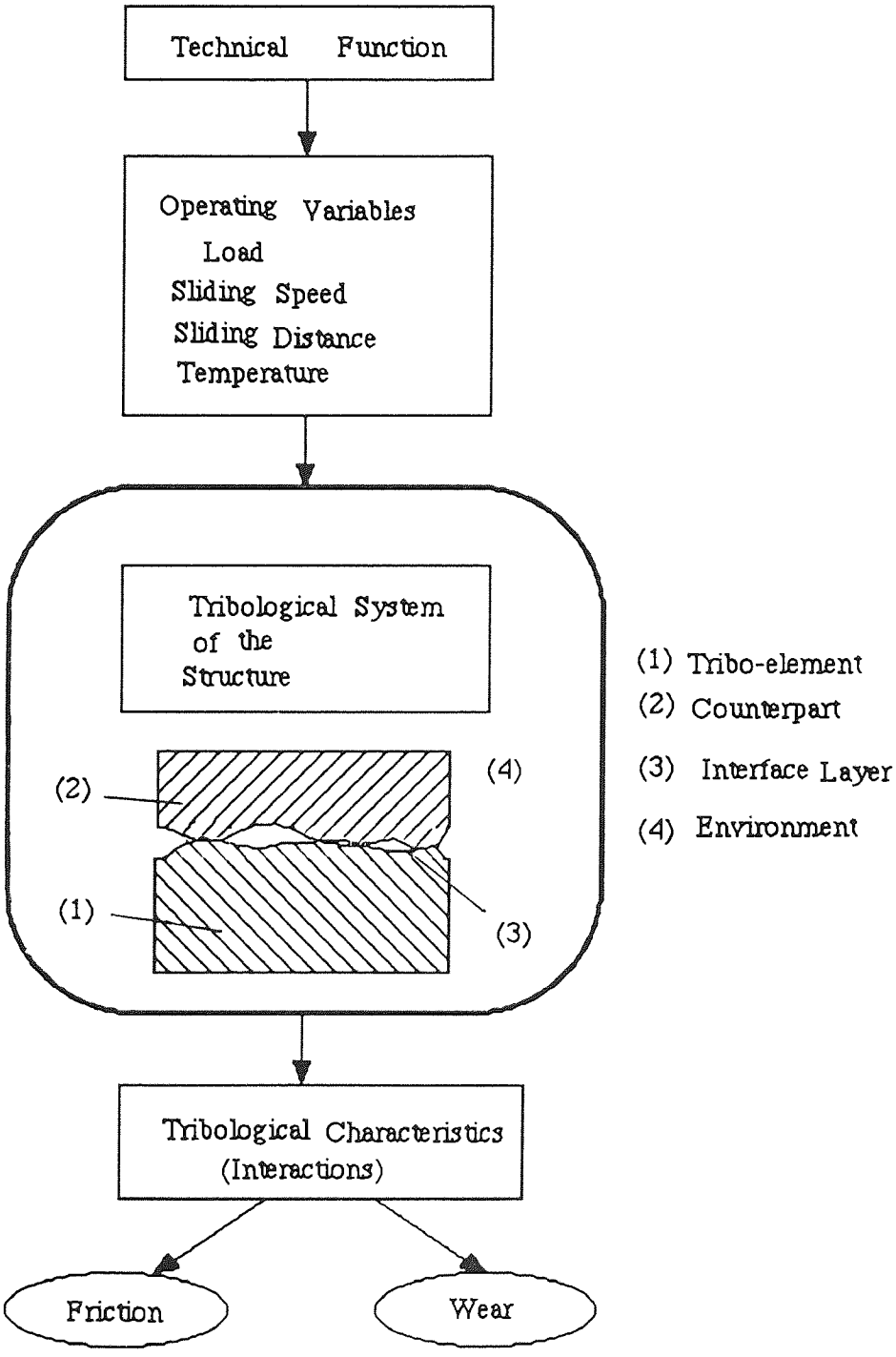

Figure 2. 3. Representation of a of tribological system.

2.3.1 Mechanisms of Friction and Wear

2.3.1.1 Mechanisms of Friction

The relationship between friction and wear of composite materials is very complicated and not fully understood. There is no absolute correlation between the two. The wear rate of a composite can be changed by orders of magnitude simply by varying certain factors of the system. The frictional force is associated with the expenditure of energy in the contact region, and it is the process of energy dissipation which may lead to the destruction of the surface layers of the composites and its eventual wearing. An intimate relationship exists between frictional and wear because without one the other can not exist.

Friction is defined as the resistance force tangential to the common boundary between two bodies when under the action of an external force, one body moves or tends to move relative to the surface of the other.[60] In engineering applications, friction is used to both of its extremes, for instance, low friction in bearing applications and high friction in braking operations. Amonts-Coulomb laws of dry friction are often referred to as a framework within which friction is generally considered by engineers.[61] They are as follows :

(1). When tangential motion between two contacting bodies occurs the frictional force always acts in a direction opposite to that of the relative velocity of the surfaces,

(2). The frictional force is proportional to the normal force,

(3). The frictional force is independent of the apparent area of contact.

When surfaces are loaded against each other they make contact only at the tips of asperities. The pressure over the contacting asperities is assumed high enough to cause them to deform plastically. This plastic flow of the contacts causes an increase in the area of contact until the real area of contact is just sufficient to support the load. Under these conditions the real area of contact A is given by the expression :

$$A_r = \frac{W}{P_m} \tag{2.8}$$

where Pm is the penetration hardness (yield pressure) of the softer material. The adhesion theory of friction assumes that friction is mainly determined by the shear strength of the cold-welded junctions formed between bodies in contact. Despite the considerable amount of work that has been devoted to the study of friction, there is still no simple model to predict or calculate the friction behaviour of a given pair of materials. The complexity of the overall friction stems from the simultaneous operation of several energy dissipative mechanisms between the materials which are strongly dependent on the system in which they function.

The coefficient of friction between metal and fibre-reinforced composites is due to the various combined effects of ploughing and adhesion. The relative contribution of these components depends on the condition of the sliding interface, which is affected by the history of sliding, the specific materials used, surface topography and the environment. The frictional force can be divided into two components: the adhesive component of friction which occurs in an interfacial region of very small thickness, and the ploughing component of friction which occurs within a relatively much larger volume of material adjacent to the region of contact.

The adhesion component consists of pure adhesion where the surface energies plays a dominant role. The dependency of surface energies suggests that the use of the same material for both sliding surface will result in a higher contribution to the frictional force, whereas, the use of different materials with respect to types of atoms, atomic distances and bond characters will result in a lower contribution factors. The adhesion component of friction may also consist of plastic deformation and material separation due to the asperities ploughing through the material resembling a fracture-like process. The ploughing component, which usually dominates when a very hard surface slides over a relatively softer one, consists of simple plastic flow or cutting and sometimes cracking and elastic grooving. It is thought that the ploughing component involves two

mechanisms for fibre-reinforced materials sliding against steel. One mechanism involves the ploughing of the steel by the fibres while the other involves the ploughing of the composite by the steel asperities causing elastic fibre bending and viscoelastic matrix deformation. Thus, the composite's compliance becomes of importance which in turn is affected by the matrix modulus and the fibre volume fraction. Consequently, the resulting frictional force between two mating solids in relative motion was obtained from the following basic mechanisms due to interactions of the opposing asperities in these two sliding surfaces. [62] These are : (1) Adhesion between asperities, wear particles and flat rubbing surfaces, (2) Interlocking of asperities, plastic deformation perpendicular and parallel to the direction of motion, (3) Ploughing of hard surface asperities.

Adhesion of asperities takes place by chemical or structural affinity between the two surfaces when they loaded together. Strong welds are formed at some asperity junctions and for the sliding to continue these welds must be broken. The break will occur at the weakest part of the junction, which may be the original interface or in the weaker of the two materials.

The other asperity interactions that results in a resistance to motion is the deformation and displacement of material during relative motion. A microscopic interaction is the deformation and displacement of interlocking surface asperities, and a more macroscopic interaction is the ploughing of grooves in the surface of the softer material by the harder. Another source of ploughing of one or both surfaces is the wear particles trapped between them therefore in most cases friction is the result of the contributions of adhesion, ploughing and interaction of asperities.

2.3.2 Mechanisms and Types of Wear

Wear is defined as the progressive loss of substance from the operating surface of a body occuring as a result of relative motion at the surface due to mechanical, chemical and thermal effects. [63] Loss of material can be the result of a variety of mechanisms such as adhesion, abrasion, corrosion and surface fatigue. In any particular instance of wear, one

may have any of these mechanisms operating either singly or combined. They may operate completely independently of each other or they may interact, and the situation can be extremely complicated. For example, the initial wear debris formed in sliding may become oxidised by frictional heating and the hard oxide may then act a fine abrasive to the surfaces. In general, it is also accepted that wear can be classified as either mild or severe as proposed by Archard and Hirst.[64] In a mild wear situation, the contact resistance is high and small fragments of debris are formed due to sliding gently. In a severe wear, it is characterised by low contact resistance and large metallic particles, rough and deeply torn surface are produced because of heavy loading. Let us now consider the types of wear in detail.

2.3.2.1 Adhesive Wear

Adhesive wear occurs when the pressure applied between two contacting asperities leads to localised plastic deformation.[65] This adhesion was thought to be due to atomic attraction and a reduction in the total surface energy of the sliding system and hence is favoured by clean surfaces. Adhesion wear is also referred to as "cold welding". The number of asperity junctions and contact areas will tend to increase as sliding and deformation continues. Therefore, strong cold welds are formed at some asperity junctions. These welds must be sheared for sliding to continue and eventually rupture at a point of weakness which may be along the original contact or in the subsurface of one of the sliding partners. The later case being normally associated with fatigue. This process implies the transfer of material from one surface to another, which may subsequently lead to the production of debris by the removal of transferred material if shear takes place away from the surface or may also cause a reversal of the process by transfer of material back to the original surface. In the absence of adhesion, the other asperity is the deformation and displacement of interlocking surface asperities by ploughing of grooves in the softer materials.

Abrasive Wear

Abrasive wear arise because of the ploughing out of a soft surface by a harder surface. This type of wear can be divided into two categories. These being two body abrasion where rough surface asperities plough a softer, moving surface and three body abrasion where wear is due to loose hard particles trapped between two moving surfaces. The mechanism of material removal from the softer surface includes microploughing combined with high plastic deformation, microcutting and eventually microcracking. Characteristics of these mechanisms are the appearance of longitudinal grooves in the sliding direction, this type of feature being knowing as gouging, scoring or scratching depending on severity. The severity of the process is related to the sharpness of the abrasive asperities or particles.

Delamination Wear

Delamination wear takes place as a result of relative sliding motion between two surfaces under a normal contact load. The delamination process occurs by the following set of mechanisms [66]:

(1) When two sliding surfaces come into contact, normal and tangential loads are transmitted through the contact regions by adhesive and ploughing actions. The asperities of the softer surface are easily deformed and some are fractured by the repeated loading. A relatively smooth surface is generated, either when these asperities are deformed or when they are removed.

(2) Once the surface becomes smooth, the contact is not just an asperity-to-asperity contact, but rather an asperity-plane contact; each point along the softer surface experiences cyclic loading. The surface traction exerted by the harder asperities on the softer surface induces plastic deformation which accumulates with repeated loading.

(3) As the subsurface deformation continues, voids are nucleated below the surface. Void nucleation very near the surface is not favored due to the triaxial state of large

compressive stress which exists just below the contact regions. In materials which contain hard particles void nucleation is preferentially initiated at the particle matrix interface.

(4) Once the cracks are present because of either the crack nucleation or pre-existing voids, further deformation and repeated loading causes cracks to extend and to propagate, joining the neighbouring ones. The cracks tend to propagate parallel to the surface since the state of loading is repeated along the surface.

(5) When these subsurface cracks reach a critical length they become unstable and propagate to the surface, generating thin wear sheets. The thickness of the wear sheets is controlled by the location of subsurface cracks growth which is controlled by the both loads at the surface.

Since the delamination process is controlled by deformation, void nucleation and crack propagation, the microstructure of the material and the state of stress are two important parameters of the wear behaviour. Such microstructural parameters as hardness, number of second phase particles or inclusions and morphology of the particles affect the wear process since they control the mechanical behaviour of materials.

Surface Fatigue

As is known from the mechanical behaviour of bulk materials under repeated mechanical stressing, microstructural changes in the material may occur which result in gross mechanical failure. Similarly under repeated tribological loading, surface fatigue phenomena can be occurred on two scales [67] and microscopic fatigue. Macroscopic fatigue wear occurs at non-conforming loading surfaces, whereas microscopic fatigue takes place at the contacts betweeen sliding asperities. In loaded sliding contacts due to the asperity height distribution these are strained to different extents, so that the contact stress will vary from a very low level of elastic stress up to a level of fracture stress of the weaker of the materials in general. Truly elastic stresses will cause no damage, while the fracture stress will results in the formation of a wear particles during a single

interaction. However, at intermediate stresses i.e., at any stress above the fatigue limit below the fracture stress, the asperity will be subjected to a single fatigue cycle and the accumulation of such cycles with continued sliding will eventually cause of the formation of a wear particle by local surface fatigue fracture.

Impact Wear

Impact wear arises from repetitive impact of two surfaces. The most common mechanism of impact wear is by formation and propagation of subsurface cracks in ductile materials and propagation of surface cracks in the brittle materials. This is similar to the erosion wear in the sense which occurs by impact of small solid particles on the surface.

2.3.2 Friction and Wear of Metal Matrix Composites

In the past much of the research on MMCs has been carried out with a view to structural applications. As a result such mechanical properties as the elastic modulus, yield strength, fatigue and creep behaviour of MMCs have been extensively investigated. In contrast, tribological properties have received only modest attention until recently. In the investigations that have been carried out on the tribology of fibre-reinforced MMCs, fibre orientation has been identified as the key microstructural parameter which affects composite wear. However, there is some disagreement as to its effect. Therefore, research work related to fibre orientation, fibre volume fraction and sliding velocity of the MMCs will be reviewed here.

Giltrow et al [68] studied the friction and wear properties of carbon fibre-reinforced metals, in their pioneering study of composites containing up to 25% vol chopped fibres in a variety of metal matrices prepared by a powder metallurgical method. They found that the wear rates decreased with increasing fibre content. The fibres, however, were ineffective in reducing the friction coefficient. Microscopic studies also showed that extensive tearing produced rough surface on pure metals, while the worn surfaces of the composites were found to be much smoother .

Eliezer et al [69] investigated the high speed tribological properties of continuous graphite fibre-reinforced metal matrix composites. The fibres were incorporated into copper and tin alloys by a liquid metal infiltration technique. They reported that the coefficient of friction and the wear rate of the composites depended on the proportion of Sn, orientation of fibres, sliding velocity, graphite grain size and degree of liquid metal infiltration within fibres. They found that the friction coefficients and wear rates decreased with increasing tin content in the matrix. The normal direction was found to give better sliding behaviour, and wear and friction were observed to decrease with increasing sliding velocity. Eliezer and Khanna [70] presented a qualitative model to explain the wear behaviour of two types of graphite composites. They utilized the fact that films are formed on the surface, and that tensile stress exists behind the asperity contact which will cause debonding of the fibres and matrix interface. But a defect of this model is that it fails to explain the wear behaviour for Type II graphite fibres where a film can not be formed. But with increasing velocity, the amount of oxide on the counterface shall decrease and this will also decrease the wear rates. The decrease, however, will be limited to low speeds. AES analysis also showed that formation of film between the fibres and matrix was present covering copper, iron, oxygen but iron and copper oxides was predominant over the sliding surface.

Amateau et al [71] studied the tribological behaviour of unidirectional graphite-fibre composites made by liquid infiltration. They found that the initial wear rates were high but decreased in time to lower steady state values. The drop in wear rate with time was due to a decrease in abrasion caused by the formation of a transferred film, and by the smoothing of the sliding surface by abrasion. In their study two types of fibres were used for the purpose of a comparison. They found that composites with Type I (HM) fibres gave higher wear but lower friction coefficients. Also the dependence on the matrix material was greater for the Type I fibres. This was not in accord with previous observations.

Wear behaviour of continuous and discontinuous graphite fibre-reinforced glass composites was studied against gray cast iron counterface by McKittrick et al.[72] They reported that the coefficients of friction and wear rates were found to be lower in the unidirectional fibre composites than chopped-random fibre composites. It was also found that Type I fibre composites had lower wear and friction coefficients than Type II fibre composites. The effects of sliding time and speed on the wear rate and friction of unidirectionally orientated graphite/aluminium matrix composites were studied by Pearsall et al.[73] It was found that the friction and wear rate of the composites decreased with increasing the sliding time until steady state value was reached. The steady state wear rate was also proportional to the reciprocal of the sliding speed and friction was observed to be dependent on velocity. Nayeb-Hashemi et al [74] reported that wear rate and friction coefficient of continuous graphite-fibre composites were found to decrease exponentially with sliding time. It was also found that the wear rate increased with increasing matrix hardness in the case of N and AP fibre orientations. However, wear rate increased with increasing thickness of reaction zone when the fibres were orientated in the P direction. A wear model was proposed for the case where the fibres were parallel to the sliding direction. Experimental data were also in close agreement with the model's prediction. Scanning and Auger electron microscopy observations indicated that the high initial values of friction coefficient and wear rates were found to be due to a high degree of matrix adhesion to the counterface. However, the low steady state values of friction and wear were found because of the formation of a film that impedes adhesion and confers some degree of self-lubrication. This film was observed to consist of a mixture of matrix and counterface materials and carbon from the fibres.

As for the case of particulate reinforcement graphite, there have been numbers of reports describing the wear behaviour of aluminium alloy graphite particle composites under dry sliding conditions. [75, 77, 78, 83] Studies have shown that lubrication of tribofilm was evident in most cases. For example, Rohatgi et al [76] studied the friction and wear of metal matrix graphite particle composites with using different materials.

They reported that the friction coefficient of low graphite (5%) composites depended on the matrix characteristics, while friction becomes independent of the matrix material at high volume fractions of graphite (15 %), due to the covering of the sliding surface by a graphite film. Their study showed that the wear rate decreased with increased sliding velocity in low graphite composites. The wear rate, however, was very low and independent of sliding velocity in composites containing large amounts of graphite. However the film could not form in the absence of air, so that a quite high friction coefficient was obtained in the composites tested in vacuum. Jha et al [77] observed a completely contrary trend where wear rate increased with graphite content (14 Wt %). Also Biswas et al [81] reported that the dry sliding wear of Al-Si alloy particle composites containing 2.7 and 5.7 Wt % graphite particles was found to be higher than that of the matrix alloy. Similar findings were reported by Gibson and co-workers [82] for composites containing higher (>8 Wt %) graphite content.

Saka et al [84] investigated the friction and wear behaviour of several fibre-reinforced metal matrix composites, comprising graphite/Al, stainless steel/Al and Al_2O_3/Al-Li alloy matrix. They reported that graphite/Al composite showed the lowest coefficient of friction and wear. In contrast, stainless steel/Al exhibited a high friction and high wear. SEM observations of the worn surfaces revealed that fibre pull-out was the predominant mechanism of wear, especially, in the graphite/Al and SS/Al composites, whereas fibre pull-out plus abrasion was dominant for the Al_2O_3/Al composites in transverse sliding.

Tao et al [85] studied the tribological properties of carbon fibre-reinforced zinc alloy composites produced by the vacuum liquid infiltration method. The study showed that the tribological properties of the composites were better than those of the zinc-alloy when the specimens were tested without lubricant, but were not better than that of the alloy when an oil lubricant was used. The friction and wear behaviour of the composite were obviously affected by the orientation of carbon fibres. The best wear characteristics were found to be the specimens with AP orientation under oil lubrication. The wear and

friction behaviour of unidirectional carbon-fibre glass matrix composites was also investigated by Lu et al.[86]

Dry sliding and abrasive wear testing was conducted on composites rubbed against different metals and SiC papers. They found that the highest wear resistance and the lowest friction coefficients were observed in AP direction when sliding took place against smooth hard metals. In contrast, the abrasive wear rate in the AP direction of the composite was higher than those of the other two directions. In addition two types of coloured wear debris were observed and these played an important role in the wear mechanisms during sliding. Sliding wear behaviour of laminated composites of copper and amorphous $Ni_{78}Si_{10}B_{12}$, fabricated by diffusion bonding was studied by Alpas and Embury.[87] They reported that wear in the copper layer occurred because of extensive plastic deformation and subsurface cracks. Metallic glass layers were effective in increasing the wear resistance of the composite by supporting the load with less deformation. Alpas and Zhang [88] also studied the sliding and abrasive wear behaviour of silicon carbide particle-reinforced aluminium composites. A commercial (2014) alloy was reinforced with 20 vol % of SiC. They indicated that the volume loss of the material increased linearly with sliding distance after a short incubation period. The highest wear was found in the case of abrasive wear. Subsurface cracks and delaminated surface layers were observed during this period.

The wear behaviour of A356 Al alloy/SiC particle composites was studied by Pramila Bai et al.[89] The composites contained fibres up to 25 vol % produced by a casting method. They found that the incorporation of SiC particles into the aluminium alloy improved the wear resistance of the matrix considerably. They also observed that iron rich layers were evident on the surface of the composites. A model for wear rates of polymer-based composites was applied by Ramesh et al [90] to predict the wear rates of nickel/silicon nitride composite coatings under sliding conditions. The results showed that the measured wear rates seem to agree with the semiquantative model.

Hosking et al [91] investigated the wear properties of the aluminium alloy composites containing particulate non-metals. Two types of wrought alloy (2014-2024) were reinforced with 2 to 30 Wt % of Al_2O_3 and SiC particles (up to 142 μm in size) using a stirring technique. They found that silicon carbide particle reinforced composites exhibited slightly superior wear resistance to alumina-reinforced composite (20 Wt %). They also reported that the wear mechanism of the matrix alloys was adhesive in nature, while composites with a high weight percent of non-metals showed an abrasive wear mechanism on both disc and pin surfaces. Alahelistan et al [92] studied short fibre alumina-reinforced composite materials containing up to 30 vol % reinforcement. The fibres were incorporated into the Al, Mg and 9Al-Mg-Zn matrices by a squeeze-casting technique, and were tested with the plane of fibres parallel to the sliding direction. The study showed that the wear properties of MMC materials depend very much on the tribo-system and the type of MMC. An optimum wear resistance was found at a fibre content of about 10 vol% in dry sliding wear. Magnesium and alloy tests also indicated an increasing two-body abrasion resistance with increasing fibre content. The abrasion rate of aluminium, however, was not affected by the fibre content.

Arikan and Murphy [93] studied the friction and wear behaviour of δ–alumina fibre reinforced zinc based alloy (30 wt % Zn, 2 wt % Cu). They found that the coefficients of friction of the composites were higher than that of the unreinforced matrix alloy and were independent of fibre content and load. The wear rate decreased with the increase in volume fraction of fibre and load (26% vol max used), and the reduction in wear rate was very significant when the fibres were orientated with their axis perpendicular to the sliding plane. In order to identify the large effects of differences in orientation, further tests were carried out under high load conditions by Murphy and Arikan [94] and the worn surfaces of the pin were examined by SEM. It was concluded that the presence of fibres reduced the amount of sub-surface plastic deformation in comparison to the unreinforced matrix alloy.

For the case of unidirectional and chopped alumina fibre-reinforced aluminium composites, Fukunage and Sakai [95] studied the effect of volume fraction of fibre on composites produced by an infiltration process in vacuum. The volume fractions of fibre were 30 and 50 vol % for unidirectional and chopped fibre composites respectively. They found that the volume fraction of fibre had a considerable effect on the wear rate. The wear rate was also obtained small to depend on the critical sliding speed and normal load. The normal direction gave the most excellent wear resistance of the various fibre alignments. Abrasive and sliding wear and friction behaviour of continuous α alumina/Al-Li matrix composite was investigated by Greenfield et al.[96] They reported that the highest coefficient of friction for unreinforced materials and the highest wear rate were observed in the anti-parallel direction. On the other hand, the lowest wear rate and the greatest reduction of friction were obtained in the normal sliding direction.

Saka and Karalekas [97] studied the effect of fibre volume fraction on the wear behaviour of particle-reinforced metal matrix composites. The composite containing up to 40% spherical Al_2O_3 particles dispersed in a copper matrix was prepared by hot pressing blends of copper and Al_2O_3 powder. They reported that wear volume exhibited considerable increase for oxide concentrations up to 30 percent, and then decreased. The friction coefficients of the composite showed a linear increase with increasing oxide concentration due to spreading of copper over the Al_2O_3 particle surface. The result of SEM micrographs indicated that delamination was a possible mechanism of wear in particle-reinforced composites. Abrasion and erosion wear behaviour of Al/δ–alumina fibre composites (30 %) were investigated by Hutchings et al.[98] They reported that the extent of fracture of the reinforcing phase plays a critical role in determining the wear behaviour, and fibre breakage was also increased with abrasive particle size, angularity and hardness in the case of two-body abrasion. Also it was increased with impact angle and velocity for erosive wear. A study of wear behaviour of TiC fabric-aluminium composite materials was performed by Sherman and McHugh.[99] The composites were

produced by a casting method using both Al-Si alloy and Al-Cu alloys. They found that the composite offered better wear resistance than that of the base alloys.

From the above literature review, it is seen that no study on the friction and wear behaviour of Borsic-reinforced aluminium matrix composites has been reported.

2.4 Concluding Summary

Metal matrix composites are currently promising for high temperature and wear resisting materials as well as for high specific stiffness and strength materials. One of them has been brought to the practical use as a light weight constructional material for a space vehicle, aircraft and automobile components.

Continuous fibres or particles of such materials as carbon, alumina, silicon carbide and boron have been made commercially, then MMCs have been produced using different techniques on a fairly large scale. The friction and wear properties necessary for practical machine design, however, have not been made clear yet. Since graphite behaves as a lubricant, carbon fibre-reinforced/Pb, Cu, Ag, Ni matrices, [68] copper-tin alloy, [69, 70] copper-silver based alloy, [71] glass, [72] aluminium matrix alloy, [73), (74] ; Particle graphite-reinforced/Al matrix alloy, [75-84] zinc alloy, [85] glass matrix, [86] ; Alumina-reinforced/Al alloy, [91, 92, 95, 96, 98] zinc based alloy, [93, 94] copper, [97] have been already tested on their wear properties. As for the other fibres only a limited numbers of reports are met with on the wear properties of silicon carbide-reinforced/Al alloys [88-92] and TiC fabric reinforced/Al alloy composite. [99]

In the case of the B(SiC) fibre-reinforced aluminium composites, however, this review of the literature has clearly shown that wear behaviour of these composites has not been established. It is, therefore, the primary objective of the present study to investigate the sliding wear characteristics of the continuous B(SiC)/Al composite at room temperature without lubricant under a variety of experimental conditions. In particular, the effect of fibre arrangement relative to the sliding surface on the wear resistance must be fundamentally studied for preparing engineering data on wear

resistance of this type of composites, and for discussing the wear mechanisms by observing the worn surface of the pin and analyzing the worn surface.

At present, there is also limited data available with respect to microstructure and tensile properties of B(SiC)-reinforced composite materials. Thus, another objective of the current investigation is to test the tensile strength of the composite under different conditions. Finally, B(SiC) fibre-reinforced plastic matrix composite is to be produced by a hot-pressing technique and used to study the effect of fibre orientation on the wear behaviour of the composite under the similar conditions to metal matrix composite, and examine the worn surface in determining the wear mechanisms.

It is hoped to compare the friction and wear behaviour of the both metal and plastic matrix composites in order to deduce the nature of friction, wear and surface for the sliding system as defined.

CHAPTER THREE

3.0 EXPERIMENTAL PROCEDURE

3.1 Introduction

This work was carried out principally on continuous B(SiC)-reinforced/2014 alloy matrix composites, ready produced in a previous research programme by liquid metal infiltration route.

The experiment mainly consists of four parts. The first step of the experiment was conducted to determine the tensile data of composite and matrix alloy, examined the fracture surfaces by scanning electron microscopy. The second step of the investigation was carried out to measure friction and wear rate of the composite materials to determine the effect of fibre orientation under dry sliding conditions. This covered normal, parallel and anti-parallel orientation of fibres to the sliding direction. Third step of the investigation was conducted to examine the worn surfaces, wear debris and the effect of additive on wear of the composite. The technique used for the sample analyses consists of scanning electron microscopy (SEM), X-ray photoelectron spectroscopy (XPS) on worn surfaces of pin.

Finally, a subsidiary experiment was carried out to produce B(SiC)-reinforced plastic matrix composites by a hot pressing technique and assess the friction and wear behaviour of the composite material and matrix, supplemented by observations of the worn surfaces. A comparison was carried out between the behaviour of metal matrix and plastic matrix composites.

3.2 Materials and Detail of Experiments

Fundamentally MMC materials studied in this work contained continuous B(SiC) boron fibres in a 2014 aluminium alloy with composition : 92 % aluminium, 4.8 % copper, 1.7 % iron, 0.79 % silicon and 0.68 % manganese. The B(SiC) fibres contained a tungsten

core about 15 μm in diameter and were made by thermal deposition of boron on a tungsten fibre. The resulting fibres about 140 μm in diameter, were coated with silicon carbide to a thickness of 2.5 μm. The fibres had a tensile strength of 2.9 GPa and Young's modules of 400 GPa.[5]

The composites were made by a liquid metal infiltration technique for a previous programme. For this process, the B(SiC) fibre reinforcement was in the form of wide woven tape made up of continuous fibres interlaced with titanium tapes. The reinforcement was thus approximately parallel. Layers of tape were cut and stacked together to give the required volume of reinforcement ranging from 16% to 32 % in the resulting composites. The plates formed were rectangular in shape and measured 110x140x10 mm. These were put into a hot die, evacuated and pressure infiltrated with aluminium alloy to produce the composite. Details of the fabrication procedure of the composite are described elsewhere.[100, 101] Mechanical tests were carried out to obtain axial strength data of B(SiC)/Al composites and examine the fracture surfaces of the samples by SEM.

In addition, B(SiC) fibre-reinforced plastic matrix composites were produced in this research programme by hot pressing technique, using the same fibre in a Daniel Press. In the hot pressing technique, the press was heated to 180 ^{o}C. For producing of composite specimens by hot pressing, a plate was designed and made from mild steel in the form of rectangle which was about 250x200x8 mm. The plate also had a 120x100x8 mm internal size for die cavity. Another two plates about the similar size was used to prepare a preform of the composite. The internal sized plate was placed on the one of the plate. The woven type of the B(SiC) fibres were cut about 120x100 mm and plastic foil also prepared in a same way. They were built up layer by layer in the desired orientation and volume fraction onto the foil layer of the matrix in the die cavity. The process was continued until reaching a certain thickness and closed with the second plate. Then the assembly was inserted into the press and platen was closed for 4.0 min for premelting without pressure and then 80 kg/cm^2 pressure was applied and released after keeping it

about above time. The assembly was cooled down below 100° C. Finally, the upper platen was removed and samples were taken out. The matrix used in this composite was a high density polyethylene which had a density of 887 kg/m^3. For the wear tests, some of the required components such as the composite plates of various of volume fractions, a woven type of unidirectional B(SiC) fibre, disc and wear pin samples, and die are shown in Figure 3.1. Samples were cut for wear tests which had fibres normal, parallel and anti-parallel to the proposed sliding surface.

Dry sliding wear tests were carried out to determine the effect of fibre orientation on the wear resistance of both metal and plastic based composite materials. For this process, three basic fibre orientations are identified in terms of the sliding direction because of the nature of unidirectional composite materials. Figure 3.2 illustrates a fibre reinforced composite block indicating three sliding directions. i.e., normal, parallel and anti-parallel orientations. Normal orientation (N) is defined as the fibres being perpendicular to sliding direction; in the parallel orientation (P), the fibres are parallel to the sliding plane and parallel to the rubbing direction, while in the anti-parallel orientation (AP), the fibres are parallel to the sliding plane but perpendicular to the rubbing direction. Worn surfaces, sections of worn surfaces, and wear debris were observed using both back scattered electron microscopy (BSEM) and secondary electron microscopy (SEM).

3.3 Microstructures of the Matrix and Composites

The specimens were prepared for microstructure examination as follows : Samples were cut from each plate which covers different fibre content by using a electrical discharge machining (EDM), and prepared by mounting small pieces into bakelite powders. They were ground on silicon carbide water proof abrasive papers of grades 200-400-800 and 1200. They then were polished carefully up to 1 μm by diamond compound on napeless paper using an automatic polishing machine to minimise relief effects. The specimens were cleaned with alcohol, then they were dried prior to examination in the optical or scanning electron microscope (SEM).

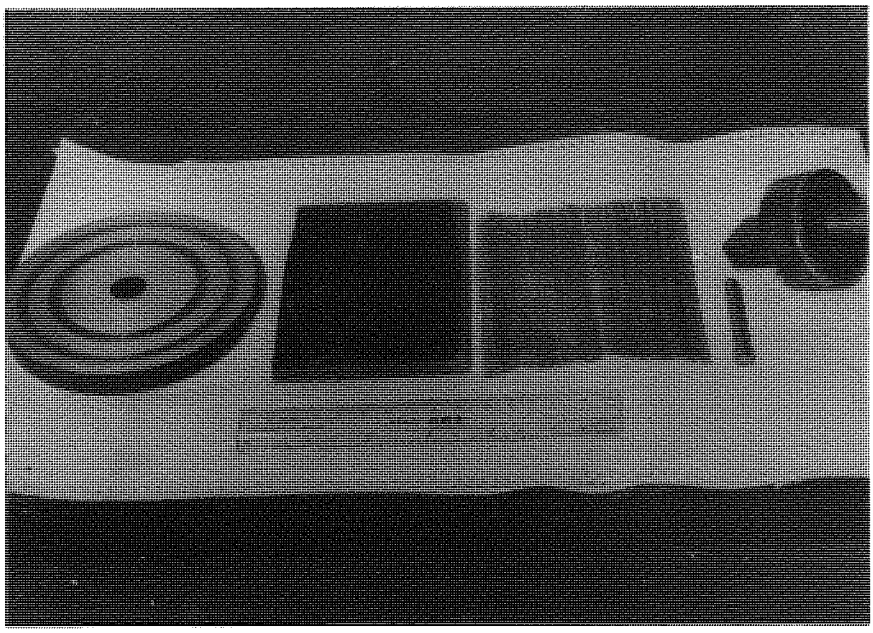

Figure 3.1. Some components used for wear tests including B(SiC) fibre, wear pin, composite plate and disc, and die.

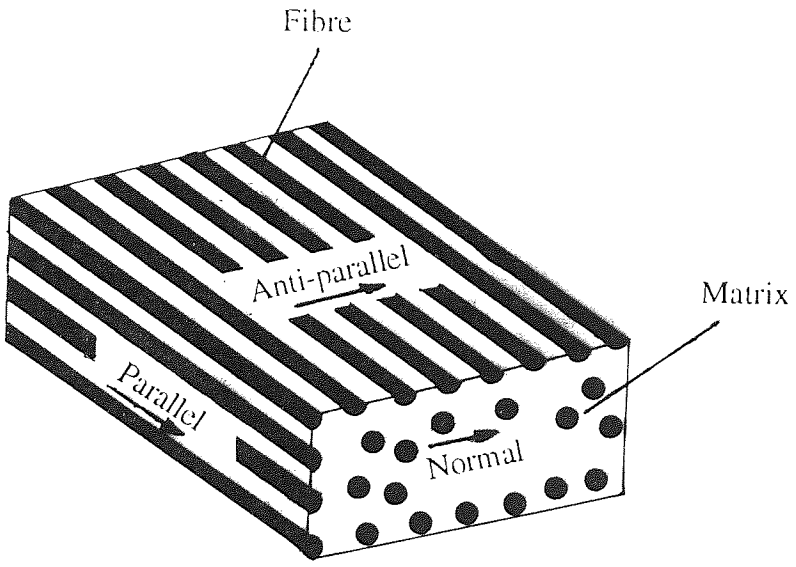

Figure 3.2. Fibre-reinforced composite block showing sliding directions.

TABLE 2

CALCULATION OF THE SPEED TO THE SELECTIVE TRACK RADIUS.

Speed (m/s) track radius (mm)	0.6	1.0	1.6	2.0	3.0
28	206	340	548	686	1028
32	180	300	480	600	900
36	159	273	425	531	796
40	143	238	382	478	717
44	130	217	348	435	652
47	122	203	325	407	610
52	110	184	294	368	552

For a track radius of r, and a revolution rate of n revolutions per minute, the rubbing speed is given by

$$V = \frac{2 \pi r n}{60} \qquad (3.1)$$

This equation can be used for a given any track radius. For example, for a 32 mm track radius and 1.0 m/s, the required r.p.m. setting is 300 r.p.m.

3.4 Wear Test Machine

A pin-on-disc type friction and wear testing machine was used in this experiment as shown in Figure 3.3. This machine consists principally of a flat-ended cylindrical pin (A) which was able to be loaded endwise against the flat surface of a rotating disc mounted on a turntable (B) which had a vertical axis of rotation. The turntable could accommodate discs varying in diameter from 20 to 100 mm. It was driven by a servo-controlled D.C motor with speeds in the range of 100 to 600 rpm. The speed was indicated on the motor control, panel and a vernier gauge on the machine measured the radius of the running track. When this radius was changed to give a new disc wear track, the motor speed was varied to maintain the same relative velocity at the pin/disc contact point. Two transducers (C, D) were fixed to the machine to measure the torque between the pin and disc, and change in the length of the pin with the vertical linear transducer.

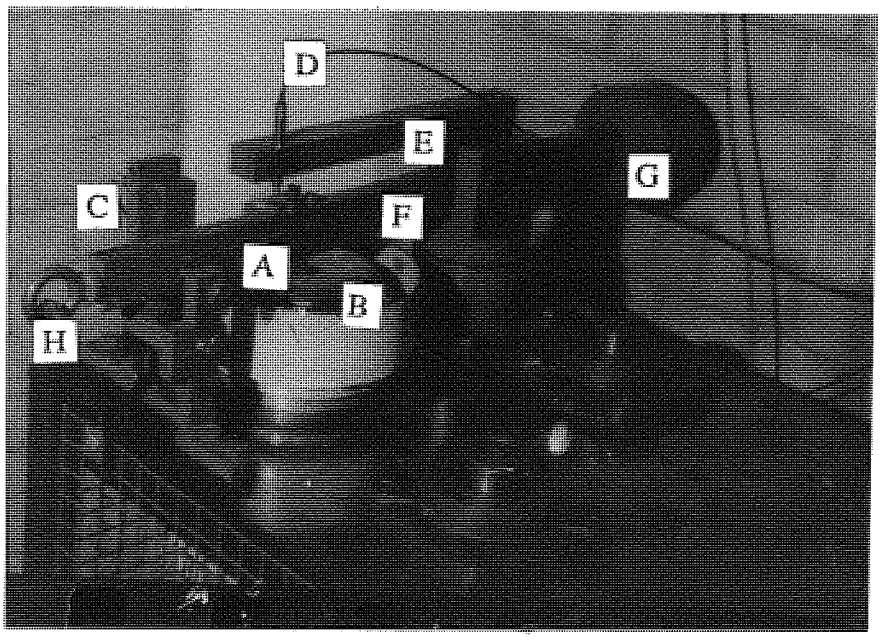

Figure 3.3. Pin-on-disc wear machine. A) Wear pin, B) Rotating disc table, C) Force transducer, D) Vertical linear transducer, E) Upper carriage lever arm, F) Vertical displacement carriage arm, G) Counterbalance, H) Load carrier arm,

3.5 Specimen Design and Preparation

The first preparatory stage was to cut the samples for both tensile and wear tests, by using a electrical discharge machining (EDM) since the composites were too hard to cut with ordinary cutting tools, see in Figure 3.4. The electrode required for EDM to cut the samples was in a cylindrical shape. Tensile samples for mechanical testing and the electrode made for wear pin samples are shown in Figures 3.5 and 3.6.

To produce the both composite samples and alloy matrix for tests using EDM, the following procedures were carried out :

(1). The electrode was designed from the brass due to small diameter electrode and finer surface finish on the workpiece, and produced in the workshop, and the composite workpiece and electrode was set. The machine was switched on position, but not dielectric tank during this process and dial indicator and the micrometer was also moved to the top of their slides.

(2). The electrode was mounted in its holder on the magnetic chuck and secured the electrode holder mechanically by engaging the two retaining latches on the sides of the magnetic chuck, and the workpiece was placed in the required co-ordinate position relative to the electrode by moving the worktable with X and Y handwheels. To assist in aligning the electrode and workpiece, the machine touch indicator lamp would lighted when the two come into contact.

(3). The depth of the machining was set to about 9.5 mm using a feed control and touch indicator. The feed control was rotated anti-clockwise to advance the electrode towards the workpiece and when it touched, it would remain in servo contact. The dial indicator was slid to bring it into contact with its anvil, then the feed control was adjusted to a position where the electrode remains in contact with the

workpiece and no movement is shown on the dial indicator. The micrometer was set to zero point to read the required depth of machining.

(4). The head height was set at the required height, and there was a sufficient clearance to change the workpiece. Using an Allen key, the clamp on the lower limit switch cam and the cam was slackened and set to a position. When machining is completed, the head would rise only this position.

(5). To start the cutting process, the tank door was closed, the adjustable weir was rotated to a position where the weir height is 30 mm above the surface to be machined on the workpiece. The dielectric pump was started and the setting adjusted to the selected value.

(6). The feed control was rotated to its fully anti-clockwise position then switched on the generator. The 10 ampere output was selected from the generator. A number of transistors from starting of 0.2 A, in accordance with generator setting were selected to set the pulse on control in order to obtain the appropriate spark gap for these samples of about 0.15 mm. The feed control was rotated clockwise to advance the electrode towards the workpiece and when it was close enough machining will be commenced. At this point, the flushing dielectric was turned on.

(7). The dial indicator was slide to a position where it follows the movements of the electrode then the feed control and the pulse OFF control was adjusted. The stability of machining could be affected by the feed control, the quality of the spark gap flushing and the pulse OFF setting. Therefore, these three controls were adjusted and maintained together to produce stable condition during the cutting of whole test pieces, evidenced by a continuous green light. These cutting process continued until the certain length was reached and machining stopped. The composite block was released from the work table and cut very gently using a saw with fine teeth perpendicular to the cross section of the samples to make cylinders and it is about 6 mm in length.

The wear pin specimens were made from the MMC materials and the unreinforced matrices by following the above procedures, and were approximately 6 mm in length and 6.33 mm in diameter and were bonded to a cylindrical steel extension pin 50 mm long with a brass sleeve using an epoxy adhesive. For all wear tests the pins were kept dimensionally constant. The pin was then held in a brass holder by the use of a cup nut in the wear machine.

As for the case of preparation of PMCs, the PMCs used in these tests were initially cut from the block into the approximate size needed. In all cases the test specimens were turned in a lathe to he size and shape required, like MMCs, and it was cut gently with saw. They then were bonded to the cylindrical steel and held in the brass holder.

The second stage was to grind all of the relevant wear surfaces to the best possible surface finish. For wear pins, further polishing was undertaken in situ on the respective wear testers using 800 grade silicon carbide paper bonded to a wear disc reversed specially for this purpose. Polishing in this manner gave a pin surface finish of better than 0.5 μm CLA, with very little edge rounding such that the whole pin surface areas rapidly able to conform at the onset of a wear test.

The pins were, after polishing, cleaned with acetone in an ultrasonic cleaning unit to remove any unwanted debris remaining after the polishing process, dried and weighed by a microbalance, hence, the pin would be ready for experimental use.

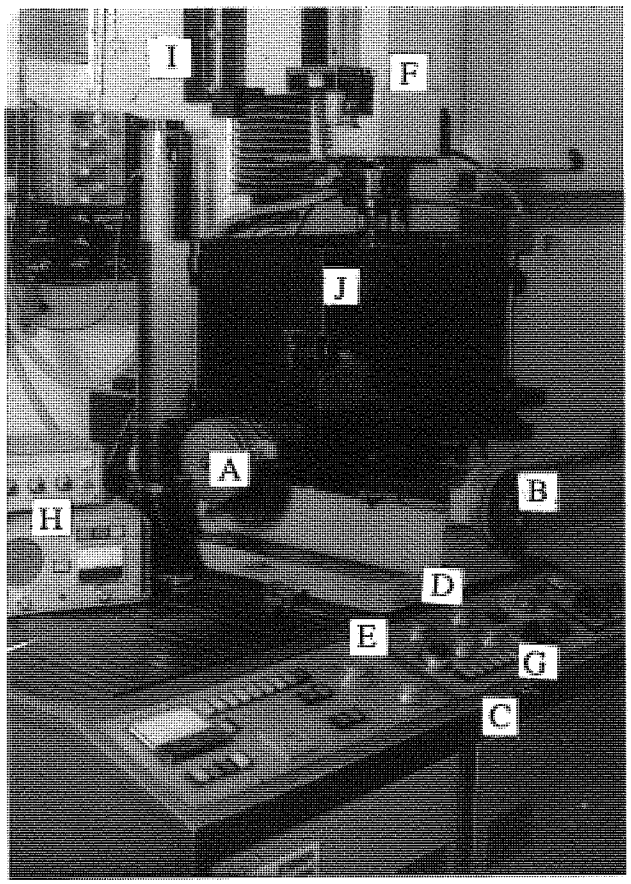

Figure 3.4. Complete view of electrical discharge machining (EDM) used for cutting of MMC materials. A) X axis handwheel, B)Y axis handwheel, C) Control panel, D) Electrode feed control, E) Flushing timer speed control, F) Flushing timer height control, G) Pulse on-off time control, H) Indicator lamp, I) Depth control panel, J) Work tank dielectric control unit.

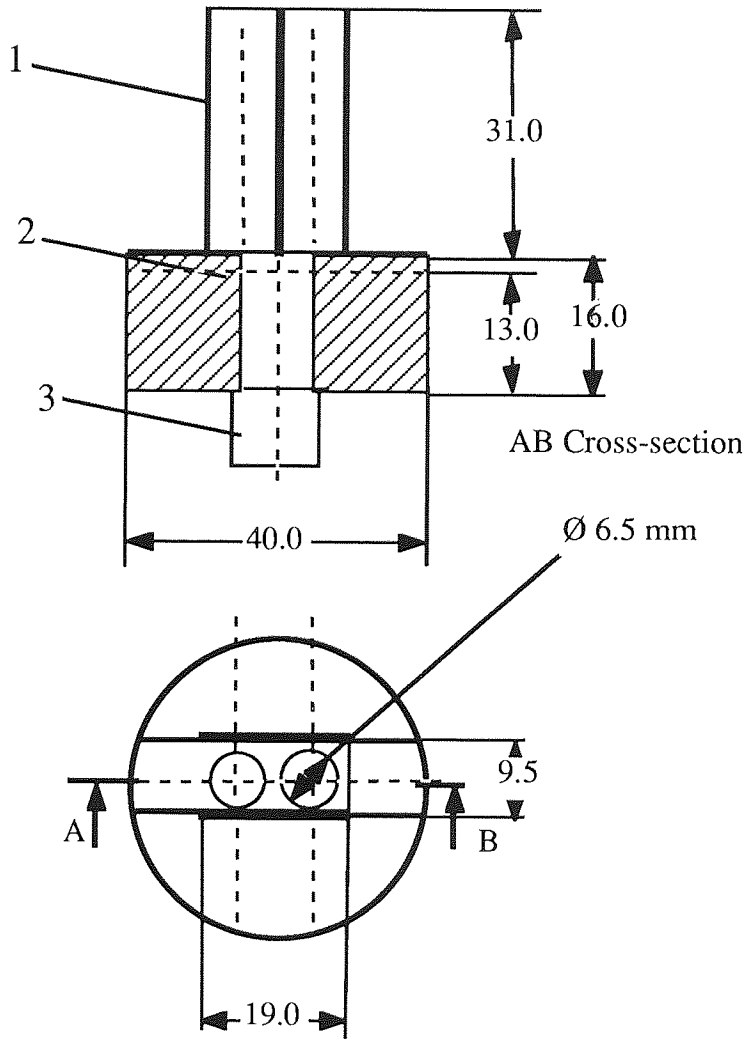

Scale : 1/1

All dimensions in mm.

Figure 3.5. Electrodes made of brass for EDM. (1 : Brass die, 2 : Holder, 3 : Morse conic of handle).

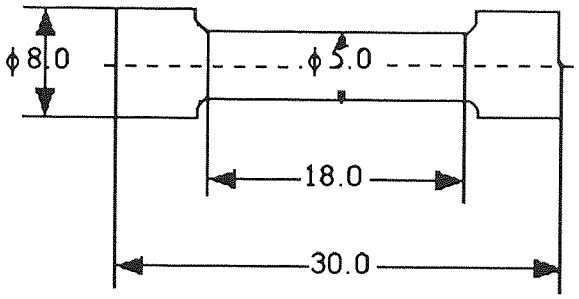

Scale : 2/1

All dimensions in mm.

Figure 3.6. Hounsfield tensile specimen dimensions.

3.6 Counter Disc Materials and Surface Topography

The disc specimens were made of hardened bearing steel En 31. The disc surfaces were flatly ground to give a surface finish of approximately 0.15 μm center-line-average (C.L.A). The measurements being made on a Talysurf 4 system. For use with the wear machine, the thickness of the discs were 12 mm and the dimensions of the discs were 120 mm in diameter. Since the diameter of disc was 120 mm, three tests can be done on the disc surface periphery rubbed by 6.33 mm diameter pin. In the first test, the pin was rubbed close to one edge of the disc. After completing the test, the disc is removed and turned over so presenting a new track to the new pin, i.e., the second test now uses the other edges of disc surface periphery. The En 31 steel disc had a hardness value of 59-63

Rc. The disc table was cleared off and the counter disc located using the pin in the disc table. The disc was locked into place by using a central screw.

Considering the surface topography, it is important to mention that apart from knowing whether dry or lubricated conditions prevail in certain application, the most important parameter which determines the wear behaviour is surface texture. The whole texture of the surface has a geometry property characterized by a serious of irregularities having different amplitudes and occurences. In general, the assessment of surface texture is conducted in terms of distribution, size and shape of asperities through optical methods like a reflection microscopy or mechanical methods like a profilometry.

The most common profilometry method used to define the texture of the surfaces is the Stylus method, in which a fine diamond stylus tranverses the surface and its vertical movements are recorded and amplified. In production engineering, one of two parameters is usually used to define the texture of surfaces. These parameters are the C.L.A. (center-line-average in a profile registry) roughness value, and the R.M.S. (root-mean-square of asperity in a registered profile) value. The C.L.A value is defined as the arithmetic average value of the vertical deviation of the profile from the center line, and the R.M.S. value as the square root of the arithmetic mean of the square of this deviation. The CLA value is more widely used in frictional applications to indicate surface conditions. The CLA value of disc surface and wear scars of the composite sample is shown in Figure 3.7. In all case, the surface roughness of the contacting triboelements, and hardness of the disc will be maintained constant.

3.7 Wear Test Procedures

The pin and disc were cleaned ultrasonically in order to prevent any transfer of contaminates before each test and then weighed. In the first step, the pin was fixed on the upper carriage lever arm with the disc locked in position on the turntable. The upper carriage lever arm was balanced by placing a block so that the beam (gimbal) was horizontal. The collet was tightened up and locking screw tightened so as the pin came into contact with the disc surface, the required load was applied by the load carrier

without putting lateral pressure on the pin. In the second step, the pin/disc assembly and setting procedures were carried out in order to start the test and the experiment was started by turning on the motor, letting its speed stabilize, and then lowering the arm to allow the pin to come into contact with the disc. The time of starting and gain settings of the recorder were noted down. Upon completion of the test, a note was made of the ending time.

Thirdly, the disc and pin were removed, wiped clean and weighed. The pin and wear debris were finally stored in a desiccator for subsequent microscopic analysis. In order to achieve the best operating conditions without lubrication, a first set of experiments for wear tests was carried out for loads of 12 N to 60 N, in steps of 12 N at a constant speed of 1.0 m/s using metals and composites. For these tests, one pin was used on one wear track with the load being periodically increased. Having established the operating conditions, each test was run with a new pin on a new track on the disc. The wear test lasted for 2 hr in both materials. The results obtained with numbers of samples taken from different locations of metal matrix composites (MMCs) and aluminium alloy matrix are given in Table 6.

A second set of experiments on the pin-on-disc assembly were as follows : The sliding velocities were 0.6 and 1.6 m/s respectively for the composite materials with the applied loads of 12 N up to 42 N. The results for composites and matrix alloy are given in Tables 5 and 7. Finally, wear tests were conducted on B(SiC)-reinforced plastic matrix composite materials (PMCs) under the similar conditions as mentioned above. The results for the plastic matrix composites are also shown in Tables 9, 10 and 11. The wear of both MMC and PMC pin samples was measured from weight loss to the nearest 0.1 mg and then converted into volume loss using density data. The wear rate and coefficient of friction were also calculated by using a LVDT, as explained in the following section.

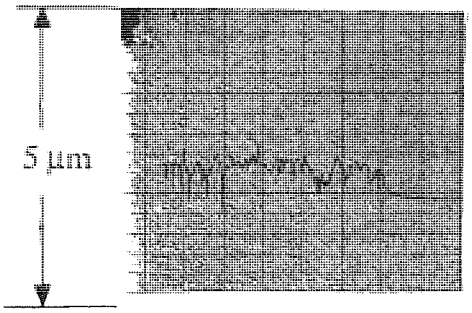

a). Cross-sectional profiles of ground disc surface before test : 0. 12 CLA.

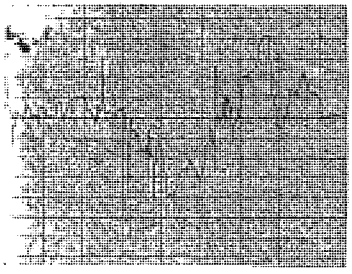

b). 32% vol composite in the N orientation : 0. 32 CLA. (load 22 N and 1.6 m/s)

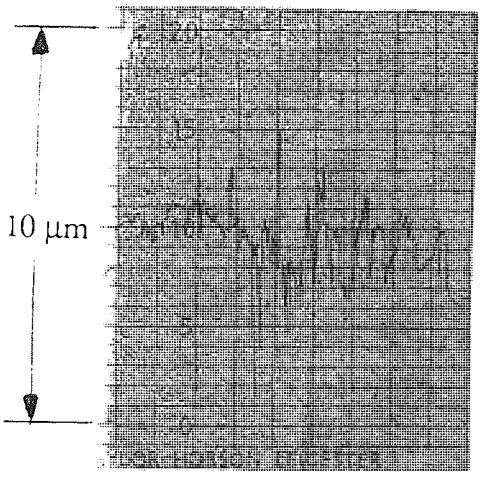

c). 32% vol composite in the P orientation : 0. 48 CLA. (Load 22 N and 1.6 m/s).

Figure 3.7. Cross sectional profiles of as ground disc surface before test and cross sectional profiles of wear scars of B(SiC)/MMC pin after dry sliding for 11.32 km against smooth steel under different loads a). Disc surface, b). Normal orientated, c). Parallel orientated samples.

3.8 Wear and Friction Measurement

Wear rate is defined in this study as the volume removed per unit sliding distance, expressed in units of mm^3/km in order to calculate the volume removed from a circular pin. We need know the pin diameter and the linear reduction of the pin as it wears or the weight loss of the pin samples. The worn volume (w) in mm^3 for a 6.3 mm diameter pin such as the one used in the present work is then given by

$$W = \frac{\Delta m}{\rho v t} \qquad (3.2)$$

Where Δ m is the mass loss during the wear test, ρ the density of the pin, v the wear velocity in km/s and t the duration of the experiment in seconds. Another method of wear measurement, used to check the validity of data obtained from the mass of the pin measurements made before and after wear testing, was to measure the linear reduction in length of the pin as it wears. In practice, the linear reduction was measured by the use of Linear Variable Differential Transducers (LVDT) in contact with a flat plate on the load arm which wears the pin. The displacement was calibrated by inserting feeler gauges of different thickness between the LVDT contact pin and the plate, and noting the change in contact of the chart recorder.

Figure 3.8 shows a plot of the wear pin versus chart displacement. As the pin wore, the load arm moved downwards hence giving a continuous measurement of pin displacement on a chart recorder. The continuous measurement of specimen length provided information which was subsequently used to produce wear versus load and wear versus time data. Wear rates were calculated from graph traces and compared with those calculated from mass loss determination of equation (3.2). A quite good fit was obtained between those of two measurements.

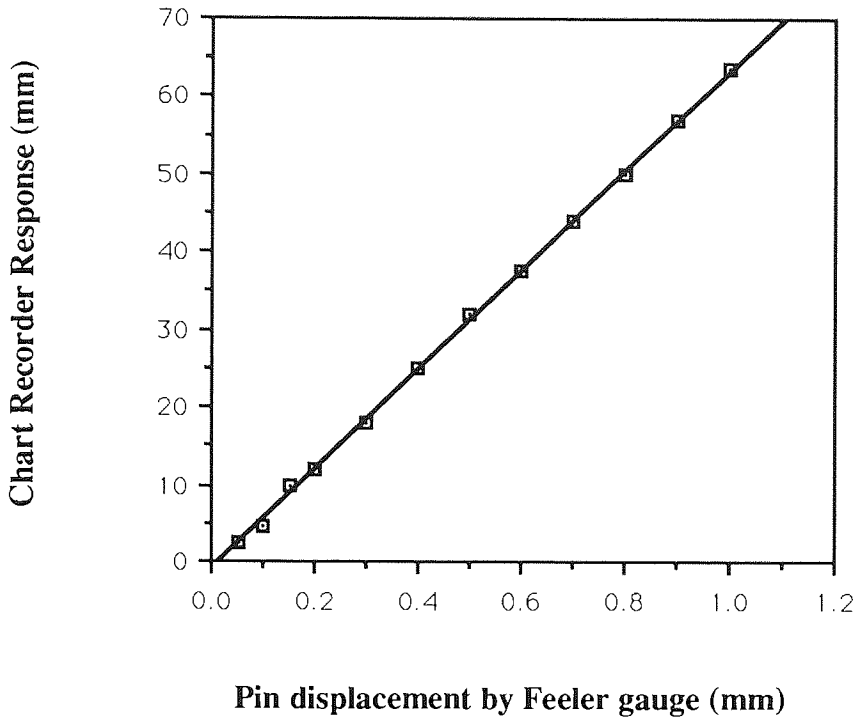

Set range : 200 mV on chart recorder

Figure 3.8. Calibration of pin displacement measurement.

A strain gauge was also used to measure frictional force at the pin. This was performed by rigidly fixing the transducers in a position where it would resist the motion of the pin-holding arm as sliding progressed. The frictional force, therefore, was calibrated on a chart recorder by applying different loads against the load cell by means of a weight. This arrangement gave a sensitivity of which 1 kgf equals to 13.2 mm on the chart which was sufficient to measure the coefficient of friction in unlubricated condition. Figure 3.9 shows a plot of friction force against pin displacement. The frictional force between the specimen contact surface and the counterface in the pin-on-disc device were monitored continuously during test and coefficient of friction was calculated in applying the Amontons-Coulomb law of dry friction. Drift characteristics were also plotted for the friction and wear transducers as shown in Figure 3.10 on the chart recorder after two hours running, starting from cold.

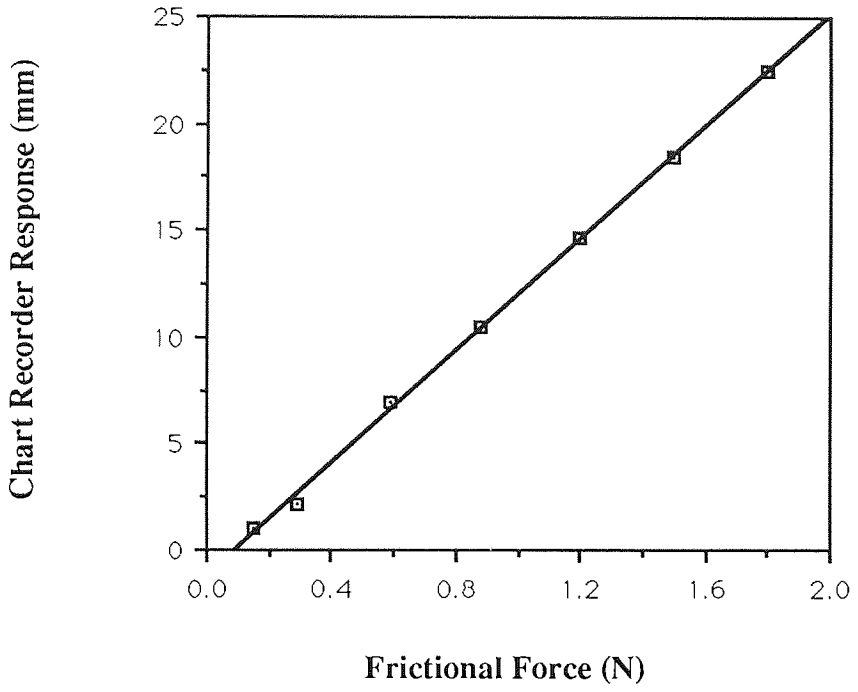

Set range : 5 mV friction setting on chart recorder

Figure 3.9. Calibration of frictional force measurement.

3.9 Microscopy

Microscopy provides an essential way of analysing the rheology, topography, metallurgy and to an extent the chemistry of worn surfaces and debris. Three main microscopy techniques were used, these being optical microscopy, scanning electron microscopy, using secondary electron emission (SE) and scanning electron microscopy (SE) using a back-scattered electron emission (BSE). Optical microscopy was the most readily available and simplest other than mounting in bakelite, polishing and etching in 2 % Nital to use of the three techniques, requiring no specific sample preparation in the image. The disadvantage of the technique was, however, a relatively low maximum magnification, and in order to obtain high magnification and high resolution scanning electron microscopy was used in SE mode.

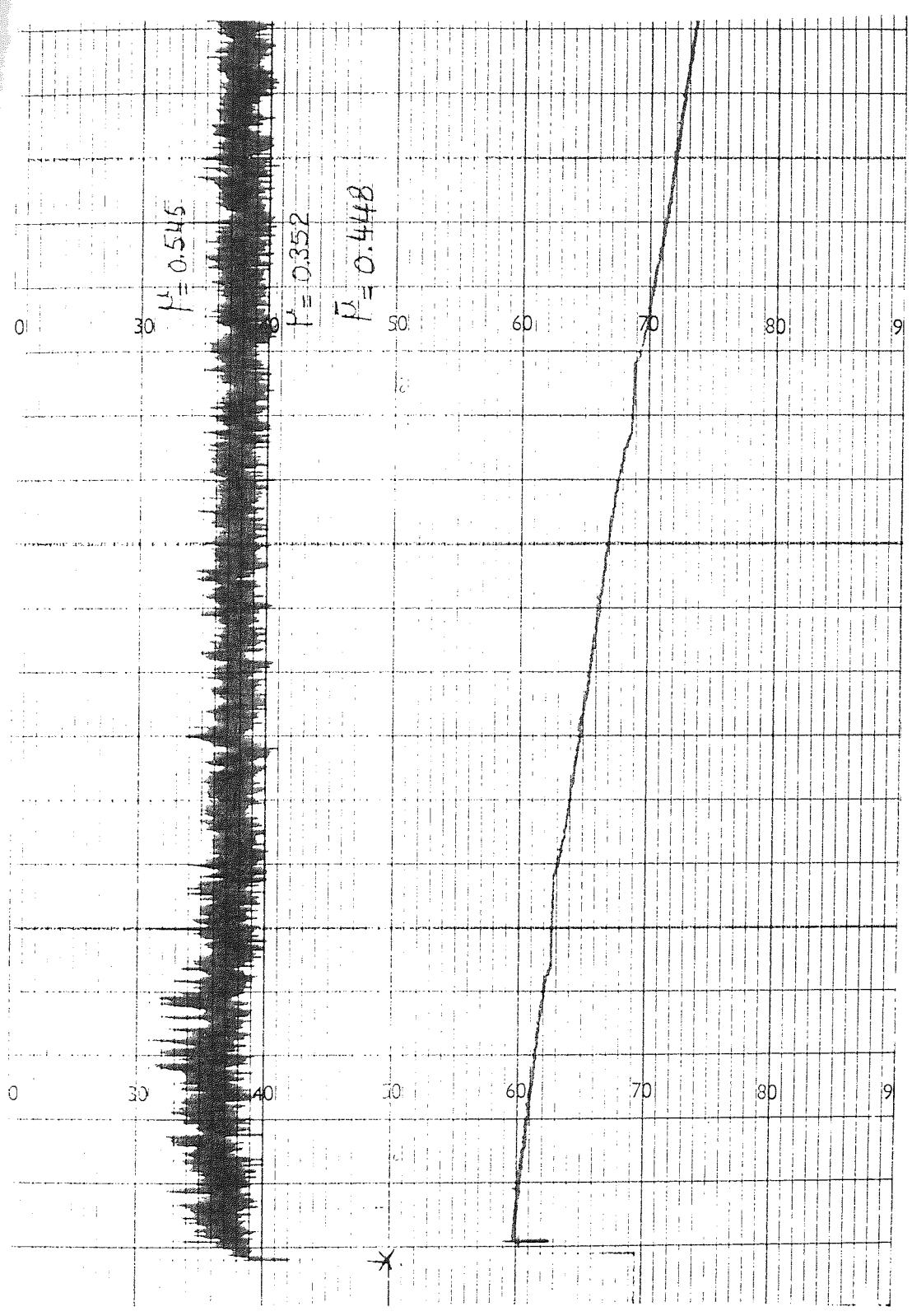

Figure 3.10. Characteristic friction and wear plots on chart recorder during dry sliding test.

This technique also had the advantage that the depth of field was extremely large, giving excellent topographical information. One disadvantage of the technique is that chemical contrast is largely due to topographical variations. Thus, an oxide layer looks much the same as metal and it is difficult to comment on the chemical nature of features seen on the electron micrograph.

One way in which chemical contrast can be obtained is by producing an image from the backscattered electrons produced by elastic or near elastic collisions between primary beam electrons and the atomic nuclei on the sample. These electrons have the same energy as the beam electron which was that of the bulk of the electrons emitted from the sample. Since the angle of backscattering of a beam electron depends on the atomic number of the nucleus which diverts it from its path, the number of back-scattered electrons depends on the average atomic number of the sample. Image brightness can thus be linked to the chemical nature of the sample. The addition of signals from diametrically opposed pairs of BSE detectors enhances the chemical contrast and reduces the topographical contrast in the resulting image, and this was used to enhance the BSE images obtained from the wear pins.

In this investigation, a Cambridge Stereoscan "90" SEM was used extensively to examine the wear surfaces produced from the pin-on-disc machine experiments and the fracture surfaces of the tensile samples. SE images were used to study the worn surfaces of the pin and the fracture surfaces of the tensile tested samples. Some of the worn pins were sectioned normal to the wear surface, either parallel to the wear tracks or normal to them. These samples were mounted in bakelite, ground and polished to 1 μm then examined in the SEM using BSE contrast to study the mechanism of wear and sub-surface metallurgical changes produced by wear.

The surfaces to be studied, were first cut to a suitable length for scanning electron microscope and stuck onto aluminium stubs using Bostick. These were then placed in a technical 'hummer' which evacuated the air inside a chamber and then deposited the material within a thin layer of usually silver or gold under high voltage conditions to

prevent charging and hence increase resolution. Colloidal silver was also painted down the side of the specimens to provide a conducting path from the surface to the metal stub.

3.10 X-ray Photoelectron Spectroscopy

X-ray Photoelectron Spectroscopy is a most useful technique in identifying of elements present in worn surfaces. Samples of the pin surfaces were analyzed after wear by using the XPS, which equipment is in the Thorton Research Centre of the Department of Electronic Engineering and Applied Physics. The purpose of the analyses was to observe changes in selected samples obtained under similar operating conditions and compare them with each other. In this technique, the samples were irradiated with monochromatic X-rays which produce photoelectron emission from atoms very near to the surface. Measurement of the photoelectron energies allows the identification of elements present in the near- surface region and it was able to give information on the chemical compounds present. Measurement of the numbers of electrons emitted at a given energy allows atomic concentrations to be determined.

CHAPTER FOUR

4.0 EXPERIMENTAL RESULTS

4.1 MECHANICAL PROPERTIES AND WEAR OF B(SiC) REINFORCED METAL MATRIX COMPOSITES

4.1.1 Introduction

The experimental results presented here are divided into sections similar to those used for the description of the experimental work. The first section resulting from 4.1 to 4.18 gives detail of microstructures, mechanical test data and fracture surfaces of the composites.The remaining sections from 4.19 to 4.38 are related to the friction and wear data of MMC materials. More sensitive techniques such as Secondary Electron Microscopy (SE), Backscattered Electron Microscope (BSE) and X-ray Photoelectron Spectroscopy (XPS) were used to quantify the hypothesis of the wear mechanism of the MMC materials sliding on hardened steel. Figures 4.39 to 4.53 are concerned with the observation of sections through the worn surfaces parallel to the sliding direction, while Figures 4.54 to 4.65 are related to the surface observation of N orientated MMCs. Figures 4.66 to 4.88 indicate the observation of P and AP orientated MMCs, but observations of sections through the worn surface parallel to the sliding direction of the N, P and AP orientated sample are shown in Figures 4.89 to 4.95. Finally, XPS spectral analyses of the MMC materials are presented in Figures 4.96 to 4.101.

4.1.2 Microstructure of Matrix and Composites

The microstructures of the materials studied in the investigation are shown in Figures 4.1 to 4.4. Figure 4.1 shows an SEM image of the aluminium alloy matrix disc in atomic number contrast. The microstructure consisted of small dendrites of aluminium with interdendritic films about 15 μm in size and rounded particles of a $CuAl_2$ phase which were about 10 μm in diameter. Figure 4.2 shows a transverse cross-section of the

microstructure of a B(SiC)/2014 composite containing the 16% volume fraction of continuous fibre at low magnification. The boron fibres (dark) have a tungsten wire core (white) and they also have a surface coating of SiC (grey) in this atomic number contrast SEM image. But the structure of the Al alloy matrix in the composite is slightly coarser than in Figure 4.1, with dendrite arm spacing of about 30 μm. A little porosity is also evident as well as some intermetallics. Figure 4.3 shows the microstructure of a bidirectional orientated composite containing 21% volume fraction of fibre. As is shown in the figure, the microstructure was composed of fibres which was orientated in both 0^{o} and 90^{0}.

The distribution of fibres within the structure varied, some areas having sparse reinforcement, particularly composites with low fibre content. In other words, the distribution of B(SiC) fibre in high volume fraction composites was more uniform. Most fibres in the composite had a diameter close to 140 μm as shown in Figure 4.4.

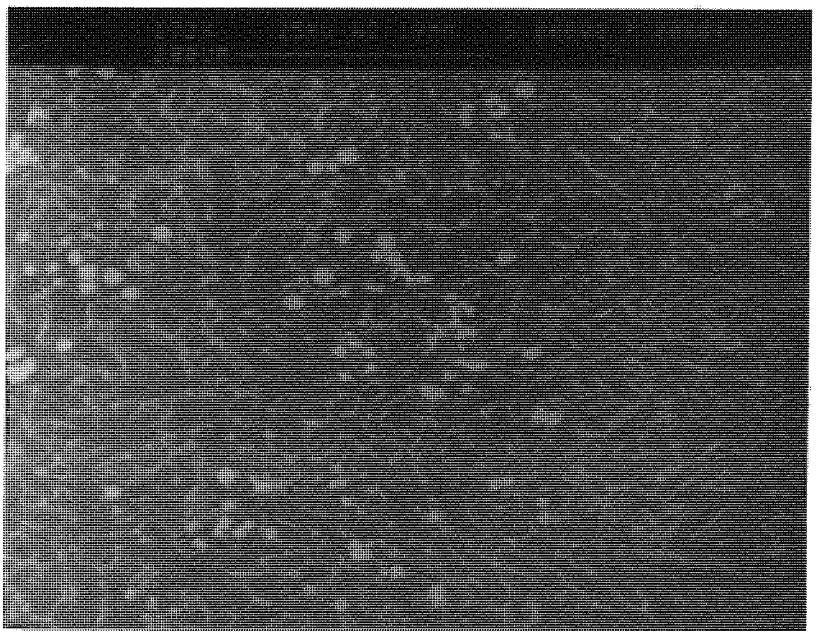

Figure 4.1. Typical SEM (BSE) micrograph of cast aluminium alloy matrix (2014).

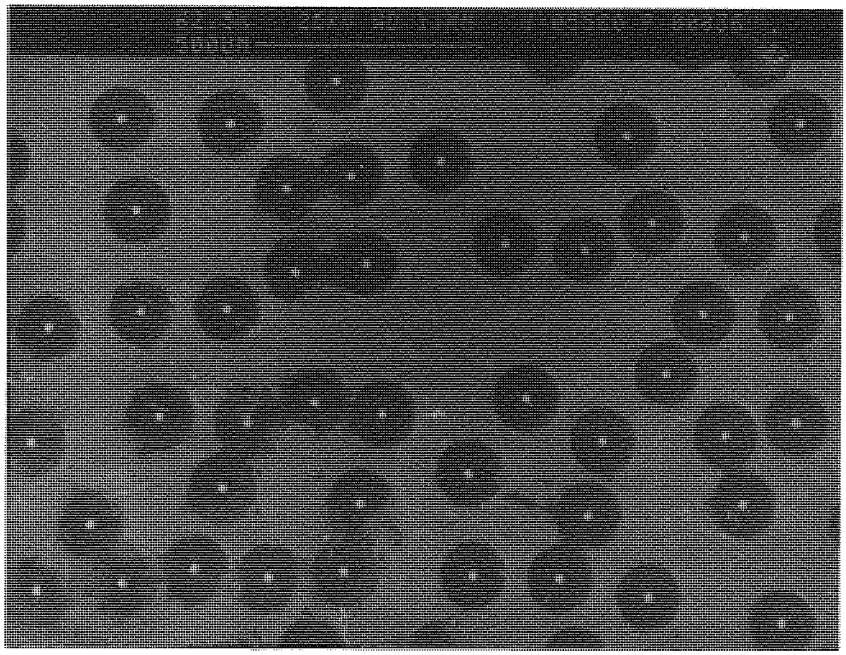

Figure 4. 2. SEM (BSE) micrograph of the MMC containing 16% B(SiC) fibre.

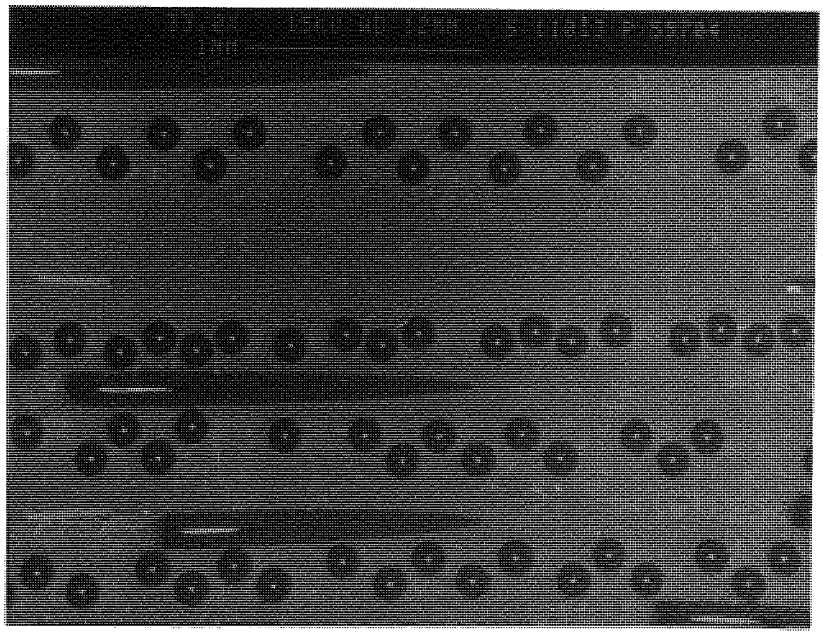

Figure 4. 3. SEM (BSE) micrograph of the MMC containing 21% B(SiC) fibre.

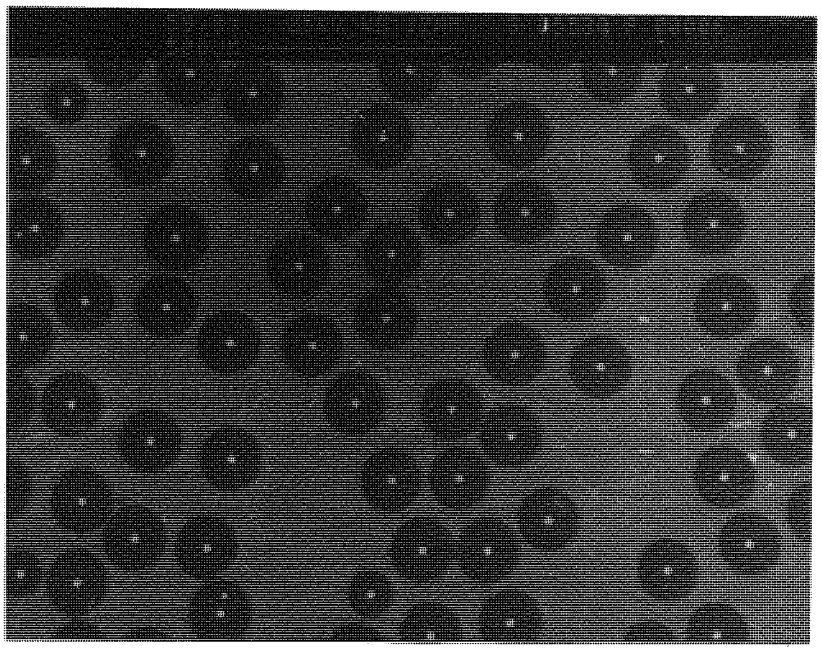

Figure 4.4. SEM (BSE) micrograph of the MMC containing 32% B(SiC) fibre.

4.1.3 Density Measurement and Hardness Tests

The density of the composites was obtained by the Archimedian method of weighing small pieces cut from the composite disc first in water and then in air. The hardness of test specimens of the composites and aluminium alloys were measured having been metallurgically polished up to 1 μm finish. Brinell hardness was measured using a 5 mm diameter ball at a load of 250 kgf for the aluminium alloy matrix and 750 kgf for Borsic reinforced composites. The average Brinell hardness of each specimen was determined from three indentations. As for the plastic matrix composite, the density of the composites was obtained in a similar way as that for the MMC materials. However the unreinforced plastic was weighed in acetone due to its density being less than that water. The results of the density measurements for both MMC and PMC materials, together with the results of Brinell hardness of the MMC materials are shown in Table 3. The variation of density of MMC and PMC materials and hardness of MMC materials with the volume fraction fibres is shown graphically in Figures 4.5, 4.6 and 4.7 respectively.

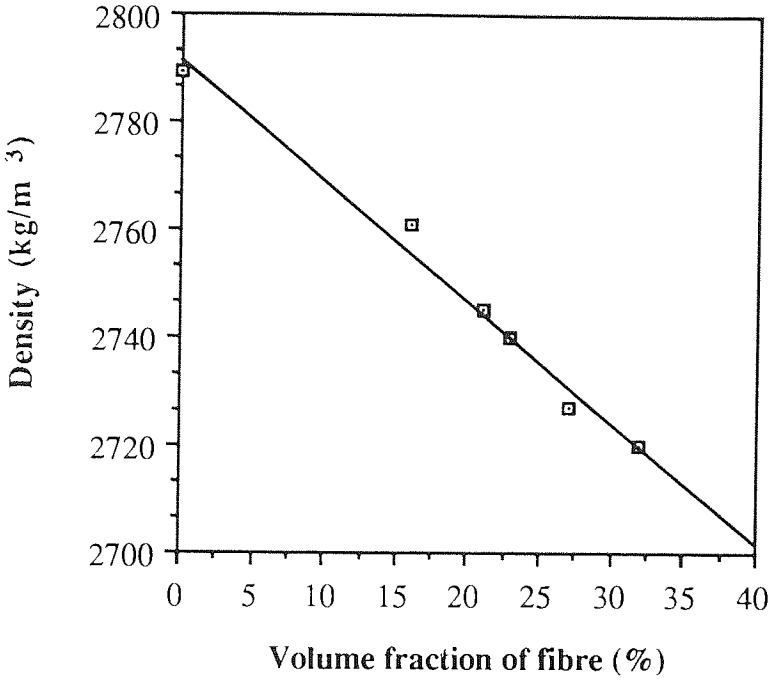

Figure 4.5. Variation of density of B(SiC)-reinforced MMC materials.

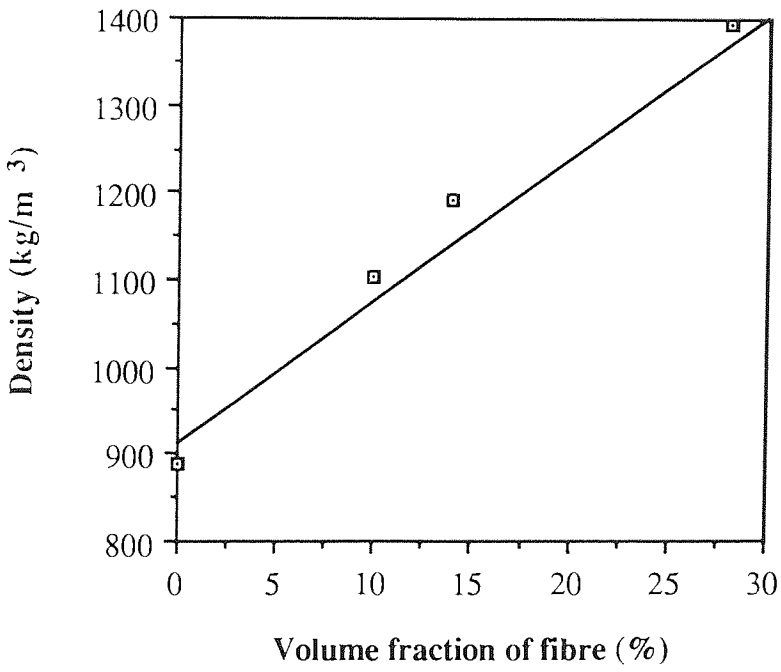

Figure 4.6. Variation of density of B(SiC)-reinforced PMC materials.

TABLE 3

HARDNESS AND DENSITY OF THE METAL MATRIX AND PLASTIC MATRIX COMPOSITES.

Types of Tested Materials	Volume fraction (%)	Hardness (BHN)	Density (kg/m^3)
Aluminium matrix	0	87	2789
B(SiC)/Al composite	16	220	2761
B(SiC)/Al composite	21	148	2745
B(SiC)/Al composite	23	212	2740
B(SiC)c/Al composite	27	343	2727
B(SiC)/Al composite	32	424	2720
HDPE plastic matrix	0	-	887
B(SiC)/Pl composite	10	-	1100
B(SiC)/Pl composite	14	-	1193
B(SiC)/Pl composite	28	-	1393

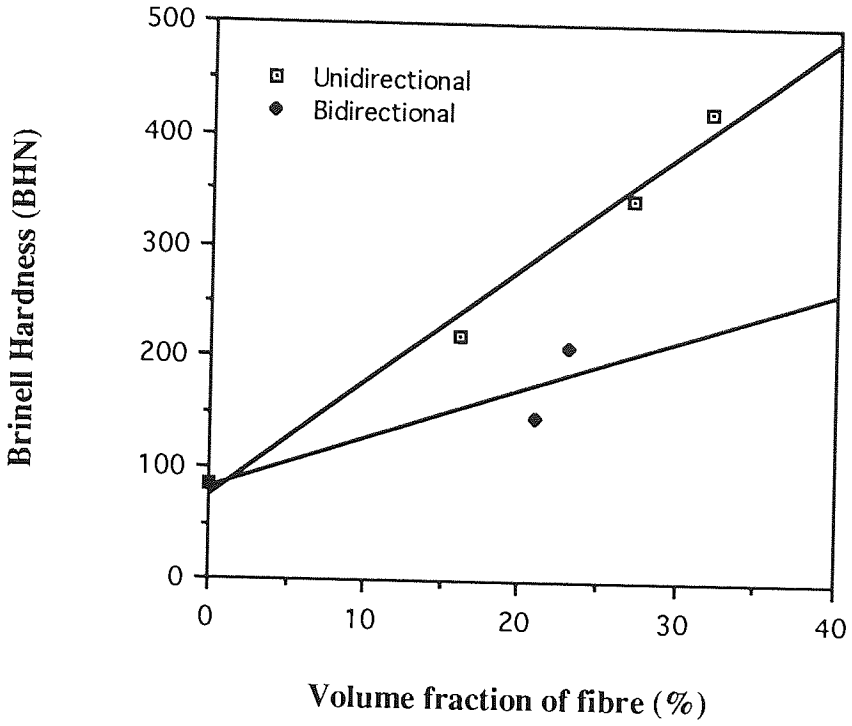

Figure 4.7. Variation of Brinell hardness of the B(SiC)-reinforced MMC materials.

4.1.4 Tensile Tests

4.1.4.1 Test Results

The tensile tests were carried out to determine the mechanical properties of the composite materials and its alloy. The results of composite and aluminium alloy tensile strength are shown graphically in Figure 4.8 as a function of fibre volume fraction and tabulated in Table 4. The data in the graph and table include the experimentally-determined mean of the tensile strength and the expected tensile strength, calculated from the Rule of the Mixtures (ROM).

The effect of temperature on tensile mechanical properties of the composite materials was measured at 150 ^{o}C and 300 ^{o}C. The results of the tensile tests for Al alloy matrix and its composites containing various fibre contents are also listed in Table 4 and shown in Figure 4.9.

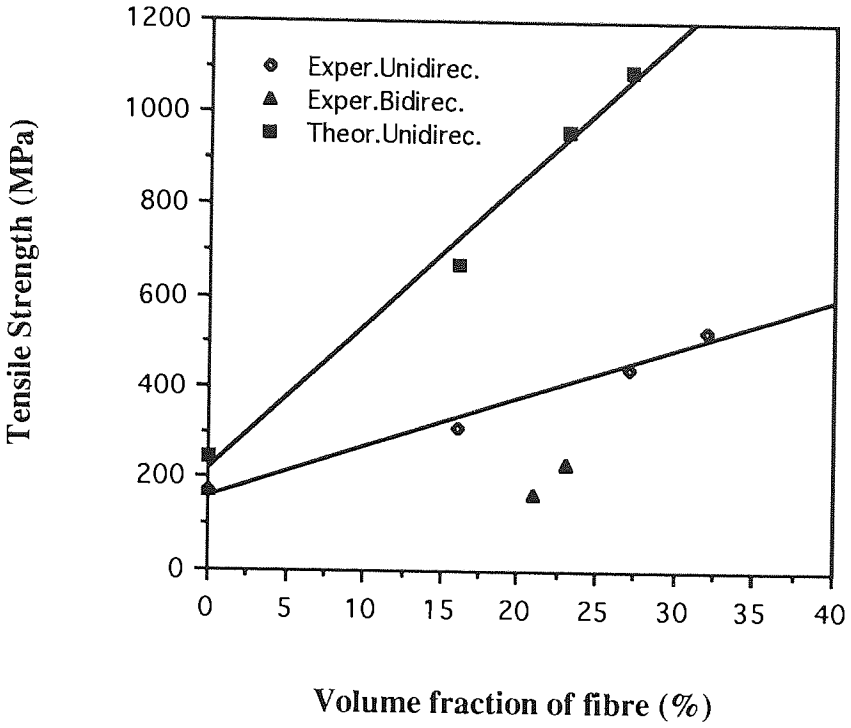

Figure 4.8. Ultimate tensile strength of the B(SiC)-reinforced MMC materials as a function of fibre volume fraction.

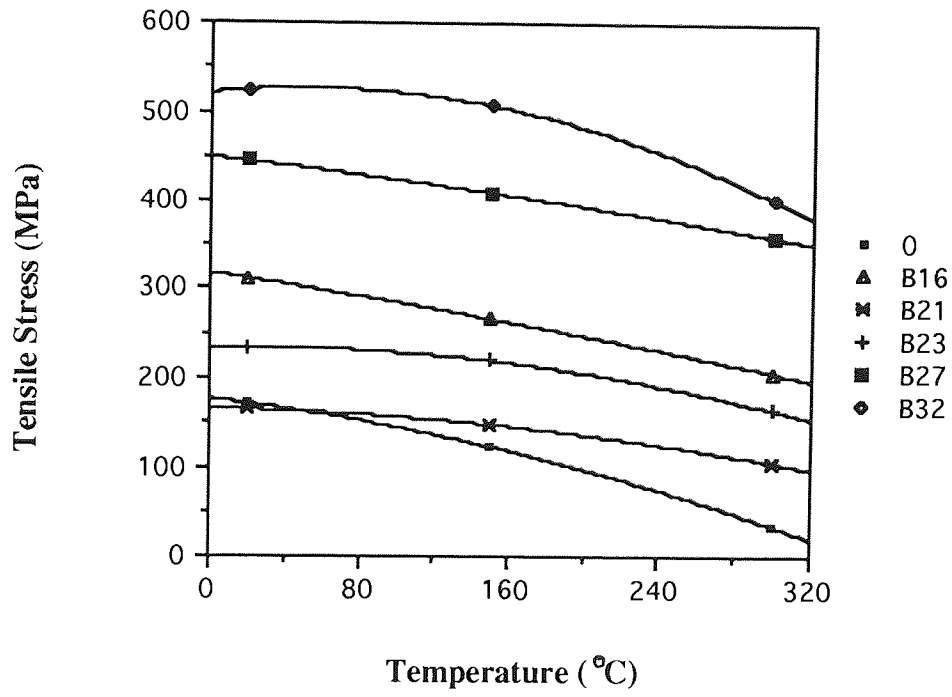

Figure 4.9. Influence of temperature on the tensile strength of the B(SiC)-reinforced MMC and its matrix alloys.

TABLE 4

THE TENSILE STRENGTHS (MPa) OF B(SiC)-REINFORCED METAL MATRIX COMPOSITE MATERIALS.

Metal Matrix Composite Materials and its matrix alloy	Tensile Strength (20 ^{o}C)	Tensile Strength (150 ^{o}C)	Tensile Strength (300 ^{o}C)
2014 Al matrix	172	123	34
Al-%16 B(SiC) composite	312	267	207
Al- % 21 B(SiC) composite (bidirectional)	165	148	105
Al-%23 B(SiC) composite (bidirectional)	235	220	165
Al-%27 B(SiC) composite	445	410	360
Al-%32 B(SiC) composite	524	507	402

4.1.4.2 *Fracture Surfaces of the Composites*

The mechanical property variations noted above were accompanied by the following changes in fracture morphology. Figures 4.10 and 4.14 show the SEM micrographs of the fractured surface of B(SiC)/Al matrix composite after tensile testing at room and high temperature respectively. Figure 4.10 shows the fracture surface of the composite containing 16% volume of unidirectional fibre at room temperature. This low magnification figure exhibits that the fracture path was not planar and was locally irregular due to the uneven distribution of fibres. The fibres were also seen to be virtually in contact at some points in the structure of the composite and widely spaced at other points.

In the case of the bidirectional 0/90 B(SiC)-reinforced composite materials, the fracture surface of the 21% B(SiC)/Al matrix composite is shown in Figure 4.11. Increased magnification of the same sample showed some fibres had separated from the matrix, as shown in Figure 4.12 in addition to evidence of pulling-out of fibres.

The fracture surface of the 27% B(SiC) fibre composite tested at room temperature is shown in Figure 4.13 and SE microscopy revealed no evidence of debonding from the brittle fracture surface but a small amount porosity was present in the matrix. The fibres were also fractured near the plane of the matrix. As for the case of high temperature test conditions for the matrix alloy and its composite, the fracture surface of Al alloy matrix confirmed that failure appeared to occur by formation of microvoids and their growth as shown in Figure 4.14 at higher magnification.

Figure 4.15 shows the fracture surface of the 16% B(SiC)/Al matrix composite at low magnification. It was observed that the surface of the unreinforced alloy was slightly dimpled, indicative of plastic deformation, while some fibres were split near the centre. In addition, there was an interfacial debonding and matrix fracture.

SE micrograph of the fracture surface of the unidirectional 32% B(SiC)/Al matrix composite is shown in Figure 4.16 at 150 ^{0}C temperature under low magnification. The

figure indicates that the fracture surface was smooth with no significant fibre pull-out and titanium tape used for the binding fibres, was also observed on the surface of the sample. At the high temperature of 150 ^{0}C, the fracture surface of a 32% B(SiC)/Al matrix composite sample is shown in Figure 4.17 at higher magnification. Catastrophic damage to the fibres and titanium wire was observed with no evidence of debonding. This was the indicative of the fact that failure occurred simultaneously in the matrix and fibre, but a small amount of fibre pull-out was also observed for this sample. Brittle B(SiC) fibre fracture surface is shown in Figure 4.18. This figure indicates typical high strength fibre fracture where the initiation site was in the tungsten core.

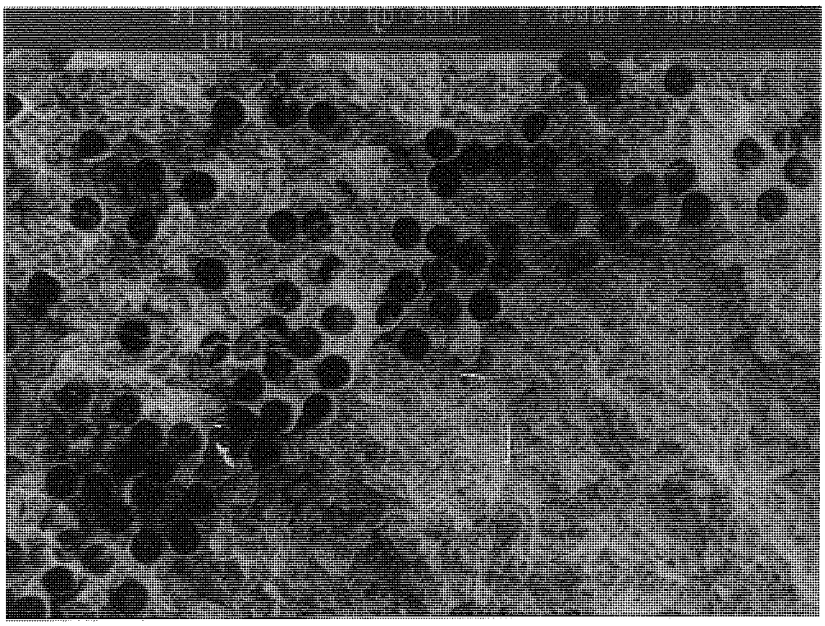

Figure 4.10. SEM micrograph of fracture surface of 16% B(SiC)/2014 aluminium composite tested at room temperature, showing undulation and dimpling.

Figure 4.11. SEM micrograph of the fracture surface of 21% B(SiC)/2014 composite tested at room temperature, showing considerably pulling-out of fibres.

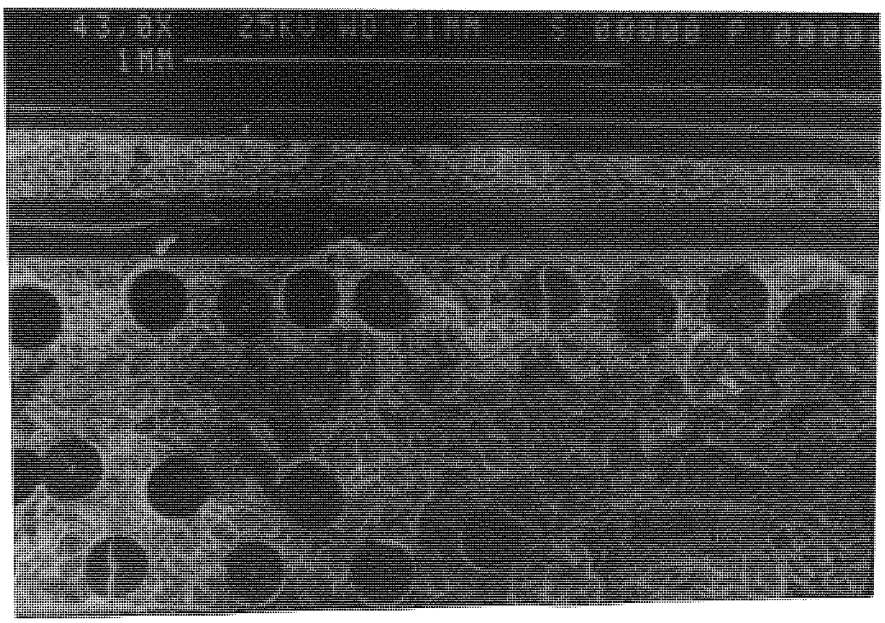

Figure 4.12. Increased magnification view of the same sample as Figure 4.11.

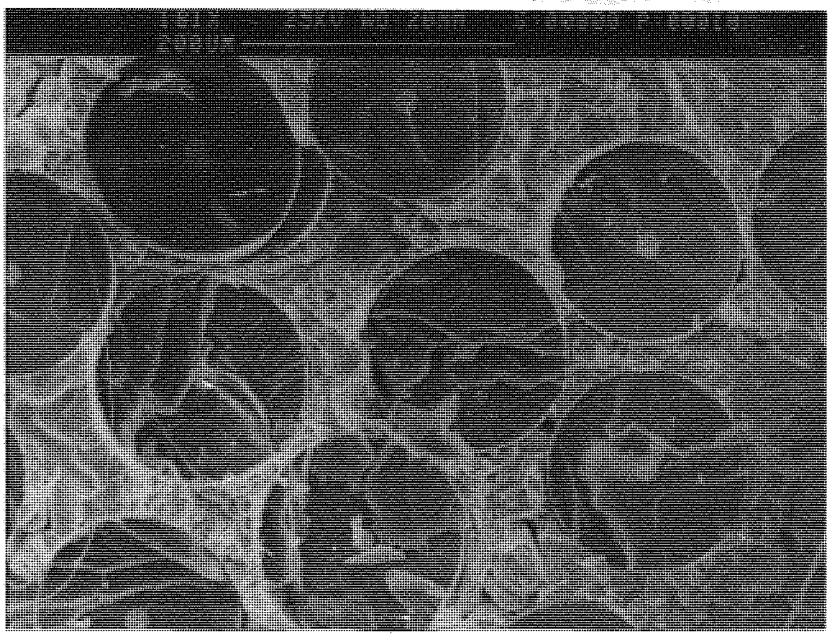

Figure 4.13. Higher magnification of 27% B(SiC)/2014 matrix composite tested at room temperature, showing brittle fibre fracture and small porosity in the matrix.

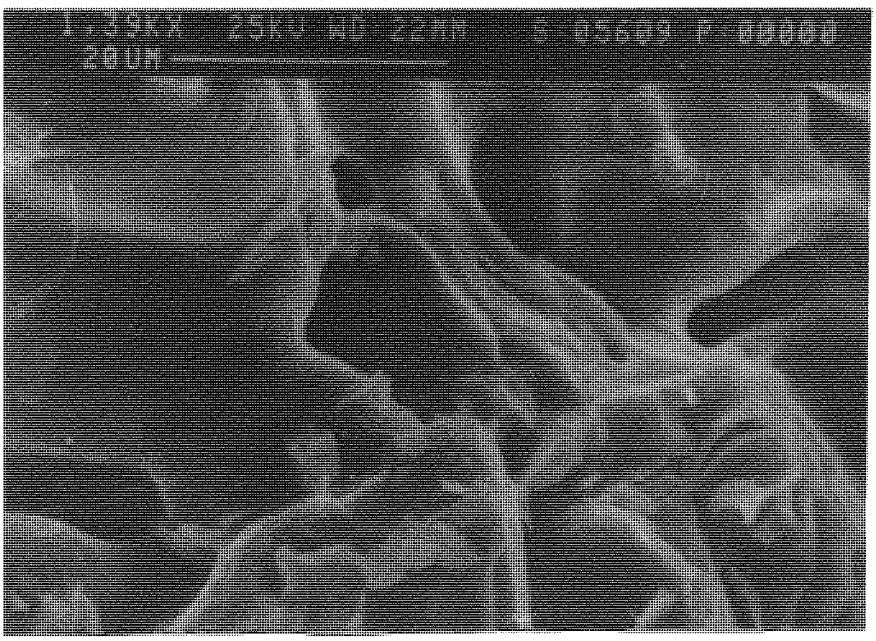

Figure 4.14. SEM image of the fracture surface of the aluminium matrix tested at 300 ^{o}C, showing microvoid formation and growth.

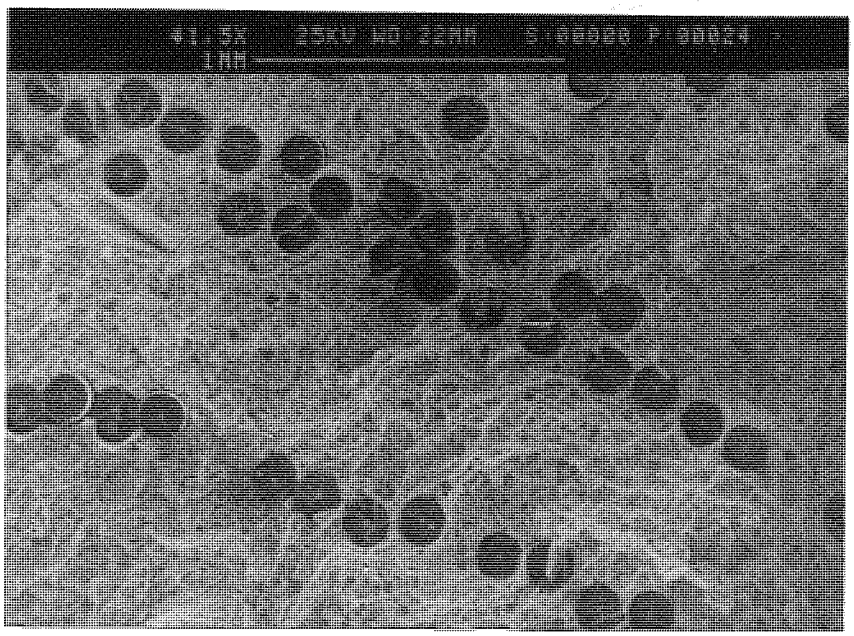

Figure 4.15. SEM image of the fracture surface of 16% B(SiC)/2014 matrix composite tested at 300 ^{o}C, showing dimpling and fibre cracks.

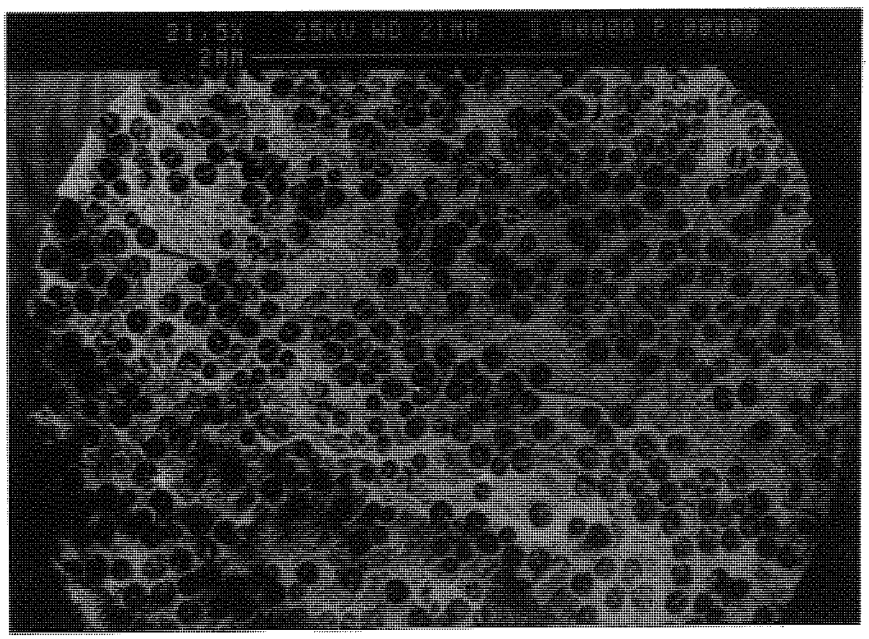

Figure 4.16. SEM micrograph of fracture surface of 32% B(SiC)/2014 matrix composite tested at high temperature showing smooth surface appearance.

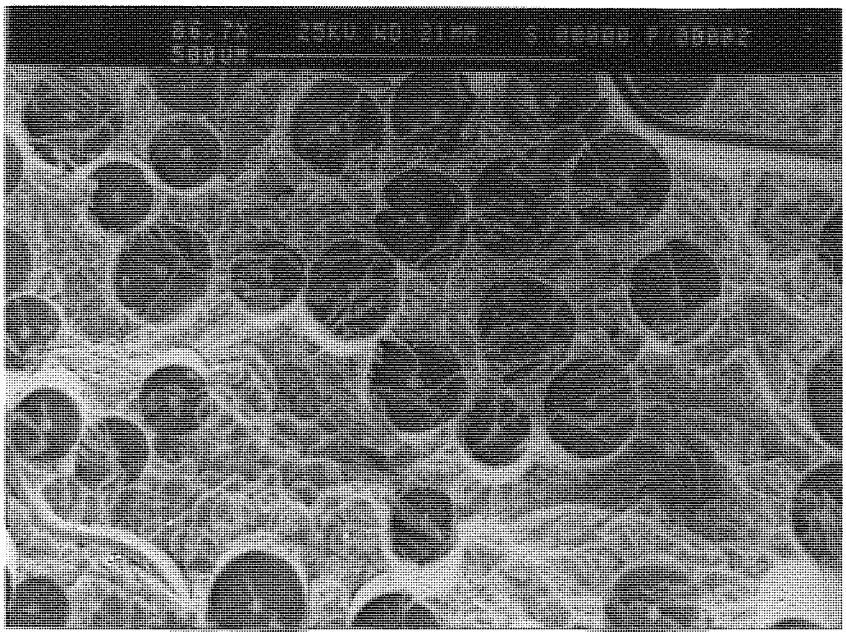

Figure 4.17. SEM image of the fracture surface of 32% B(SiC)/Al matrix composite tested at 150 ^{o}C, showing fractured fibres.

Figure 4.18. SEM image of the fracture surface of 32% B(SiC)/Al matrix composite tested at 150 ^{o}C, showing the crack initiation from the tungsten core and catastrophic failure.

4.1.5 Wear Properties of B(SiC)-Reinforced Metal Matrix Composite Materials

4.1.5.1. Effect of Load and Sliding Speed

The effects of varying the applied normal load and the sliding speed were investigated employing the pin-on-disc test apparatus. All tests were performed on metal matrix B(SiC)-reinforced aluminium composites employing three fibre orientations i.e. N, P and AP sliding direction against the smooth steel. The loads used for these experiments were between 12 N to 60 N inclusive, with surface sliding speeds of 0.6, 1.0 and 1.6 m/s respectively. The effect of load on the average volumetric wear rate of the B(SiC) reinforced MMCs is presented in Figures 4.19 to 4.25 for these three orientations. The figures are grouped in terms of speed with Figures 4.19 to 4.20 representing tests at 0.6 m/s, Figures 4.21 to 4.23 representing tests at 1.0 m/s, and Figures 4.24 to 4.25 representing tests at 1.6 m/s. The results of the tests carried out at different loads are listed in Tables 5, 6 and 7 respectively for sliding speeds of 0.6, 1.0 and 1.6 m/s.

Figure 4.19 shows the volumetric wear rate as a function of load for B(SiC reinforced MMC and its alloy matrix. The tests were carried out in the N orientation for a speed of 0.6 m/s. At this specified sliding speed under different loads, the volumetric wear rate increased as the normal load increased. This figure further revealed that the volumetric wear rate increased non-linearly with load and showed concave behaviour. This was very sharp for the matrix, while a low tendency was observed in the MMCs. Figure 4.20 also shows the volumetric wear rate as a function of load for the MMCs under the same speed but for the P orientated composite sample. It was observed that the volumetric wear rate increased as the normal load increased. Again the increase in wear rate was non-linear with load.

For the tests conducted at 1.0 m/s sliding speed, Figures 4.21 to 4.23 show the average volumetric wear rate as a function of the load for B(SiC)-reinforced aluminium matrix composites, tested in the N, P and AP orientations respectively. The first figure indicated that the volumetric wear rate increased with increasing load. Among the

composite, the 16 vol% fibre composite showed a slightly higher wear rate than the others. However there was a considerable difference between the lowest volume fraction of fibre composite and the unreinforced matrix.

Figure 4. 22 shows the average volumetric wear rate as a function of load for the B(SiC)-reinforced MMC pin, tested in the P orientation. From this figure, it is appeared that volumetric wear rate approximately increased linearly as the load increased. Also Figure 4.23 shows the average volumetric wear rate as a function of load for B(SiC) reinforced MMC materials. Test was conducted in the AP orientation under the same sliding conditions. Again similar trend was observed in this orientation; namely, average volumetric wear rate increased linearly with increasing load, as evidenced in Figure 4.23.

Figure 4.24 shows the volumetric wear rate as a function of load for B(SiC) reinforced MMC slid in the N orientation at 1.6 m/s. This figure indicated convex curve for the matrix alloy with load. In other words, there was an increasing trend in wear rate for the alloy matrix below 42 N, a decreasing rate thereafter. For the composites linear increases in wear was observed with load, except for the 16% B(SiC)-reinforced composite. For the P orientation, the volumetric wear rate as a function of load for the MMCs is shown in Figure 4.25. This figure also revealed that the volumetric wear rate increased linearly with load.

The effect of sliding speed on the volumetric wear rates of the matrix and its composite is shown in Figures 4.26 and 4.27 for the N and P orientation respectively. For this continuous dry sliding test, the distance travelled was maintained at 4.32, 7.20 and 11.52 km under the conditions of the different sliding speeds of 0.6 m/s, 1.0 m/s and 1.6 m/s. It could be seen that wear rate of the matrix alloy increased considerably up to 1.0 m/s and then wear rate decreased as the sliding velocity increased. For the N orientated composite, however, the volumetric wear rate decreased slightly with sliding speed in a range of 1.0 and 1.6 m/s as shown in Figure 4.26. In the case of P orientation, as shown

in Figure 4.27, the wear rate increased slightly up to 1.0 m/s and then decreased with sliding speed.

4.1.5.2 Effect of Fibre Content

Figure 4.28 shows the volumetric wear rate as a function of fibre content in unidirectional B(SiC)-reinforced MMCs for the N orientation at various loads at 1.0 m/s. The figure revealed how fibres incorporated in a metal matrix improved the resistance of the materials to the dry sliding wear. A little dependence in wear rate was observed with increasing fibre content.

Figure 4.29 shows the volumetric wear rate as a function of fibre content for B(SiC) reinforced MMCs, but the tests were conducted on the P orientation at various loads at 0.6 m/s. Again a considerable reduction in wear rate was observed for this orientation, and the wear rate seemed to be almost independent of fibre volume fraction. From the results in both Figures 4.28 and 4.29, it is clear that B(SiC) fibres were very effective reinforcements as far as the wear of MMC is considered.

4.1.5.3 Effect of Fibre Orientation

The wear results described in the present work were all obtained to determine the effect of fibre orientation on the wear behaviour of the B(SiC)-reinforced MMC materials. The average volumetric wear rate distributions of the composite for these orientations are illustrated graphically in Figure 4.30 as a function of fibre sliding direction, and listed in Table 5. The tests shown in Figure 4.30 were carried out at a load of 60 N and a sliding speed of 1.0 m/s. From the Figure, the wear volume decreased considerably in MMCs tested for all orientations in comparison to the alloy matrix. Among the different sliding directions of N, P and AP orientation, the N orientation showed the lowest wear rate when dry sliding against steel. An increase in the wear rate was observed as the fibres proceeded from N to AP and AP to P orientation. The P orientation resulted in the highest wear rates while the AP orientation gave intermediate wear rates for a distance slid of 7.2 km, but the difference was small.

wear rates while the AP orientation gave intermediate wear rates for a distance slid of 7.2 km, but the difference was small.

Figure 4.31 shows the volumetric wear rate as a function of fibre volume fraction for the N and P orientated MMC samples, but the tests were done at a lower speed of 0.6 m/s and a lower load of 12 N. A significant reduction in wear rates were observed from the figure, and different wear results were evident in respect to the two sliding directions. Again the lowest wear rate was found in the N orientation. A high degree of difference was observed between unidirectional and bidirectionally orientated reinforced composites in this case where the 21% fibre was bidirectionally orientated.

As for the high sliding speed of 1.6 m/s, as shown in Table 7, no big difference was obtained between these two sliding directions, but the P orientation seemed to be lower in some cases than the N orientated samples under this high load condition.

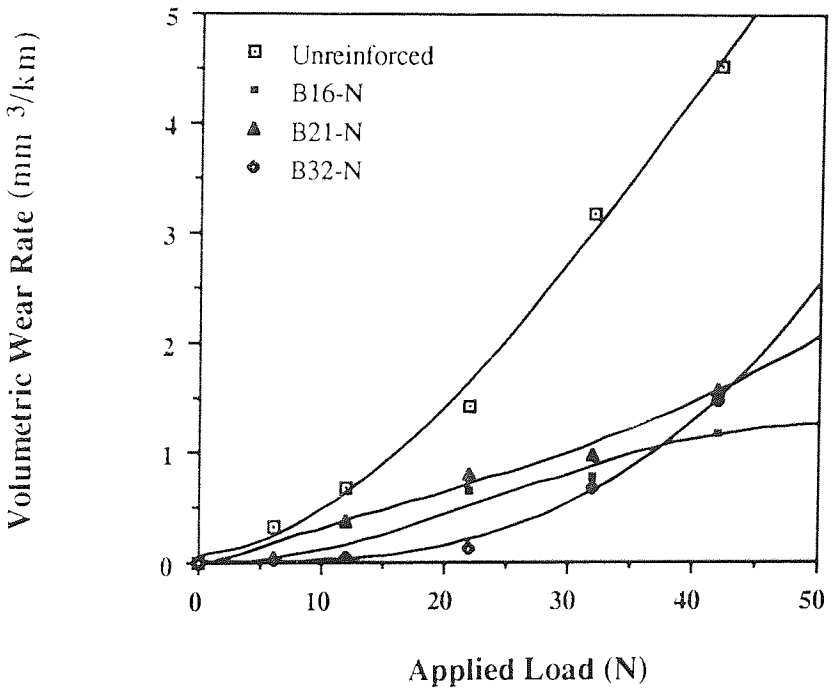

Figure 4.19. Average volumetric wear rate as a function of load for B(SiC)reinforced MMCs sliding in the N orientation (Speed = 0.6 m/s).

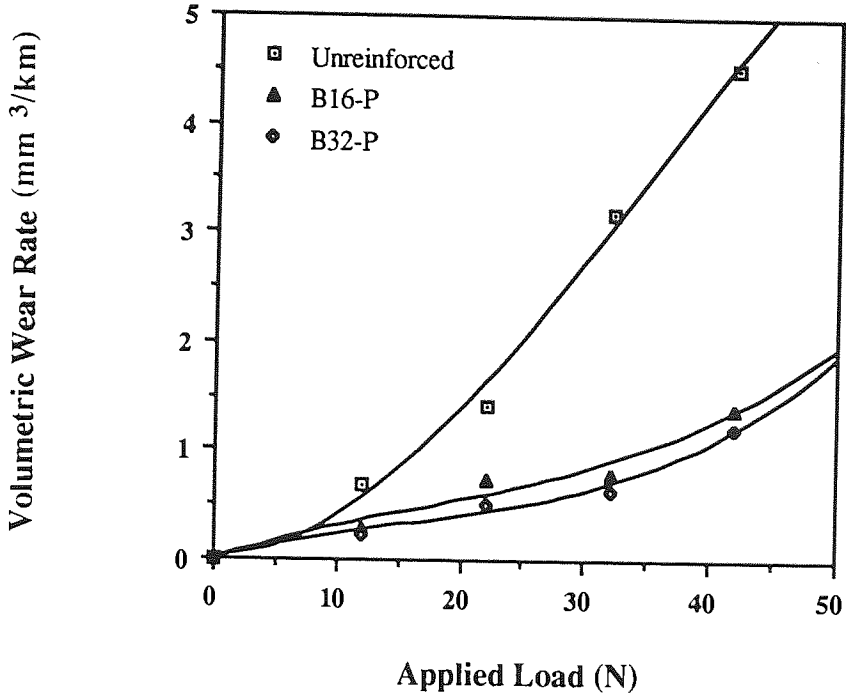

Figure 4.20. Average volumetric wear rate as a function of load for B(SiC)-reinfrced MMCs sliding in the P orientation (Speed = 0.6 m/s).

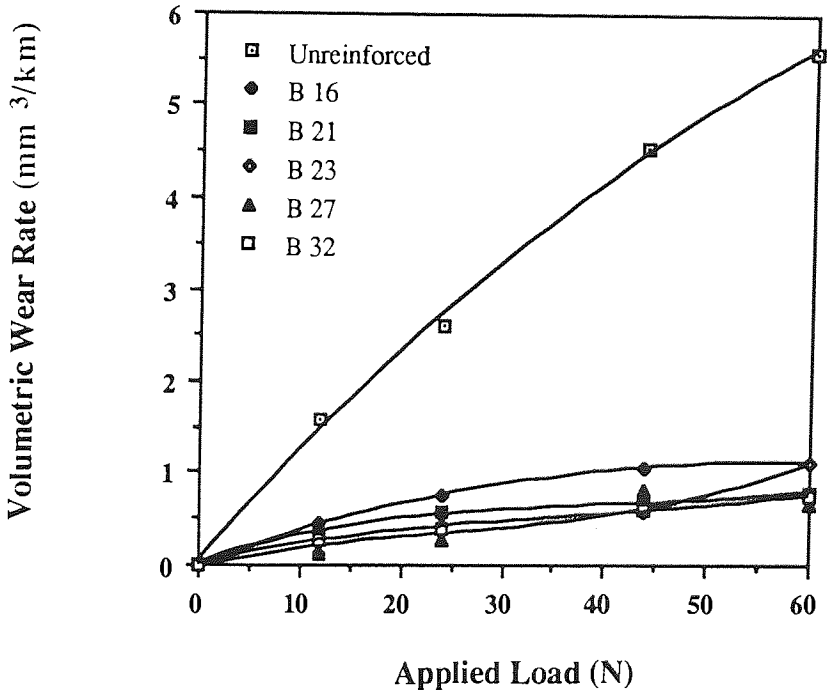

Figure 4.21. Average volumetric wear rate as a function of load for B(SiC)-reinforced MMCs sliding in the N orientation (Speed = 1.0 m/s).

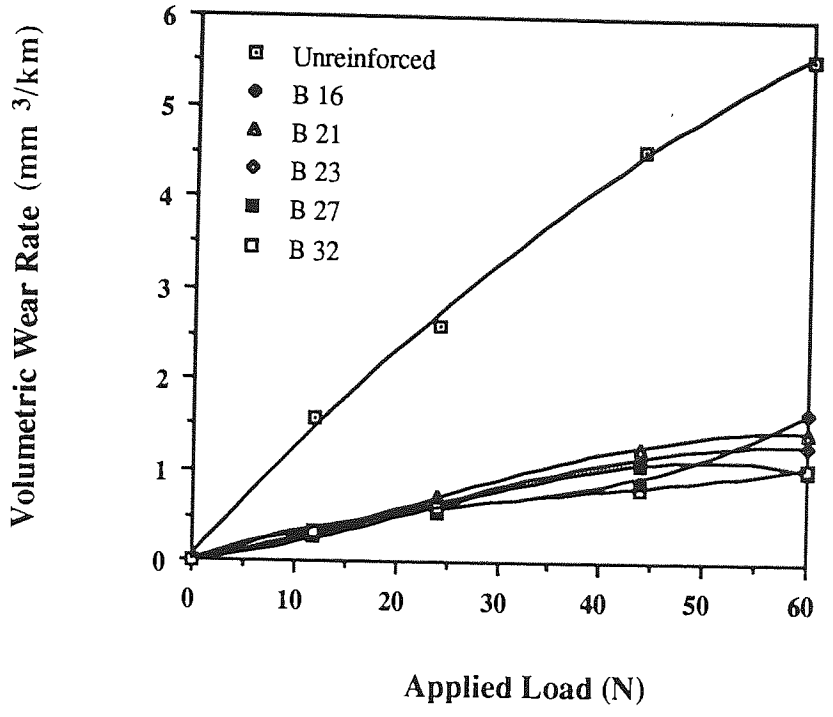

Figure 4.22. Average volumetric wear rate as a function of load for B(SiC)-reinforced MMCs sliding in the P orientation (Speed = 1.0 m/s).

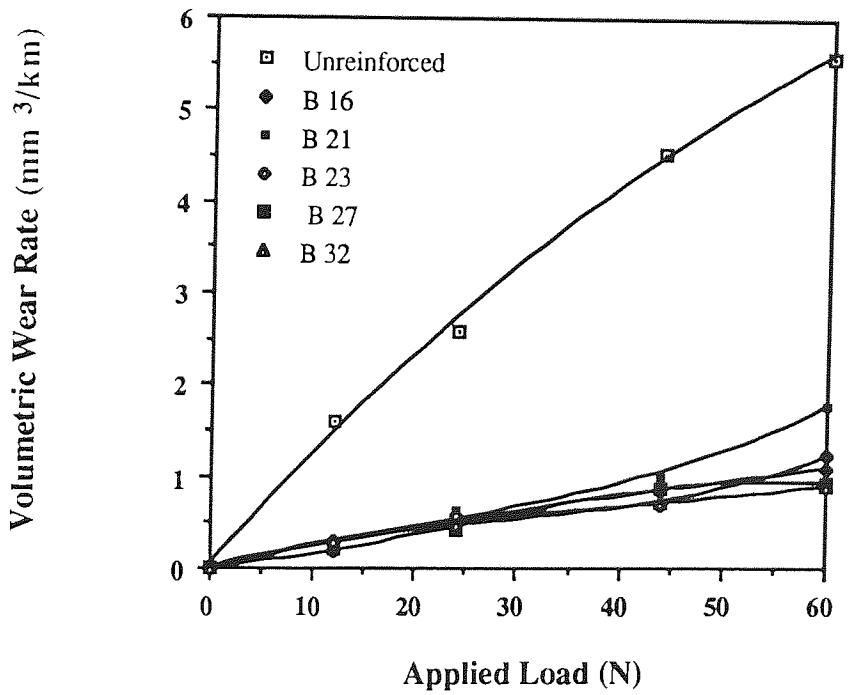

Figure 4.23. Average volumetric wear rate as a function of load for B(SiC)-reinforced MMCs sliding in the AP orientation (Speed = 1.0 m/s).

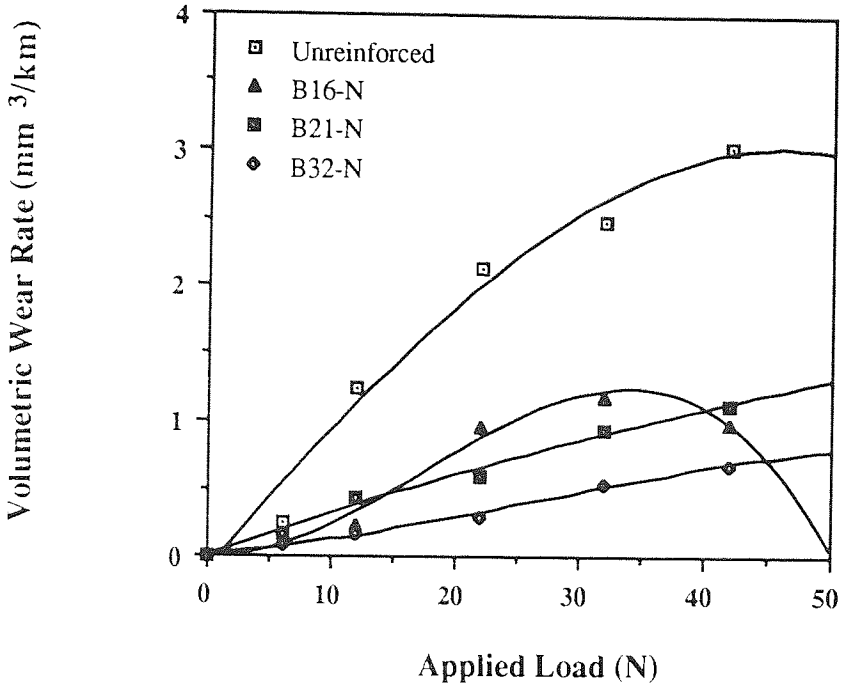

Figure 4.24. Average volumetric wear rate as a function of load for B(SiC)-reinforced MMCs sliding in the N orientation (Speed = 1.6 m/s).

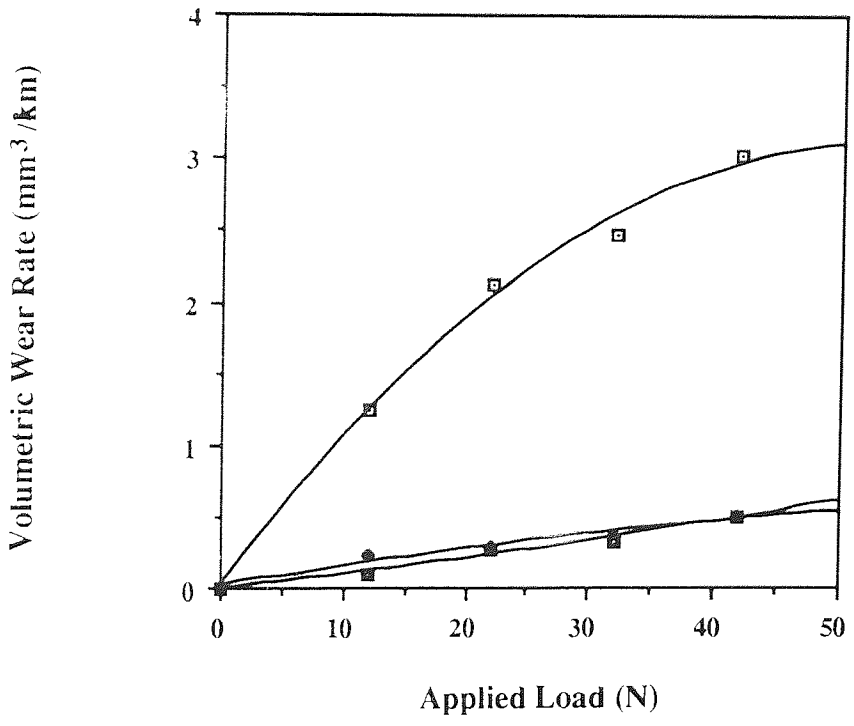

Figure 4.25. Average volumetric wear rate as a function of load for B(SiC)-reinforced MMCs sliding in the P orientation (Speed = 1.6 m/s).

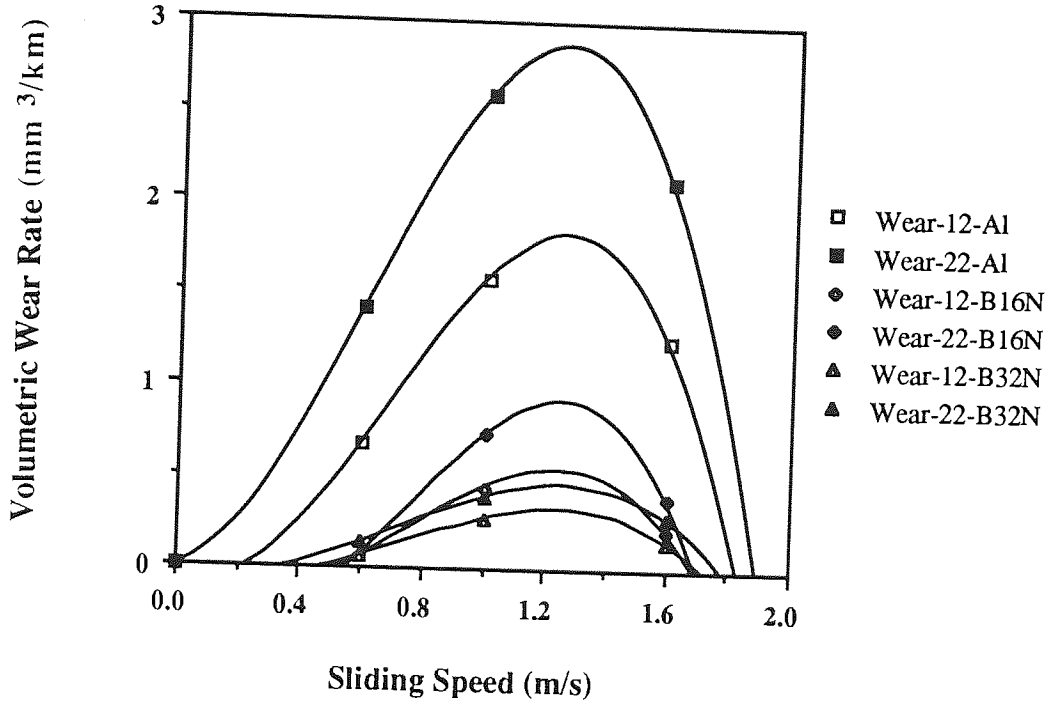

Figure 4.26. Average volumetric wear rate as a function of load for B(SiC)-reinforced MMCs sliding in the N orientation. (Speed = 1.6 m/s)

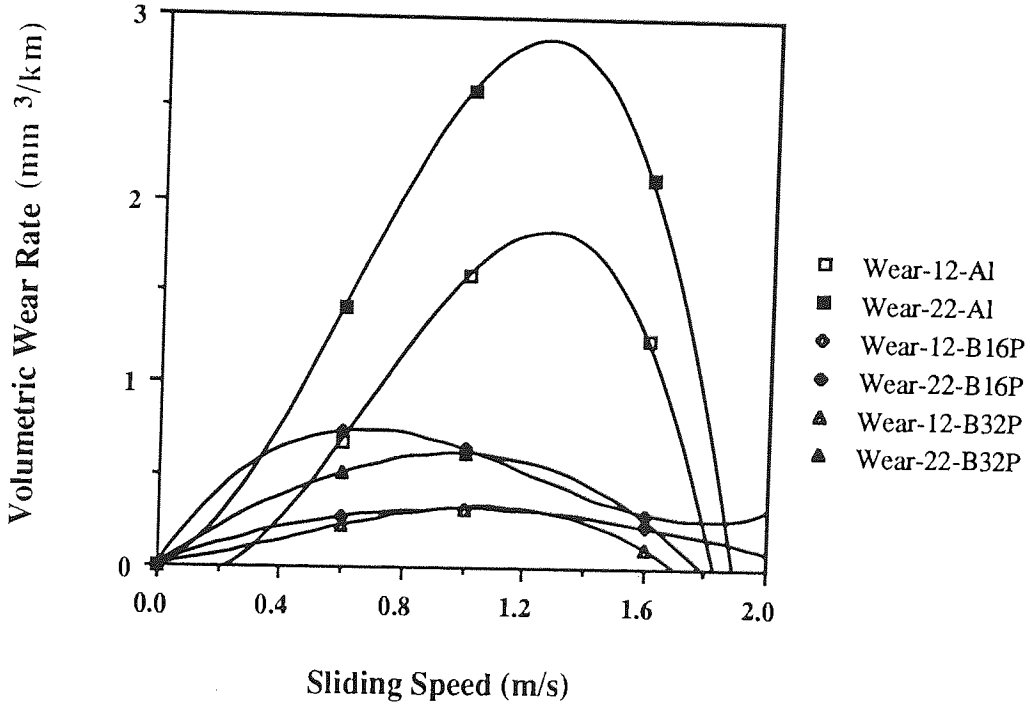

Figure 4.27. Volumetric wear rate versus sliding speed for the MMCs sliding in the P orientation against smooth steel.

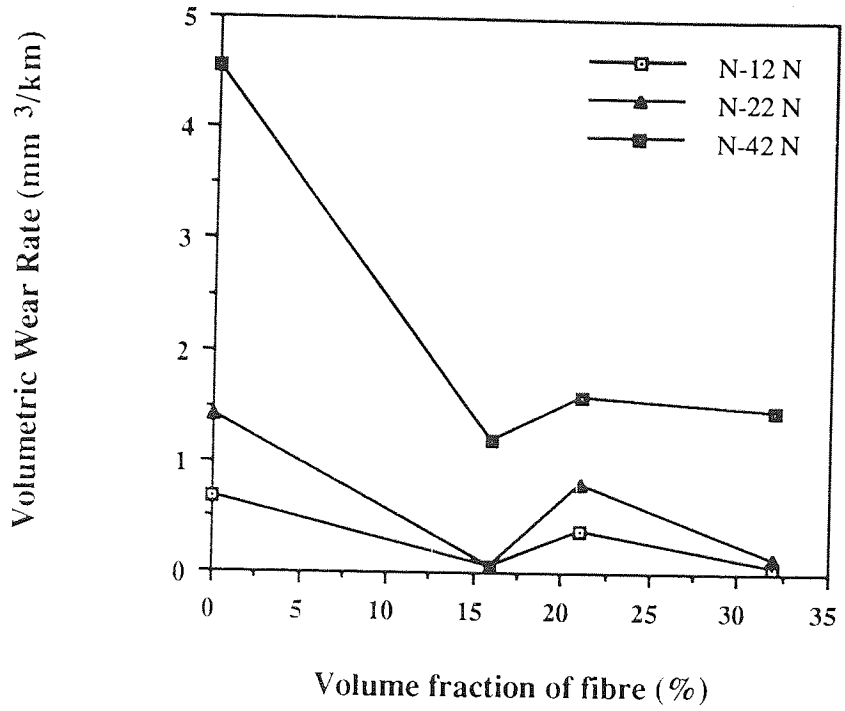

Figure 4.28. Volumetric wear rate as a function of fibre content in unidirectionally B(SiC)-reinforced MMCs for the N orientation at various loads.(Speed =1.0 m/s)

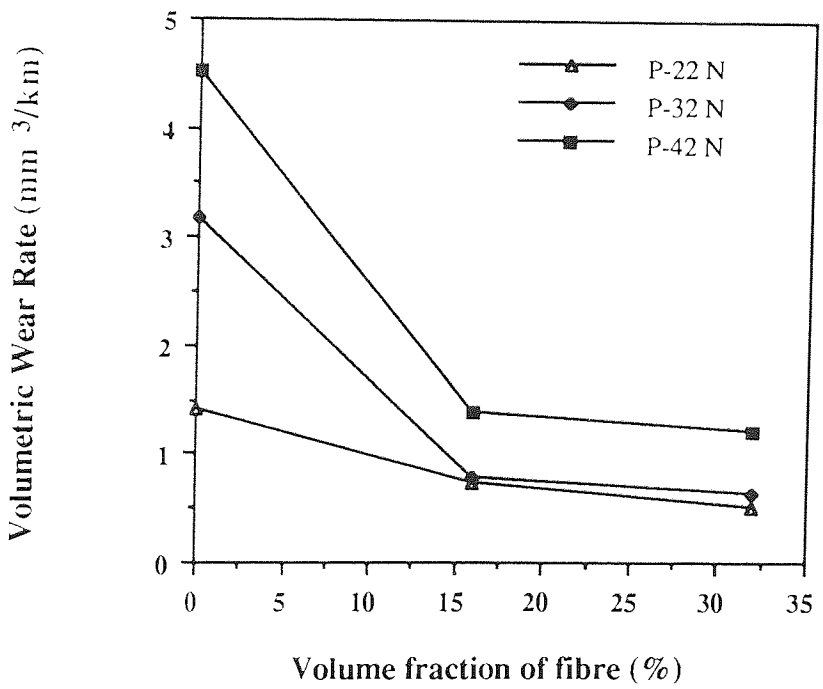

Figure 4.29. Volumetric wear rate as a function of fibre content in the unidirectionally B(SiC)-reinforced MMCs for the P orientation (Speed = 0.6 m/s).

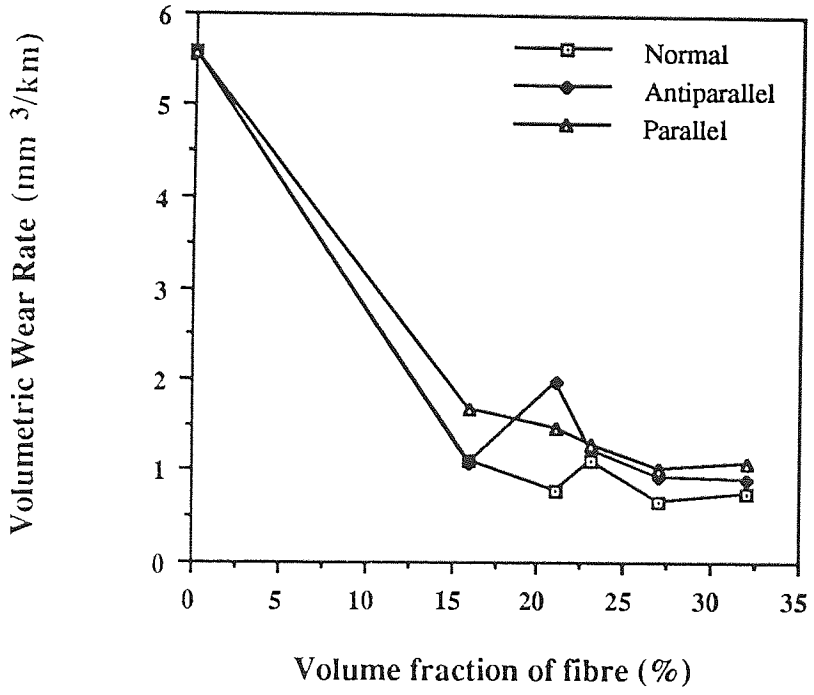

Figure 4.30. Volumetric wear rate as a function of sliding direction for the N, P and AP orientations of B(SiC)-reinforced MMCs (V = 1.0 m/s and L= 60 N).

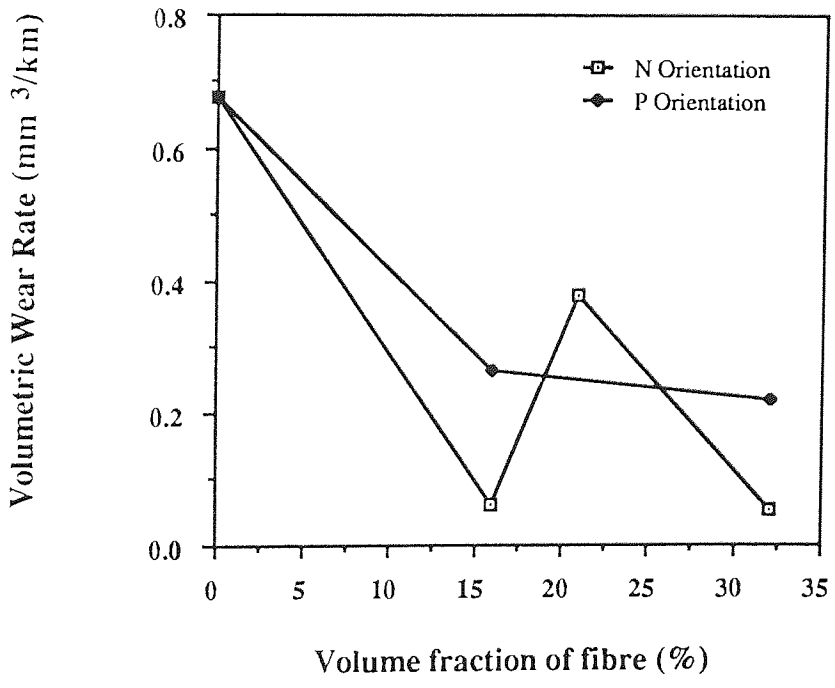

Figure 4. 31. Volumetric wear rate as a function of sliding direction for the N, P and AP orientations of the B(SiC)-reinforced MMCs. (V = 0.6 m/s and L = 12 N)

4.1.6 General Friction Results

Average coefficients of friction as a function of fibre volume fraction in the metal matrix and its composites are shown in Figures 4.32 to 4.38 for the three orientations. Each figure shows data for two speeds, i.e. 0.6 and 1.0 m/s. Figures 4.32, 4.33 and 4.34 show the coefficient of friction versus fibre volume fraction for a speed of 1.0 m/s under different loads in the N, P and AP orientation respectively. It was found that the coefficient of friction of the matrix alloy was about 0.31 to 0.40 under these conditions. The friction coefficient of B(SiC)/2014 MMC was generally much larger than that of the unreinforced matrix. From Figures 4.32, a slight decrease in friction coefficient was observed with increasing load and also with increasing fibre volume fraction at this speed of 1.0 m/s.

Figure 4.33 shows little variation with either load or fibre volume fraction for the P orientation, but first of all, the friction coefficient increased highly up to the 21% B(SiC) fibre, particularly for low load condition, whereas the friction coefficient was lower under high load of 60 N and tended to increase with increasing fibre content, then decreased thereafter. The minimum average coefficient of friction of about 0.53 was observed for the P orientation.

Figure 4.34 shows the coefficient of friction versus volume fraction of fibre for a speed of 1.0 m/s under different loads in the AP orientation. The friction coefficient gradually increased up to 21% volume fraction of fibre and then some decreases were observed in the 23% volume fraction of fibre. The coefficient of friction was remained constant for the 23 and 27% volume fraction of fibre at all loads, and then slightly decreased with increasing volume fraction of fibre to 32%, especially at low loads. The coefficient of friction generally decreased with the load. The maximum average coefficient of friction of about 0.65 was obtained in this orientation at this sliding speed.

Figure 4.35 shows the coefficient of friction versus fibre content at a speed of 0.6 m/s in the N orientation. The friction coefficient was found to be high, and large scatters

were observed, in particular for a 32% volume fraction of fibre. Also some indication of decreasing friction coefficient with load were evident in all these tests.

Figure 4.36 shows coefficient of friction versus fibre volume fraction for a speed of 0.6 m/s at various loads in the P orientation. The coefficient of friction first increased very slightly with load up to the 16% fibre and then decreased with increasing volume fraction of fibre, except for a load of 12 N where the increase carried on. In addition, the coefficients of friction were usually grouped together, especially at high volume fraction of fibre used, i.e. 32% and no significant variations were observed with load.

The effect of sliding speed on friction coefficient for the MMC pins is shown in Figure 4.37 for the N orientated samples. The samples were tested at a load of 12 N at all sliding speeds. From the figure, it could be seen that friction of the matrix alloy and composite decreased with increasing sliding speed. A significant difference was observed between the matrix and its composite in that the matrix had a much lower coefficient of friction. Moreover, a sharp decrease in coefficient of friction was observed for all fibre volume fractions of the composite at a speed in excess of 1.0 m/s.

Figure 4.38 also shows the coefficient of friction versus speed for the MMC pins sliding in the P orientation against smooth steel. The tests were carried out for a loads of 12 N and 24 N. As shown in the figure, the effect of sliding speed on the friction coefficient was clear. It was appeared that friction coefficient increased up to 1.0 m/s in most cases and then decreased sharply with sliding speed. However, for the matrix alloy, friction coefficient decreased with increasing speed, but the effect of volume fraction of fibre on friction coefficient was small, especially at the highest speed of 1.6 m/s. Comparing the 16% and 32% fibre composites at loads of 12 N and 24 N, it appeared that higher load increased friction in the 16% fibre composite, but reduced it in the 32% fibre composite.

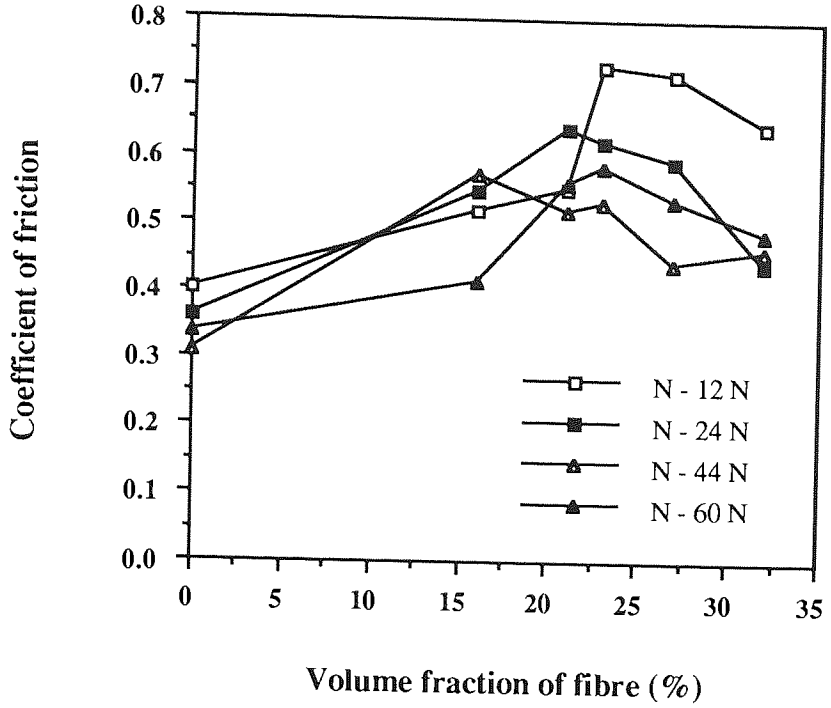

Figure 4.32. Coefficient of friction versus volume fraction of fibre for a speed of 1.0 m/s under different loads in the N orientation.

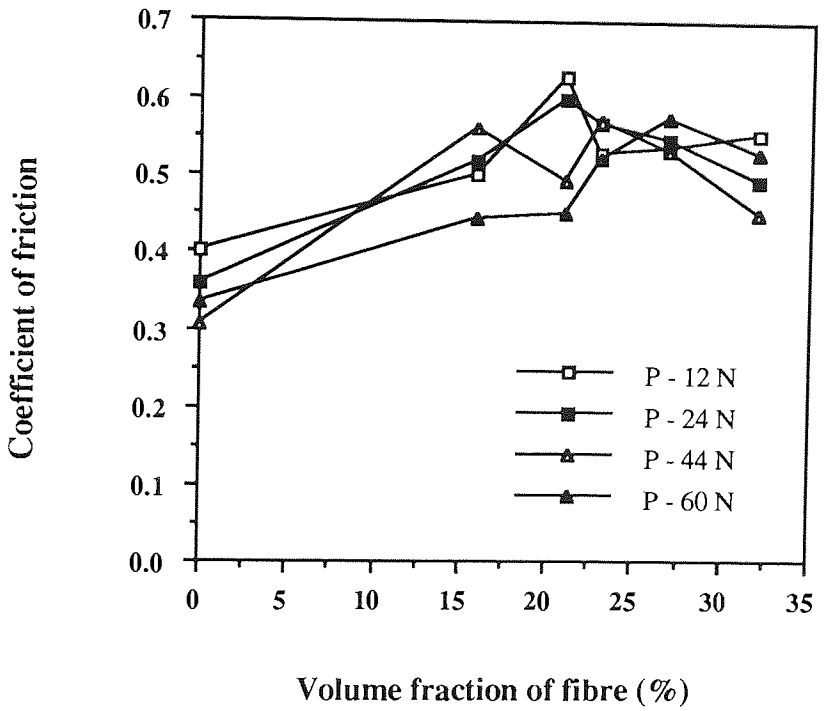

Figure 4.33. Coefficient of friction versus volume fraction of fibre for a speed of 1.0 m/s under different loads in the P orientation.

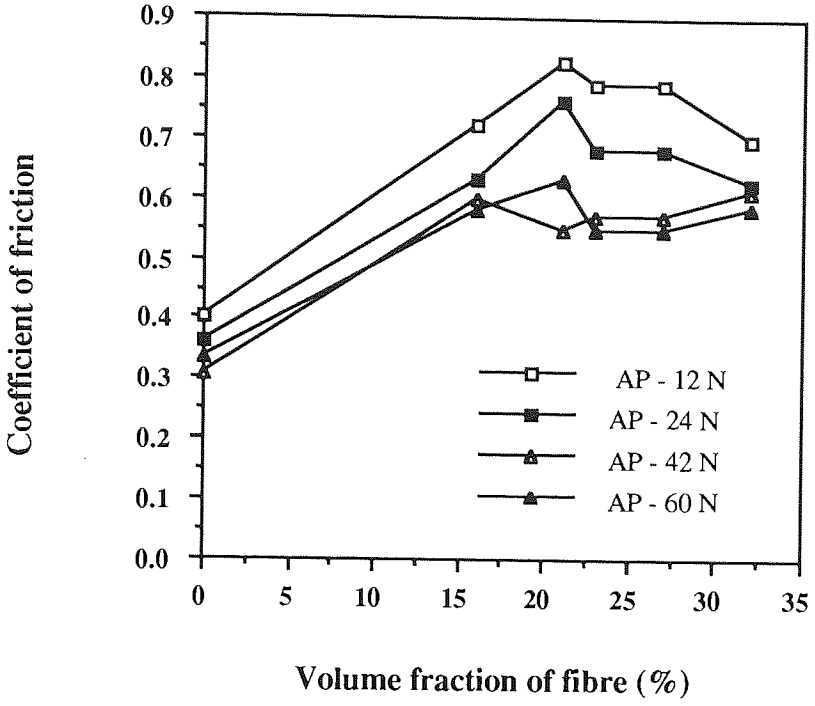

Figure 4.34. Coefficient of friction versus volume fraction of fibre for a speed of 1.0 m/s under different loads in the AP orientation.

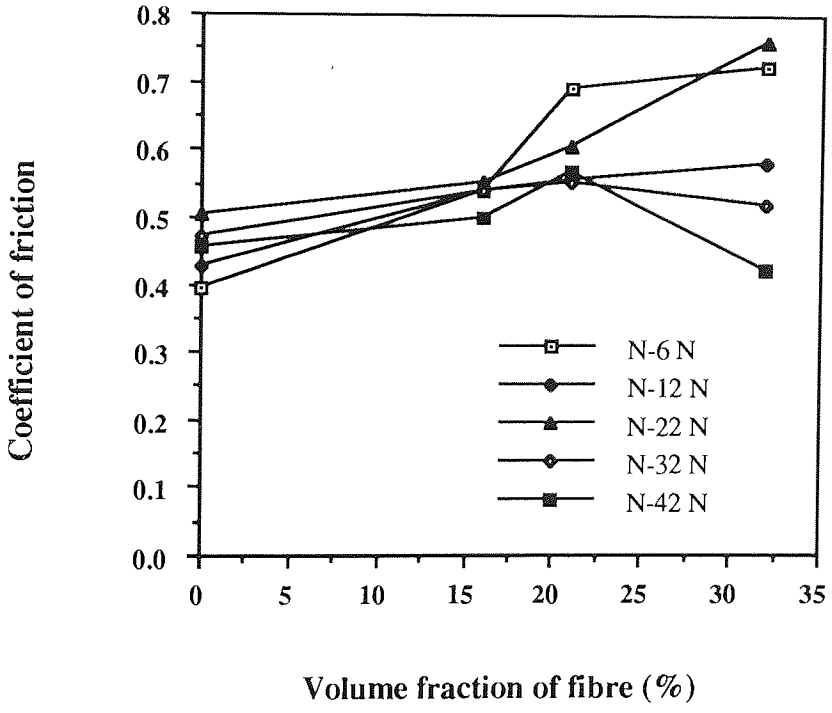

Figure 4.35. Coefficient of friction versus volume fraction of fibre for a speed of 0.6 m/s under different loads in the N orientation.

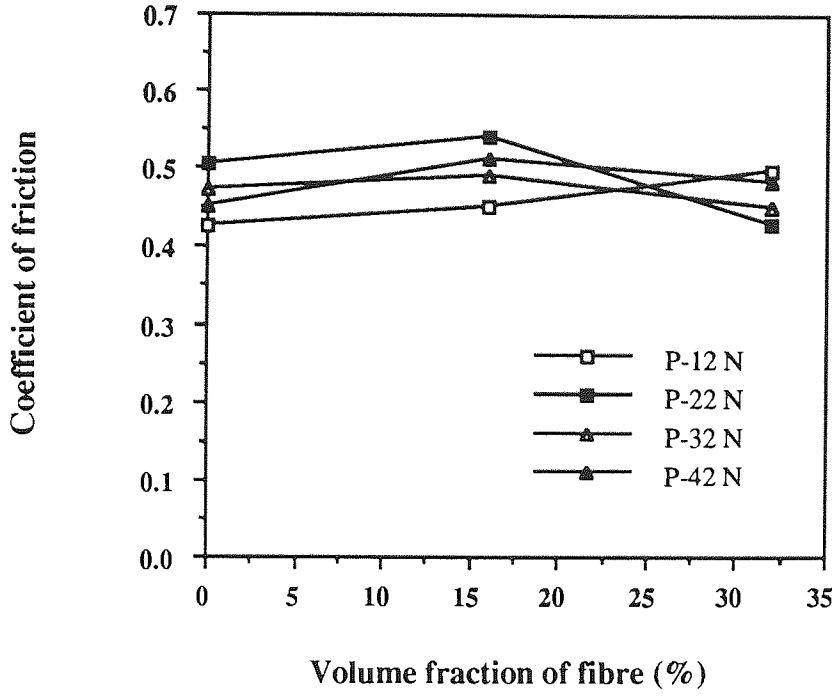

Figure 4.36. Coefficient of friction versus volume fraction of fibre for a speed of 0.6 m/s under different loads in the P orientation.

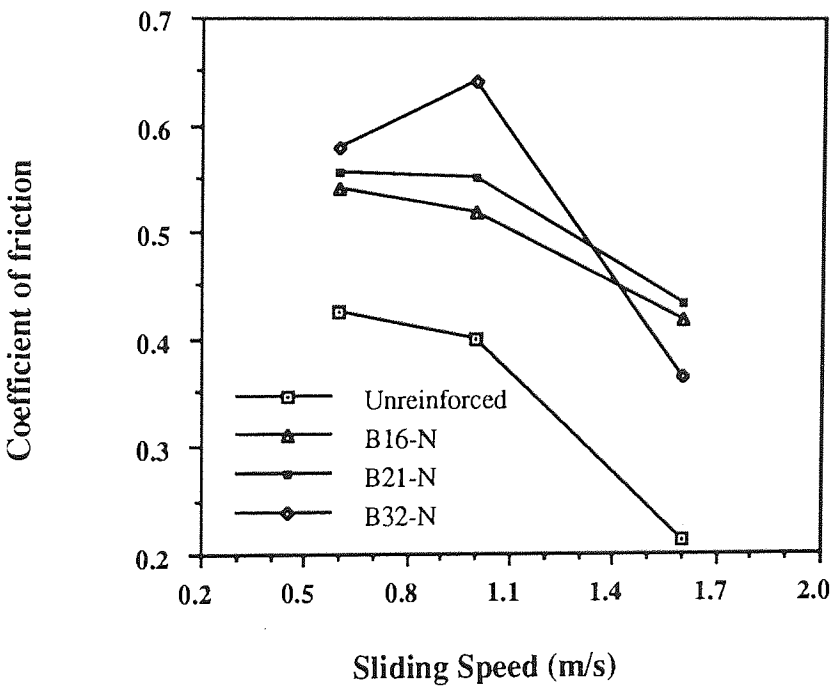

Figure 4.37. Coefficient of friction versus sliding speed for MMC pins sliding in the N orientation against smooth steel under a load of 12 N.

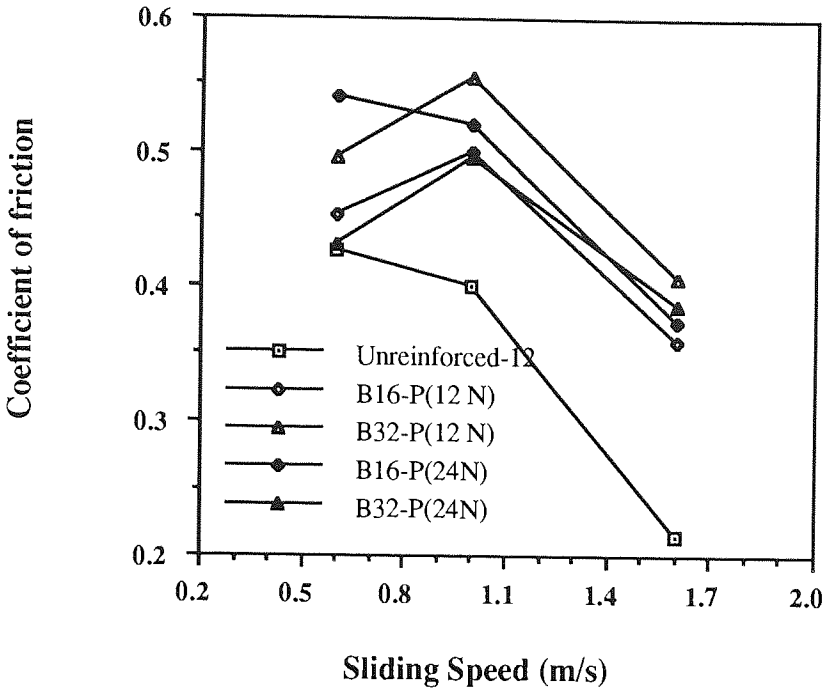

Figure 4.38. Coefficient of friction versus sliding speed for the MMC pins sliding in the P orientation against smooth steel under loads of 12 and 22 N.

4.1.7 Surface Observations and Wear Mechanisms

From the results of the previous section of 4.1.5, the wear behaviour of the unidirectional reinforced MMCs was found to be excellent compared with the Al alloy matrix under same conditions. In order to find out the cause of this behaviour, metallographic surface observations of the matrix and its composites were carried out by means of SE and BSE microscopy.

4.1.7.1 Unreinforced Aluminium Matrix

Figure 4.39 shows the worn surface of 2014 aluminium alloy pin tested at 1.0 m/s and 24 N load, the sliding direction was from right to left. Extensive grooving took place over the surface parallel to the sliding direction, while Figure 4.40 and 4.41 show similar micrograph for the same condition in both SE and BSE contrast at high magnification. In these micrographs flat ridges of deformed metal lie on the surface, and only rather shallow ploughing grooves were observed. A small amount of oxide particles was embedded over the surface was shown by the BSE image.

An SE image of the worn surface of the matrix pin is also shown in Figures 4.42 and BSE image in Figure 4.43 for a speed of 1.0 m/s but a load of 60 N. These micrographs indicate plastic deformation and microchips formation over the surface in SE image, but relatively smooth wear track with parallel furrows in the sliding direction was further evidenced for the ploughing mechanism. The deformed metal layer and transferred iron to the pin surface were observed in the BSE image. The length of a deformed layer of transferred iron was more than about 250 μm. Figure 4.44 shows a similar micrograph of the matrix alloy pin, tested under the same conditions, and severe local spalling was observed in this SE image, where the sliding direction was from right to left. The spalling of the wear sheet was lifted from the surface since the cracks have just reached the surface. Moreover, mild abrasive wear was also evident on the part of the sample.

Figures 4.45 and 4.46 show the worn surface of the matrix pin under similar conditions in SE and BSE contrast, and more massive damage and plastic deformation was observed in SE image and a number of equated particles were also shown to be reattached to the worn surface in the BSE image. Figures 4.47 and 4.48 show a cross-section of the worn surface of the matrix pin after sliding at 1.0 m/s and a 60 N load, near to the trailing edge. These micrographs show fragments of hard oxide particles and the formation of elongated holes, voids were observed in SE mode, while the fragmented wear debris was compacted on the surface and filled a groove as shown in Figure 4.48.

Figure 4.49 shows the subsurface layer parallel to the wear track of the pin for a speed of 1.0 m/s and 44 N load. The delamination crack along the sliding direction of the wear track was more than 120 μm long and nearly continuous. The top surface of the wear sheet was smooth, while the fractured surface was rough. At a critical length, these cracks shear to the surface, yielding a wear particle in the form of a long thin sheet as evidenced by this figure. A distorted zone was also evident in the matrix close to the surface.

Figure 4.50 shows another similar feature of a subsurface crack formed underneath the wear track of a matrix pin which was tested at 0.6 m/s and 22 N, but the length of the crack and the thickness of surface layer were lower than the previous one. The thickness of the surface layer was about 3-5 μm. The wear sheet then would remove from the plane of the surface due to residual stress and strain in the sheet or due to the repeated loading. In addition, a strain hardening layer was also evident at high magnification.

As for the case of high sliding speed condition, Figure 4.51 shows the worn surface of a matrix pin sectioned parallel to the sliding direction for a speed of 1.6 m/s and 22 N load in BSE image at high magnification. This figure illustrates the extent of plastic deformation and the layer of compacted fragments on the surface, and multiple delamination cracks underneath the surface were observed. Similar features are shown in Figure 4.52 which was another subsurface section of the same sample. The length of the

subsurface layer was about 190 μm and the maximum thickness layer was 10 μm. The another important observation was the formation and growth of voids and a distorted matrix microstructure.

Figure 4.53 shows typical wear debris from the 2014 aluminium alloy pin collected after the wear experiment. Two types of wear particles are observed : large flake type particles and small equated particles which were frequently found adhering to each other in agglomerated masses. The average length of the plate-shape particles was about 180 μm while small agglomerated particles varied significantly.

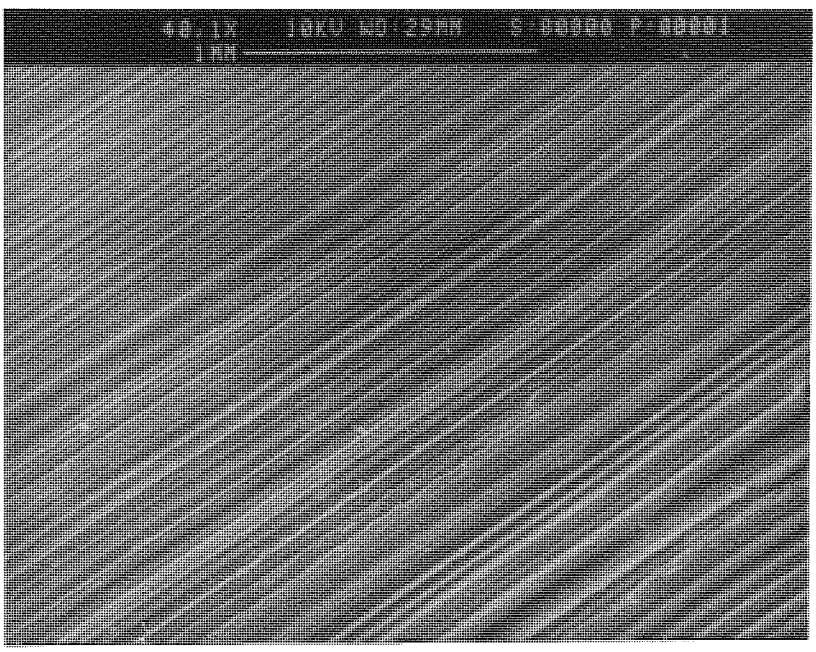

Figure 4.39. SE micrograph image of wear surface of the 2014 aluminium alloy pin after sliding at 1.0 m/s speed and 24 N load, showing extensive grooving, leading edge to left.

Figure 4.40. SE image of the wear surface of the matrix pin after sliding at 1.0 m/s speed and 24 N load, showing flat ridges deformed metal and grooving at high magnification.

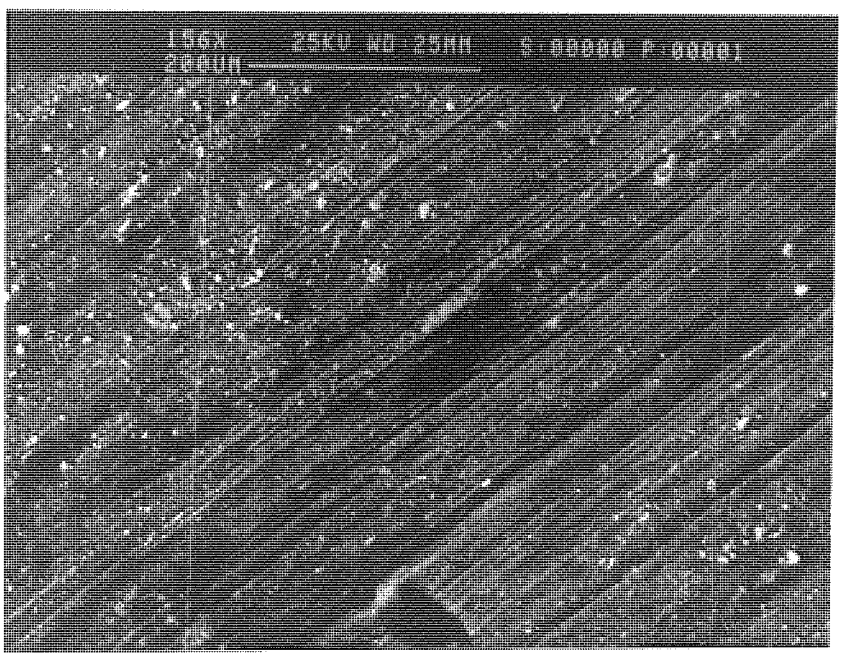

Figure 4.41. Backscattered electron image of the same sample of Figure 40, showing some oxide particles embedded in the matrix.

Figure 4.42. SE image of the wear surface of the matrix pin after sliding at 1.0 m/s speed and 60 N load, showing plastic deformation and microchip formation, leading edge to left.

Figure 4.43. BSE image of Figure 42, showing deformed layer and iron transfer to the pin surface.

Figure 4.44. SE image of the matrix pin after sliding at 1.0 m/s speed and 60 N load, showing several local spalling and grooving, leading edge to left.

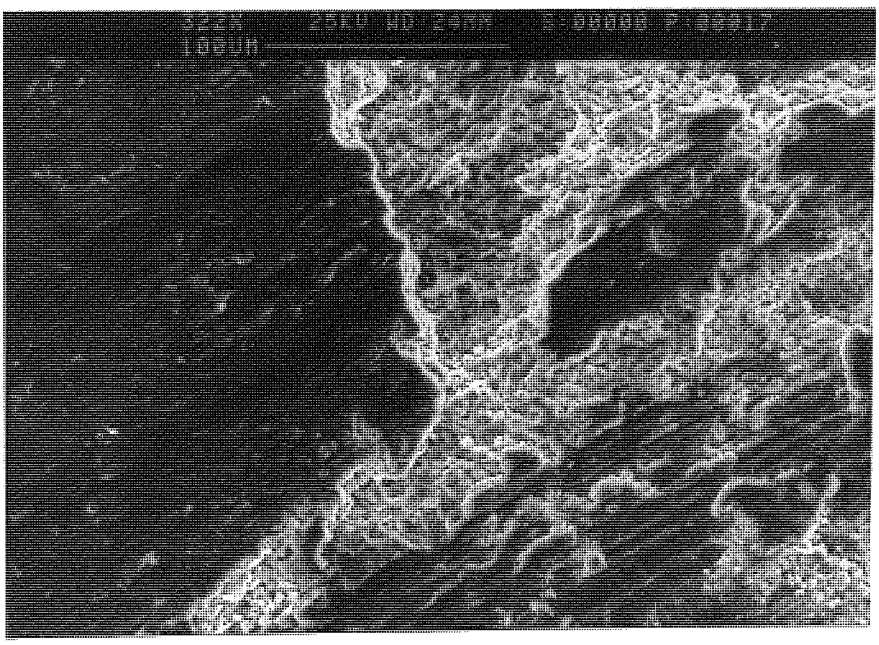

Figure 4.45. SE image of the wear surface of the matrix pin after sliding 1.0 m/s speed and 60 N load, showing extensive damage and plastic deformation, leading edge to right.

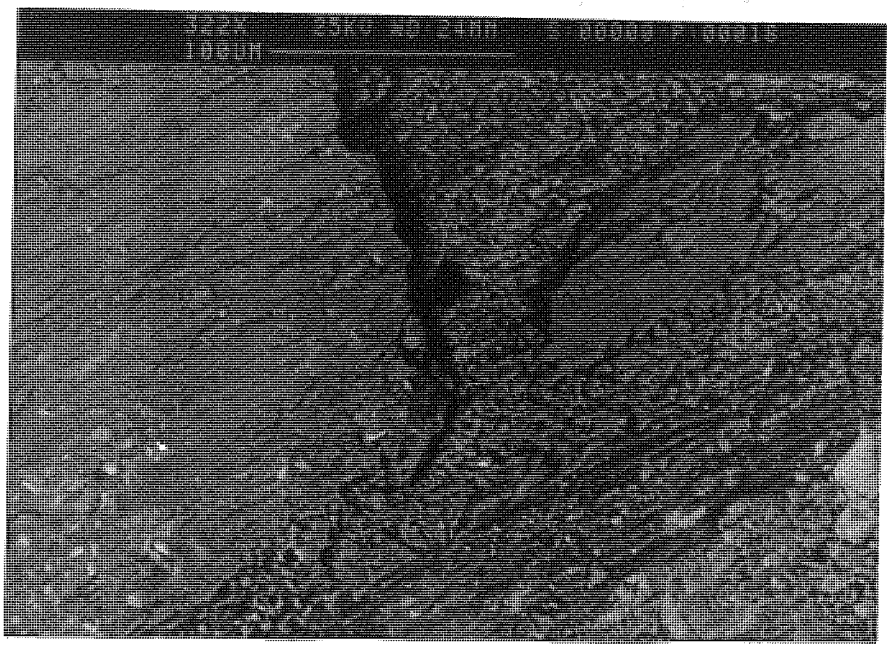

Figure 4.46. BSE image of the same sample as Figure 45, showing surface fatigue cracks and particles attached to the surface.

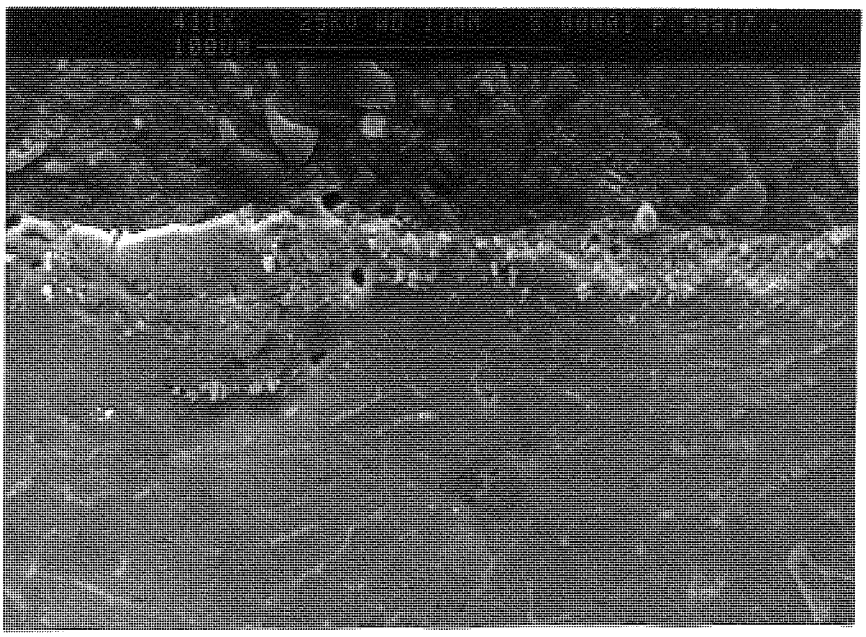

Figure 4.47. SE image of the wear surface of cross-section of the matrix pin after sliding at 1.0 m/s speed and 60 N load, showing fragments of oxide particles and formation of voids around the hard particles.

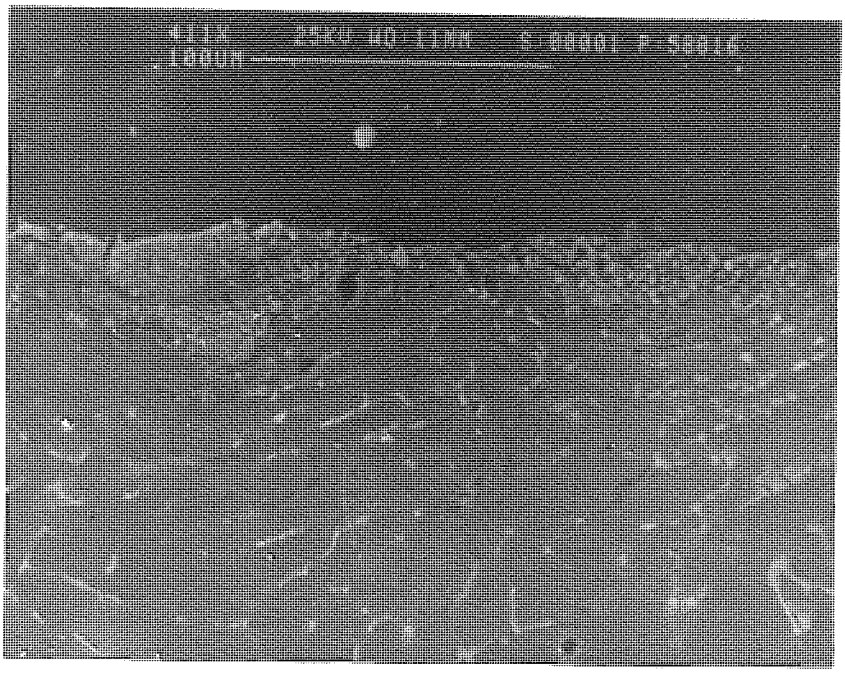

Figure 4.48. BSE image of Figure 47, showing fragments of embedded oxide particles and cracks.

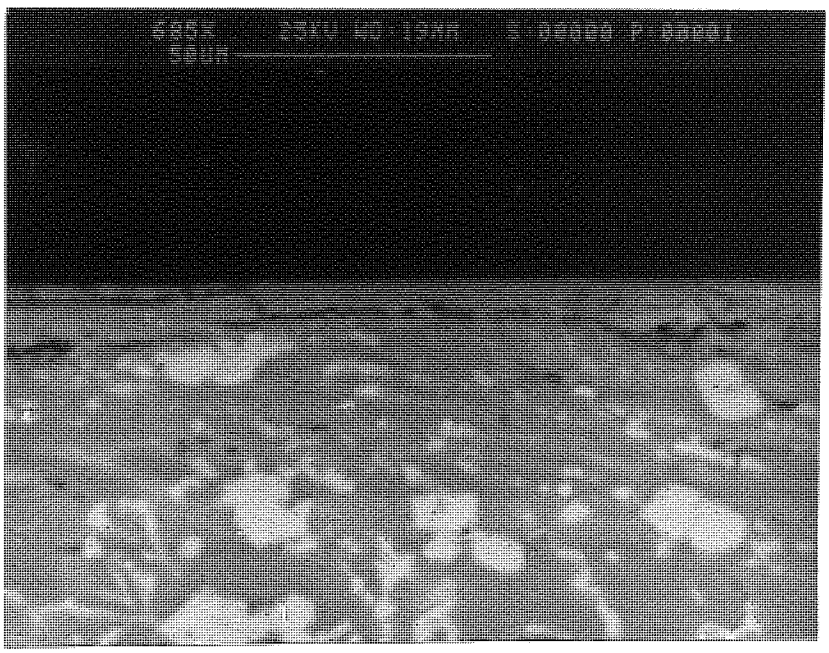

Figure 4.49. BSE image of the wear surface of the matrix pin parallel to the slidingdirection, for a speed of 1.0 m/s and 44 N load, showing cracks and subsurface deformation.

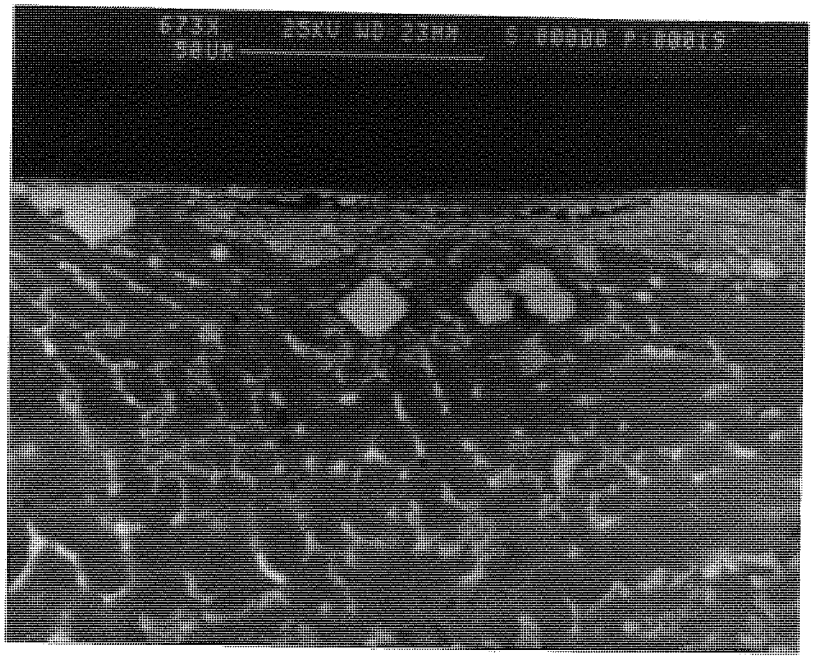

Figure 4.50. BSE image of the wear surface of the matrix pin parallel to the rubbing direction, for a speed of 0.6 m/s and 22 N load, showing subsurface deformation and strain hardening at high magnification.

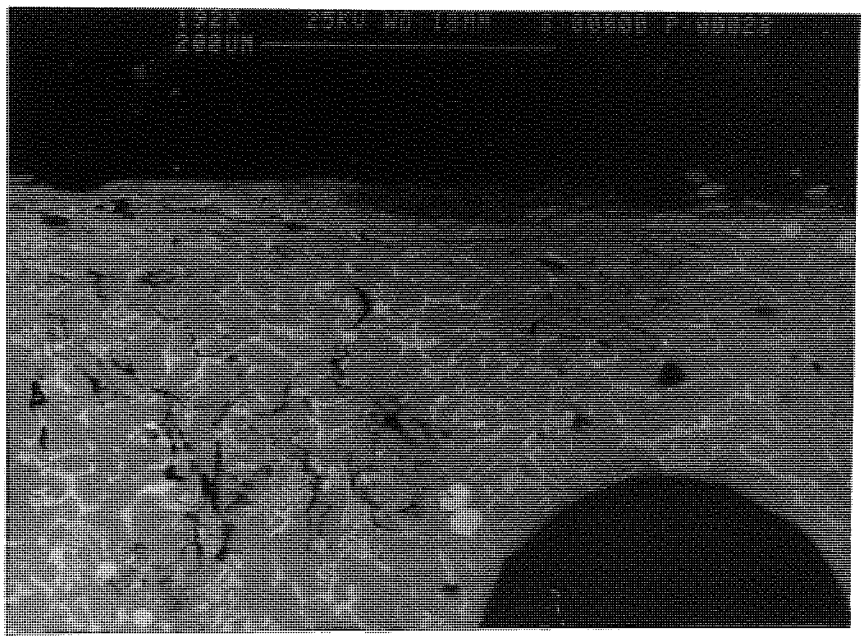

Figure 4.51. BSE image of the wear surface of the matrix pin parallel to the slidingdirection, for a speed of 1.6 m/s and 22 N load, showing subsurface and continuous cracks, and a deformed fragmented layer over the surface.

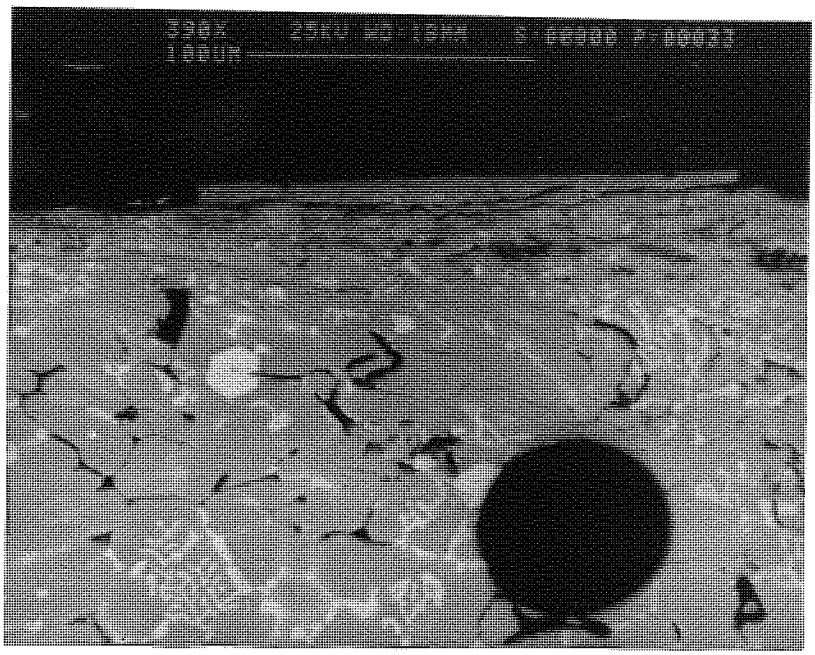

Figure 4.52. Higher magnification of Figure 51, showing subsurface layer and growth of voids on the distorted zone.

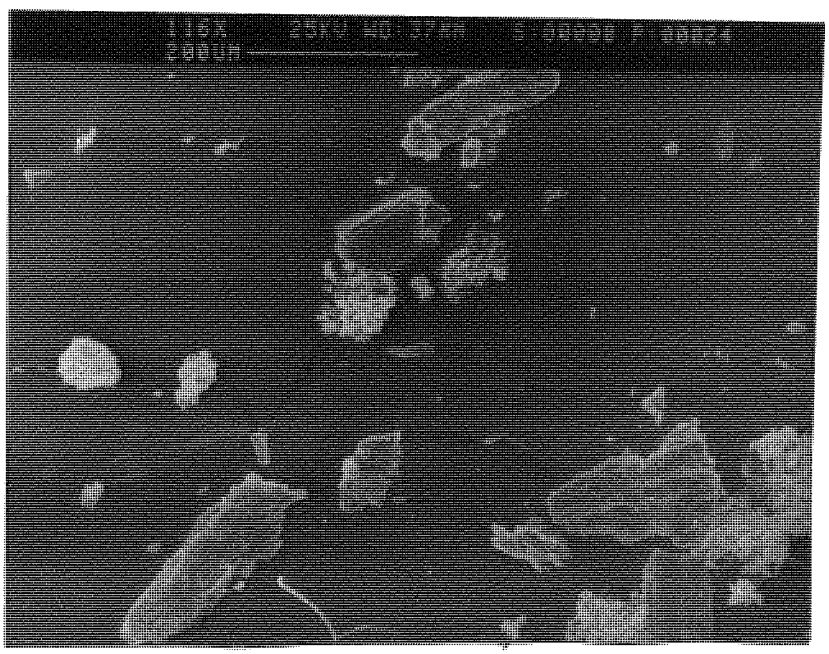

Figure 4.53. SEM micrograph of typical wear debris generated from the aluminium matrix, showing flake type particles and agglomerated finer debris.

4.1.7.2 *Unidirectional Fibre Reinforced Composite*

Under SEM examination, general images of the worn surfaces of the B(SiC)-MMC materials were studied with respect to the three main orientations (N, P and AP) as shown in Figures 4.54 to 4.65, Figures 4.66 to 4.81 and Figures 4.82 to 4.94 respectively. It was observed that different forms of wear dominated for each orientation.

Considering first the worn surface of the composite in which the fibres were perpendicular to the sliding direction (N) under different testing conditions such as load, speed, distance etc. Figure 4.54 shows the worn surface of the composite pin containing 32% volume fraction of fibre tested at 1.0 m/s and 44 N in SE image. The sliding direction was from left to right. This micrograph showed a relatively smooth surface appearance at low magnification in spite of employing a high load. There was a much reduced amount of plastic deformation of the pin, but there was some smearing of the matrix over the fibre edges. An increased magnification view of the same sample of the composite pin is shown in Figure 4.55 in SE image. It was clearly observed that fibres were cut from the ends in a slicing manner. These fractured fibres might be due to trailing edge effect. The maximum length of these particles was about 25 μm but they depended on the testing parameters and varied from place to place. Matrix smearing was also observed over the fibre ends.

The worn surface of the composite pin containing 16% volume fraction of fibre is shown in Figure 4.56 at low magnification in SE image. Leading edge was from right to left. This micrograph shows that fibre fracture occurred and caused grooving over the surface of the pin. It was observed that more fibre fracture appeared because of the non-uniform distribution of fibres in the composite pin. Increased magnification of the same sample is also shown in Figure 4.57, indicating similar surface appearance. A small amount of fractured particles was visible. Some fibres were fractured not from the end but also from the middle of the fibres. The length of these particles was about 45 μm. Also small particles were embedded into the matrix.

Figure 4.58 represents a similar micrograph, but for a load of 60 N at high magnification, leading edge was from left to right. A smooth surface appearance and reattachment of wear debris was exhibited in their SE image. A quite uniform debris was evident and the maximum dimension of the debris was about 10 μm. In addition, there was also evidence of fibre fracture from the ends and matrix smearing over the fractured part of the fibres. The backscattered electron image of this sample is shown in Figure 4.59 and exhibited some hard oxidised particles embedded in the matrix and reattached to the fibre surface. Again, matrix smearing was evident and fractured particles were also observed over the whole surface of the pin. The maximum size of these particles was about 12 μm.

Figure 4.60 shows the worn surface of the 32% B(SiC) fibre composite pin in SE image. The test was conducted at a speed of 0.6 m/s and load of 22 N , leading edge was from right to left. This micrograph showed similar surface appearance but some disruption was observed over the pin surface. The fibre fracture and matrix smearing was predominant mechanism as shown in Figure 4.61. The fracture of fibre was seen to be brittle type from the micrograph, but smooth surface obtained, some fibre debonding was also observed at high magnification. The small wear grooving was evident over the surface due to abrasion of small asperity particles. The BSE image of the same micrograph as shown in Figure 4.62, clearly revealed that the small fracture particles were embedded over the composite pin. It was about 5-12 μm. Moreover, smearing of the matrix on the fractured fibres ends was also observed in this micrograph.

Let us look at the orthogonal (bidirectional) orientated composite pin, Figure 4.63 shows the worn surface of the composite containing 21% volume fraction of fibre, tested for a speed of 0.6 m/s and 22 N load at low magnification, leading edge was from right to left. Extensive fibre fracture was observed in both parallel and normal orientated fibre surface in SE image. The fibre thinning and fracture in the P and fracture in the N orientated fibre at different size was also evident from the micrograph. Some craters were also seen in the matrix and the size of these craters seemed to be uniform shape. Increased

magnification of Figure 4.64 shows that catastrophic fibre fracture had occurred in both cases. The length of the fibre fracture depended upon the operating variables. A small amount of ploughing was also observed which was nearly continuous. It was appeared that the depth of the fibre fracture region was greater in this orientation, although a few intact fibres were also evident in the surface of the pin, particularly at the N orientated fibres due to strong bonding between the fibres and matrix. Figure 4.65 shows the worn surface of the same sample at higher magnification. From this micrograph, it could be seen that a substantial fibre damage and fracture had occurred and as a results of this, fibre removal was observed at the right side of the worn surface. Furthermore, the microstructure was also distorted from the bottom of this sample.

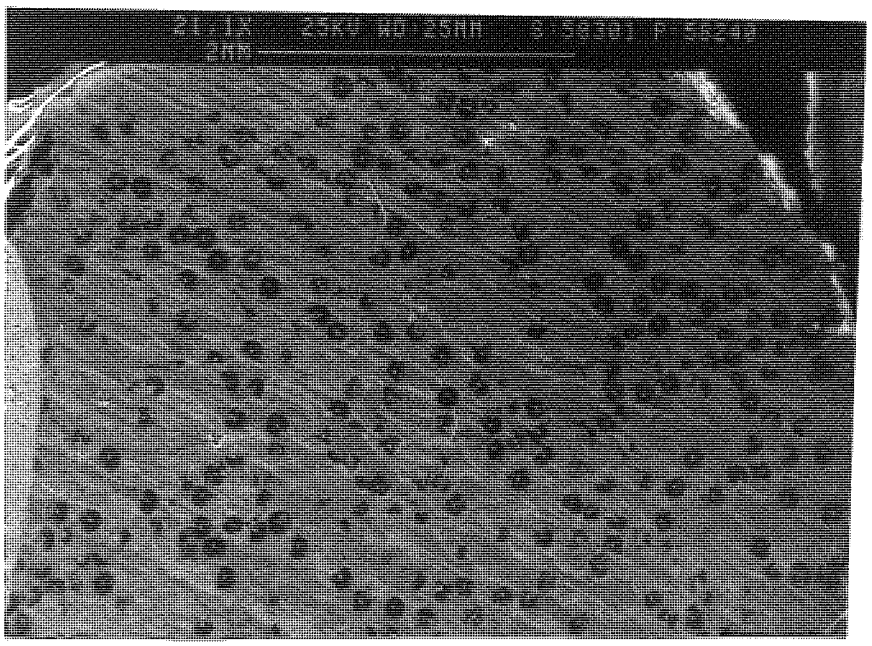

Figure 4.54. SE image of a worn surface a B(SiC)-reinforced MMC pin tested in the N orientation at 1.0 m/s speed and 44 N load, showing relatively smooth surface, leading edge left to right. ($V_f = 0.32$)

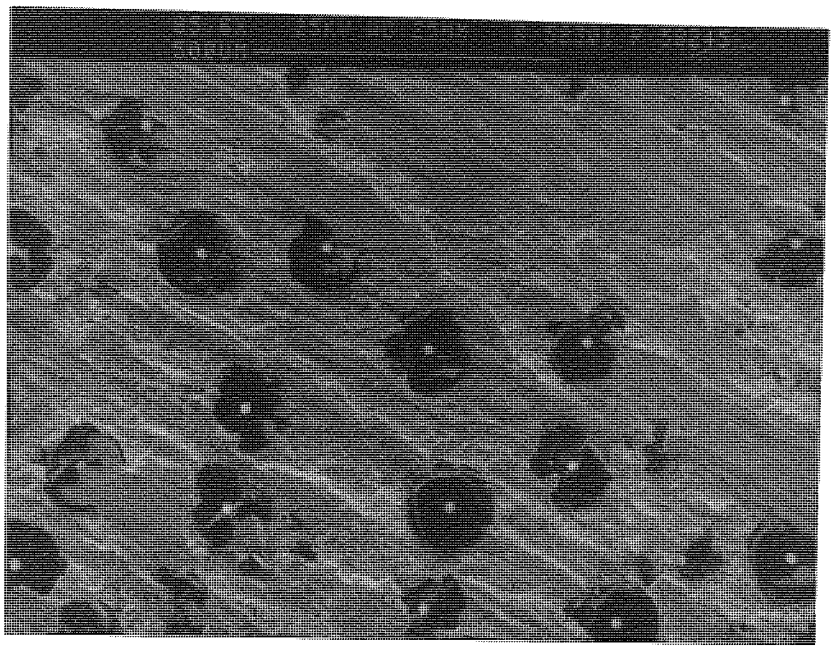

Figure 4.55. Increased magnification of Figure 54, showing matrix smearing over the fractured fibres.

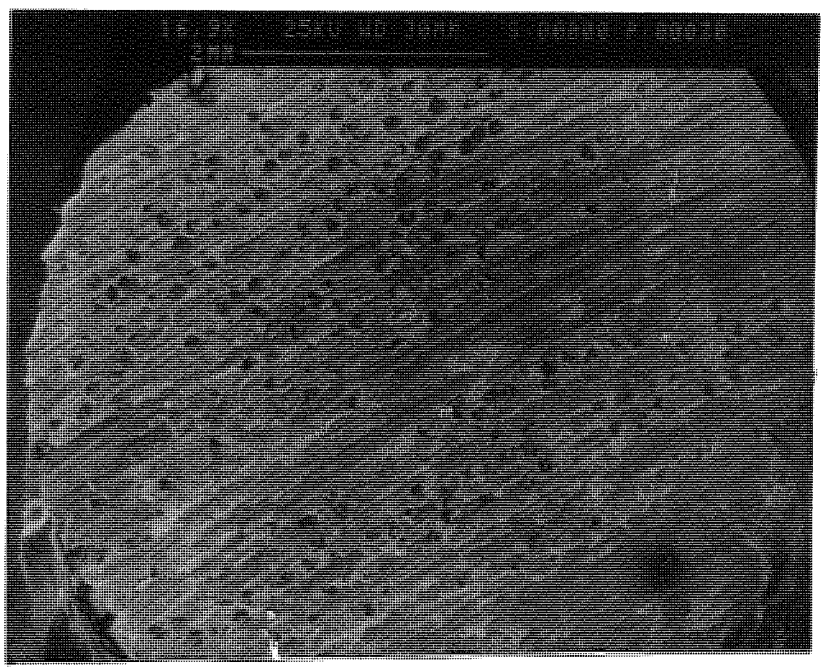

Figure 4.56. SE image of the worn surface of the B(SiC)-reinforced MMC pin tested at 1.0 m/s and 12 N load, showing some grooving and fractured fibres, leading edge right to left. ($V_f = 0.16$)

Figure 4.57. Increased magnification of Figure 56, showing breakages of fibres.

Figure 4.58. SE image of the worn surface of the B(SiC)-reinforced MMC pin tested at 1.0 m/s speed and 60 N load, showing smooth surface and reattachment of debris over the fractured fibre, leading edge left to right. ($V_f = 0.16$)

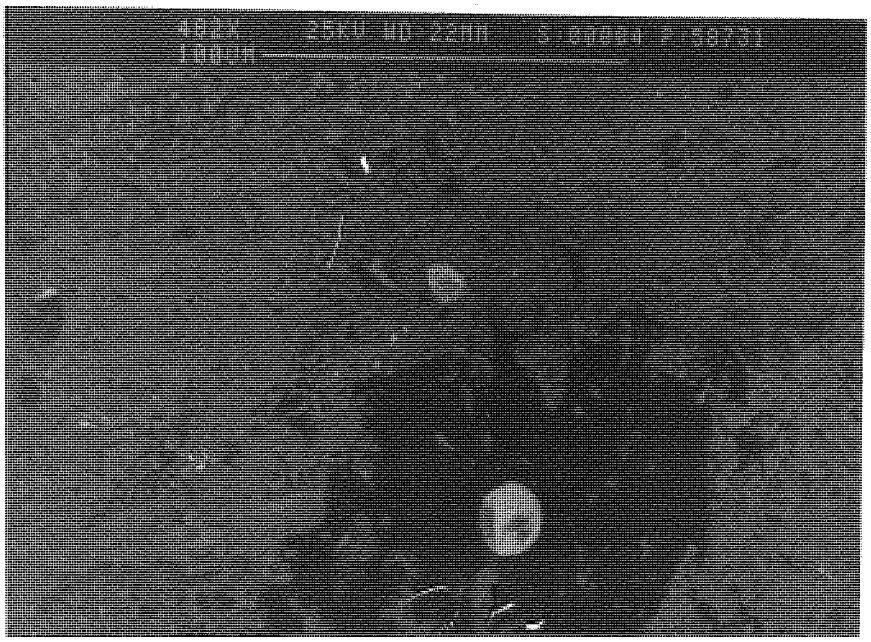

Figure 4.59. BSE image of the same sample of Figure 58, showing oxide particles embedded in the matrix and partially covering the fibre.

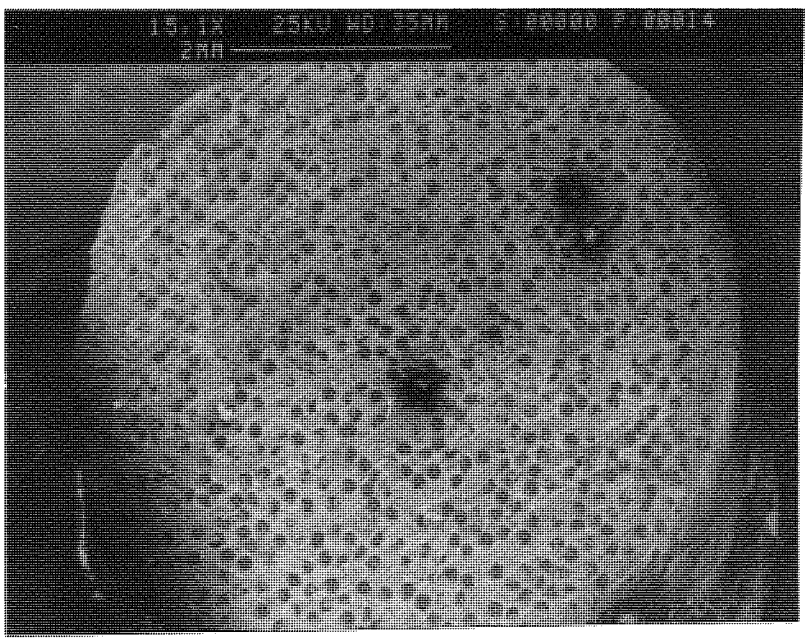

Figure 4.60. SE image of the worn surface of the B(SiC)-reinfoced MMC pin tested at 0.6 m/s speed and 22 N load, showing smooth surface, leading edge right to left. (Vf = 0.32)

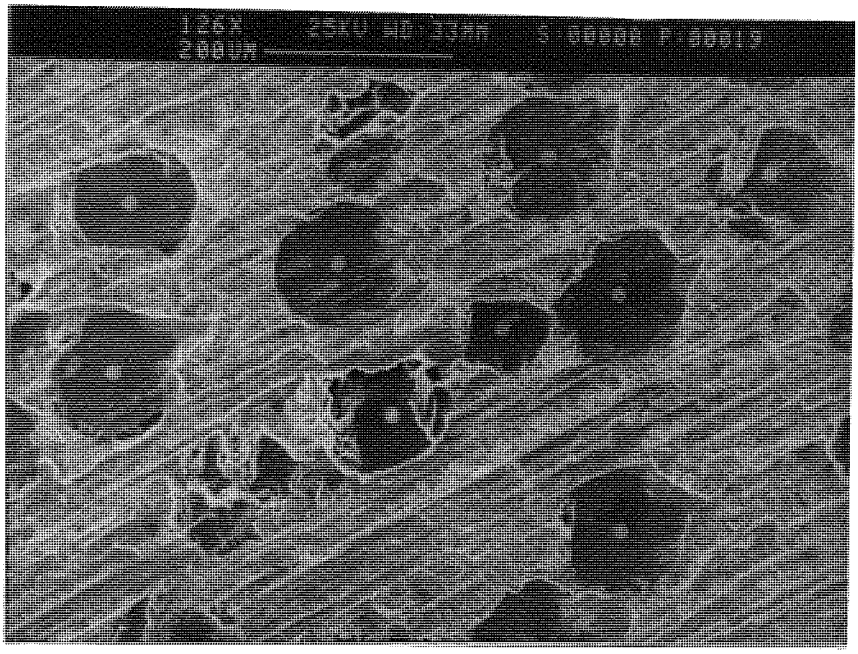

Figure 4.61. Higher magnification of the same sample of Figure 60, showing fracture of fibres in a brittle type and smearing of matrix.

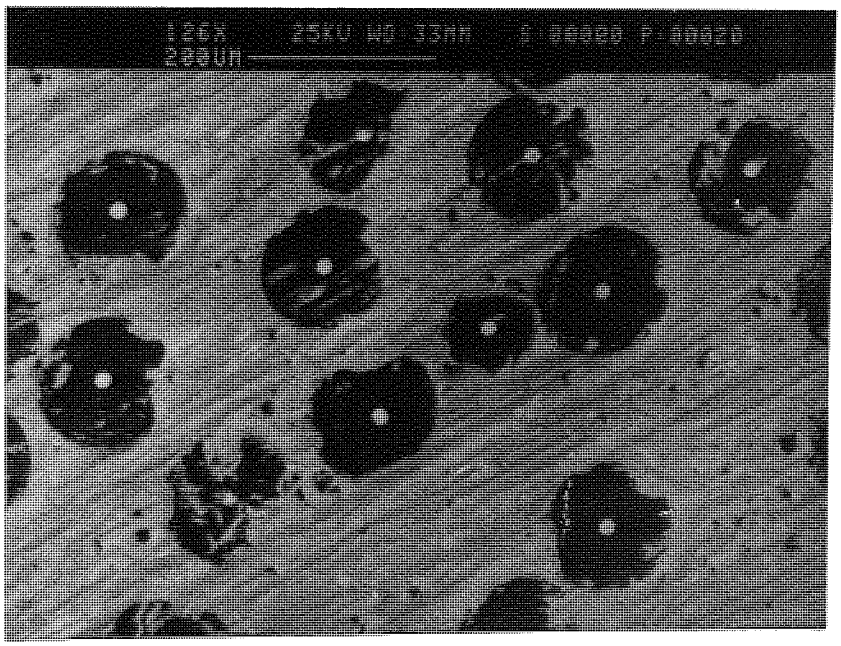

Figure 4.62. BSE of Figure 4.61, showing matrix smearing over the fractured fibre and embedded fractured particles in the matrix.

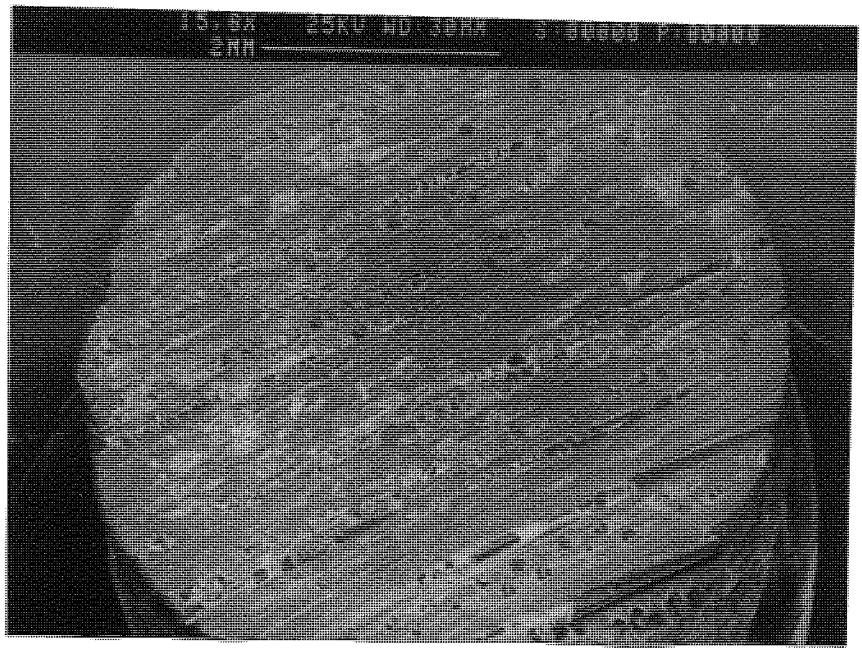

Figure 4. 63. SE image of the worn surface of a B(SiC)-reinforced MMC pin at 0.6 m/s speed and 22 N load, showing fibre fracture and removal from the surface, leading edge right to left.($V_f = 0.21$)

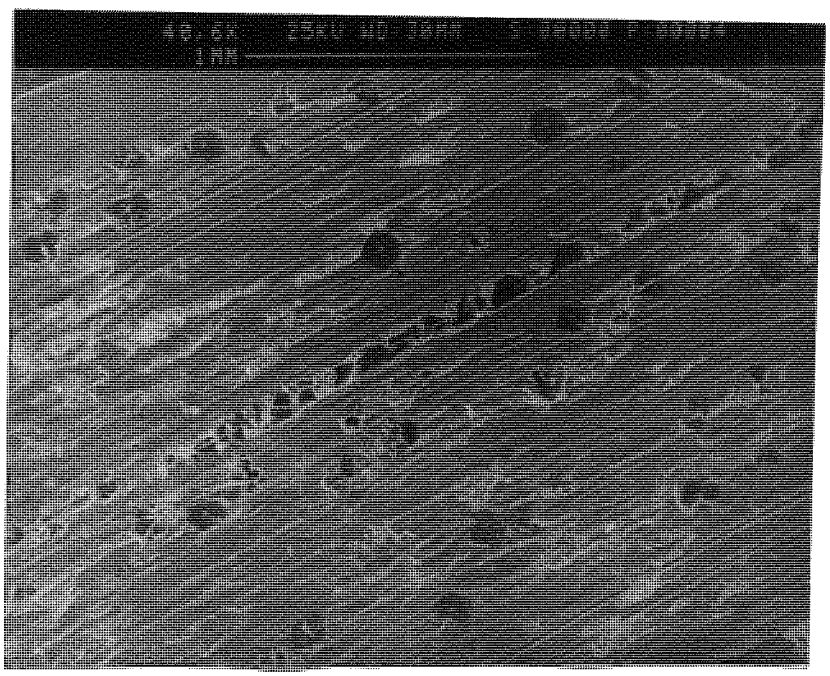

Figure 4.64. Increased magnification of Figure 63, showing more damage to the parallel orientated fibre.

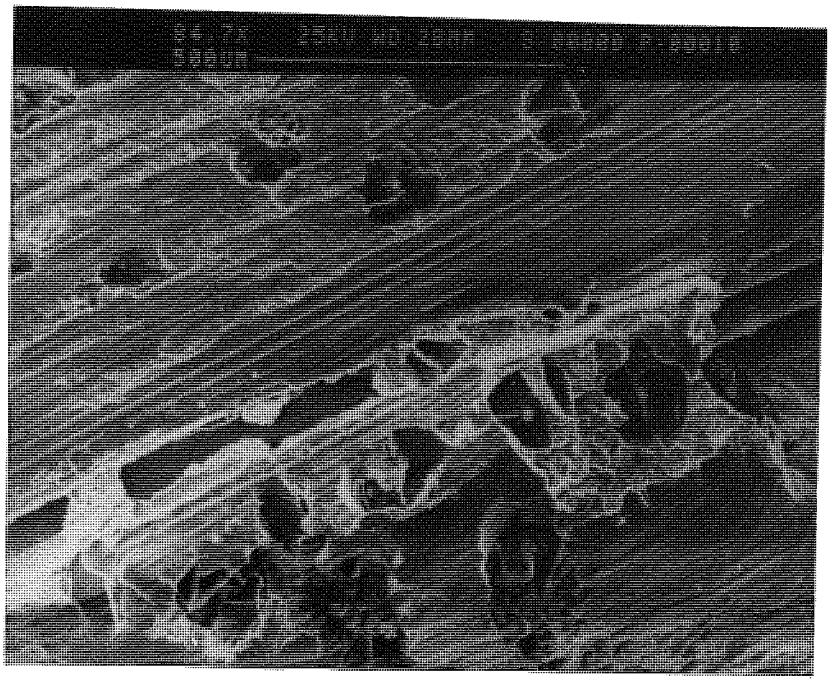

Figure 4.65. Higher magnification of the same sample of Figure 64, showing substantial fibre fracture and fibre removal from the parallel orientated place, beside distorted region at the bottom part of the sample.

A general picture of the dominant wear mechanisms which occurred in the N orientation was the microcracking, microfracturing of the fibre ends in a small pieces and the fractured part of the fibres were smeared by the matrix alloy. No evidence of fibre pull-out or sub-surface deformation could be observed in this orientation. Also broken fibre particles were embedded into the matrix.

As for as the P orientation is concerned, a general observation of the worn surface of the composite materials has been made using SE and BE image under the identical test conditions as in the N orientation samples. Figure 4.66 represents the worn surface of the 32% B(SiC) composite pin tested in the P orientation, leading edge was from right to left. This low magnification micrograph showed that fibres were peeled away from the surface for a speed of 1.0 m/s and load of 24 N. The fracture of tungsten cores and boron fibres

was also observed as shown in Figure 4.67 in BSE image. The removal of fibres was also visible over the composite pin surface.

Figure 4.68 shows the worn surface of the pin tested in the P orientation under same conditions at increased magnification, leading edge was from left to right. It appeared that the fibres first cracked into short segments owing to the tension and bending and the brittle nature of the fibres, then some of them were pulled out and tilted at an angle to the sliding direction. The size of the cracked particles varied considerably and the minimum length of these particles was about 30 μm. A smooth surface was observed between the exposed fibres.

Figure 4.69 shows the worn surface of the the composite pin at higher magnification in SE image. This figure indicated that the mechanism of ploughing and plastic deformation was the predominant for the sample. This might be because the some fibres removal from the contact region was further influenced by the ploughing and cutting of the matrix in between the exposed fibres, caused abrasion and increased the roughness of the disc and this was evidenced in Figure 3.9. Figure 3.9 shows the cross-sectional profiles of wear scars of B(SiC)/MMC pin against smooth steel under 22 N load for P and N orientations, at a speed of 1.6 m/s. In the P orientated composite sample, the roughness of the counterface was increased from initial roughness 0.12 μm CLA to a roughness of 0.48 μm at the end of the test.

Figures 4.70 and 4.71 show similar features but for the lower load of 12 N, in SE and BSE images respectively, leading edge was from left to right. First figure indicated that fibre bending and plastic deformation was observed at high magnification. The brittle fibre fracture was also evident due to tension effect and extensive debris particles were accumulated close to the fibre edge. The BSE image shows that iron had been transferred into the matrix surface, and matrix smearing over the fibre could be seen readily in this micrograph. Fragmentation of the debris was also evident in this mode.

Figure 4.72 represents a composite pin tested at a speed of 1.0 m/s and a load of 60 N load at high magnification. The sliding direction was from left to right. This figure showed

fibre thinning due to wear, and fracture including fracture of the tungsten core. Plastic deformation was also evident over the fibre surface, and there were many fractured fibres and cores. The size of the fibre core fracture could be varied significantly. Backscattered electron image of the sample is shown in Figure 4.73. The fractured fibres and cores were observed besides that some fractured particles about 10 μm.in size were embedded into the matrix.

Figure 4.74 shows the worn surface of the composite pin tested at 1.0 m/s speed and 24 N load, the 32% volume fraction of fibre was used for this test of the composite. The leading edge was from left to right. Again this figure indicated that extensive fractured/cracked fibres and cores were observed, the pieces of which were of a large size. The maximum length of the cracked fibre pieces was about 120 μm. Some debonding and loose particles were also evident. With repeated sliding, this resulted in short segments being removed from the surface of the sample.

As for the case of low sliding speed, Figure 4.75 shows the worn surface of the composite pin tested for a speed of 0.6 m/s and 12 N load. The sliding direction was from right to left. Fibre and core cracking were observed over the surface while some fibre removal was also evident in this sample. Titanium tape, used for binding fibres, was also observed on the pin surface as shown in BSE image of Figure 4.76, while a significant number of broken fibres and removal of fibres from their places are also shown in Figure 4.77 at increased magnification.

Figure 4.78 shows the worn surface of the composite pin reinforced with 27% volume fraction of fibre tested under identical conditions at low magnification. The sliding direction was from right to left. From this figure, fibre fracture and pulling-out appeared because of tension, in addition to the removal of fibres from the near edge. It was noted that at the edge of the sample, a lip was formed made of matrix material including pieces of fractured fibres.

As for the high sliding speed, Figure 4.79 represents the composite pin containing a 16% volume fraction of fibre tested for a speed of 1.6 m/s and at 12 N load. The sliding

direction was from right to left. This figure showed extensive fibre fracture at low magnification. Some shallow craters and grooving were also evident over this sample. Increasing velocity appeared to increase slightly the surface grooving. The increased magnification micrograph of Figure 4.80 also indicated that a considerable amount of fibre cracking and bending had occurred. Some removal of fibres was evident in the SE image which was about 400 μm long. A smooth surface appearance was observed over the matrix surface. Figure 4.81 shows the similar information of BSE image of the same sample.

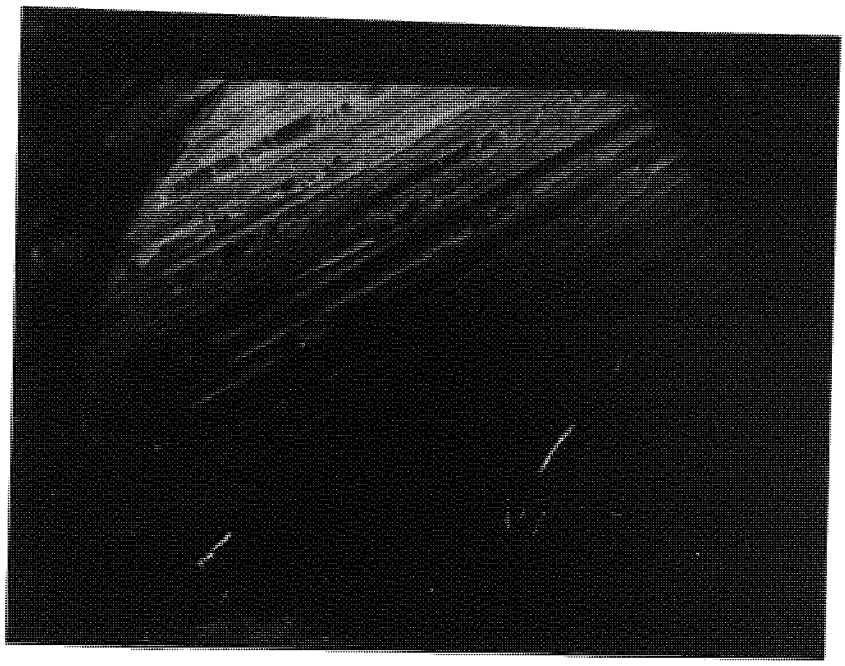

Figure 4.66. SE micrograph of a worn surface of a B(SiC) MMC pin tested in the P orientation for a speed of 1.0 m/s and 24 N load, showing peeling of fibres, leading edge upper right to lower left.($V_f = 0.32$)

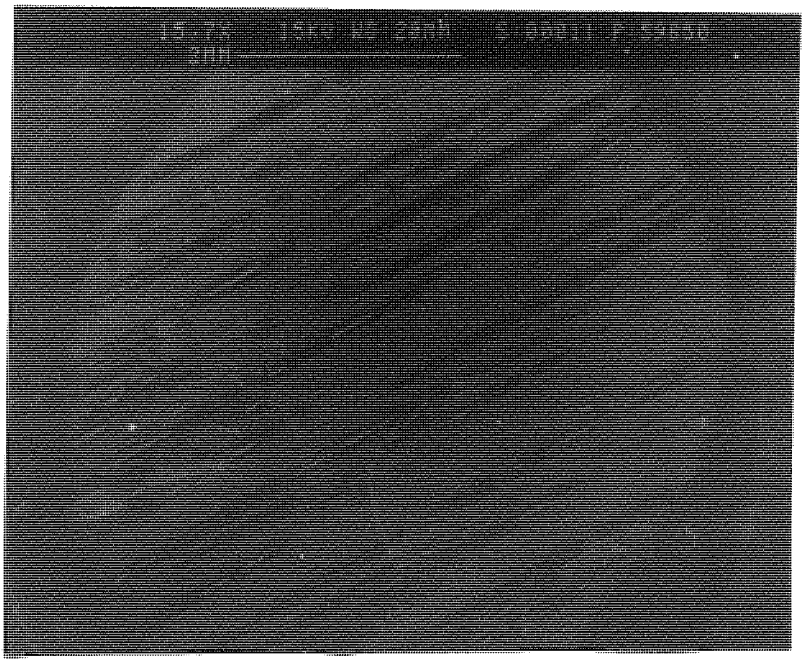

Figure 4.67. BSE image of the same sample of Figure 66, showing fracture of boron fibres and their tungsten cores.

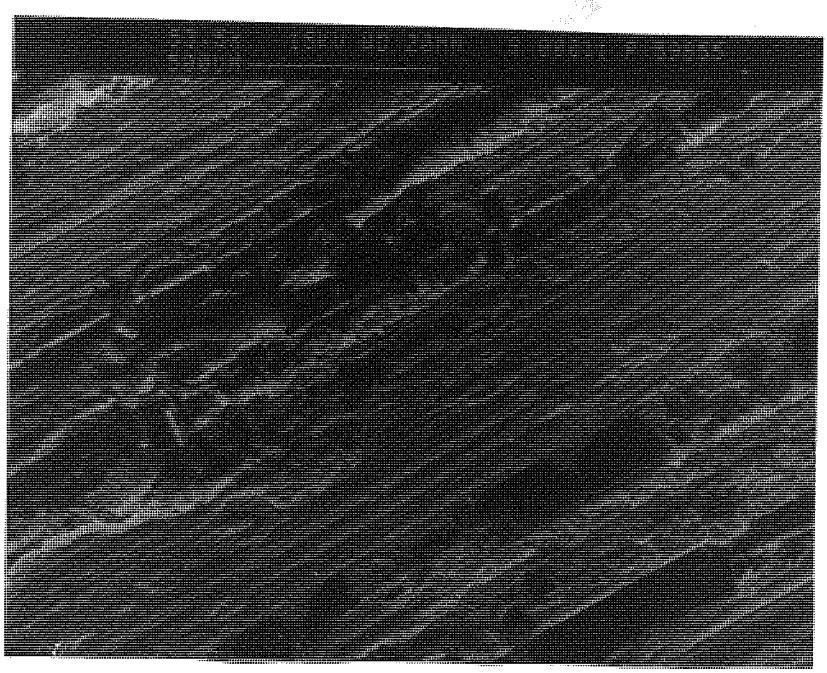

Figure 4.68. SE micrograph of the worn surface of the B(SiC)-reinforced MMC pin for a speed of 1.0 m/s and 24 N load, showing the cracked fibres and reversal of fibre to the sliding direction, leading edge lower left to upper right.($V_f = 0.32$)

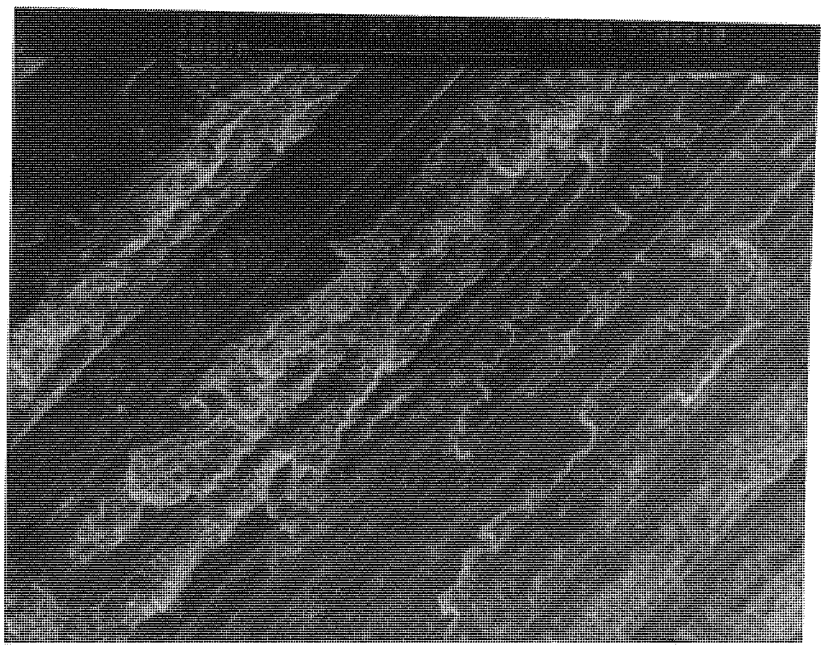

Figure 4.69. SE micrograph of the worn surface of the MMC pin under similar test condition at high magnification, showing microploughing and plastic deformation.

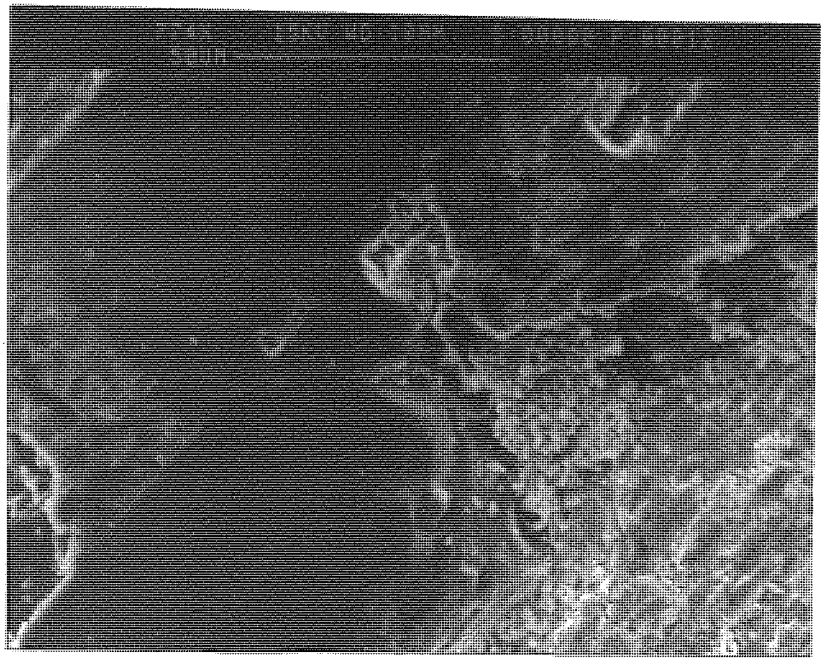

Figure 4.70. SEM micrograph of the worn surface of the MMC pin tested in the P orientation for a speed of 1.0 m/s and 12 N load, showing fibre bending,brittle fracture and plastic deformation under high magnification.

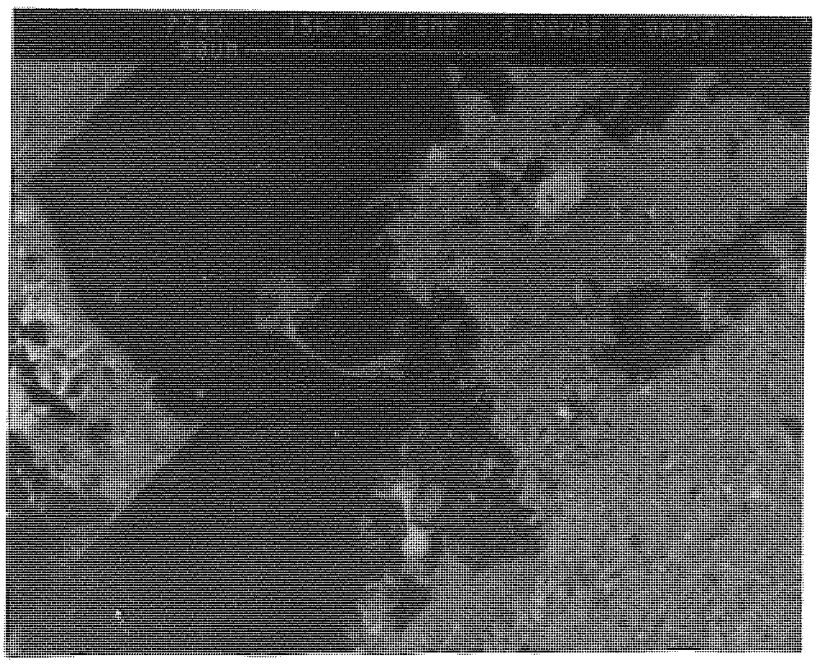

Figure 4.71. BSE image of Figure 70, fragmentation particles close to the fibre edge, transferred iron and smearing of matrix over the fractured fibres.

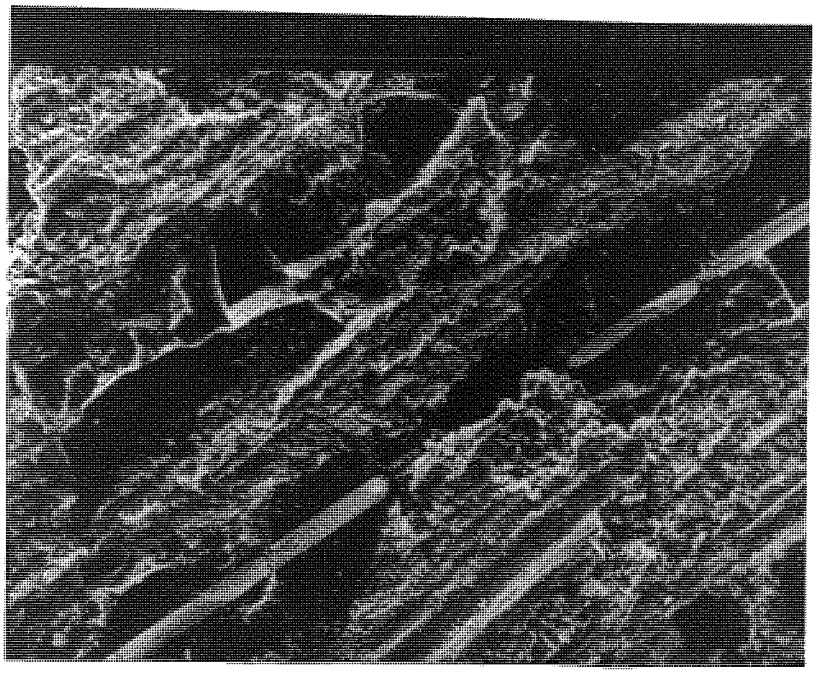

Figure 4.72. SEM micrograph of the worn surface of the B(SiC)-reinforced MMC pin for a speed of 1.0 m/s but under 60 N load, showing fractured tungsten core and fibre and matrix smearing, leading edge lower left to upper right.($V_f = 0.32$)

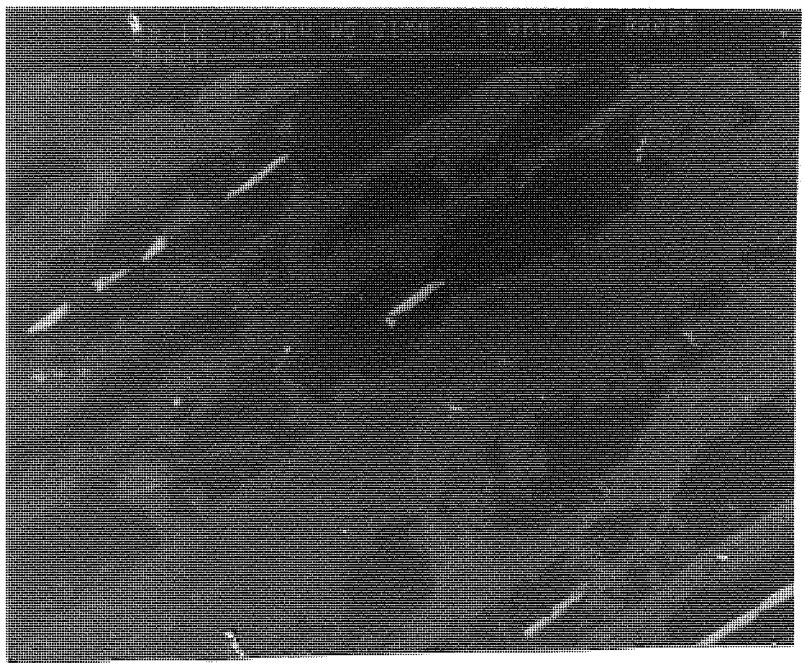

Figure 4.73. BSE image of Figure 72, showing fractured cores and fibres and their embedding into the matrix.

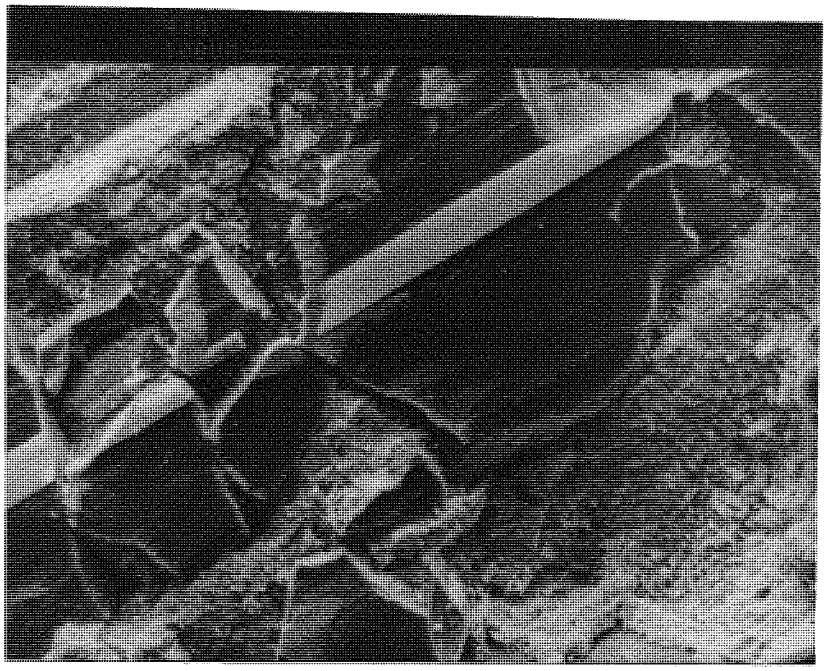

Figure 4.74. SE micrograph of the worn surface of the B(SiC)-reinforced MMC pin tested under same speed but 24 N load condition, showing catastrophic fibre and core fracture and debonding, leading edge to upper right.

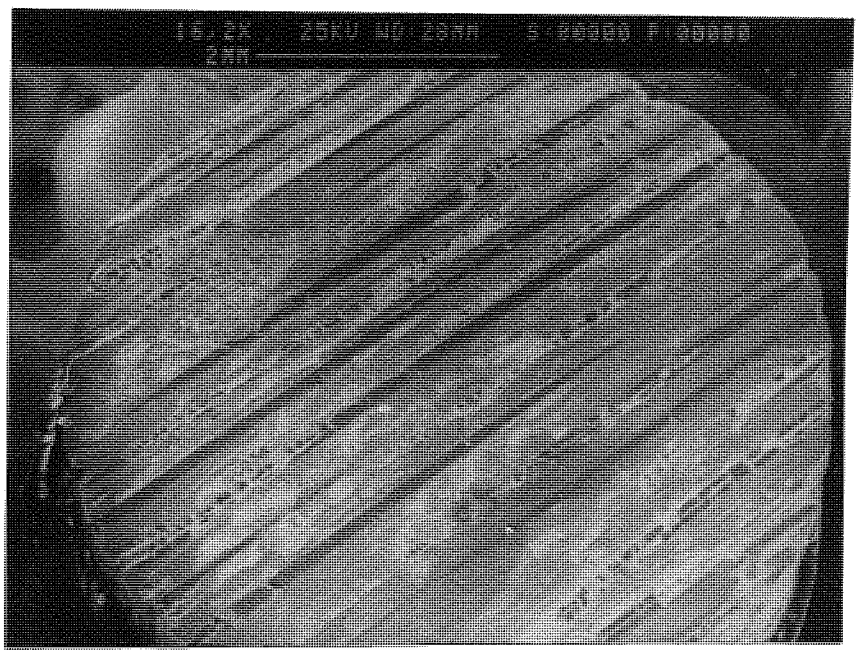

Figure 4.75. SE micrograph of the worn surface of the B(SiC)-reinforced MMC pin tested in the P orientation for a speed of 0.6 m/s and 12 N load, showing some of the broken fibres and fibre thinning, leading edge to lower left.

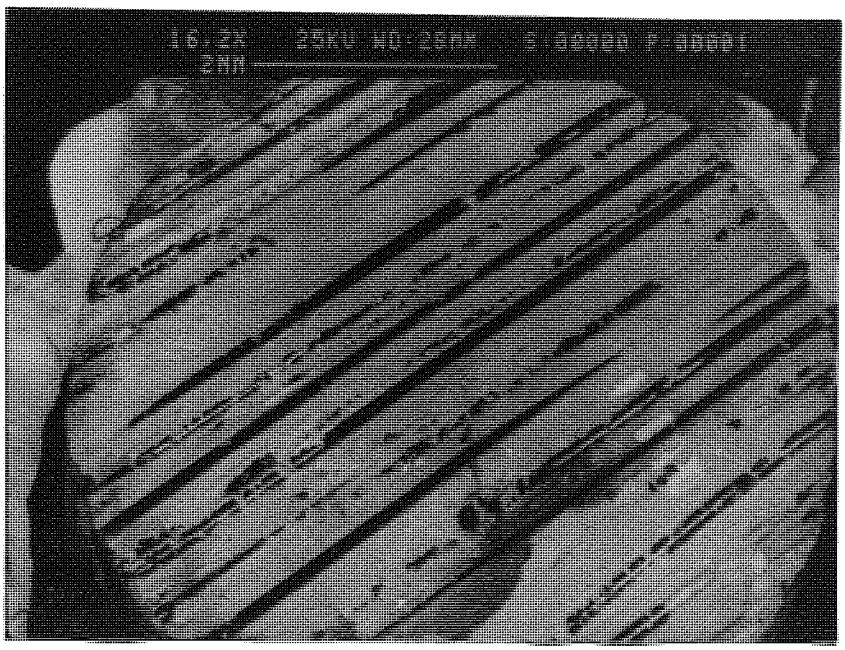

Figure 4.76. BSE image of Figure 75, showing broken fibres, cores, and titanium wire.

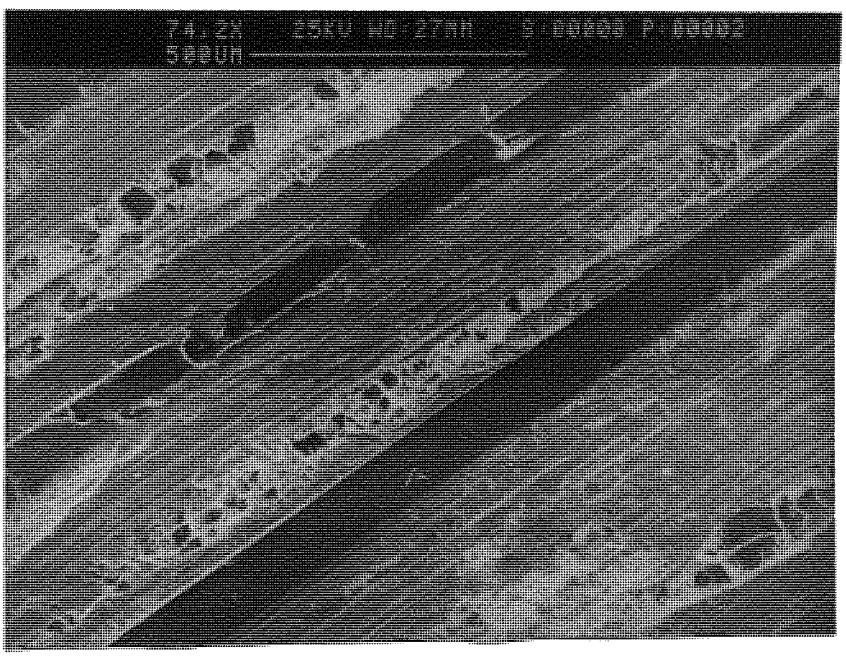

Figure 4.77. Increased magnification of Figure 4.76, showing significant broken fibres and removal of fibres from their places.

Figure 4.78. SE micrograph of the worn surface of the B(SiC)-reinforced MMC pin tested in the P orientation for a speed of 0.6 m/s and 22 N load, showing broken fibres and pulled-out fibres, leading edge to left.($V_f = 0.27$)

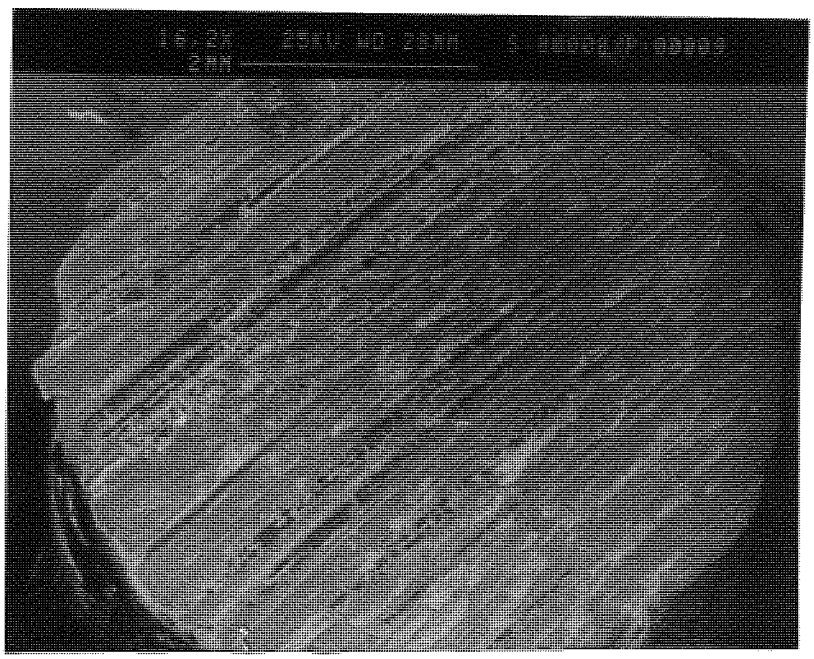

Figure 4.79. SE micrograph of the worn surface of the B(SiC)-reinforced MMC pin tested for a speed of 1.6 m/s and 12 N load, showing extensive fibre breakage and shallow craters, leading edge to left.($V_f = 0.16$)

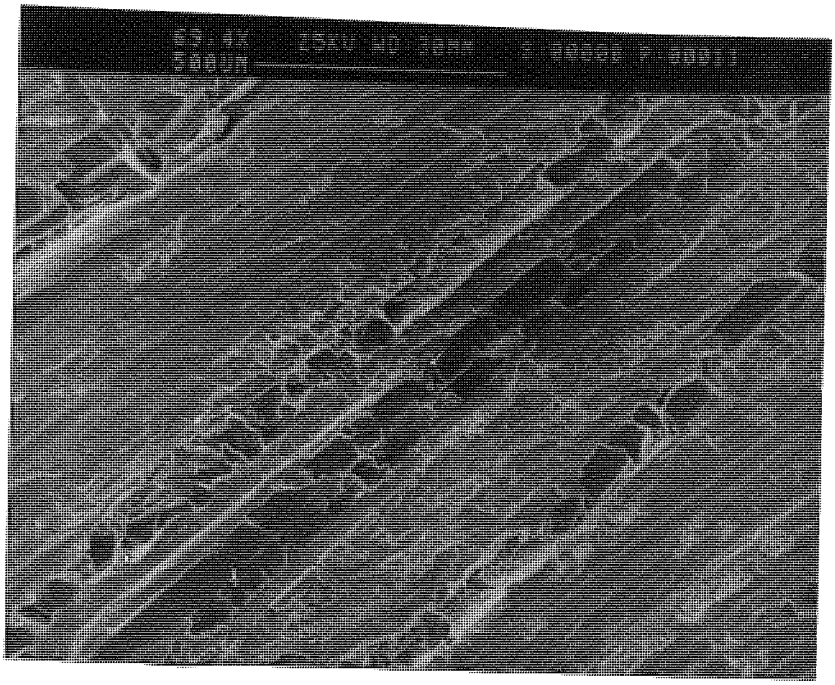

Figure 4.80. Increased magnification of Figure 79, showing considerable cracking of fibres into short segments and fibre bending.

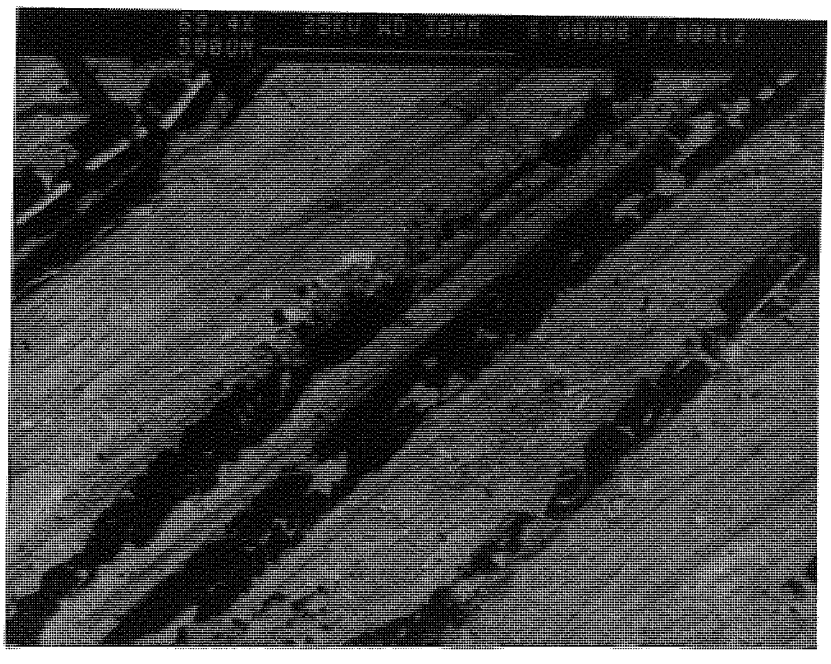

Figure 4.81. BSE image of the same sample of Figure 4.80.

Apart from the microscopic worn surface observation of the composite, the appearance of the wear debris as observed in the SEM, was found to be dissimilar to that of the tests of the aluminium matrix alloy. The typical wear debris obtained from the composite pin is shown in Figure 4.82. Small powdery agglomerated particles are present here. There was no change in appearance of the debris as a function of sliding speed and load.

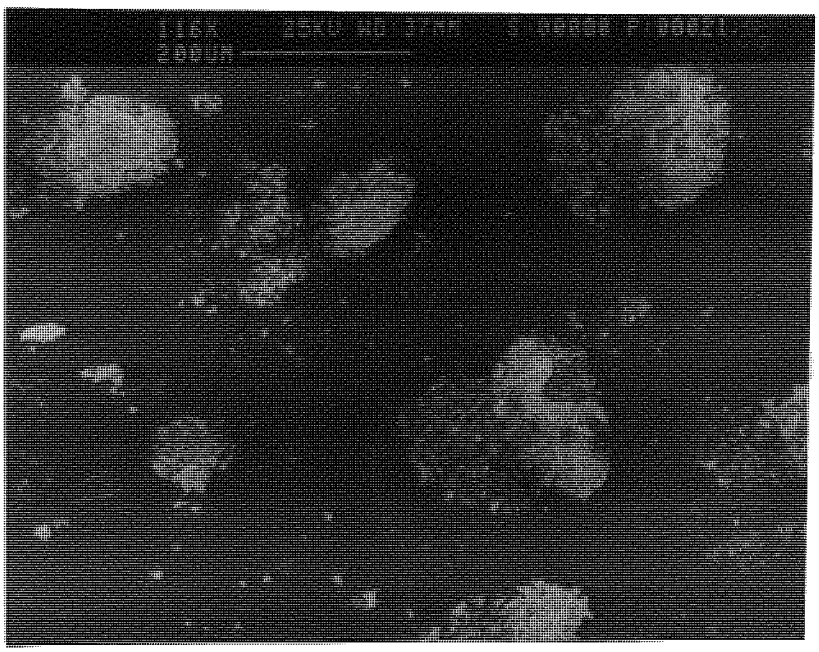

Figure 4.82. SE micrograph of typical wear debris generated from the B(SiC)-reinforced MMCs showing agglomerated fine particles.

A slightly different situation exists for the AP orientation although similar test conditions were used. For example, Figure 4.83 shows the worn surface of an MMC pin tested in the AP orientation at 1.0 m/s speed and 24 N load under low magnification. The sliding direction was from top to bottom. It was appeared that the fibres were broke into short pieces by deforming to a high degree due to bending. These separated fibre particles were then subsequently removed separately or some of these particles remained attached to

the surface. The shortness of these particles varied significantly from place to place. There was evidence more broken fibres at the right part of the pin surface while a small amount of grooving and a lump of matrix attached to the worn surface was also observed.

A BSE image of the same sample is shown in Figure in 4.84. It was observed that broken fibres and tungsten core particles were embedded in the surface, and smearing of the matrix was also evident over part of the broken fibres. Figures 4.85 and 4.86 show similar features for a composite pin at increased magnification in SE and BSE images respectively. The sliding direction was from top to bottom. The first figure showed that fibres were heavily fractured and the matrix smeared over the fractured fibres. The surface appearance looked smooth in spite of the fact that these fibre fractures had occurred. The latter one also indicated fracture of fibres, and small amounts of these particles were reattached to the surface. Some iron from the steel disc was transferred to the pin surface.

Highly plastically-deformed matrix was also observed at high magnification as shown in Figure 4.87. The deformed plastic matrix was smeared over the fractured fibre surface. The size of the pieces of fractured fibre was large, about 50-80 μm, and brittle fracture of the tungsten core can be seen. Similar features were found in the BSE image, which showed the sharply fractured core and smeared matrix over the surface of the pin. A BSE image of the worn surface of the composite is shown in Figure 4.88 at high magnification. The test was conducted at a speed of 1.0 m/s and 22 N load. This figure exhibited that catastrophic failure of fibres had occurred and resulting in heavy plastic deformation and matrix flow.

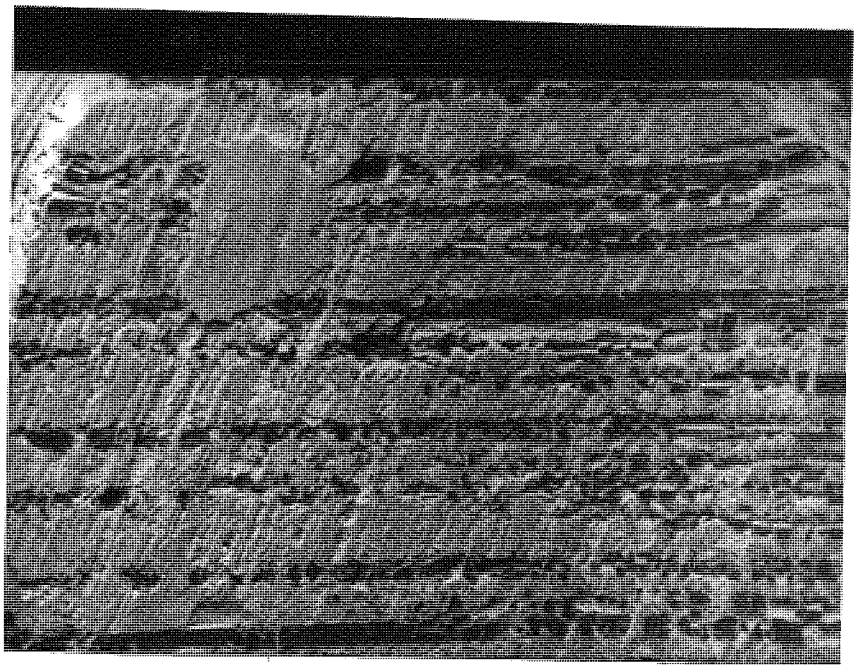

Figure 4.83. SE micrograph of a worn surface of a B(SiC)-reinforced MMC pin tested in the AP orientation at 1.0 m/s and 24 N load, showing fibre bending, fibre fracture and fibre removal from the place, leading edge at bottom.($V_f = 0.32$)

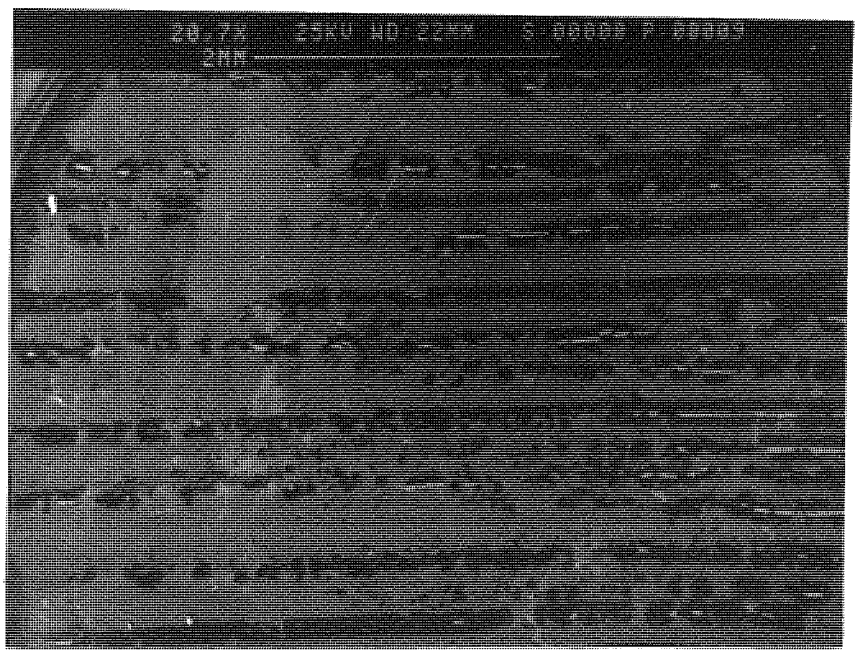

Figure 4.84 BSE image of Figure 83, showing pulled-out, fractured fibres embedded in the matrix.

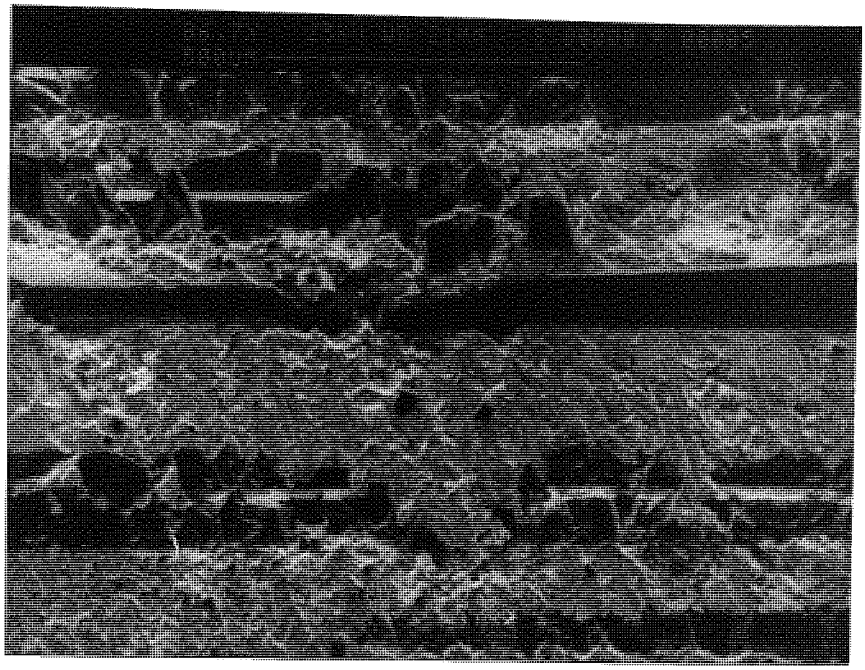

Figure 4.85. SE micrograph of the worn surface of the B(SiC)-reinforced MMC pin tested under the same condition of 24 N and 1.0 m/s speed in the AP orientation, showing fibre fracture and matrix smearing, leading edge to bottom.

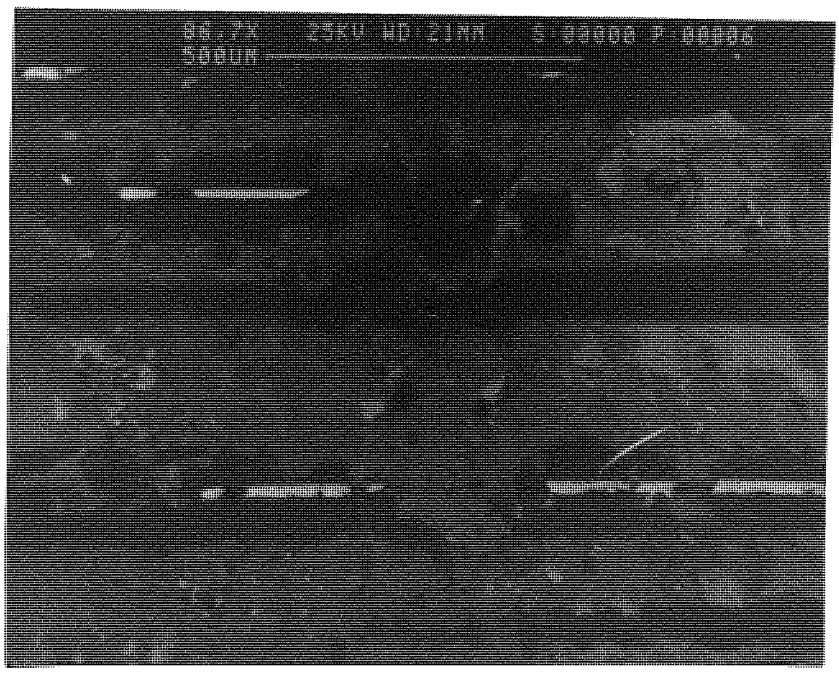

Figure 4.86. BSE image of Figure 85, showing fractured fibres smeared by the matrix and transferred iron.

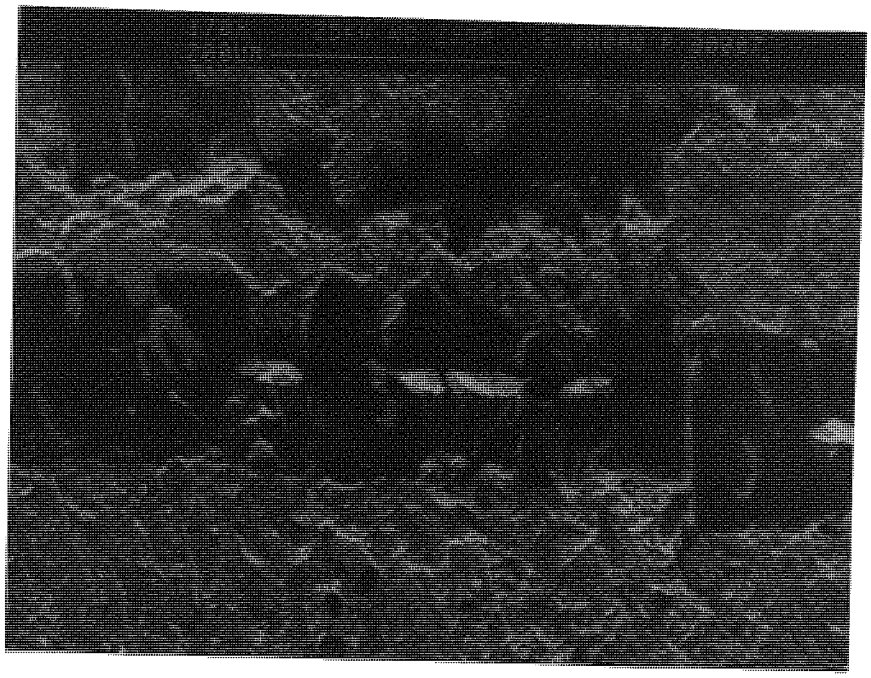

Figure 4.87. Increased magnification of Figure 86, showing plastically deformed matrix and damaged fibres and core ($V_f = 32\%$), leading edge to bottom.

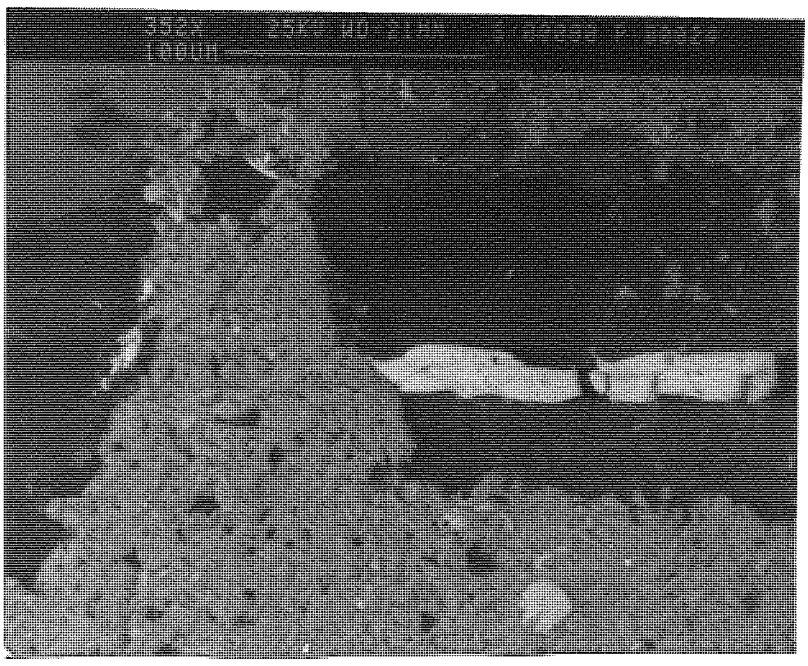

Figure 4.88. BSE image of SE micrograph, showing extensively broken fibre, core and embedded particles, leading edge to top.

The general wear mechanisms were similar to the P orientation. This might be due to having identical surface appearance but showed some minor difference. The predominant wear mechanisms were cracking, fracturing and pull-out of fibre. However, microploughing mechanism was absent for this orientation.

As discussed in the previous section in general, the N orientation generated the lowest wear rates while the AP orientation showed intermediate wear rates, but the P orientation exhibited the highest wear rates. The observation of the worn surface conducted by SEM showed a slightly different wear mechanisms for each of the main orientations. Therefore, the sections through the surface of the wear pin were examined under the same technique to determine the cause of this behaviour. The experimental tests were carried out under the same condition, namely the composite pins were tested for a speed of 1.0 m/s and 44 N load used for all orientations.

A characteristic micrograph of section through the wear surface of the pin tested in the normal to the sliding direction is shown in Figure 4.89 at high magnification. In this micrograph, there was a fibre (black) which was vertical to the horizontal plane at the right and the matrix (grey) on the left side of the sample and deformed matrix layer on the top of the micrograph, and a SiC layer (light grey region) between the fibre and matrix was observed. This figure further demonstrated that the fibre ends were cut or fractured in a slicing manner and splinters of fibres were generated. The length of the pieces of fractured fibre was about 20-25 μm long and the deformed metal was approximately 10 μm deep.

Backscattered electron image of the same sample is shown in Figure 4.90, showing smeared matrix over the fibre ends and SiC surface layer on the boron fibre appeared large width because of shallow-angle section. As far as high sliding speed is considered, the worn surface of a composite pin is shown in Figure 4.91 at low magnification by mixture of SE and BSE image.in which the test was conducted at a speed of 1.6 m/s and load of 22 N. This figure also showed that fibre breakage had occurred, but a bigger fibre-damaged area was readily seen on the pin surface. The depth of damage to the fibres was about 80-150 μm, hence more fibre breakages resulted in higher wear rates in this case. Higher

magnification of the same sample is shown in Figure 4.92. Fibre breakage and smearing of the fibres was observed, but fibre damage was also found to be more and the minimum and maximum length of the fibre breakage was about 20-170 μm.

In the case of the parallel orientation, Figure 4.93 shows a section through the wear surface of the composite pin parallel to the sliding direction, tested under similar condition at high magnification. The profile of the worn surface showed evidence of a subsurface damage zone, and matrix cracks beside fibre splinters. This zone was composed of areas of fibre/matrix debonding. The sub-surface layer was about 40-60 μm, while the average length of fibre splinters were about 30-60 μm. The BSE image of Figure 4.94 shows the deformed layer underneath the wear track. It also shows many oxide debris particles.

Figure 4.94 shows a section through the wear surface of the composite pin tested in AP sliding direction under similar conditions. This section was normal to the sliding direction so that damage to the fibre could be studied. A substantial fibre breakage was observed close to the wearing surface beside a small amount of subsurface deformation, while the high magnification BSE image of the surface of Figure 4.95 showed a subsurface deformation layer and surface fatigue cracks. The depth of the layer was about 100-120 μm, and titanium layer resulted from the binding tape in the pin was also evident over the surface in BSE mode. The surface fatigue cracks were about 40-60 μm long. Some adherence debris was also observed over the surface.

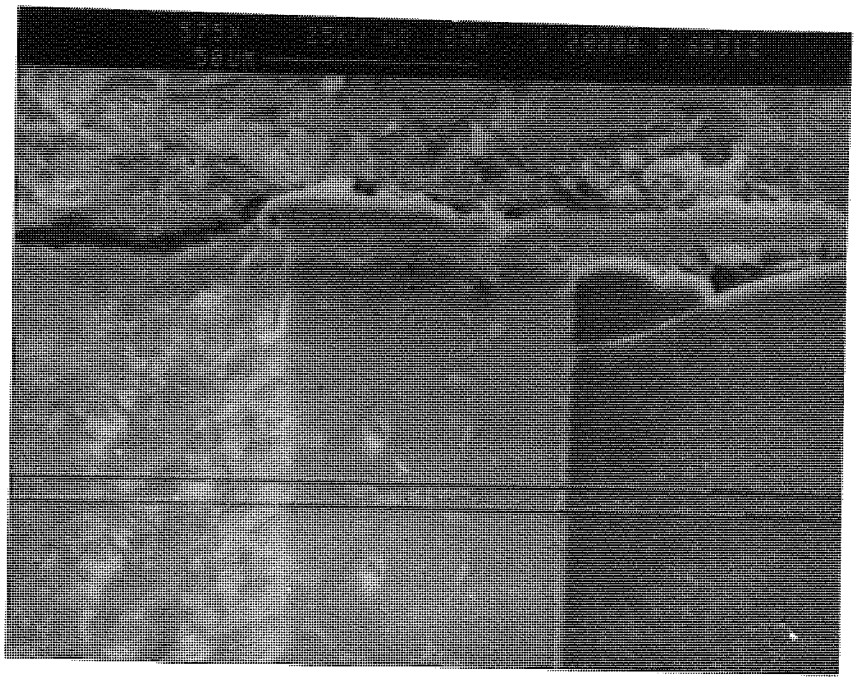

Figure 4.89. SE micrograph of section through the wear surface of the MMC pin tested normal to the sliding direction for a speed of 1.0 m/s and 44 N load, showing fractured of fibre end, deformed and smeared by the matrix material.($V_f = 27\%$)

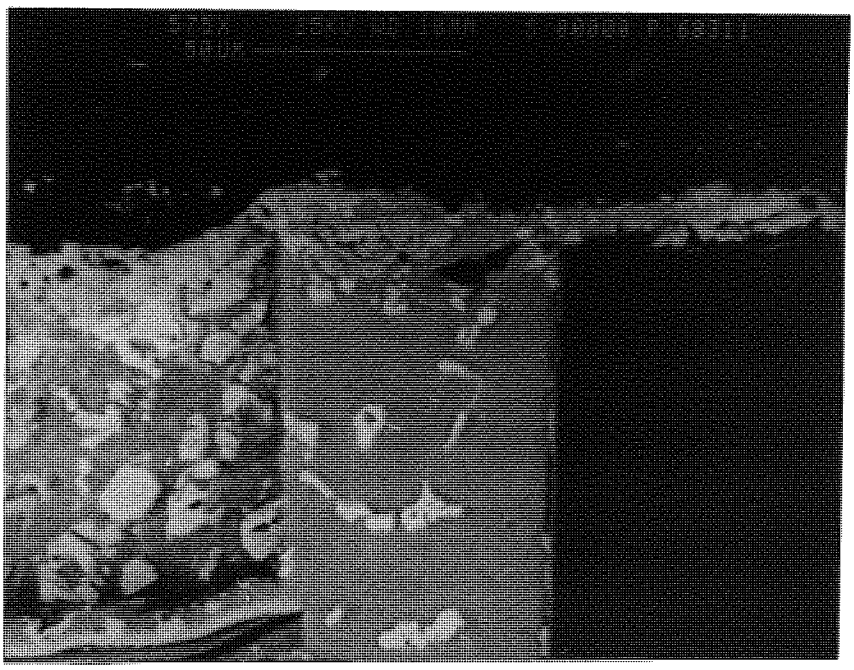

Figure 4.90. BSE image of the same sample of Figure 89, showing the damaged matrix over the fractured fibre end.The light grey region in the SiC surface layer on the B fibre, the apparent large width due to a shallow-angle section.

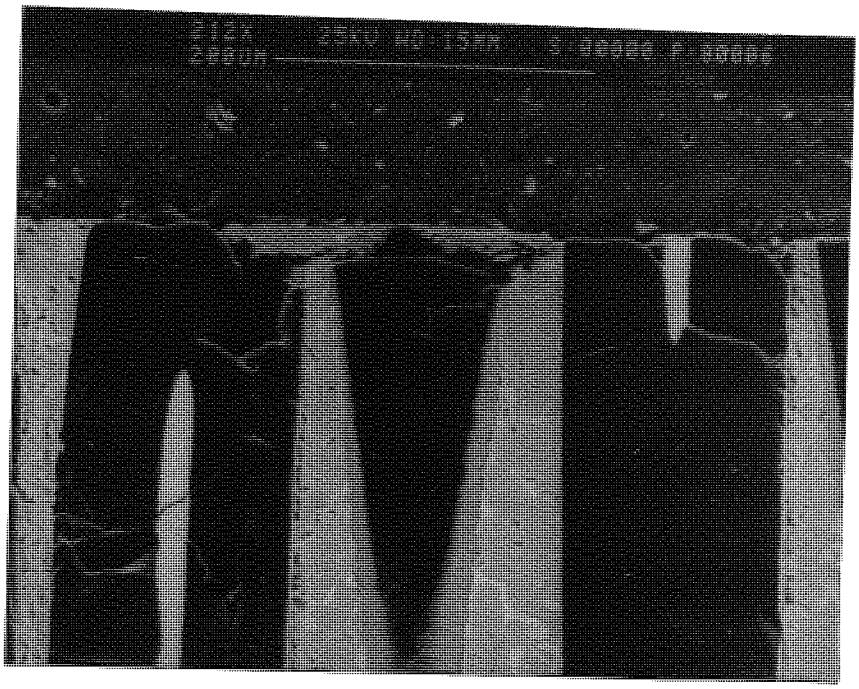

Figure 4.91. SE micrograph of the worn surface of the MMC pin tested normal to the sliding direction for a speed of 1.6 m/s and 22 N load, showing deep fibre fracture underneath of the surface beside matrix smearing at high magnification.($V_f = 0.32$)

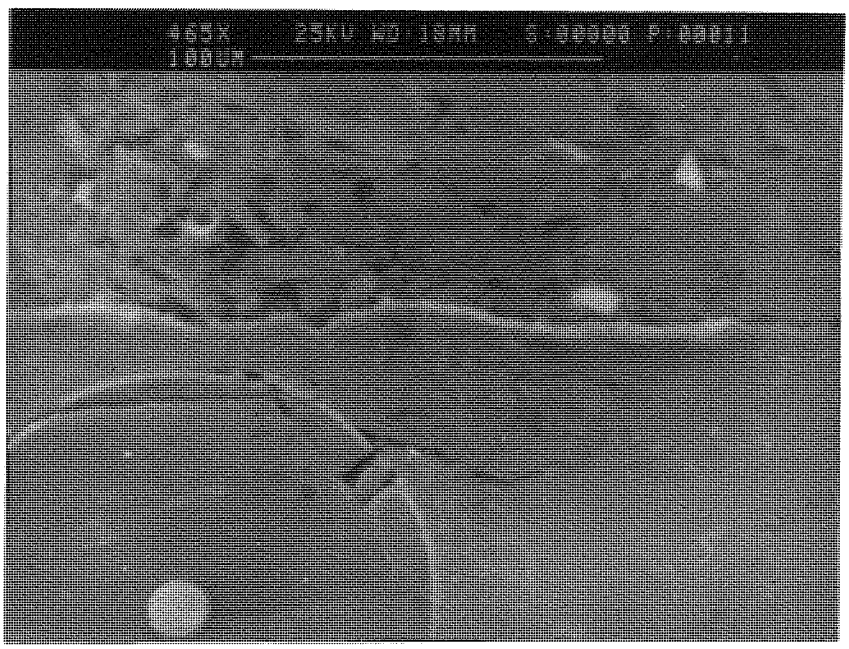

Figure 4.92. SE micrograph of section through the wear surface of the MMC pin tested parallel to sliding direction under similar condition showing subsurface plastic deformation.

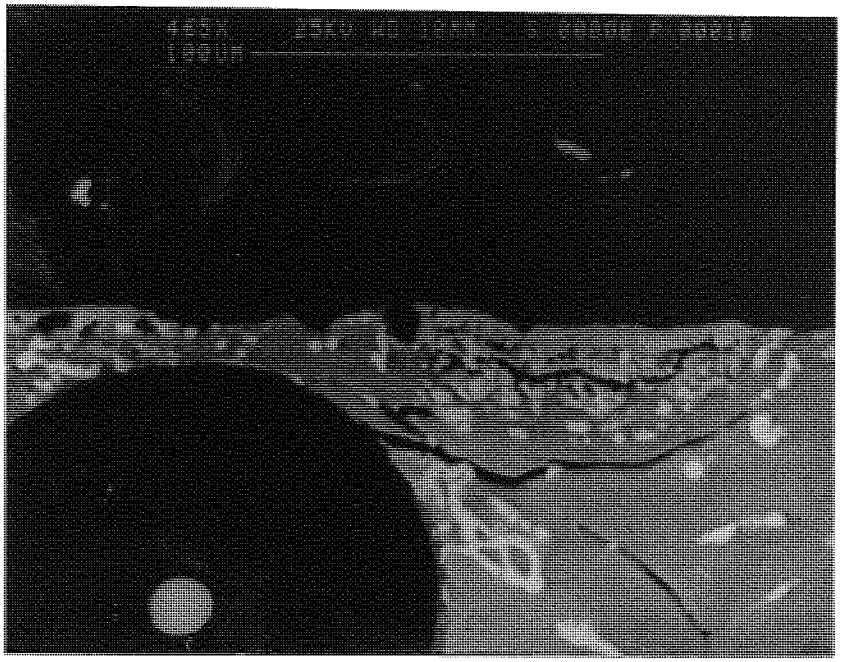

Figure 4.93. BSE image of the same sample of Figure 4.92, showing deformed layer and cracks.

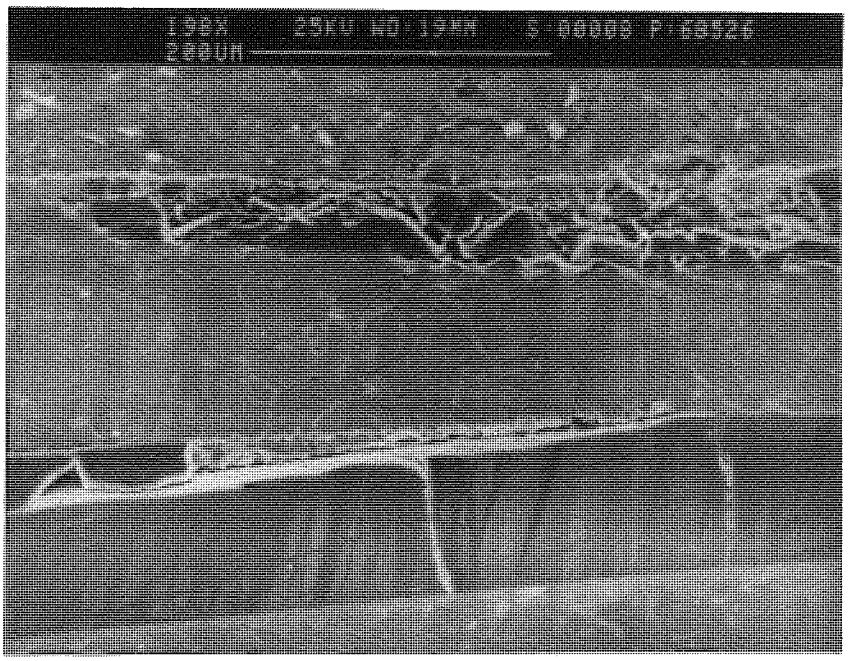

Figure 4.94. SE micrograph of section through the wear surface of the MMC pin tested AP sliding direction under similar condition, showing extensively fractured fibres.

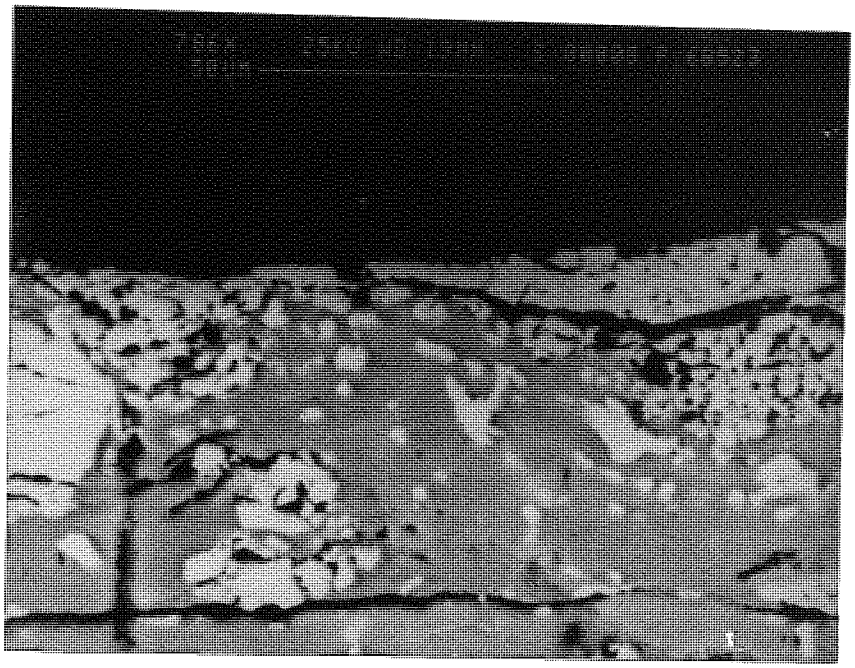

Figure 4.95. BSE image of section through the wear surface of the MMC pin at higher magnification, showing the deformed layer and cracks due to surface fatigue.

4.1.8 X-Ray Photoelectron Spectroscopy on Worn Surface

The worn surfaces of the MMC pins were analyzed by XPS to determine the nature of the surface composition. Tests were conducted under similar conditions only for the N and P orientations of the 32% composite. Typical XPS spectra are shown in Figures 4.96 to 4.101 and the chemical compositions of the worn surface are listed in Table 8. Figure 4.96 shows the XPS plot recorded for a worn pin tested in the N orientation at a speed of 0.6 m/s under 22 N load. This figure indicated that O, C, B, Al, Fe, Si and N were present. The oxygen peak was more intense than the others, carbon, iron and boron gave small peaks but the others were very small.

Figure 4.97 shows similar spectral information for an N orientated sample tested at a speed of 1.6 m/s under 12 N load. This spectrum were chosen from a selection of the experiments to illustrate the dependency on such factors as load and speed. Similar elements were detected on the worn surface of the pin, but the carbon peak was relatively high in this case of the orientation.

Figure 4.98 shows another spectrum of the same load, but the test was conducted at a speed of 0.6 m/s in the P orientation of the composite under the same load. The spectrum of all elements were generally the same as those with the exception that B and Al peaks were more pronounced and O and C was predominant in this sample. The numerical results obtained from XPS were recorded and showed similar trends to those shown in the above figures. However, a more in-depth look was taken of these spectra with respect to the effect of fibre orientation. Such an example is shown in Figure 4.99,which shows a greatly expanded part of the recorded spectrum of Figure 4.96. In this figure, basically two components boron containing boron oxide (B_2O_3) and iron boride (FeB_2) were formed, and corresponding to binding energy peaks of about 36.0, 26.2 amplitude (in k constants of 2 kc and 13 kc) respectively. Apart from O, the main elements presented on the worn surface of the sample were Fe, B, Al and C. As atomic percentages, the amounts of the

elements were as follows : Fe : 9.49%, B : 21.56%, Al : 3.40% and C : 29.00 % in this XPS plot, as shown in Table 8.

In the case of the expanded region of Figure 4.97, shown in 4.100, the similar components of boron oxide and metallic boride appeared but with quite different contents. For example, both the FeB_2 peak and B_20_3 boron peak had amplitudes of 2 kc, i.e.FeB_2 boron had decreased a factor of 6 or more whilst B_20_3 was about the same. Evidenced that total FeB_2 had decreased considerably amount of is given by the compositions listed in Table 8, thus total B decreased from 21.46% to 9.38% and Fe also decreased from 9.49% to 2.20%, whereas Al and C increased significantly from 3.40% to 12.45% and from 29.00% to 43.00% respectively for this case of this test condition, (high speed and low load).

Figure 4.101 shows the expanded area of the P orientated sample of Figure 4.98 and the same two components were also observed here, but FeB_2 boron had increased slightly to 3.4 kc in amplitude, while B_20_3 boron remained at 2kc as in the other samples. Table 8 shows a total boron content of 12.1% (up to 9.4%), but much lower Fe content then before. In the other samples the ratio or Fe/B was very roughly equal to the 1/3 ratio expected, but their case the Fe/B ratio was very low.

Considering these results with the data in Table 8, it is clear that the amount of O in the surface is more or less independent of wear conditions and orientations. However the B content changed appreciably, more B in the N orientated low speed, high load samples and also most of this extra boron in the form of an intermetallic compound FeB_2.

The situation in the P orientated sample is less clear, the amounts of Fe, despite the low load, is higher than in the low load N orientated sample according to the graph, but much lower according to Table 8 analysis. The reason for this is not known.

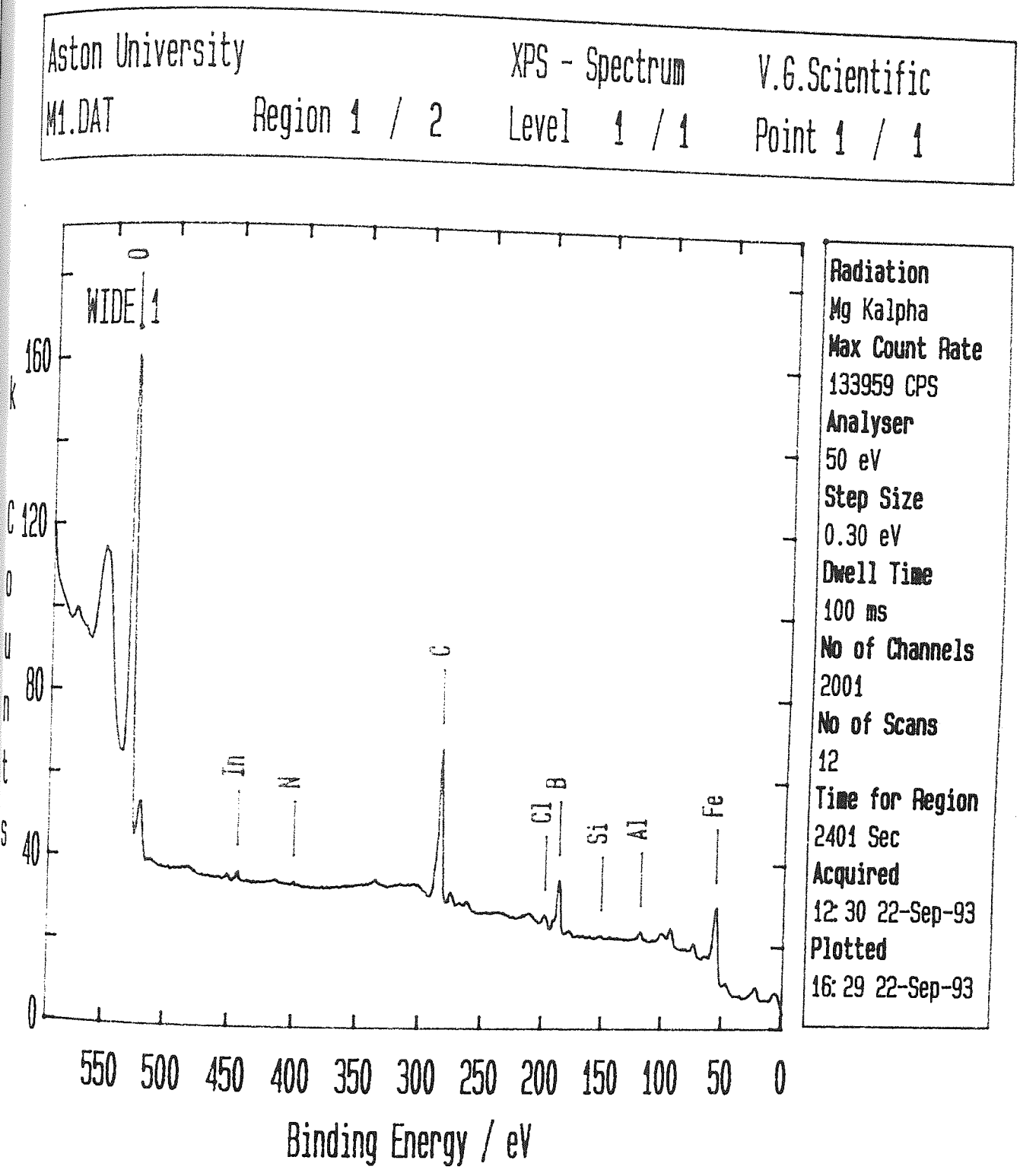

Figure 4.96. XPS analyses of a worn surface of a composite pin sample run at a speed of 0.6 m/s and a load of 22 N in the N orientation.

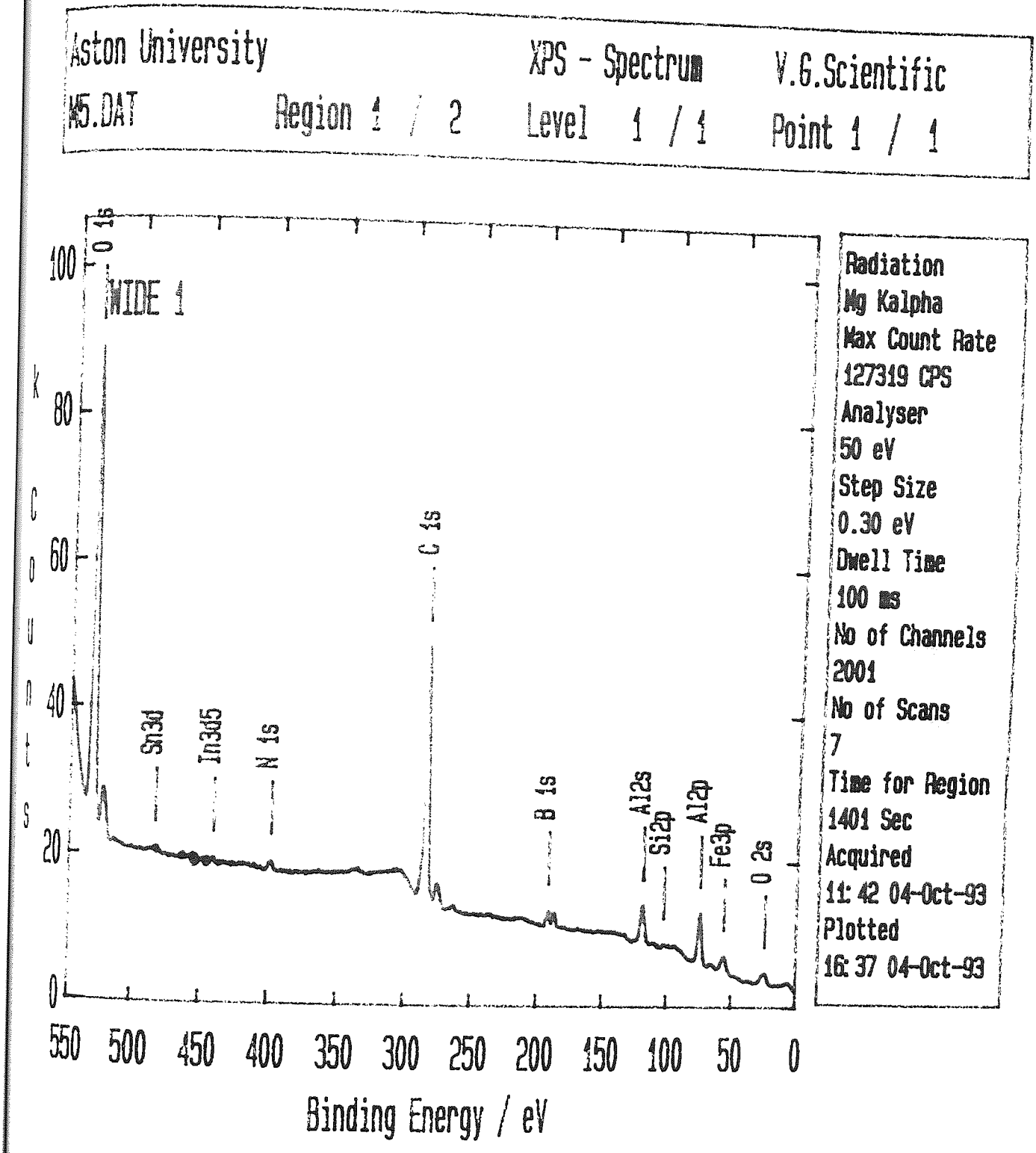

Figure 4.97. XPS analyses of the worn surface of the composite pin run at a speed of 1.6 m/s and a load of 12 N in the N orientation.

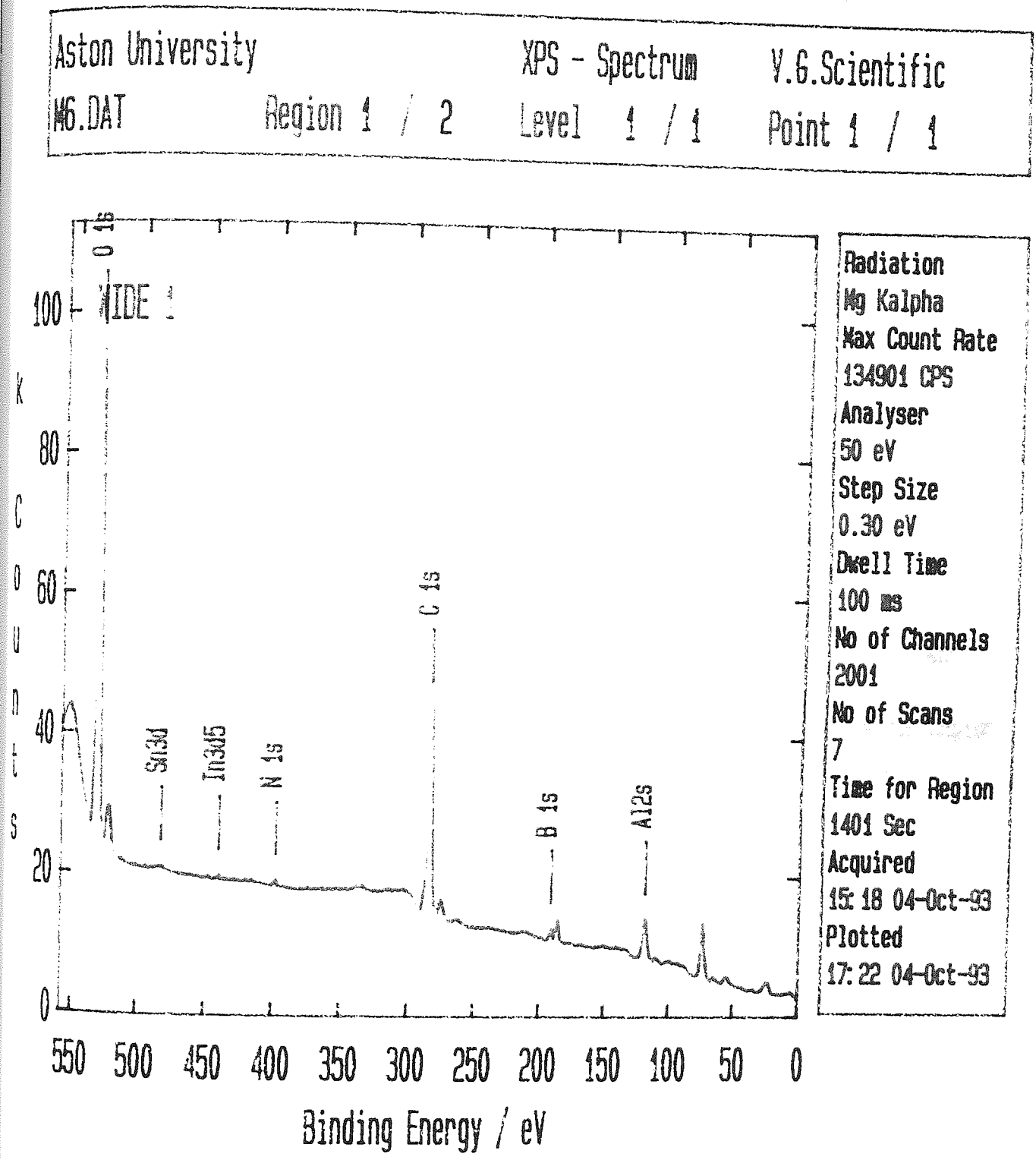

Figure 4. 98. XPS analyses of the worn surface of the composite pin run at a speed of 1.6 m/s and a load of 12 N in the P orientation.

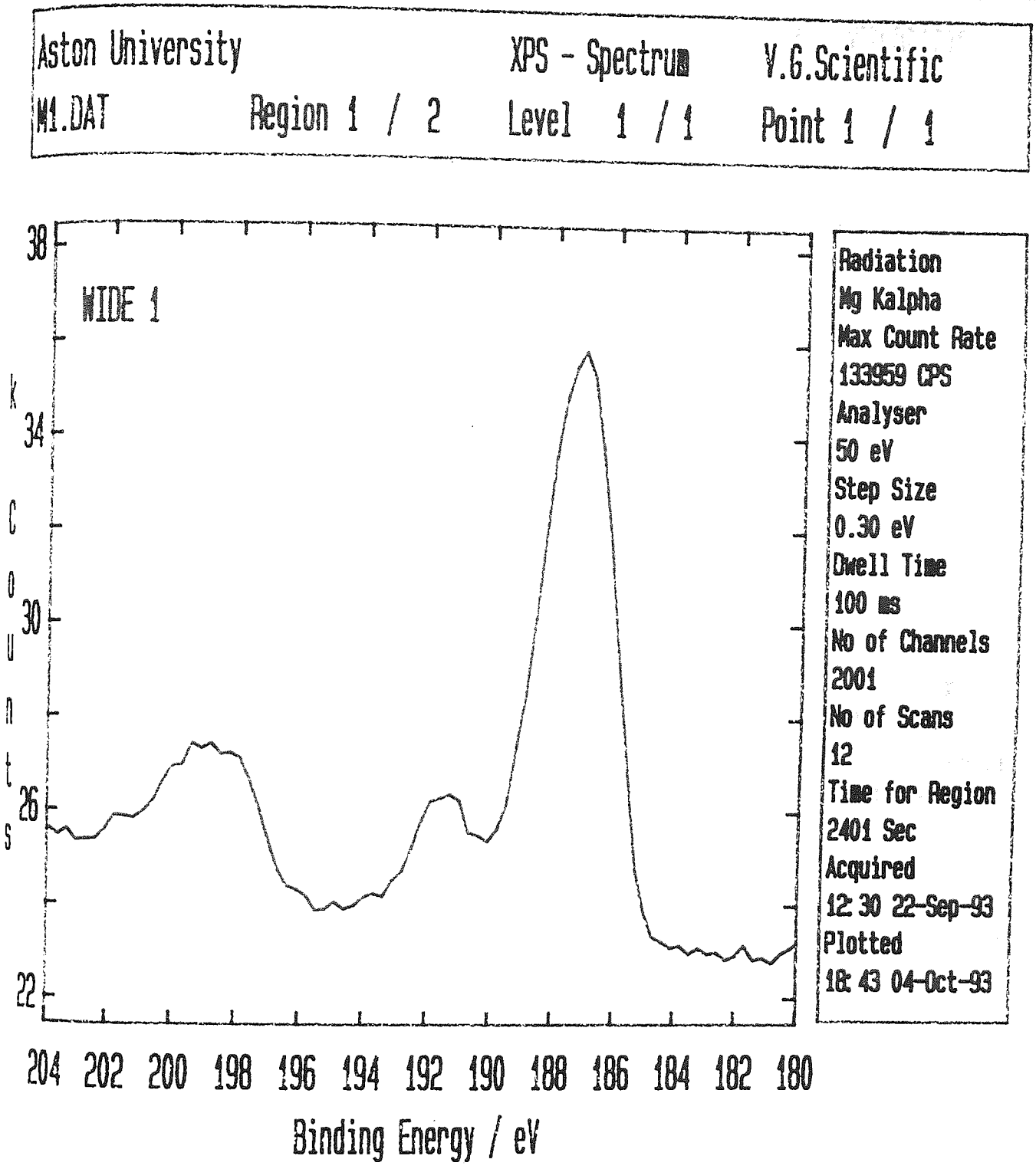

Figure 4.99. XPS analyses of the worn surface of the N orientated composite pin.(Load = 22 N, Speed = 0.6 m/s)

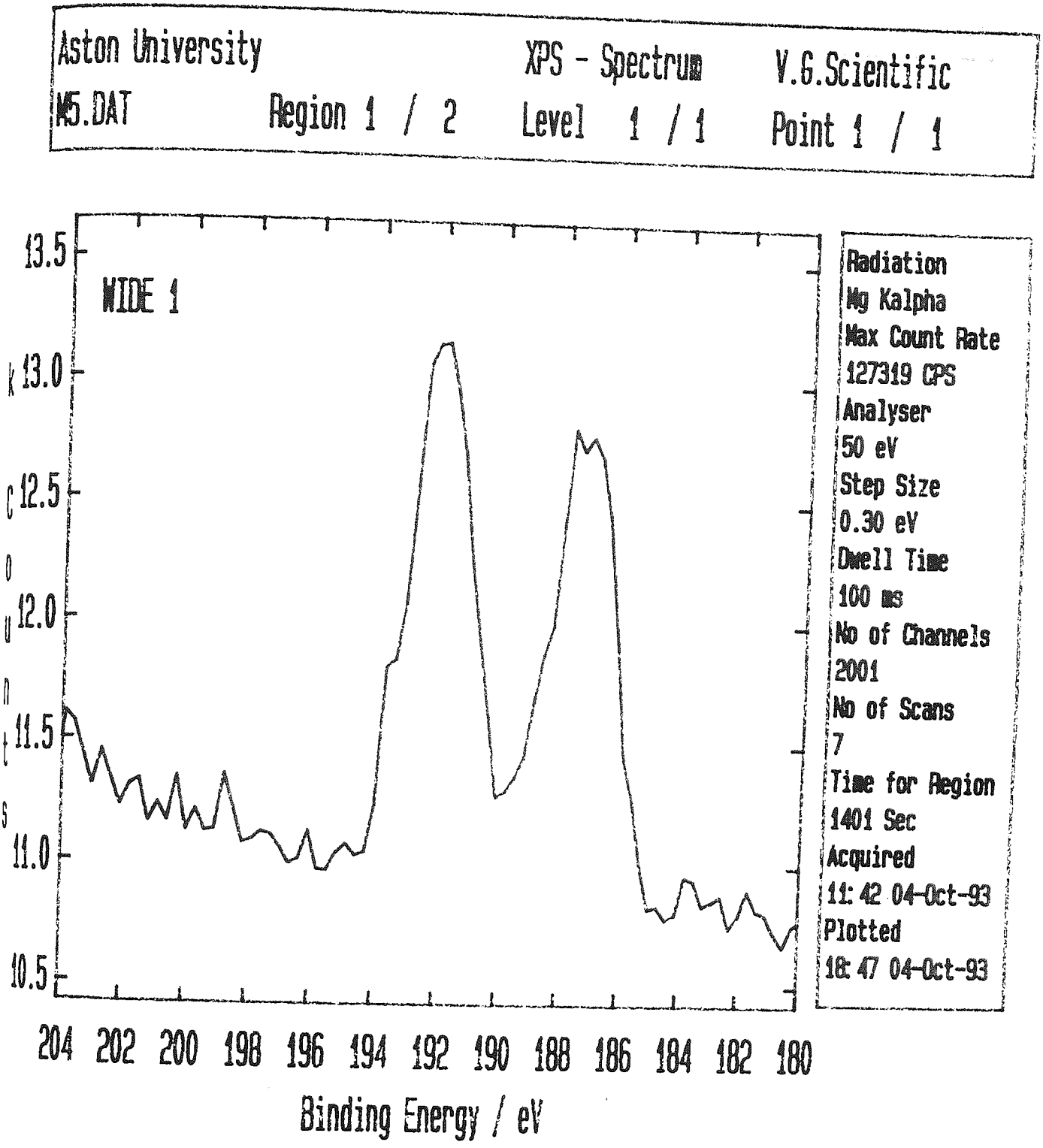

Figure 4.100. XPS analyses of the worn surface of the N orientated composite sample.(Load = 12 N, Speed = 1.6 m/s)

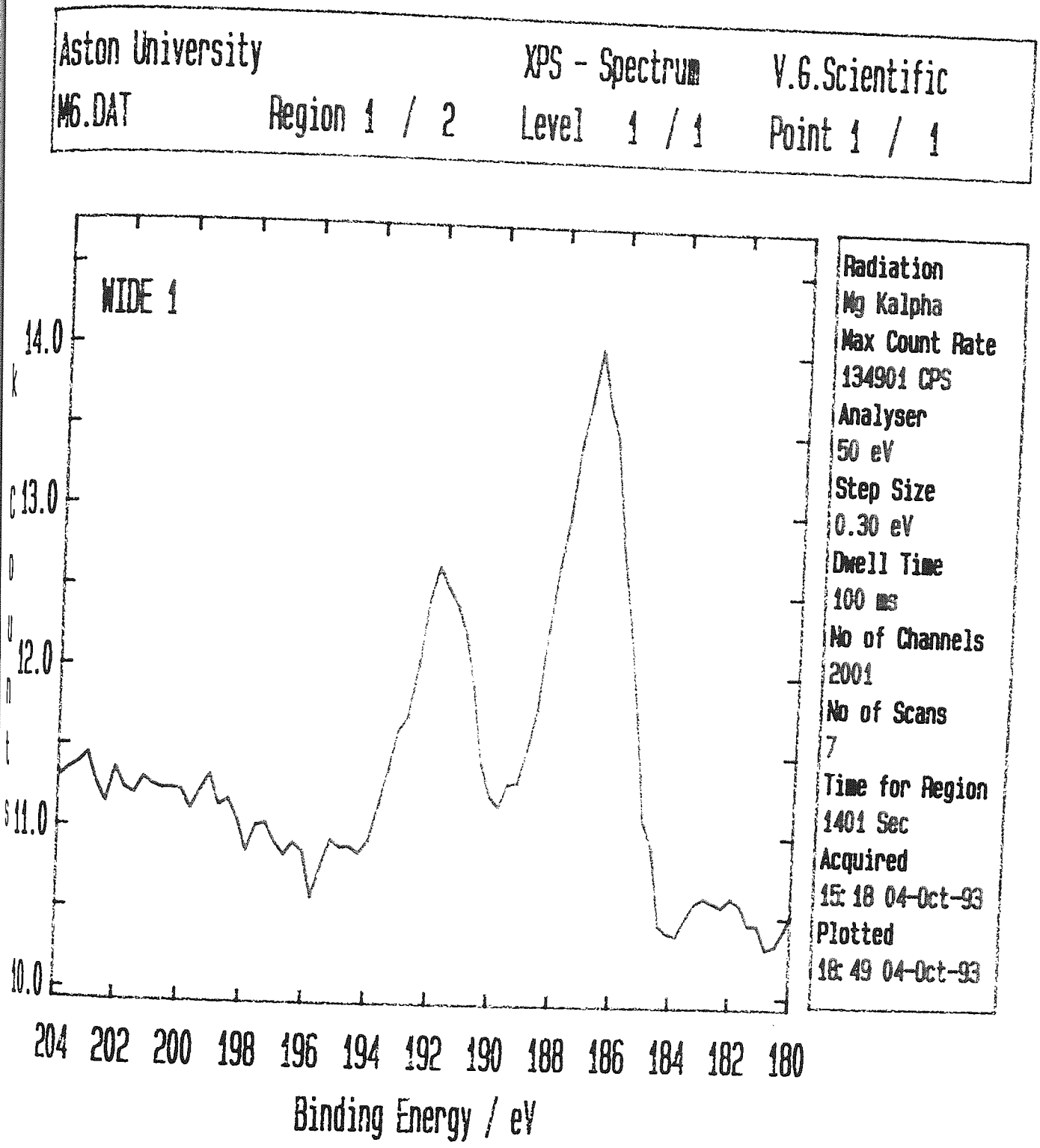

Figure 4.101. XPS analyses of the worn surface of the P orientated composite sample (Load = 12 N, Speed = 1.6 m/s).

4.2 WEAR OF B(SiC)-REINFORCED POLYMER MATRIX COMPOSITE MATERIALS

4.2.1 Introduction

In the previous section, the mechanical behaviour and wear results of the B(SiC) reinforced composite and its aluminium matrix have been reported under various conditions. In this section, the wear behaviour of the B(SiC)-reinforced plastic matric composite (PMC) and its HDPE polymer matrix (especially, effect of fibre orientation) was investigated under identical test conditions in order to facilitate a comparison of the two materials in terms of the wear volume and microstructure. The first sections from 4.102 to 4.109, are related to wear data of the PMC materials, while friction data are presented in Figures 4.110 to 4.112. The last sections from 4.113 to 4.127 are concerned with SEM observation of the worn surfaces of these composites.

4.2.2 Effect of Sliding Speed and Load

In this section, dry sliding wear tests were conducted to determine the effect of fibre orientation (N, P and AP) on the wear resistance of B(SiC)-reinforced PMC materials under different operating conditions using the pin-on-disc technique. The test conditions used were as follows : the operating wear velocities were 0.6, 1.0 and 1.6 m/s respectively with applied loads of 12 N up to a maximum of 22 N. The wear tests lasted for about one hour and the wear rates were calculated from the previous equation used for the MMC materials. The results of the tests carried out at different conditions are listed in Tables 9, 10 and 11 for sliding speeds of 0.6, 1.0 and 1.6 m/s respectively.

The average volumetric wear rate as a function of sliding speed of the B(SiC)-reinforced PMCs is shown in Figure 4.102. The tests were conducted on the N orientation at a load of 22 N. It could be seen that the wear rate of the HDPE matrix was found to be noticeably larger than that of its composite. The convex curve showed evidence of reduced wear above a critical speed of 1.0 m/s. For instance, the wear rate of the polymer matrix

increased up to value of 1.75 mm^3/km at 1.0 m/s and then dropped sharply to about 0.73 mm^3/km at a maximum sliding speed of 1.6 m/s. Only a little variation was observed in the case of the composite.

Figure 4.103 shows the average volumetric wear rate of the P orientated sample as a function of sliding speed for the PMCs. The tests were carried out under the same load condition, but for the P orientation. Again, a peak was observed in the matrix wear rate, and the wear rate of the PMC decreased highly compared with the unreinforced matrix. It was also appeared that 14% fibre composite showed a higher wear rate than the 28% fibre composite. However, same trend was observed in all sliding speed used for this case. There was no real tendency to increase the wear rate with sliding speed, possibly the composites were showing at the same behaviour pattern as the matrix, but with a much smaller peak at a speed of around 0.3 m/s.

As for as the effect of the load on the wear rate of the PMCs, Figure 4.104 shows the average volumetric wear rate as a function of load for the B(SiC)-reinforced PMCs, including N, P and AP orientation and the matrix. The sliding distance was maintained at 4.32 km. From the figure, for any load, wear rate of the PMC for all orientations was lower than that of the HDPE matrix, and the wear rate of matrix increased with load quite strongly. The increase in the lower volume fraction composite was little except for the P orientation, but in general there was an increasing trend in volumetric wear rate with load for the PMCs.

Figure 4.105 shows the volumetric wear rate as a function of load for the PMC, but the tests were carried out at a speed of 1.0 m/s for all orientations. It was observed that the rate of increase of volumetric wear rate with load was much higher in the matrix than in any of the differently orientated composite samples, whereas the rate of increase of wear rate in the P orientation was also slightly higher than the others. It was clear from the graph that the N orientation gave the lowest wear rate under the same test conditions.

4.2.3 Effect of Fibre Content

The effect of the volume fraction of B(SiC) fibre on the volumetric wear rate of HDPE plastic matrix is shown in Figures 4.106 for the N. The load applied in the tests was 22 N and two sliding speeds of 0.6 and 1.0 m/s were used for the tested materials. It was obvious that by introducing fibres into the HDPE matrix, the volumetric wear rate was substantially reduced in both of the speed conditions. For example, in the N orientation, the average volumetric wear rate in the composite was found to be about eight orders of times smaller in magnitude than that of the matrix at a speed of 0.6 m/s. The reduction in volumetric wear rate was also considerable at a speed of 1.0 m/s compared with the unreinforced matrix. As shown in Figure 4.106, it appeared that the volumetric wear rate also increased slightly as the fibre content increased in this orientation at a load of 22 N and, especially at a speed of 0.6 m/s. The other words, the increase in sliding speed resulted in the lower wear rate at this test conditions.

Figure 4.107 shows the volumetric wear rate as a function of fibre content of the composite in the P orientation. The tests were carried out at a load of 22 N and at speeds of 0.6 and 1.0 m/s. Again, a moderate reduction in volumetric wear rate was observed by the incorporation of fibre in the HDPE plastic matrix and it was about three times lower in magnitude than that of its matrix at 0.6 m/s speed.

From the figure, however, the volumetric wear rate decreased with increasing fibre contents although the tests were carried out under the same condition. The result also showed that the wear rate of 14% fibre composite was higher than that of 28% fibre composite. According to the results obtained here for the P orientation, the volume fraction of fibre had a moderate influence on the volumetric wear rate of the B(SiC)-HDPE polymer matrix composite.

4.2.4 Effect of Fibre Orientation

The effect of fibre orientation on the wear behaviour of PMC materials was carried out using N, P and AP main sliding directions is shown in Figures 4.108 and 4.109. These

figures showed that anistropic behaviour was evident in these orientations. Namely, the N orientation gave the minimum wear rate and the P orientation showed the highest wear rate while the AP orientation exhibited similar results to the N orientated samples in some cases, particularly under low speeds of 0.6 and 1.0 m/s.

In the case of high sliding speed condition, Figure 4.109 shows the volumetric wear rate as a function of fibre volume fraction for the PMCs sliding in the N, P and AP orientations under the same load. Again, the highest wear rate was found in the P orientation. For example, when the N and AP orientated samples containing 14% fibre were tested at a speed of 1.6 m/s and 22 N load, the volumetric wear rates were obtained to be about 0.056 and 0.370 mm^3/km respectively.

4.2.5 General Friction Results

The average coefficient of friction as a function of fibre volume fraction of B(SiC)-PMC and HDPE matrix is shown in Figures 4.110 to 4.112 and tabulated in Tables 9, 10 and 11. The tables showed that three speeds were used, i.e. 0.6, 1.0 and 1.6 m/s. The first figure indicated that the coefficient of friction of the HDPE matrix was decreased considerably by the incorporation of B(SiC) fibre at 14% and 28% levels. Furthermore, the figure revealed that the N orientation showed the highest of coefficient of friction, while the P and AP orientation exhibited the low value of coefficient of friction and no significant variation was observed between them. In the N orientation, the coefficient of friction also increased again with fibre content, especially at the high load. However, in the P orientation, the coefficient of friction only decreased slightly with fibre content. Also a slight increase in the coefficient of friction with load was observed in the AP orientation under high load condition.

Figure 4.111 shows the coefficient of friction versus volume fraction of fibre in the PMCs tested at a high speed of 1.6 m/s, and at loads of 12 N, 22 N in the three main orientations. From the figure, the coefficient of friction of the PMCs was generally found to be much lower than that of the unreinforced HDPE polymer matrix. It appeared that the

coefficient of friction tended to decrease with increasing volume fraction of fibre in HDPE plastic matrix composite for the P and AP orientations, but a slight difference was evident for these samples. However the opposite trend was observed in the N orientation, where the friction coefficient increased again with either fibre content or load.

The effect of sliding speed on the friction coefficient of the composite is shown in Figure 4.112. This figure indicated that the AP and P orientation results were similar to each other, and much lower than the N orientation. It was also observed that coefficient of friction increased with increasing sliding speed in the all orientations at much the same rate.

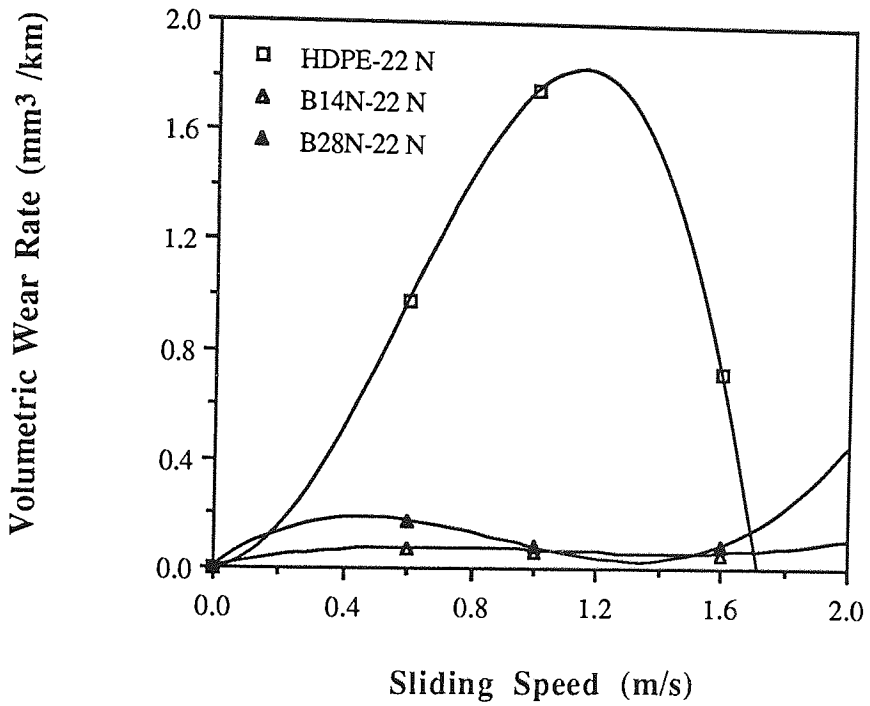

Figure 4.102. Volumetric wear rate as a function of sliding speed for the B(SiC)-PMC materials in the N orientation. (Load = 22 N)

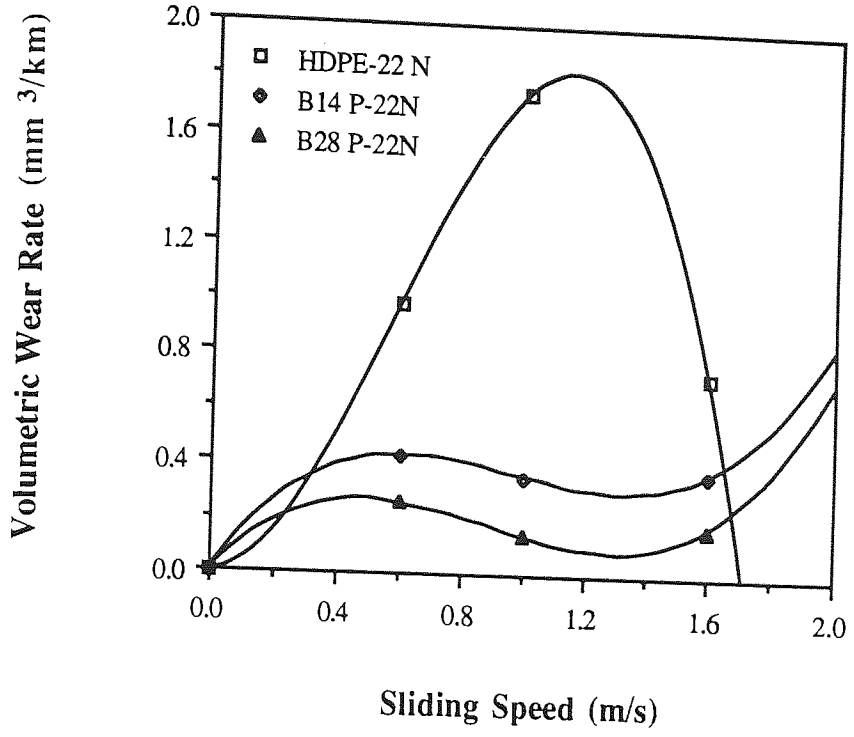

Figure 4.103. Volumetric wear rate as a function of sliding speed for the B(SiC)-PMC materials in the P orientation. (L = 22 N)

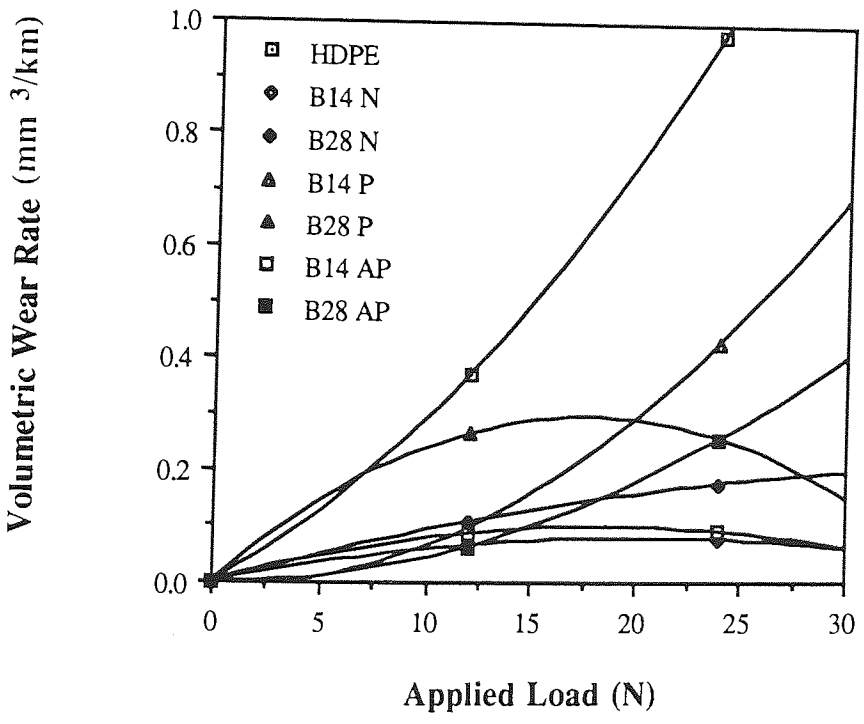

Figure 4.104. Volumetric wear rate as a function of load for B(SiC)-PMC materials tested at a speed of 0.6 m/s.

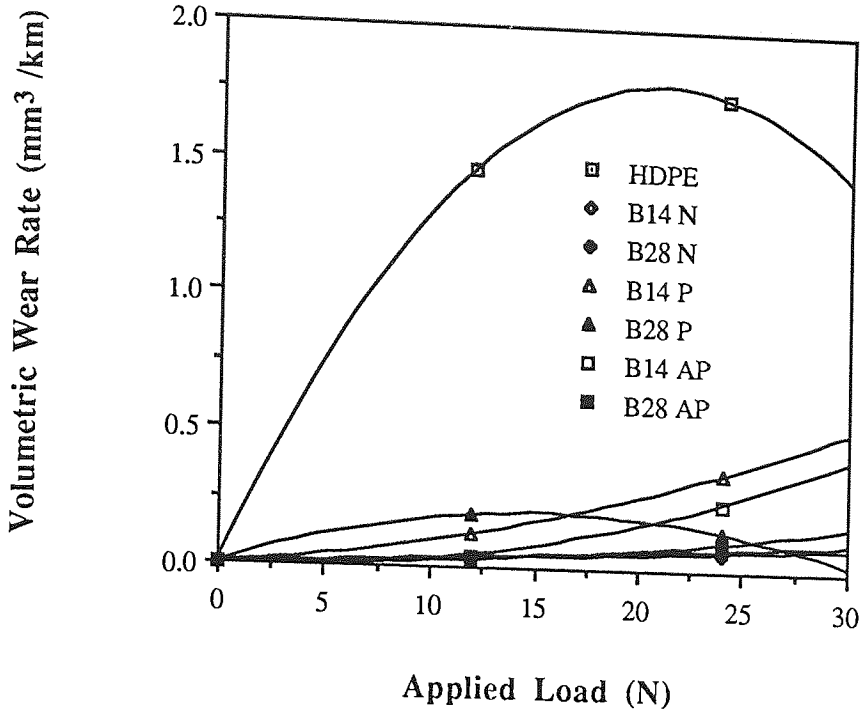

Figure 4.105. Volumetric wear rate as a function of load for B(SiC)-reinforced PMCs tested at a speed of 1.0 m/s.

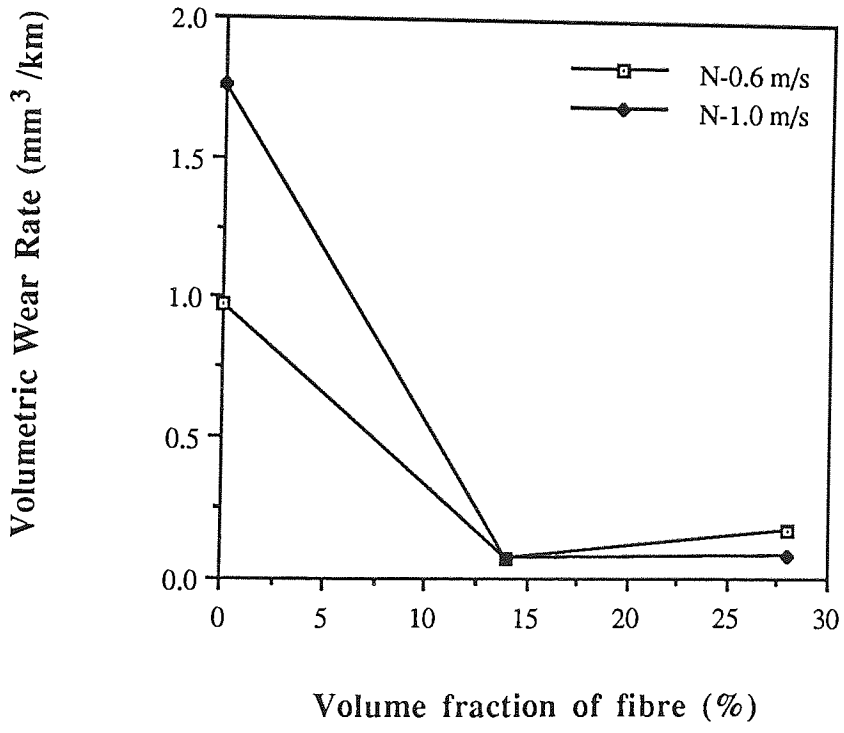

Figure 4.106. Volumetric wear rate as a function of fibre content in unidirectionally orientated B(SiC)-reinforced PMCs tested for the N orientation.(Load = 22 N)

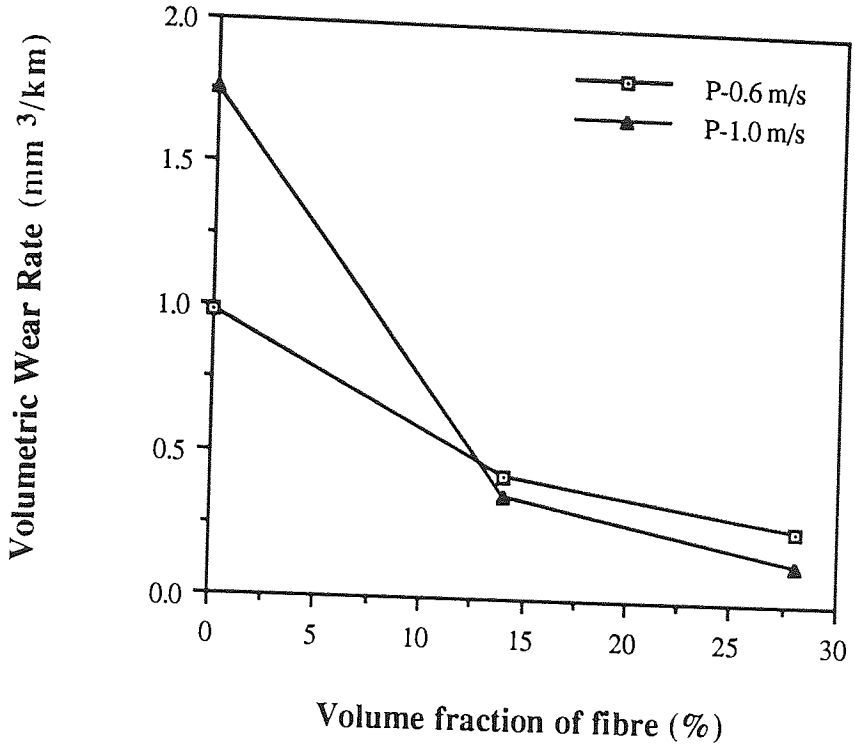

Figure 4.107. Volumetric wear rate as a function of fibre content in the unidirectionally reinforced B(SiC)-reinforced PMCs tested for the P orientations. (Load = 22 N)

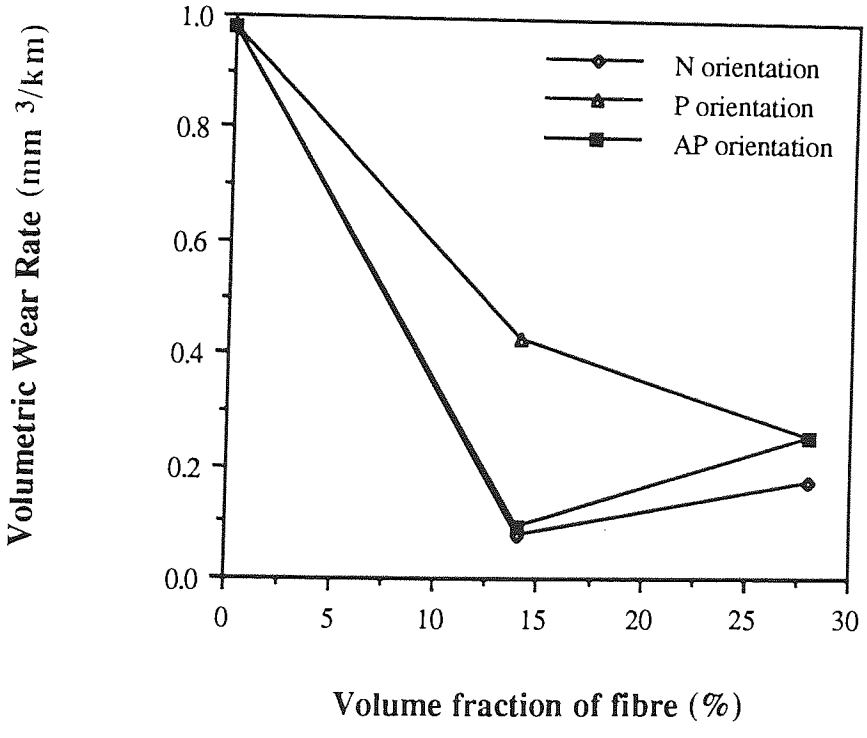

Figure 4.108. Volumetric wear rate as a function of fibre content for the PMCs sliding in N, P and AP orientations. (Speed = 0.6 m/s and Load = 22 N)

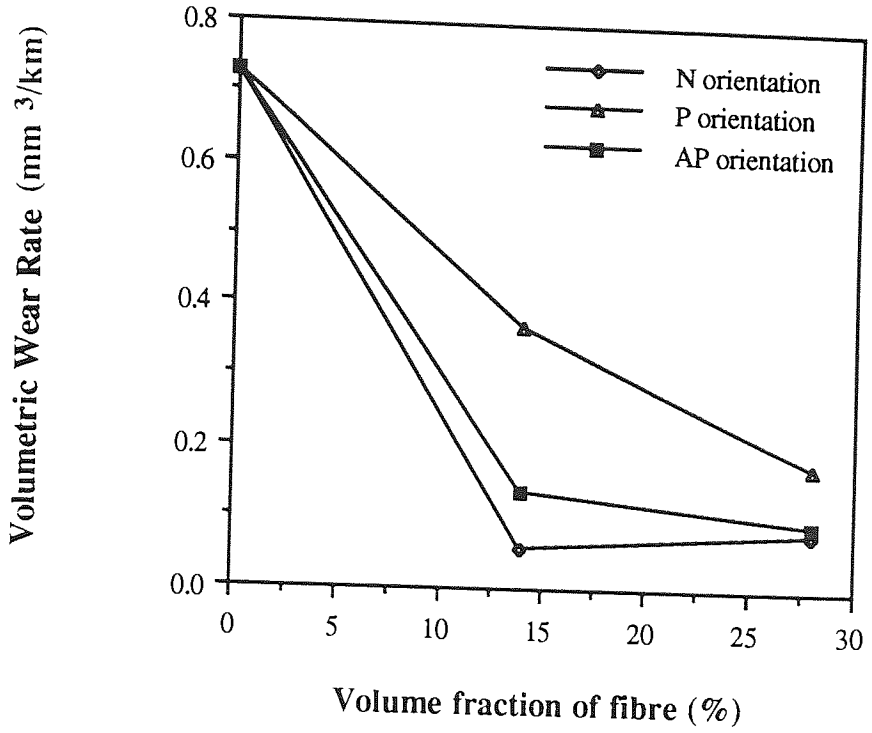

Figure 4.109. Volumetric wear rate as a function of fibre content for the PMCs sliding in N, P and AP orientations.(Speed = 1.6 m/s and Load = 22 N)

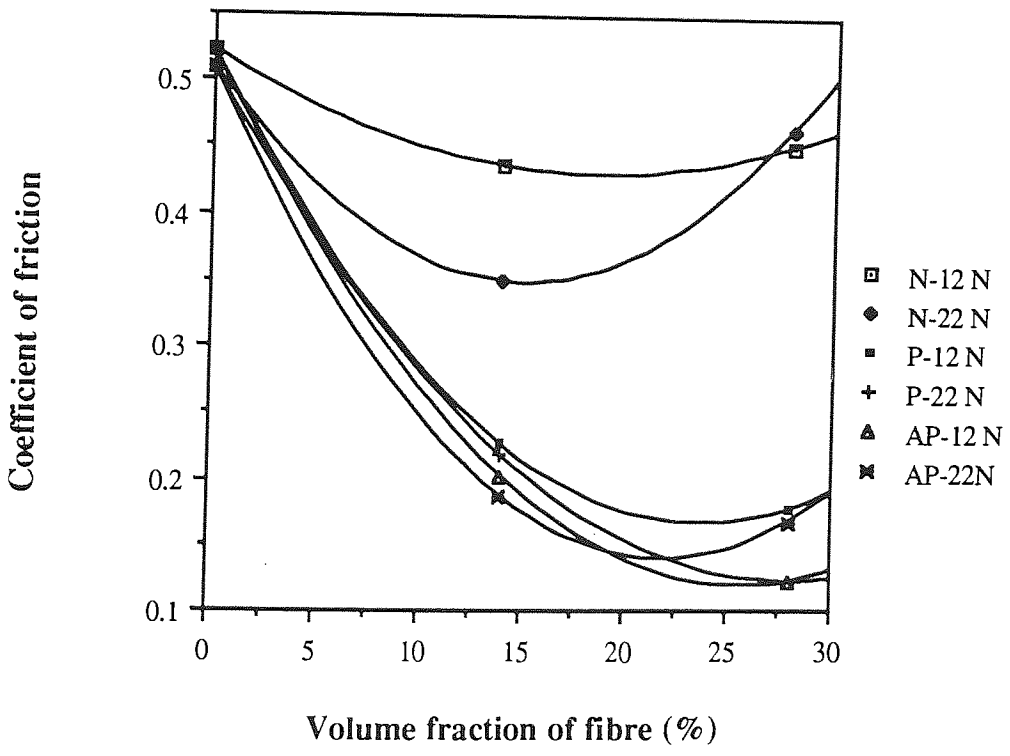

Figure 4.110. Coefficient of friction versus volume fraction of fibre reinforced PMCs tested in the N, P and AP orientations at a speed of 0.6 m/s.

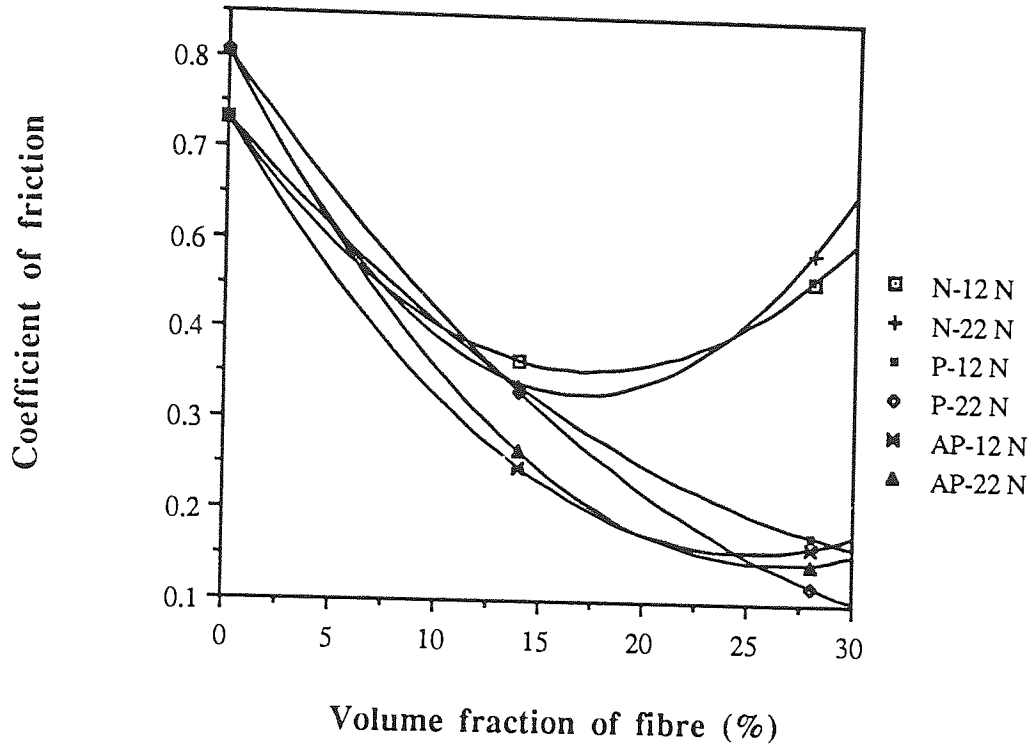

Figure 4.111. Coefficient of friction versus volume fraction of fibre reinforced PMCs tested in the N, P and AP orientations at a speed of 1.6 m/s.

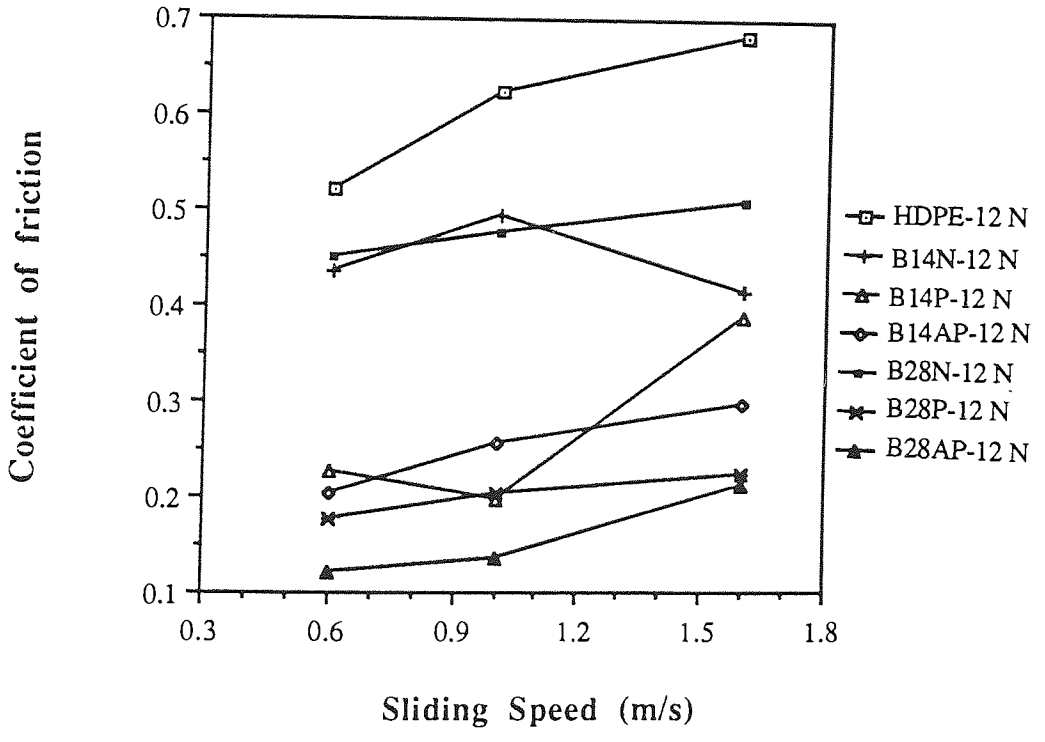

Figure 4.112. Effect of sliding speed on coefficient of friction for the PMC pins tested in the three main orientations at a load of 12 N.

4.2.6 Surface Observations and Wear Mechanisms

Different surface appearances were microscopically observed for the wear surfaces of the HDPE matrix and its composites. The polymer matrix had a ductile surface, and wear had produced several plough furrows to the sliding surface. Such an example of a worn surface of the matrix specimen is shown in the SE micrograph of Figure 4.113. The leading edge was from right to left. This SE micrograph indicated that the failure of the matrix had taken place predominantly by microploughing and microcutting. The same sample is shown in Figure 4.114 at increased magnification and showed the thin layer which was produced during the wear and some cracks over the layer was also observed at this magnification. Figure 4.115 also shows the worn surface of the polymer matrix, but test conducted at a speed of 0.6 m/s and load of 12 N. The sliding direction was from left to right. This micrograph taken under high magnification revealed the many lumps of the matrix over the surface of the sample and the surface seemed to be smooth. The thickness of the lumps was observed to be a thin over the sample in addition to evidence of a small amount of debris particles.

Under low and high magnification the general worn surfaces of the B(SiC)-reinforced plastic matrix composite materials (PMCs) were examined in SEM. It was observed that different forms of wear mechanisms dominated for each of the main orientations (N, P and AP). An SE micrograph of the PMC pin tested in the N orientation is shown in Figure 4.116, leading edge was from right to the left. It was apparent that the fibres ends were broken, creating fibre splinters which was reattached to the surface or removed from their place. The length of the fibre splinters were variable. The same sample is shown in Figure 4.117 at increased magnification. This figure also showed that fractured fibres were embedded in the surface and some cavities and tearing of the matrix by splinters were also evident in this case. The type of fibre fracture as shown in this figure at high magnification, demonstrated that the fibres were broken from the end piece by piece and was accompanied by plastic deformation of the matrix.

Under low magnification, SE micrograph of the worn surface of the composite pin tested in the N orientation is shown in Figure 4.118. The leading edge was from right to left. The tests were carried out at a speed of 1.6 m/s and 22 N. The micrograph revealed that more fibre breakage had occurred and fibre fracture rich area was also observed at the left of the composite sample, near to the trailing edge. The same sample is shown in Figure 4.119 at high magnification. The fractured fibres and splinters were embedded in the surface of the sample in addition to observation of the ductile layer of the plastic matrix. This figure further revealed that the fibre ends were not planar with the HDPE matrix surfaces. The fibres ends were proud of the surface. The lengths of the protrusion were about 25 μm. Further wear would then caused to the length of the debonded fibre as evidenced by the figure.

Figure 4.120 shows the worn surface of the PMC pin tested at a speed of 0.6 m/s and 22 N load, leading edge was from right to left. The volume fraction of fibre used in the composite was the 14% B(SiC) fibre. The SE micrograph revealed that most of the fibres in the HDPE matrix had pulled-out from the place. In other words, the very dark and continuous portions seen in the micrographs corresponds to the cavities on the worn surface of the composite sample. The cavities on the worn surface must be produced by the frictional force due to softening of the polymer matrix. These cavities also appeared to be long on the worn surface because of pulled-out of long fibres. The width of the cavities is about 40-60 μm.

Figure 4.121 shows the worn surface of the PMC pin tested at a speed of 1.6 m/s and 22 N under high magnification, leading edge was from right to left. The volume fraction of fibre used in the composite was the 28% B(SiC) fibre. Again this SE micrograph showed debonding, wear occurred by fracturing of fibres and then weaking of interfacial bond between the matrix and B(SiC) fibre, as small fragments as well as larger pieces had formed by debonding under both the sliding speed and normal load.

In the P orientation, SE micrograph of the worn surface of the composite pin is shown in Figure 4.122 under low magnification. The composite pins were tested at a speed of 1.0 m/s and 12 N, leading edge was from right to left. The surface revealed long and continuous grooves and in some places patches where the fibres had been removed from the surface during the course of wear can be seen. Titanium tape, used for binding the fibres, was also observed. The same sample of the composite is shown in Figure 4.123 at higher magnification and showed that cavities had been generated due to pulled-out of fibres during the wear process, and abrasion was evidenced by fine grooves visible in the sliding direction.

Fibres were broken due to a bending action when the PMC materials were rubbed in the AP orientation against the smooth steel. Figure 4.124 shows the worn surface of the pin tested in the same orientation at a speed of 1.0 m/s and 12 N. The leading edge was from left to right. It was observed that fibre breakage had occurred in a some pieces and these particles reattached to the surface with subsequent process. The length of the broken fibre particles varied greatly. The higher magnification micrograph of Figure 4.125 indicated fibre bending and smearing of the matrix over the bent or broken fibres, as was also evident in Figure 4.126.

As for the case of high sliding speed conditions, the worn surface of the composite pin (AP) is shown in Figures 4.126 and 4.127 at low and high magnifications respectively. The sliding direction was from left to right. From the micrograph, a smooth surface was observed although some fibre fracture had occurred. A tribofilm was evident on the surface of the polymer matrix, this was more pronounced at higher magnification.

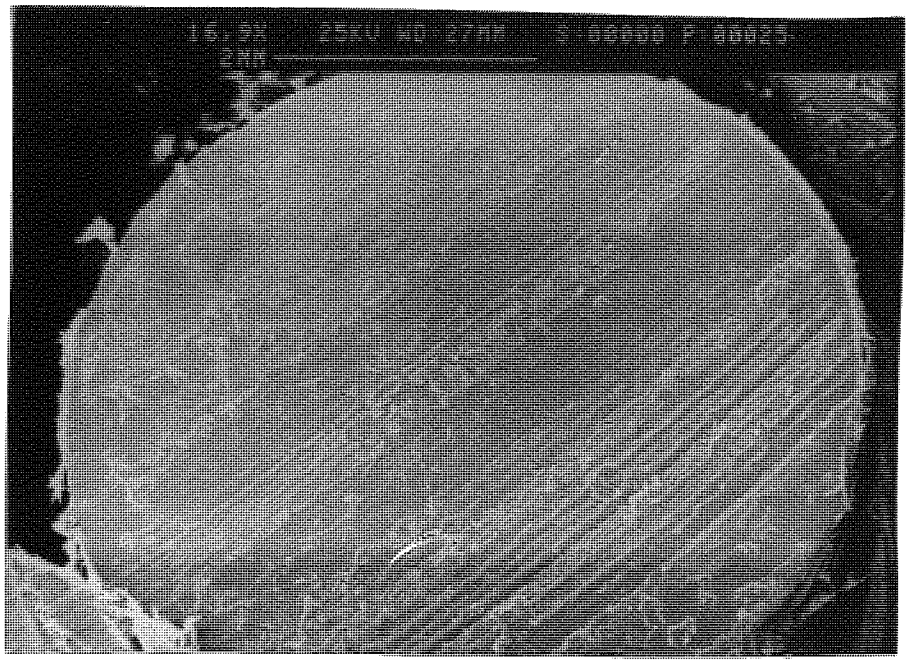

Figure 4.113. SE micrograph of a worn surface of a HDPE matrix pin after sliding for a speed of 1.6 m/s at 12 N load, showing microgrooving, leading edge to left.

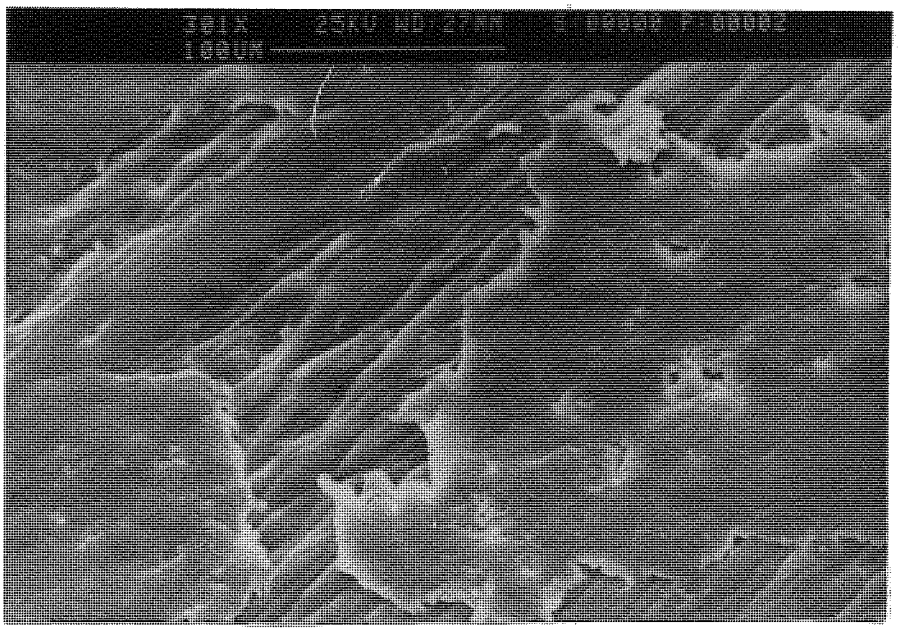

Figure 4.114. Higher magnification of Figure 4.113.

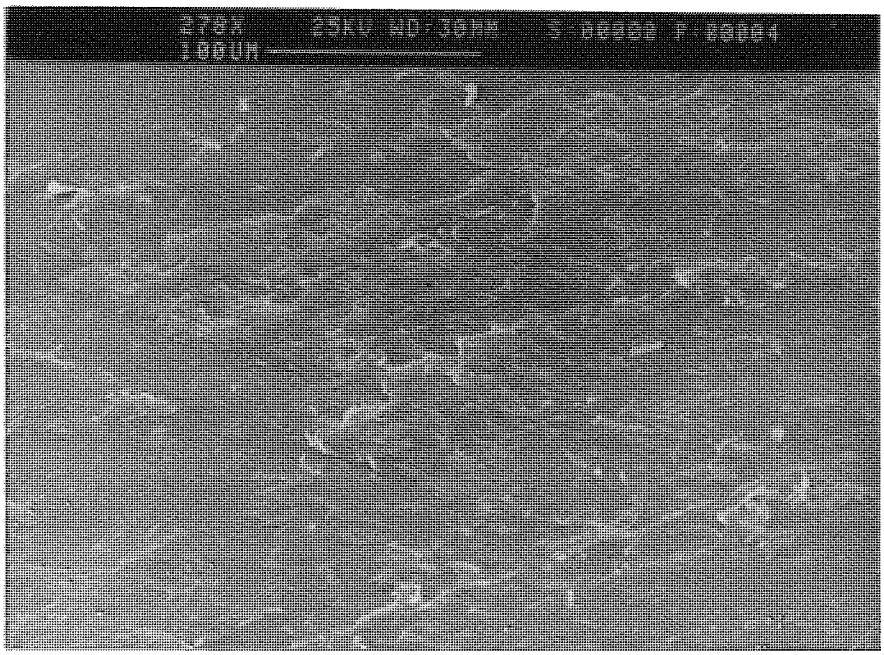

Figure 4.115. SE micrograph of a worn surface of a HDPE matrix pin after sliding for a speed of 0.6 m/s at 12 N load, showing lumps, leading edge to right.

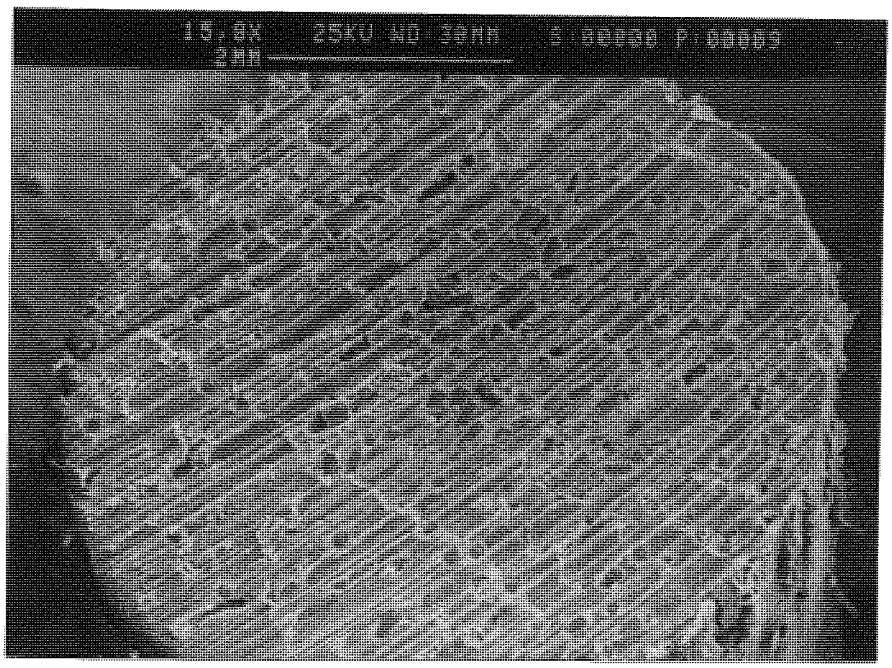

Figure 4.116. SE micrograph of the worn surface of a B(SiC)-reinforced PMC pin in the N orientation for a speed of 1.0 m/s at 12 N load, showing some broken fibre and embedded fibres in the matrix, leading edge to left .($V_f = 0.14$)

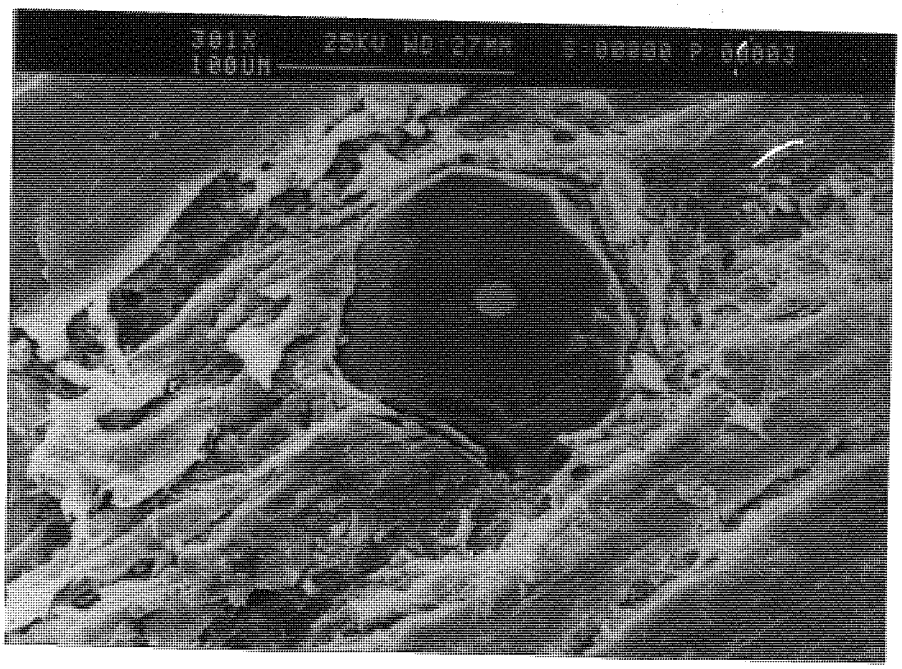

Figure 4.117. Increased magnification of SE image of a PMC pin tested at a speed of 1.0 m/s in the N orientation, showing broken fibres, cavities and debris particles.

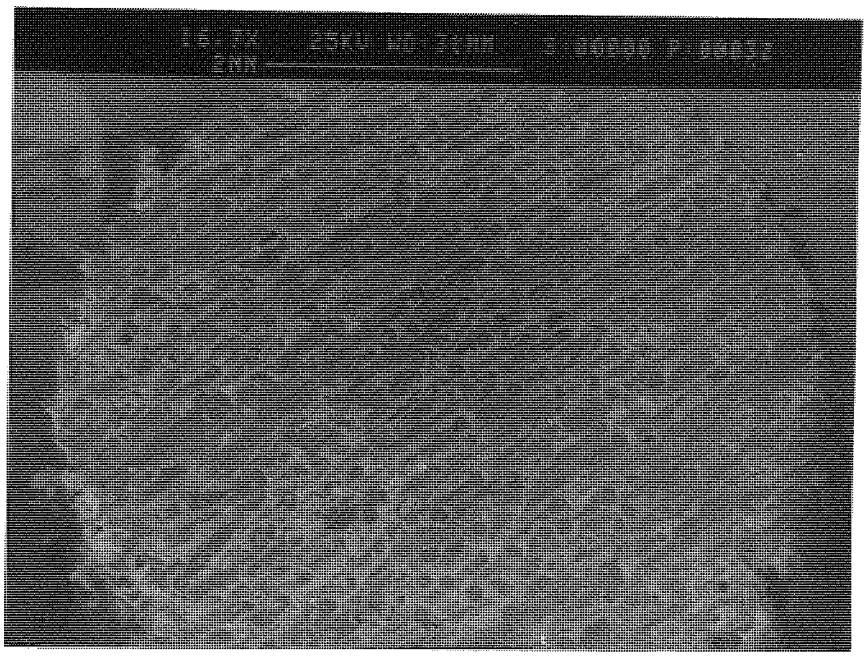

Figure 4.118. SE micrograph of the worn surface of the B(SiC)-reinforced PMC pin tested in the N orientation for a speed of 1.6 m/s at 22 N load, showing smooth surface appearance but some broken fibres as well, leading edge to right.

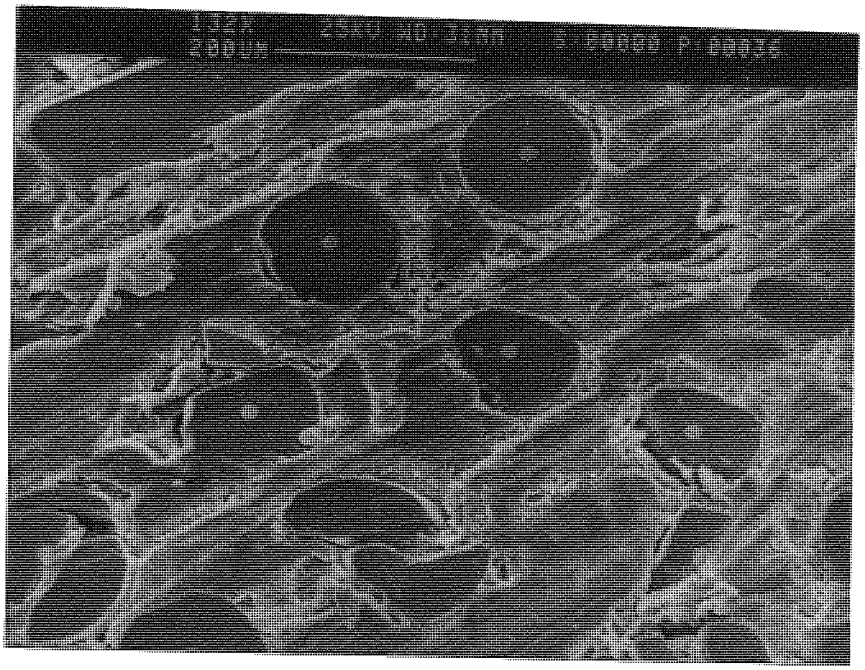

Figure 4.119. Higher magnification of the same sample of Figure 4.118, showing fracture of fibre end and plastic deformation of the matrix.

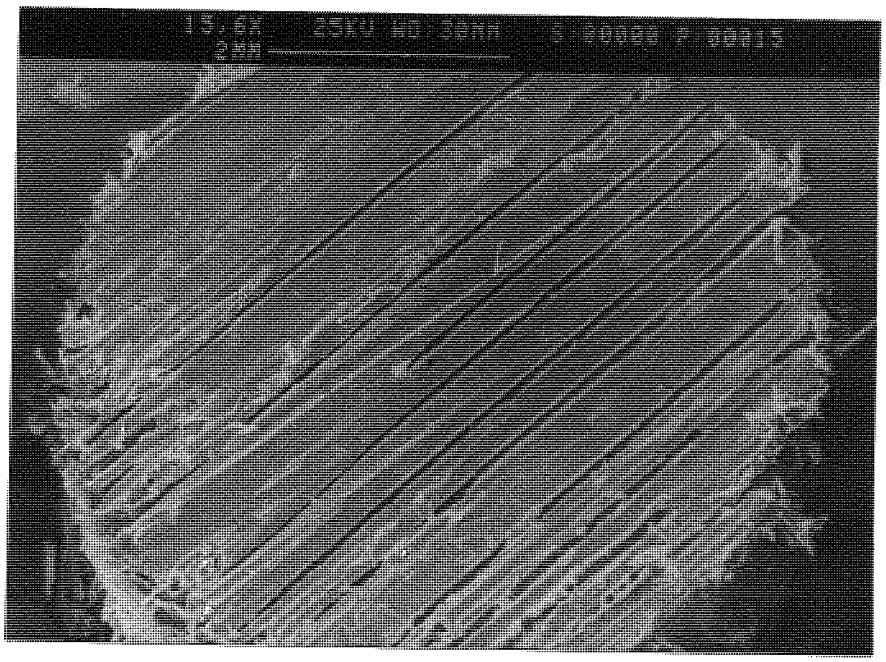

Figure 1.120. SE micrograph of the worn surface of the B(SiC)-reinforced PMC pin tested for a speed of 0.6 m/s at 22 N load, showing cavities and pulled-out of fibre near the trailing edge, leading edge to left. ($V_f = 0.14$)

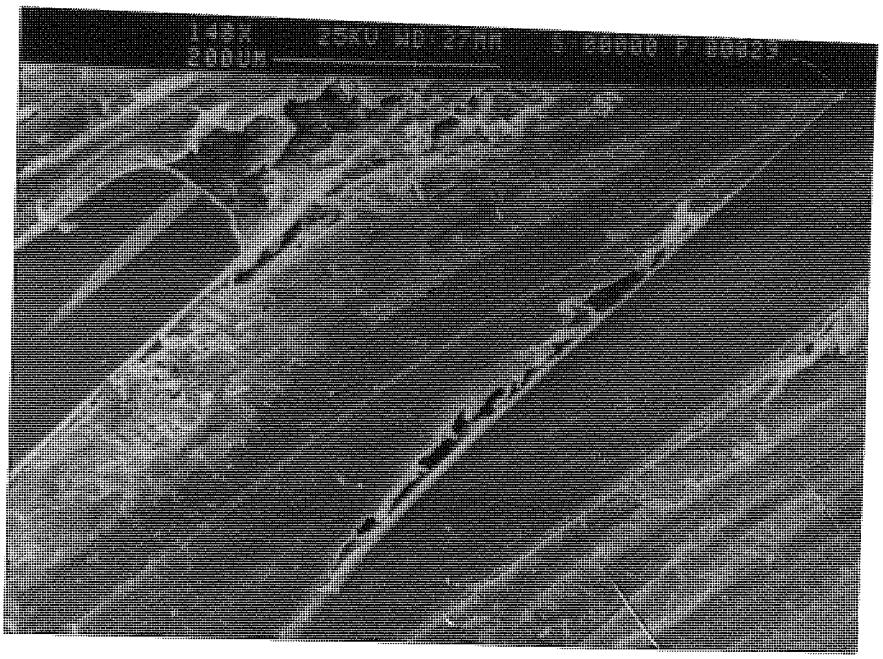

Figure 4.121. Higher magnification of the.SE micrograph of the worn surface of the B(SiC)-reinforced PMC pin tested for a speed of 1.6 m/s at 22 N load, showing broken fibre and debonding, leading edge to left. ($V_f = 0.28$)

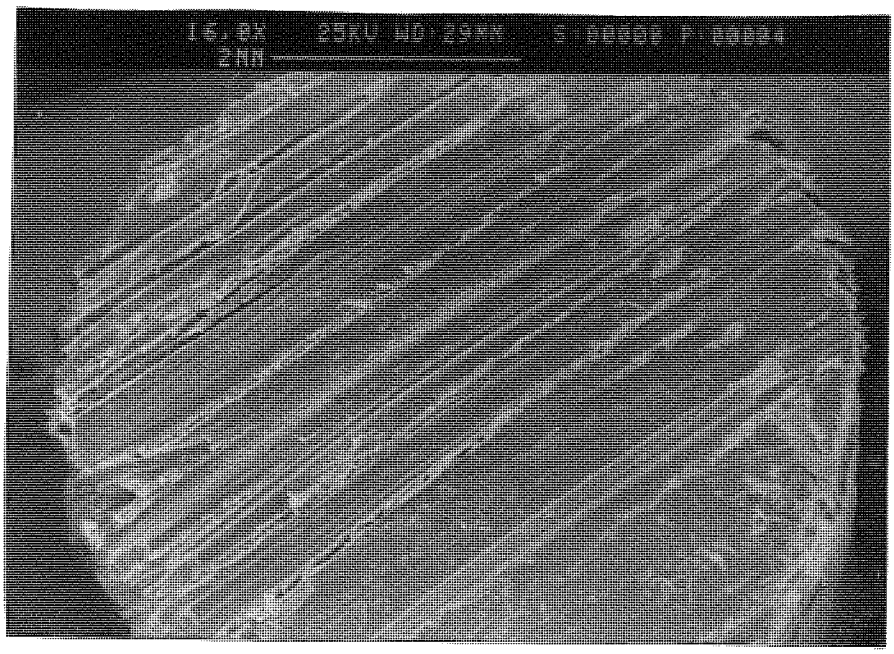

Figure 4.122. SE micrograph of the worn surface of the B(SiC)-reinforced PMC pin tested in the P orientation for a speed of 1.0 m/s at 12 N load, showing extensive grooving and pulling-out of fibre, leading edge to left.($V_f = 0.28$)

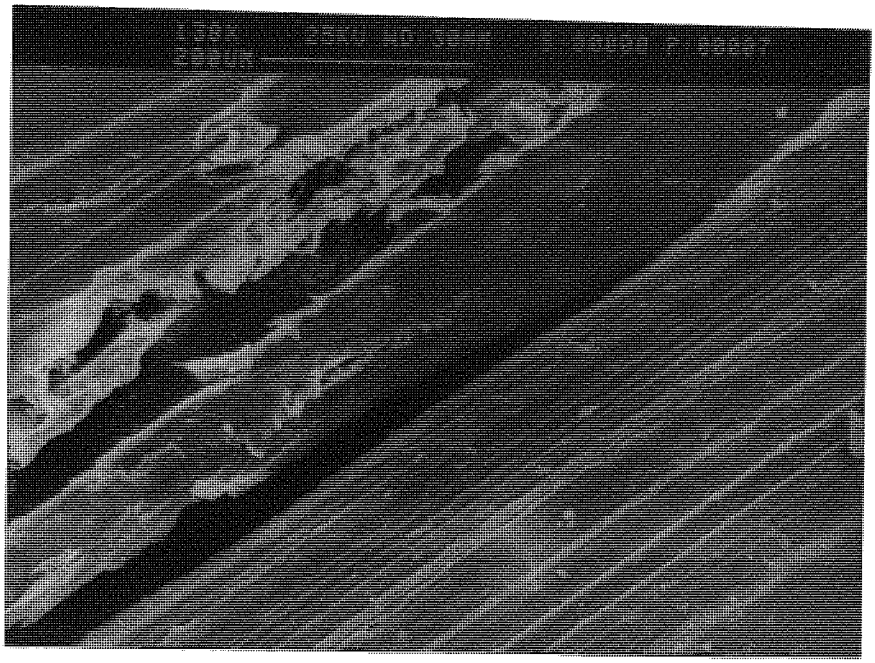

Figure 4.123. Higher magnification of Figure 4.122, showing cavities over the wearing surface due to pulling-out fibre.

Figure 4.124. SE micrograph of a worn surface of a PMC pin tested in the AP orientation for a speed of 1.0 m/s under 12 N load, showing fibre breakage and rolling-out of fibre, leading edge to right.

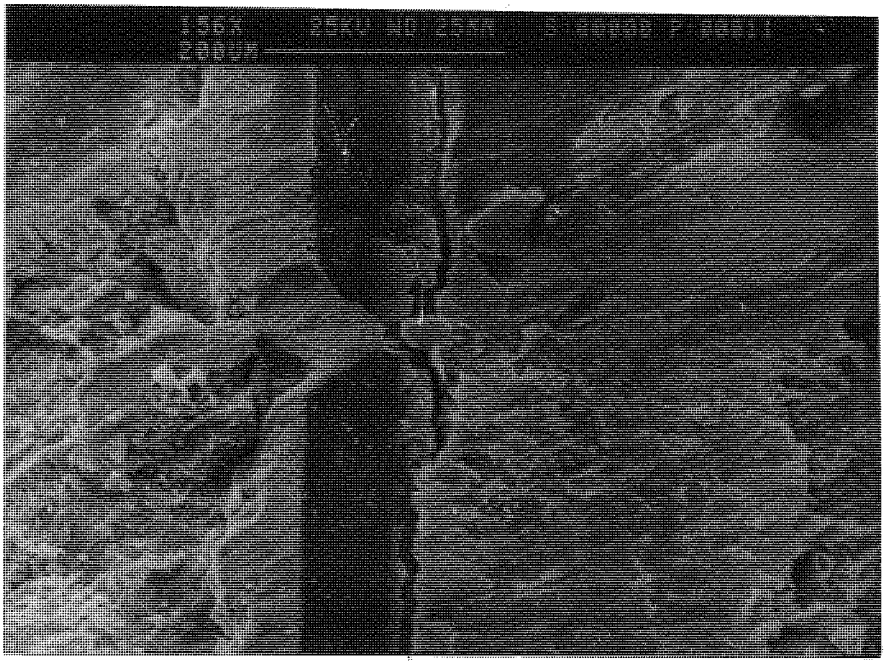

Figure 4.125. Higher magnification of Figure 4.124, showing fibre debonding and smearing of the matrix over the fibre.

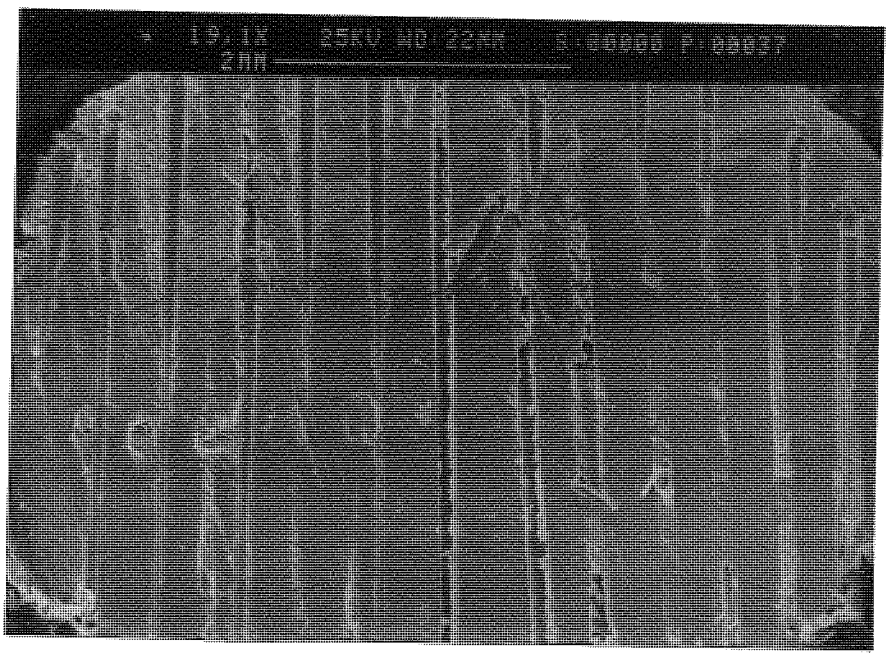

Figure 4.126. SE micrograph of the worn surface of B(SiC)-reinforced PMC pin tested in the AP orientation for a speed of 1.6 m/s under 22 N load, showing the fractures of some fibres and roll-out of fibre, leading edge to right. ($V_f = 0.32$)

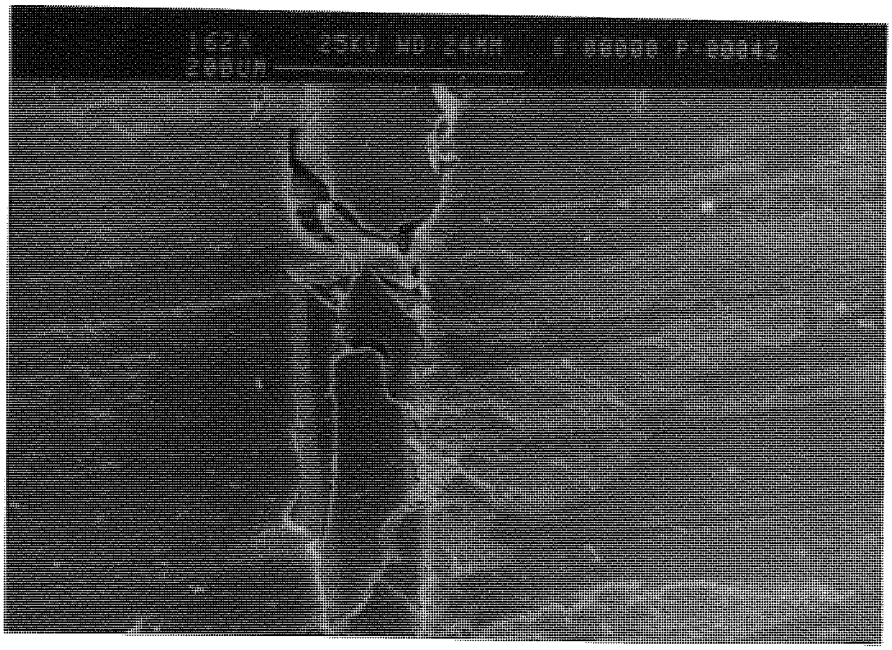

Figure 4.127. Higher magnification of the same sample of Figure 4.126 showing fracture of fibre and formation of tribofilm over the surface.

CHAPTER FIVE

5.0 DISCUSSION

5.1 Introduction

The main objective here is to discuss the experimental results of mechanical property tests of MMCs and wear tests of MMCs, besides the wear tests of the PMCs. In particular, the wear behaviour of both of the composite materials tested and wear mechanisms will be discussed and compared to those obtained by other workers, based on fibre orientation, operation variables, type of the matrix and microscopic observations. In addition, a comparison can also be made between metal and polymer matrix composite materials and a summary of the wear mechanisms and the influence of fibre on the wear rate of the composite are made and some logical suggestions are offered on how these mechanisms correlate to the measured wear rates.

5.2 Mechanical Behaviour of MMCs

The B(SiC)-reinforced/2014 aluminium matrix composites consisted of unidirectional or bidirectional orientated fibres in the aluminium alloy matrix, and their microstructures and those of the matrix alloy were shown in Figures 4.1 and 4.4. The transverse cross-section of the unidirectional array of fibre and its matrix microstructure could be seen in Figure 4.2 and comparing with Figure 4.1, the structure of the aluminium matrix in Figure 4.2 was coarser than that in Figure 4.1, with a dendrite arm spacing of about 30 μm as compared with 15 μm. This could be only related to cooling rate, as dendrite arm spacings, either because of a shorter increase at lower cooling rates, or perhaps the dendrite nucleation is controlled by the fibre spacing. Apart from that, the fibre-reinforced composite materials microstructures were reasonably homogeneous, and the distribution of B(SiC) fibre in the high volume fraction composite was found to be more uniform than in the lower volume fraction composite.This also might be because fibre spread was inversely dependent on the

volume fraction of fibre, therefore, the probability of fibre alignment increased with increasing in the volume fraction of fibre.

The density of the MMCs, as shown in Figure 4.5, decreased linearly in terms of the volume fraction of B(SiC) fibre. This behaviour was normal and as expected because these properties were not related to fibre orientation. As for the case of polymer matrix composites (PMCs) in a similar way, the density of the PMCs was also plotted in Figure 4.6 as a function of fibre volume fraction. It was apparent that the density increased quite highly with increasing fibre reinforcement. The opposite trend with respect to fibre volume fraction was observed between density of MMCs and PMCs because of the matrix effect, but both of them obeyed the simple rule of mixtures law. In addition, the variation of hardness was plotted in Figure 4.7 as a function of fibre volume fraction in the MMCs and listed in Table 3. There was a significant improvement in the hardness of aluminium alloy matrix as a result of the incorporation of B(SiC) fibres up to the 32%. This was more pronounced for the longitudinal orientated composites. For example, an increase in hardness of about 153, 294 and 387% for the 16, 27 and 32% fibre composite respectively was obtained. In the case of the 21% and 23% fibre composites, an increase in hardness of around 70% and 143% for these composites respectively was evident. However a considerable reduction was found for the bidirectional composite compared with the longitudinal orientated composite. This might be due to some geometrical effect of the bidirectional orientation of the fibres in the composite, or because of increased surface damage caused by cutting of the test specimens, which caused a localised loss of fibres in these samples.

The results of the tensile testing on the B(SiC)-reinforced aluminium matrix composite, shown in Figure 4.8 and listed in Table 3, indicated both improvements and reductions in properties when compared to typical values for 2014 unreinforced matrix. For the unreinforced alloy samples, the tensile strength was 172 MPa while the composite with 16% volume of fibre, had a tensile strength of 312 MPa in the fibre axis direction. This represents 104% improvement in strength. The improvement appeared to be almost

linear for the unidirectional orientated samples, increasing by about 11 MPa for each 1% of fibre reinforcement , e.g. the UTS was 172 MPa for 0% fibre, 312 MPa for 16% fibre, 445 MPa for 27% fibre, 524 MPa for 32% fibre reinforcement. The actual increases were about 81, 156 and 205% for the 16, 27 and 32% B(SiC) fibre composite. However, any increases in strength due to fibre reinforcement were quite small or sometimes even lower when bidirectional orientated continuous fibre reinforced composites were tested under identical conditions. For instance, a tensile strength of only about 165 MPa was obtained for 21% bidirectional fibre reinforcement, and 235 MPa for 23% bidirectional reinforcement. This probably was because matrix strengthening was predominant in these composites or existing of a weak matrix-fibre interface bonding between the matrix and fibre may be the other reason for these composites as shown in previous section. As a consequence of this the lower strength was obtained for the orthogonal composite than the unidirectional orientated composite samples. On the other hand, the tensile strength of unidirectional continuous fibre-reinforced composite showed an almost linear relationship with respect to fibre content ranging from 16% to 32% since most of the loads were carried by the longitudinal fibres.

A similar study was carried out using boron fibre by other researchers.[45] For instance, their work showed that boron fibre reinforcement considerably increased the strength properties of aluminium powder compacts due to reinforcement. In their work, the improvement was 250% and 487% for 10% and 20% volume fraction of boron respectively. Similar increases were recorded by others [102] on boron-reinforced aluminium composites produced by diffusion bonding. They obtained 268% and 573% increases when 12% and 26% of fibre was used respectively. However, the tensile strengths of these resistance-sintered composites were found to have lower values than those estimated from the rule of mixtures. This was explained to originate from the non-uniform distribution of fibres. Also similar findings were concluded by using a continuous graphite fibre composite [103]. They used 6061 aluminium matrix and pitch based-graphite fibre to make unidirectional composites by a using squeeze casting technique. They

reported an almost linear relationship with respect to fibre volume fractions ranging from 4% to 52%. Increases of 62.5%, 222% and 300% for 10, 40 and 52% volume fraction of graphite fibre respectively were obtained. However, the dominant mode of failure was apparently that of fibre pull-out, consistent with the relatively weak fibre-matrix interface. Some evidence of interfacial reaction on the fibres were also reportedby them.

Boron/magnesium matrix composites were produced by an infiltration casting route.[104] Here also the improvement was significant. For example, the failure strength of the matrix was about 25 MPa, while for the composite it was about 153 MPa. Moreover, a SE micrograph showed that strong interfacial bonding was evident between the matrix and fibre as well as the fibres were not pulled-out of the matrix because of this, strength increased highly with volume fraction of fibre in their work.

The results of effects of the high temperatures on the tensile strength properties of Al alloys and B(SiC)-reinforced composites were shown in Figures 4.9 and Table 4 and these indicated a smaller reduction in properties when compared to typical values for unreinforced Al matrix. The tensile strength of the matrix at 300 ^{o}C was about 34 MPa, corresponding to reduction of about 80% compared with the room temperature strength. For the composites the strengths were about 207 MPa and 402 MPa for the 16% and 32% fibre composites, giving corresponding reductions of about 34% and 23% respectively when compared to the room temperature strengths.

Figure 4.9 showed that the rate of decrease of strength with temperature was broadly the same for all composites. However the matrix lost strength more quickly than the composites, especially near 300 ^{o}C. Nevertheless differences chiefly arose because of the higher initial strengths of the composites compared with the matrix. The two bidirectional composites were only moderately better than the matrix, reflecting their similar low temperature behaviours.

Considering that the strength of the fibres should be very insensitive to temperatures in the range up to 300 ^{o}C, the decreasing volume of the matrix in the high fibre composites should give a reduced sensitivity to increased temperature. However the contribution of the

matrix to the tensile strength was small, so that any effects are probably concealed by scatter in the results. The behaviour of the 32% fibre composite was slightly anomalous in that it appeared to weaken a little faster than the other composites at temperatures near 300 ^{o}C.

The good high-temperature properties suggest that fibre-matrix bonding was good, particularly for the unidirectional reinforced composite. The effect of the test temperature on the tensile strength of an Al/20% boron composite was studied by some authors [45] and the tensile strength at room temperature was almost found to be maintained up to 300 ^{o}C. Scheafer and Toth et al [39, 46] also investigated the variation of tensile strength with temperature for unidirectional and cross-ply of B/6061 Al composites. For 25 vol% and 50 vol% composites, strength reductions of 20 to 40% were reported from room temperature to 400 ^{o}C. The temperature dependence of the transverse strength of the composites was also found to be independent of the reinforcement content and the transverse strength decreased with increases in filament content at all temperatures. A similar reduction in tensile strength of the B(SiC)/Al composites.was found in the current study.

Considering the fracture surface of the composites, Figure 4.10 showed the fracture surface of the 16% B(SiC) composite at room temperature and a locally irregular topography was observed. This might be as a result of containing an uneven distribution of fibres in the matrix because of the production technique used. Figures 4.11 and 4.12 showed the fracture surfaces of the 21% B(SiC) fibre composite at low and increased magnification. The predominant failure mechanism was pull-out for this case. Although the presence of holes and short lengths of fibre protruding from the fracture surface indicated that some pulling out had recovered it is possible that only very short lengths of fibre had pulled-out. Such an effect could be due to fracture of the fibre at a point which does not exactly coincide with the microscopic plane of the fracture surface, and this pulling out may represent only a minor deficiency in bond strength at the fibre/matrix interface.

Figure 4.13 showed the fracture surface of the unidirectional 27% B(SiC) fibre composite at room temperature and high magnification and revealed a brittle fracture of the

fibres. There was a river line pattern on the fibre ends which indicates that cleavage had occurred. The matrix fracture surface was more complicated. These were significant numbers of pores and the fracture was at least partially ductile in nature, with small cusps in many areas. The presence of porosity does not necessarily imply poor infiltration, the poor feeding of a fibre-filled region could simply have produced shrinkage pores during solidification. However the porosity may have contributed to a lessening of the fibre/matrix bond in places due to level was weak of the porous matrix. Despite that, the plane of fracture was generally the same for the matrix and fibres, and it is believed that a good mechanical bonding had occurred between the fibre and matrix. Therefore, a considerable improvement in properties was achieved for the case of unidirectional orientated composites.

Figures 4.14 and 4.15 showed the tensile fracture surfaces of the matrix and low volume fraction of the 16% B(SiC) fibre composite at high and low magnification respectively. The first figure revealed the formation and growth of voids in the matrix due to the high temperature of the test. For the composite fracture surface, there was evidence that a very small amount of fibre debonding had occurred around some fibres, some of which also had secondary cracks. In addition, the composite matrix was heavily dimpled. This indicates extensive ductile matrix deformation at the point of fibre failure, when the matrix had fractured rapidly but in a plastic manner.

Figures 4.16 and 4.17 showed the fracture surface of the 32% B(SiC) fibre composite at 150 ^{o}C. Under low magnification, this figure showed a broadly smooth surface with some undulations. These were due to the presence of titanium tape in the fibres bundle which was used to hold the fibres together. The second micrograph shows an unusually large amount of porosity, but this does not appear to have affected bonding because there was very little pull-out of fibres. The reasonably smooth fracture surface with few fibre ends protruding shows that the relationship between fibre fracture and matrix fracture is evidently very close. This indicates that pulling each individual fibre caused fracture close to the advancing tip of the matrix crack during failure, if not at the actual crack tip. As a

result of this, improvements in the mechanical properties were obtained for this orientated samples. Apart from this, only a small amount of fibre was pulled-out. This could be because the fracture strength of the fibre varies along the its length, the weak points might have occurred away from the position of the maximum tensile strength so that the fibre failure occurred out of the fracture plane.

Figure 4.18 showed SE image of the fracture surface of 32% B(SiC) fibre composite. The vertical cleavage shear between the fibre core and matrix was observed. This might be indication of an enough bonding between the matrix and fibre or having defects on the fibre surface.

According to the present experimental results, as shown in Figures 4.8, 4.9 and Table 4, the tensile strengths of the composites showed considerable increases with respect to the fibre volume fraction. It is easy to understand that tensile strengths of the composites with 27% volume fraction of fibre were somewhat higher than those of the composites with 16% volume fraction of fibre. This is due to the difference in volume fraction of strong fibres. This work proved clearly that composites reinforced with B(SiC) fibres, developed high strengths at room and elevated temperatures.

However the experimental values were somewhat lower than the theoretical values calculated from the rule of mixtures equation. This probably would be because the strength depends not only the properties of the components, but also on the mechanism of the failure. The failure occurs by the development of microscopic-scale damage which spreads to form a major flaw such as a crack as shown in the fracture surface of the composites. Propagation of the crack is controlled by the essentially discontinuous nature of the composite and varies highly. Apart from that, there are many other factors which could lead to this phenomenon :

(1) The fibres may be damaged when they are pressure infiltrated,

(2) The fibres are very hard and very susceptible to influence of surface defects due to production processes or mechanical abrasion,

(3) The fibres may not be well distributed in the matrix and their orientations may vary slightly away from the tensile axis,

(4) The fibres may not have the same strength and uniform diameter.

5.3 Wear Behaviour of MMCs

The microstructure of the composites consisting of unidirectional or bidirectional B(SiC) fibre in the Al alloy matrix has been correlated with the increased mechanical strengths in the previous section. Based on the present results this metallurgical structure appeared to improve wear resistance also, under the different conditions used here. A low wear rate for the composites was observed at all test conditions, as discussed in the following sections.

Figures 4.19 and 4.20 showed the effect of load on the wear rate of the B(SiC) reinforced MMCs tested in the N and P orientations for a speed of 0.6 m/s respectively, together with the aluminium alloy matrix for comparison purpose. From the first figure, it could be seen that in each case the pin wear rate increased non-linearly with loads, especially for the unreinforced matrix at low speed condition. This might be for the following reason : during the sliding process, normal and tangential loads were transmitted through the contact points by adhesion and ploughing actions. The soft asperities were easily deformed and sheared under the repeated loading actions. Simultaneously the hard asperities on the counterface or hard particles between the sliding surfaces plough and cut the soft surfaces and resulted in changes of the surface characteristics. Because of this a non-linear increase in wear rate of the matrix was observed in both figures. However, for the composites a similar but lower tendency was observed in the N orientation for the 32% fibre composite. This also might be a result of the B(SiC) fibres in the matrix breaking on exposure at the rubbing surface due to the changing in the surface characteristics of the specimen. The wear rates of the composite under low loads were about 10 times lower than those of corresponding matrix due to giving less damage to the fibres. However, this reduced to factors of 3 to 6 in the case of higher loads and speeds in the N orientated samples.

For the P orientation, as could be seen in Figure 4.20, again, wear rate increased non-linearly with increasing load under similar data. Similar behaviour was obtained between the composite and unreinforced matrix alloy, whereas, it was found to be about 3 times lower than that of the aluminium alloy matrix. The reason for increasing non-linear behaviour of the composites and their difference between the matrix was probably a result of the fibre in the matrix, which broke on exposure to the rubbing surface and changed the surface characteristics of the specimens. It should also be noted that wear rate almost was independent of volume fraction of fibre. There was a progressive difference between the matrix and both composites and a considerable reduction was obtained in both cases. For instance, the reduction was about 64% for the P orientation while it was about 80% for the N orientation.

Figures 4.21, 22 and 23 showed the effect of load on the wear rate of the MMCs tested in N, P and AP orientations for a speed of 1.0 m/s respectively. To aid comparison, volumetric wear rate of the aluminium matrix alloy was also plotted in these figures. As shown in Figure 4.21, wear increased considerably with increasing loads up to the maximum load of 60 N for the matrix alloy because of an increase in the real area of the contact. A large difference between the matrix and composite, however, was observed due to the continuous B(SiC) reinforcement. Thus, the wear resistance of the composite was found to be more than 5 or 6 times better than that of the unreinforced matrix. The effect of volume fraction of fibre on the wear rate of the composites, as shown in Figure 4.21, was almost zero between composites with 21% to 32 vol % fibre. The 16 vol% fibre composite showed a slightly higher wear rate than the others. This might be due to the lower content, but it may also be simply as a result of containing an uneven distribution of fibres in the matrix because of production technique used. However, a considerable difference was found between the lowest volume fraction fibre composite and the unreinforced matrix. For the 16% vol fibre composite, the reduction in wear rate for the N orientation was about 77% compared with the matrix alloy while for 21, 23, 27 and 32 vol% fibre composites the corresponding reductions were 84, 85, 87 and 86% respectively.

For the parallel orientation (P), as shown in Figure 4.22, wear rate also increased linearly with the loads and no big difference was obtained between the various fibre volume fraction composites up to 22 N load. However, thereafter some difference was observed for this case. This is believed to be because of forming large fibre cracks on the sliding surface which will be explained in a later section, but the 32% fibre composite showed a lower wear rate than the others. It should be noted that the wear rates of the composite were about 4 times lower than that of the matrix. Comparison between these figures showed that an increase in load caused an increase in the pin wear for both orientated samples, but factors of 5 or 6 were obtained for the N orientation, while factors of 4 were achieved for the P orientation.

As for the case of anti-parallel orientation (AP), as indicated in Figure 4.23, wear rates almost increased linearly with increasing load except for the 21% fibre composite tested at a load of 60 N. However, a small amount of scatter occurred in that case, but significantly, there was no effect of fibre volume fraction on the wear behaviour of the composites, especially at loads of 12 N, 24 N and 44 N. This could be due to a degree of fibre breakage, as will be explained in the latter section on wear mechanisms. On the other hand, like the N and P orientations, composite wear rates were lower by factors of 5 or 6 than that of the unreinforced matrix for this orientation. From this figure, an abnormally high composite volumetric wear rate was found for the 21% B(SiC) fibre composite under 60 N load. However this was a bidirectional composite in which a small number of fibres was orientated at right angles to the others. In the plane of wear chosen for the test, some fibres might be parallel to the sliding directions and the rest anti-parallel, but the relative numbers would depend on exactly which plane section coincide with the wear surface.

Further test results carried out on the composites at different conditions of load and velocity conditions, were presented in Table 7. They were also graphed in Figures 4.24 to 4.25 which showed the wear rate as a function of load for the N and P orientations respectively.

In the case of highest sliding speed, again wear rate increased with increasing load, as shown in Figure 4.24, for the N orientation. It could be noted from Figure 4.24 that above 42 N (corresponds to 1.33 MPa), the tendency of the wear rate of the matrix decrease with further increased in load. It appeared that at higher pressures the intermetallic $CuAl_2$ particles may be smeared on the surface and produced a change in the trend. Figure 4.52 appeared to show small intermetallic particles embedded in a surface film. However, for the composites a large scatter in volumetric wear rate was observed among the various volume fractions of fibres, and the 16% fibre showed a similar characteristic curve like the unreinforced matrix, but a large difference was still evident between the matrix and this composite with low volume fraction of fibre. This might be due to containing an uneven distribution of fibres in the composite sample, as seen from the microstructure of Figure 4.56. However, 21% and 32% fibre composites showed similar trends to increase proportionally with increasing the load up to 32 N, but the 21% fibre composite generated higher wear than the 32% fibre composite, probably because of the small number of differently orientated fibres in that bi-directional material. On the other hand, the lowest wear was obtained for the 32% fibre composite due to existence of a good enough bonding between the fibre and matrix and this resulted in a less damage over the sliding surface. The wear rate of the composite was found to be about 3-4 times lower than the unreinforced matrix.

For the P orientation, no fibre volume fraction effect could be observed in Figure 4.25 and wear rate almost increased linearly with different loads. The wear resistance of the composites was about 6-7 times higher than that of the base alloy. This figure further revealed that the wear rate of the P orientation was found to be lower than that of the N orientation as shown in Figure 4.24 and compared with Figure 4.25. In the N orientation, this would probably be that the fibres were loaded as cantilevers under the action of the frictional force under this sliding condition. The friction force produced larger deflections and stresses in the fibres. Increasing sliding speed increased the lateral impact cycle and thereby resulted in chattering. The chattering also accelerated debonding and fracturing of

the reinforcing B(SiC) fibre. In the P orientation, however, the deflections and stresses were not so large in comparison to the N orientation as the fibres remain supported by the matrix at all times. Thus the wear rates are lower.

Figures 4.26 and 27 showed the effect of sliding speed on the volumetric wear rate under different loads for the N and P orientations respectively. The result showed that the wear rate of the composite and its matrix alloy first increased sharply with increasing sliding speed then decreased with further increase in sliding speed, giving a maximum at a sliding speed of about 1.0 m/s. For the composites, only small variations were found at high velocities. This showed the existing of a critical speed where the wear mechanisms appeared to change from initial sliding wear to an impact wear for the composite. This could be because of heat generated at the contacting surface and this was more pronounced for the alloy matrix due to existing of high thermal conductivity than the composite. As for an increase in volume fraction and load, similar trend was observed and the composite was still in very small value. In other words, volumetric wear rate was found to be minimum at the sliding speed of 0.6 m/s and then increased highly above this critical speed condition as shown in Figure 4.26. Similar observation could be seen in Figure 4.27 for the P orientation for the case of 0.6 and 1.0 m/s respectively. Again, volumetric wear rate increased with speed like a former case. However, there was a trend to decrease the wear rate at the sliding speed of 1.6 m/s under high load in general. This might be due to occurring a strong interface bonding between the fibre and matrix or producing a finer broken debris particles of fibres. This powdery worn debris, as shown in Figure 4.81, could be caused smoothing of the counterface and resulted in a decrease in wear rate with increasing in speed.

The effect of the volume fraction of fibre on the volumetric wear rate was shown in Figure 4.28 for the N orientation. Here is interesting result that the wear rate was reduced by incorporation of fibres but the volume fraction had little effect on the wear rate. The incorporation of the 16% fibre reduced the wear rate by about 72% in comparison to matrix alloy and by 84% for the 32% fibre composite. Higher wear was recorded for the 21%

fibre composite, but this was bidirectional, and can not be directly compared. According to the results, the volume fraction of fibre had a little influence on the wear rate of the composite above 16%. Similar finding was also observed in the P orientation under different loads. There was a small indication of reduction in wear rates with increasing volume fraction of fibre as shown in Figure 4.29. It was found, however, that the reductions were about 48% for the 16% fibre compared with matrix alloy and 64% for the 32% fibre composite, both under a 22 N load. From the figures, it is evident that wear rate was almost independent of the volume fraction of fibres for both P and N orientation, provided that the fibre content was at least 16%.

Figures 4.30 and 31 showed the effect of the fibre arrangement of the composite relative to the sliding surface on the wear rate for three main orientations under fixed load of 60 N. From the figures, each of the progressive wear curves was characterized by low similar wear rates. However, some differences were found in wear behaviour and the lowest wear rates were obtained for fibres orientated normal to the sliding surface (N). The highest wear rates were achieved when the sliding was along the longitudinal direction of the fibre axis (P), while sliding transverse to the fibre axis (AP) yielded intermediate wear. It was also found that there was a considerable difference between the composite and the unreinforced matrix. The reductions in wear rates were about 87 and 81% for the N and P orientations respectively, while the AP orientation showed a reduction of 84% compared with the matrix alloy. The dependency of wear resistance on fibre orientation was due to the degree of fracturing of the fibres because of stresses induced by asperities and hard particles in the contacting surfaces. Due to the limited bending range of the fibres before fracture, the most fibre fragmentation would occur for the P and AP orientations. These fragments contribute to the wear rate of the composite. This will be discussed in a detail in a forthcoming section.

Another series of tests was conducted on the composites under different sliding conditions of low speed and low load as indicated earlier. This showed that wear rate depended on the frictional conditions as shown in Figure 4.31. An apparently higher

degree of fluctuation behaviour was observed in the N orientation, but again, the 21% composite was bidirectional and can not be compared directly with the others. If this is ignored, the behaviour of N and P orientations is similar, but the absolute wear rate of the P orientation was much higher under these conditions. This figure also demonstrated that wear rate was dramatically reduced in comparison with the matrix alloy at low loads. It is considered that this is due to forming debris particles between the disc and pin sample in the N orientation. Therefore, for 16% and 32% fibre composites, the N orientation had a wear reduction of 92% compared with the matrix under the similar condition while a 64% reduction was obtained for the P orientation compared with the matrix alloy, but for the case of the 21% fibre composite, the corresponding reduction was about 44% in comparison with the unreinforced matrix. This must be due to the bidirectional fibre orientation of this sample.

In summary, volumetric wear rate of the MMCs increased with increasing applied load and showed a slight increase with sliding speed but decreased slightly with increasing fibre volume fraction beyond the 16% fibre, whereas for the unreinforced matrix, wear rate increased significantly with applied load and sliding speed. It was also found that the sliding in the N orientation yielded the lowest wear, followed by AP and P orientations. SEM examination of the worn surface showed that the wear mechanism appeared to differ slightly among the specimens with three orientations. These mechanisms depended upon the amount of breakage of the fibres near the surface which produced a mixture of hard fibre particles, and also the extent of a plastically deformed in a surface layer, subsurface matrix layer. The details of the wear mechanisms will be discussed in the following sections.

5.4 Wear Mechanisms of Unreinforced Matrix and Composites

From the results of the previous section of 5.3, it was quite obvious that the unidirectional B(SiC) fibre reinforced composites had excellent wear properties because the

reinforcement of hard fibre in the softer Al alloy matrix provided protection to the latter. The wear rates of the composites ranged from about factors of 3 to 10 for the composite with different fibre orientations and alloy matrix under the frictional conditions encountered here. That suggested that different wear mechanisms occurred depending on the frictional conditions. To explore the mechanism, SE, BSE and XPS analyses of the worn surfaces of the matrix and composites were performed.

Let us consider the wear behaviour of the aluminium matrix first. Basically, three theories have been proposed to explain the material removal mechanisms during the sliding wear of such pairs of materials as discussed in Chapter 2. These are the adhesion, abrasion and delamination. The adhesion theory is based on the hypothesis that atomistic contact between the asperities of the Al alloy and steel gives rise to adhesion or local welding stronger than the shear strength of the softer of the two materials.[65, 66] The delamination theory is based on the concept that the normal and tangential forces introduced during sliding wear will induce plastic shear deformation of the softer surface. Various steps involved in this process are : (1) transmission of forces, (2) deformation, (3) crack nucleation and crack propagation and (4) wear sheet formation. Crack propagation generally controls the overall wear rate if delamination is the operating mechanism.

The volumetric wear rate or weight loss of the Al-matrix material removal surface increased considerably with sliding distance and operating variables as shown in Figures 4.19 to 4.25. These figures revealed that wear rate increased with increasing sliding speed and increased linearly or non-linearly with the applied load under high or low load test conditions respectively. In order to determine the reason behind these different behaviours, a microscopic examination was carried out to find out the basic mechanism of wear during the wearing process.

SE microscopy image of the worn surface of the Al-alloy matrix, as shown in Figure 4.39, revealed that continuous grooves had formed throughout the wearing surface of the sample. It was interesting that the grooves were rather long and their paths did not change over the length of the track. These grooves were probably caused by the ploughing action

of hard asperities on hardened steel or wear particles produced during the wear process. It was also noted that the size of the plate debris roughly corresponded to the size of the patches of the highly damaged zones found on the worn surface. However, under high magnification examination of the worn surfaces of the similar matrix sample, shown in Figures 4.40 and 4.41 in SE and BSE image respectively, flat ridges of deformed metal were observed on the surface, and rather shallow grooving was also evident due to smoothing of the asperities on the surface, and by repeated sliding. The BSE image of the same sample also showed the clearly smoothed surface due to asperities losing their original shape in addition to the formation of the small amounts of oxide or metal particles on the surface. This might be caused by adherence of debris particles to the surface.

Increased magnification SE images of the worn surface of the Al-matrix alloy, as shown in Figure 4.42, revealed several cases of plastic deformation covering the abrasion grooves with matrix alloy and formation of microchips due to testing under high load conditions. It was also observed that fine scoring was a continuous process. This might be as a result of abrasion by entrapped debris particles formed as work-hardened deposits on the counterface. Further sliding flattened the roughened surface and resulted in the formation of a smooth surface as evidenced the BSE image of Figure 4.43. On the other hand, another mode of material removal was edge cracking since the edge of the strip limited its ability to withstand further strain without fracture. Thus when the edge was subjected to high tensile stresses in the plane strain (longitudinal) direction, cracks normal to the sliding direction were initiated. Such a type of feature was seen on the surface of this sample. In the BSE image of the same sample, regions of high atomic number (light contrast) showed that iron was transferred to the pin surface. This suggests a typical mild of wear mechanism (oxidational) because a large area of conformity came into contact between the sliding surfaces, but it was not always the case under the sliding condition of 1.0 m/s speed.

Figure 4.44 showed heavy grooving, and local spalling as well as smoothing in the sliding direction. Surface and associated subsurface plastic deformations were predominant

features of the wear scar morphology. Under the load studied here, it was clear that the principal wear mode was that of deformation and failure due to stresses associated with both normal and friction forces and as a result of this, the presence of cracks and voids on the surface might be caused by spalling in addition to thermal softening of the matrix. Here because of the severity of deformation and its interaction with abrasion or delamination, it was dominant over the alternative mechanism of oxidational wear. Under high magnification, as shown in Figure 4.45, the SE image of the worn surface of the matrix alloy revealed extensive damage and plastic deformation in the Al alloy matrix because the surface stresses exceeded the yield strength. The high degree of plastic deformation and consequent high rate of alloy removal prevented the production of an oxide layer. However, mechanical mixtures of oxidised particles were observed on the matrix surface, as shown in the BSE image of Figure 4.46, due to increasing the frictional heating at the matrix/disc interface. On the other hand, the existence of plenty of surface cracks parallel to the sliding direction and the dark smooth appearance of the surface also suggest that the transition took place from mild to metallic wear. This could be because the oxidation layer was destroyed when it reached a critical thickness at this high load of 60 N, which caused adhesion to occur.

The cross-section of the worn surface of the matrix alloy, as shown in Figure 4.47, demonstrated the formation of elongated voids and subsurface cracks at a certain distance below the wear track. This effect is due to the generation of stresses which have maximum effects at different points below the surface. Fragmented oxide particles were also observed because of repeated welding and fracture of debris particles. The BSE image of the same sample in Figure 4.48 showed more clearly that fragmentated oxide or debris particles were compacted into the wear grooves. It is suggested that an oxide layer protects the surface and gave the observed rate of increase in wear rate at high loads. The formation of a compacted layer together with the flattened worn surface might be due to generation of heat at the pin/disc interface and fragments were produced by high stress on the tips of the asperity because true area was smaller than the apparent area and resulted in filling of the

grooves. As a result of this, the surface became smoother. Examples of such features are shown in both SE and BSE images. In the literature K. Razavizadeh and T. S. Eyre [105, 106] have studied extensively oxidative wear of Al alloys. It was concluded that the formation of oxide was induced by the frictional heating and diffusion from hot spots.

The worn surface was sectioned parallel to the sliding direction of the matrix alloy pin to find out the predominant mechanisms of wear under similar test conditions. Such examples were shown in Figures 4.49 to 4.52. The subsurface observations closely indicated that voids did form in the deformed layer beneath the wear track. It seemed that voids were nucleated by plastic flow of the matrix around hard particles or inclusions through the coalescence of microvoids and vacancies during plastic deformation of the subsurface layer. Voids and cracks could link up by shearing and void growth or by propagating of cracks between these voids. It was shown that the circular cavities formed under combined normal and shear loading deform to an elliptical shape for this matrix alloy (Figure 4.48). The material between the cavities ruptured to join the deformed voids and produce a subsurface crack at a finite distance from the sliding surface, as shown in Figure 4.49. These subsurface cracks and layer, subsequently, lead to the detachment of wear debris particles in the form of thin plates whose thickness varied considerably depending upon the test parameters. This also suggested that delamination was the basic mechanism of wear.

Figure 4.50 also showed a similar effect underneath the wear track of the matrix pin, but the thickness of the subsurface layer was found to be less than the previous test. This strongly suggested that the thickness of the delaminated layer depended on the experimental conditions. The subsurface crack under the worn surface was nearly continuous parallel to the sliding direction. It was generated by stresses lower than in the previous case. A white (high atomic number) strain hardened-layer was also observed due to covering the surface with intermetallic particles and/or iron oxides near to the worn surface. The worn surface of another matrix sample at increased magnification showed that multiple subsurface cracking took place under the wear track which was quite different

from the previous two samples. This test was at a high speed, and extensive subsurface plastic deformation had occurred. The matrix had fractured in many place along the interdendritic network of intermetallics, and near the surface these had linked to form a long cracks. However the other different feature of this sample was the formation of a surface layer lower in atomic number than the matrix. It is presume that this is alumina, a hard substance which protected the surface from wear. The wear versus load curve of Figure 4.24 showed a slowing wear rate for this test.

The formation and growth of voids, as shown in the higher magnification micrograph of Figure 4.52, the flowing of the matrix material and the distorted region elongated in the sliding direction, are clearly evidenced by this micrograph, within a zone of about 30 μm deep. The another important characteristic was that the surface was straight at the upper part of the surface layer while the bottom part of the crack was a helical shape due to residual stress existing in the sheet.

An SEM examination of the wear debris could throw some light on the likely wear mechanisms. The analyses of the debris obtained during the wear test on 2014 Al-alloy showed the presence of two major types of wear particles : (1) plate type (180 μm), (2) fine agglomerated round particles (90 μm). These respective particles sizes were approximate, and depended on the operating variables. The majority of the debris was flaky plate-like in nature (Figure 4.53), indicating that delamination was one of the primary wear mechanisms in the Al matrix, whereas the presence of other types of oxidised debris particles, although the less numerous, suggested that wear was not entirely controlled by delamination, and oxidative or adhesion wear may be partly responsible. Any vibration even of small amplitude during the disc movement would generated a cyclic loading oscillating which might be considered. Therefore, giving rise to fine debris particles. Another reason for generating the round agglomerates may be due to the magnetic nature of the debris from these dry air tests. This could be ferromagnetic iron or ferrimagnetic oxides with the spinel structure formed by oxidation of iron to form $FeO.Fe_2O_3$.

In summary, an examination of the worn surface of the matrix revealed a number of differences depending upon experimental conditions. For example, a comparison between the low and high load conditions showed that a large load gave rise to a high level of disruption, extensive plastic deformation and abrasion, and formation of delaminated layers on the surface as might be expected. However, the nature of the surface generated could change in type as well as in the severity of damage as shown by the high speed tests.

Let us now consider the wear of the composites. In the case of the three main orientations tested i.e. N, P and AP, the lowest wear rate was obtained in the N orientation, while the highest wear was generated in the P orientation, whereas the AP orientation showed an intermediate wear rate. In order to reveal the reason behind this behaviour, worn surfaces of the composites after testing were microscopically examined by SEM and BSE. The different surface appearances of the N, P and AP orientated samples were shown in Figures 4.54 to 4.87.

Let us consider the wear behaviour of the N orientation first. Worn surfaces of the composite tested at a speed of 1.0 m/s were shown in Figures 4.54 to 4.64 under various loads. The surface of the composite possessed a relatively smooth surface appearance and contained cracks which were perpendicular to the sliding surface, as shown in Figures 4.54 and 4.55 at low and increased magnification respectively. In the latter case, it was clearly observed that the fibres were cut or fractured from the ends in a slicing manner. The broken fibre pieces were on average 10-25 μm in length. Normally, the Al alloy matrix has a lower modulus than the fibre and thus the difference in the axial strains between the fibre and matrix would produce a tangential stress and corresponding compressive loading of the fibres. Wear of the matrix could also give protrusion of the fibres. Therefore the contact load is transferred from the matrix to the fibres at the end of the fibre as well as the cylindrical surface. The combination of compressive stress with shear in the fibres gives a bending action exacerbated by the unsupported length of the fibres. The maximum bending moment in the fibre occurs where the fibre is the contact with the matrix. In other words the friction forces in the sliding process apply a shear load to end of fibres in this orientation,

and cause bending of the fibres. This is because fibre fracture in bending should take place for wear to proceeded as the planes are the N orientated to the sliding surface. This factor may be responsible for fractures of the fibres from the end, but this was more pronounced in the case of high speed conditions as shown in Figure 4.90. Alternative the fibre ends could fail by shear, but bending in general produces higher normal stresses than shear.

Matrix smearing over the fractured fibres was also evident and led to the delaying of the material removal from the specimen, hence resulting in a low wear for this orientation. Similarly, Figure 4.56 showed the worn surface of the 16% fibre composite, which had a slightly rough surface appearance because more fibre breakage had taken place in this case. This also caused some grooving over the surface of the pin. The length of the broken fibre particles was about 30-45 μm. It is explained as due to possessing a non-uniform distribution of the fibres. This low volume fraction composite with possible some poor bonding, revealed by occasional fibre pull-out. Small embedded particles over the matrix surface were also evident in Figure 4.57. Again, a smooth surface was observed in Figure 4.58 in spite of the fact that a high load was applied and the micrograph was taken at high magnification. From the micrograph, an important observation was that the formation of metallic debris over the pin surface which was subsequently oxidized during sliding processes. Such metallic debris would have to be plastically deformed by repeated "three body" entrapment events. The size of the debris particles was about 10-15 μm. If a large amount of debris was deposited on the worn surface of the specimen, this culd have resulted in a decrease in the weight loss of the sample. In particular, a large amount of debris were also formed during the test conducted at a speed of 0.6 m/s, but this one seemed to be hard oxide particles and brown colour debris was covered over the pin/disc for this orientation samples and was seen easily by the naked eye. The BSE image of the sample shown in Figure 4.59, revealed the small boron and metallic and oxidized hard particles which were embedded into the pin surface.

As for the case of low sliding speed effect on the worn surface of the composite, as shown in Figure 4.60, was that a similar surface appearance resulted, but some disruption

was observed over the sliding surface of the pin, and again, the predominant mechanism was that of fibre fracture and smearing of the matrix, besides which ploughing was also evident in the higher magnification micrograph of Figure 4.61. This might be due to abrasion of small asperity particles of the counterface or the fracture fibre particles. As shown in the BSE image of Figure 4.62, the fracture fibre particles in small size were embedded over the surface.

Under similar test condition, the 21% fibre composite, as could be seen in the SE image of Figure 4.63, showed extensive fibre fractures in both parallel and normal orientated fibres of the composite structure, some craters were also observed near the region of fibre clusters. They were possibly formed when the end of the fibres in the cluster were fractured. It appeared that in both case the fibres were broken catastrophically into short segments before they were pulled-out from the matrix. The large amount of fibre fracture obtained in that case was shown in Figure 4.64. Substantial fibre fracture and fibre pulling-out prevailed for this orientation, as indicated in Figure 4.65 at increased magnification. This might be due to debonding because the debonding effect was greater in the bidirectional orientated fibres because these fibres lied parallel to the sliding surface. The increase in debonding caused more fracture chattering in the parallel orientated fibres than the in the perpendicular fibres as shown in Figure 4.65. The debonding and fracture of reinforcing fibres were found to be greater for this sliding condition. As a result of this, the microstructure of the composite was also greatly distorted at the bottom part of the specimen. The other observation was that fibre fracture appeared not only from the ends but also from the middle. This also suggested that a higher degree of debonding was obtained in this orientation.

In the P orientation, fibre breakage occurred directly in the contact region as well as subsurface regions. Figure 4.66 showed the worn surface of the 32 % B(SiC) composite pin tested at medium speed and medium load, and the appearance of the worn surface of the pin was quite different from those of the N orientation. From the micrograph, the fibres had cracked into short segments some of which had peeled away. Consideration of stresses on

a fibre partially embedded in a matrix and subjected to an axial, or near axial shear indicates that tensile stresses would be set up at an angle of 45^0 to the plane of shear. The fibre would be expected to break up into segments with angled fracture surfaces. The exact fracture geometry could vary considerably from this theoretical prediction if the direct compressive stress is also taken into account. A simple Mohr Stress Circle construction indicates that the angle of the plane of fracture would steepen from 45^0 to nearer a transverse plane. Examination of Figure 4.66 and the high magnification of Figures 4.72 and 4.74 lends some support to this fracture mechanism, in that angled fractures are visible where the fibres had broken up. However considerable displacement of the fragments makes it impossible to say whether the fibre fractures were initially or approximately parallel planes.

The ready detachment of pieces of fibre, which were much larger than in the case of the N orientation fragments are considered to be the main reason for higher wear rates in this orientation. Fracture did not necessarily prevent the fibres from sustaining a load. For example in Figure 4.67, many broken fibres had worn down to their midpoints to reveal the tungsten core, and even if displaced some fibres could become embedded again in the matrix, as shown in Figure 4.68. In this micrograph, it could be readily seen that the fibres were broken toward the sliding direction and some pieces of broken fibres on the sliding surface had turned almost perpendicular to the sliding direction. The reason for this was that the alloy matrix had softened by the frictional heating and was able to flow plastically.

Figure 4.69 showed the mechanisms of ploughing and plastic deformation on the worn surface of a composite pin tested under similar condition. In addition to the fibre damage was the the fact that fractured fibre particles or hard asperities of hardened steel could plough and cut the matrix material in between the exposed fibres, resulted in abrasion, thereby increased the surface roughness of the disc. This was also confirmed by increase in roughness of the counterface from initial 0.12 μm to 0.48 μm (CLA) to a final value measured in the transverse direction of the sliding at the end of test, as shown in Figure 3.7. However the final counterface roughness in the N orientation was the 0.32 μm (CLA). The

large plastic deformation was shown in Figures 4.70 to 4.71 in SE and BE image respectively, and an agglomeration of this debris particles close to the fibre was revealed. These were about 3 μm in size, and were clearly derived from the broken boron fibres. Very small white particles mixed with the several debris, are thought to be iron debris from the counterface. The layer white particle is probably a fragment of tungsten. Thus the matrix smeared over the fibres contained a mixture of hard particles which would help it to resist wear.

Figures 4.72 and 4.73 showed the wear surfaces produced by heavy load at moderate speed but no significant variations in surface structures were evident although there was an increase in surface damage with this increased load. This suggested that increased load increased the severity of the wear process in accordance with Figures 4.23 and 4.25. Comparison of Figures 4.75 (low speed test) with Figure 4.79 (high speed test) showed that fibre fragmentation and matrix flow were greater in the high speed tests, and low load showed increased grooving and cratering over the surface compared with Figure 4.75. This can be explained by running distance at this case. However it also appeared that low speeds could lead to more fibre pull-out, as shown in Figure 4.78. Pull-out will result in weight loss as well as more rapid wear the fibre fragmentation, the parallel fragments are usually retained on the surface. At the increased magnification, the high speed tests produced more fibre fracture, the fibres were fragmented and some had pulled as observed in Figures 4.80 and 4.81 in SE and BSE images respectively. The length of the cracks varied and the BSE image showed that most of the small debris particles were together with iron or intermetallic.

As discussed in the previous section of 5.4, the debris particles for Al alloy matrix were found to be of a flaky type. This suggested that the basic mechanism of wear was delamination. For comparison purpose, let us look at the debris particles of the MMCs tested in the P orientation. The situation was quite different if the wear debris of the B(SiC)/reinforced composite is considered under similar test conditions and a change in the mechanisms of wear might be expected. The debris produced from the composite pin, as

seen in Figure 4.82, consisted of some small equiaxed powdery particles. This also suggested that the microfractures of the fibres had occurred, and the microfractured particles which had formed because trapped between the two contacting surfaces, and with repeated sliding became further reduced in size. As a result of this, fine debris particles were produced from the composites. The formation of these debris particles may have resulted in the excellent wear resistance of the composites in comparison to the matrix alloy.

In the case of anti-parallel orientation, fibres or fibre bundles were broke up into irregular fragments in the contacting surface due to the bending action of counter disc. Figures 4.83 and 4.84 showed the wear surfaces produced in SE and BSE contrast respectively. Encounters of these fragments with the neighbouring fibres led to further fibre cracking, but many remained attached to the matrix surface. It was also found that large lumps of deformed matrix adhered to the pin surface. This could be because the removal of pieces of fractured fibres had exposed the matrix in these places to rapid wear by grooving. However the transverse deformation of the matrix appeared to entrap the shattered fibre particles, giving rise to an overall lower wear rate in the AP orientation compared with the P orientation. The presence of chopped-up fibres with smeared over matrix on the wear surface was shown in Figure 4.85 in SE image, a sample tested at a load of 24N and medium speed. The surface appearance seemed to be smooth although it contained large broken fibres particles, probably because the other reinforcement in the composite remained intact in place and supported the applied load, but when the applied load induced bending stresses that exceed the fracture strength of B(SiC) fibres, the fibre fractured and lost its effectiveness. A certain amount of iron-rich material from the counterface was also evidenced by Figure 4.86 in BSE image. This BSE micrograph indicated that the low wear rates observed in the AP orientation composites may also be associated with the formation of iron-rich layers on the contact surfaces. During sliding wear, iron and possibly other alloying elements from the En 31 steel counterface, were transferred to the surface of the composites. The iron-rich transfer layers were developed at medium loads (24 N) where

many of the fibres remained unbroken during wear and thus could act as load bearing elements. There was little evidence for any large scale plastic deformation and damage in the matrix adjacent to the wear surfaces. This suggested that the removal of material from the surface of the steel slider was due to the abrasive action of the embedded fragments of hard B(SiC) fibres. The specific details of iron transfer are difficult to determine, and the iron could be metallic, in the form of compounds or as oxides.

Surface material suggestive of oxidation could be seen in Figure 4.87 at high magnification, where brittle fibre fracture, a smooth matrix surface and smearing were shown as well. Oxidative wear is indicated by this micrograph while the fractured parts of the fibres were smeared by the matrix alloy as shown in in Figure 4.88. Moreover, small debris particles were still embedded into the matrix and formed a mechanical mixed alloy. The size of these particles was about 6-12 μm in this micrograph. Again the small sizes are considered to be the fractured brittle fibres which further reduced them to small fine particles. These became embedded into the alloy matrix and gave the observed resistance of the composite to wear.

The cross-sections of the worn surfaces of the composites gave further information. Transverse and longitudinal cross-sectional views of the subsurface of the composites for each sliding direction were shown in Figures 4.89 to 4.97. It could be seen from Figure 4.89, that regions of fibre near the surface had been deformed and fractured into small pieces. The length of the fractured particles was about 10-25 μm and this part of the fibre was smeared by the alloy matrix. The thickness of the deformed, smeared metal was approximately 10 μm. The BSE image of the same sample was shown in Figure 4.90, and revealed the matrix flowing over the fracture fibres. However, in the case of high speed, as could be seen in Figure 4.91, it was observed that more cracks appeared in the fibres underneath the sliding surface of the 32% fibre composite. It is suggested that the fibres were bent and broken during the wear process and that the wear rate depended upon the extent of this speed-dependent subsurface damage. This figure further showed deep fibre fracture and smearing due to cyclic loading where the fibres acted as a cantilevers.

The transverse sectional view of the subsurface region of parallel-tested sample as shown in Figures 4.92 and 4.93, revealed evidence of a subsurface damage zone, where cracks and fibre splinters were produced below the wearing surface in SE and BSE images respectively. The thickness of the subsurface layer to the depth of a crack was about 40-60 μm. Surface grooves had been filled with debris. Figure 4.95 showed a transverse section of the anti-parallel tested worn surface of a composite. It was observed that catastrophic fibre fracture occurred close to the sliding surface while fibres deeper down suffered less damaged while subsurface deformation layer was shown in Figure 4.96 in BSE contrast. The length of these cracks were about 100-120 μm. Again the surface grooves had been filled with debris, and cracks had formed in those region also. From the micrograph, subsurface cracks were also evident due to surface fatigue, which were about 40-60 μm deep from the surface.

In summary, the presence of B(SiC) fibres in the base alloy provided protection to the softer matrix during sliding and also improved its load bearing capacity. But fibre fracture and a subsurface damage zone played an important role in determining the wear behaviour of these composite materials with different orientations. From the results of wear surface and subsurface observations, in the N orientation, it was found that fibre fracture and splinters were found to be of small dimension, and the damaged zone was not as deep as the P and AP orientations in the case of the tests conducted at 0.6 m/s and 1.0 m/s. Therefore, the N orientation showed the lowest wear rate and the P orientation the highest wear rate. The difference in wear rates between the P and AP orientations can also be explained based on the direction of propagation of fracture planes in the fibres. In the P orientation, under the action of the friction force, fracture planes propagate at about 45^0 to the axis of the fibre, like a micro-peeling as evidenced in Figure 4.66. However, in the AP orientation, fracture planes propagate perpendicular to the fibre axis and propagation of cracks can be easier along the fibre axis. Therefore, lower wear rates were found in the AP orientation, whereas, the effect of fibre orientation on the composites depended on the tribological operational variables of load and speed.

The direct method of investigating chemical nature of the worn surfaces of the pin was that of X-Ray Photoelectron Spectroscopy and the data obtained from the technique was considered. Let us consider the X-ray spectra results for the N and P orientations given in Figures 4.96 to 4.101 together with the elemental compositions of the worn surfaces of the composites pins which were listed in Table 8. Figures 4.96, 4.97 and 4.98 showed that O, C, B, Al, Fe, Si and N were observed. Of these elements, basically oxygen and nitrogen were from the atmosphere, the presence of carbon was due to unavoidable atmospheric contaminates or residues of sample cleaning. Iron picked up from the counterface, and boron from the reinforcement and aluminium from the matrix were detected. From the figures, it could be seen that there was no significant variation in the amount of oxide over the surface under these sliding conditions and orientations.

The expanded parts of the graphs were shown in Figures 4.99 to 4.101 respectively. Figure 4.99 showed the XPS spectra for the N orientation tested at a speed of 0.6 m/s and load of 24 N. It appeared that two components of boron, namely, one in the form of boron oxide (B_2O_3) and another in form of iron boride (FeB_2) were observed here. In the case of the expanded area of the N orientated sample, but tested at a high speed of 1.6 m/s as shown in Figure 4.100, the components of boron oxide and iron boride appeared again, whereas, the content of these components were quite different. i.e. B_2O_3 was about the same amplitude of 2 kc but FeB_2 had decreased by a factor of 6. Also the total amount of boron decreased from 21.5 % to 9.4 % and Fe decreased from 9.5% to 2.2%. However Al and C increased considerably. This was the feature of the high speed test condition.

Figure 4.101 showed the expanded area of the P orientated sample tested at the sliding speed of 1.6 m/s. From the Figure, the same two components were also observed. Boron oxide remained at 2 kc peak, whereas, iron boride had increased slightly to a 3.4 kc amplitude. From Table 8, it was observed that a total boron content decreased from 12.1% to 9.4%, but iron was much lower than before.

Comparison of the XPS results from worn surface samples showed that the amount of Al decreased in the N orientation at low speed in comparison to that for the N, P

orientations at high sliding speed conditions. This might be due to formation of a tribofilm on the N orientated sample at low speed. As result of this, little fibre breakage or pulling-out of fibres had occurred, and matrix removal from the composite pin during sliding was small because the composites. This was mainly consisted of B(SiC) fibre and an Al alloy matrix. However, in the case of high speed tests, the situation became different because Al increased sharply and boron decreased highly. This indicated an opposite effect compared with the previous sample. It means that more fibre breakage took place in both N and P orientations at this speed and some of the pieces were removed, while the rest of it formed a mechanically mixed alloy due to heavy sliding speed. Thus, Al increased considerably because of removal of the fibres from their places and C increased slightly due to atmospheric or surface contamination. However, for the P orientation, despite the fact that the same test conditions were used, the amount of Fe was found to be lower than the N orientated sample although the Al alloy matrix was similar content in both composites. This could be due to differences in surface topography.

It is worth comparing the results observed here with those of similar materials tested, especially considering the effect of fibre orientation on continuous carbon-fibre reinforced metal matrix composites [69, 72, 84] and on continuous alumina-aluminium composite materials.[95, 96] Similar conclusions were reported for alumina-zinc based composites with randomly dispersed fibres.[93, 94] All of these workers considered that specimens in which the fibres were arranged perpendicular to the sliding surface had better wear resistance than those in which the fibres were arranged parallel to the sliding surface because the former case needed extra energy in order to damage the fibres. As for the current study, this idea was also true. The wear rate was indeed low enough but in our case tests were made for three different orientations : N, AP and P. The principal mode of wear was explained by microfracture, cracking of the fibre ends, and matrix smearing on the fractured part of the fibre at rubbing speeds under 1.0 m/s. Also the formation of oxide debris films were observed, preventing the direct contact between the pin and disc for the case of low sliding speeds, e.g. 0.6 m/s. There were a few conflicting reports on the difference in wear rate

between P and AP orientations. For example, one investigation found that the AP orientation was even better than the N orientation [86] while the P orientation produced the minimum wear rate in the SS/Al matrix composite. [84] However, H. Nayeb-Hashemi et al [74] also found that the P orientation produced more wear than the others due to pulling out mechanism.

The present results agreed with previous in that they showed that wear loss of alignment P was larger than that of the AP orientation. The reason became clear when the their worn surface were observed by SEM. The fibres on the worn surfaces of the P orientation were cracked into short segments due to shear by the hardened counterface disc. After fracture the broken fibres separated from the matrix, and many were lost from the surface. Because the grooves left by displaced fibres were parallel to the sliding direction, fibre particles and other debris were not trapped in these grooves. Thus the matrix was left unprotected by either fibres or a debris layer. This would cause slightly increased wear compared with the AP orientation, because fractured fibre particles in the AP orientation were either embedded in the matrix or could be lodged between the fibres for this orientation. However there are still disagreements among investigators. For example, Amateau [109] showed the orientation of fibre did not significantly affect the wear rate and coefficient of friction of an Al alloy composite containing graphite fibres. He argued that a thick graphite transfer layer dominated the frictional behaviour and masked the effect of orientation. However later McKittrick and Amateau [72] observed strong anistropic wear behaviour in graphite-copper based alloy composites and explained that only a thin adherent debris layer was detected, which could not mask the effect of fibre orientation. Therefore, the lowest and highest wear occurred in the N and P orientations respectively. By contrast, Lu and Friedrich [86] reported the lowest wear rate for the AP orientation in carbon fibre glass matrix composites. This was explained by the fact that the formation of brown debris played an important role. A similar finding was also reported by Tao, Wang and et al. [85]

5.5 Friction Properties of MMCs

It appeared that the tribological behaviour of B(SiC)-reinforced MMCs has not been studied so far. It is not possible to compare the results of the present study with those of other investigations.

The friction coefficients of the MMCs of the present study were shown in Figures 4.32 and 4.34 for three orientations, tested at a speed of 1.0 m/s under various loads. The variation of the friction of the unreinforced matrix alloy with applied loads was small with an average value of 0.35 over the range of loads used. For the matrix, the coefficient of friction was found to decrease as the normal applied load increased. This is attributed to the increase in sliding interface temperature which increased with frictional heat at higher loads. However, the introduction of the fibres increased the coefficient of friction considerably in all orientations. This might be due to a greater ploughing component in the friction of fibre composites particles incorporated in the composite specimen because these fibre particles abraded the counterface significantly and resulted in the fractured fibre particles and counterface particles embedded in the matrix surface. Intermediate friction coefficients were found when the fibres were orientated normal to the sliding direction as shown in Figure 4.32. Its average value was 0.56 for a speed of 1.0 m/s. The 23% fibre composite showed the highest value of friction at the lowest load of 12 N. There was also a trend to a decreasing friction coefficient with increasing load and fibre content. The reason for the reduction in friction coefficient at higher loads is thought to be because of chipping and fragmentation of the fibre ends at higher compressive loads. As the fibre content increased, the average stress on the fibre ends decreased and limited the depth of penetration of the fibre into the counterface disc, and therefore leading to a final reduction in friction coefficient.

For the P orientation, friction coefficients formed a close group as shown in Figure 4.33. The lowest friction was obtained for this orientation because the counterface made direct contact with the B(SiC) fibre. Average friction coefficients were virtually identical and were about 0.53. No fluctuations in friction force were seen throughout the test, but some

indication was observed of a reducing in the friction coefficient with increasing volume fraction of fibres especially at high load. A small increase was also noted for the 21% fibre composite, and the reason may be due to the existence of a bidirectional composite of orientation which could trap the fracture debris particles between the pin and disc. However, the highest coefficients of friction of about 0.65 were obtained when the sliding direction was transverse to the fibre axis as shown in Figure 4.34. This suggested that larger wear particles were created in this orientation as evidenced in Fig.4.86. The particles could either be lost from the contact zone after being broken from the composite surface or remained there for a fixed time as a transferred layer and plough the specimen effectively. The coefficient of friction thus depended on the total amount of the various particles in the wear debris, hence, the coefficient of friction was high. It was observed that the AP orientation demonstrated some fluctuation in friction force during the test. This was in contrast to the case of longitudinal sliding in which the friction force remained more or less constant throughout the test period. Again, the friction coefficient of the 21 vol% composite was higher because of more fibre breakages. The friction coefficient was also found to be lower at high load, but friction tended to decrease slightly as the fibre volume fraction increased in particular for loads of 12 and 24 N. From the result of the composite tested under a constant speed of 1.0 m/s, there appeared to be an increase in friction coefficients in order of P>N >AP type geometry.

As for the case of low sliding speed, shown in Figures 4.35 and 4.36, the coefficient of friction of the unreinforced matrix increased up to 0.50. For the matrix, there was a trend to an increasing friction coefficient with increasing load up to a certain point, followed by a decrease. This phenomenon is recognised in other studies, and may be attributed to the ploughing of abrasive particles and generation of heat. For composites with the N orientation, the friction coefficient was found to be about 0.53 and no considerable increase was observed with increasing load, in fact it remained almost constant for the 16% fibre composite. However, a large scatter appeared especially for the 32% fibre composite. This might be due to production of debris particles on the contacting surface under low loads.

There was also a trend to decrease in friction coefficient with fibre content and load in this high fibre composite. This might be because of the reduction in the exposed area of matrix due to fragmentation of fibres.

For the P orientation, the effect of volume fraction of fibres was less clear. It appeared that coefficient of friction tended to decrease slightly with increase in volume fraction of fibres as shown in Figure 4.36. The lower friction coefficient was found for this orientation with respect to the N orientation, but the difference between them was little and no big variation with loads was evident. This also suggested that friction coefficient may be dominated by the surface properties.

The variation of coefficient of friction with sliding speed for the matrix alloy and its composite sliding against steel disc was shown in Figure 4.37. The variation of coefficient of friction in both matrix alloy and composites appeared to be relatively small at speeds between 0.6 and 1.0 m/s, except with 32% fibre composite. The friction coefficient was found to be high which was about 0.65 for the 32% fibre composite because of fractured and embedded particles over the surface. However, in the case of higher speeds, the friction coefficient was more dependent on a speed for the matrix alloy because of increasing sliding temperature between the matrix and counterface. For the composite, the friction coefficient of both 16% and 21% fibre composites had some slight trend, thus displaying a little dependence on speed. This might be as a result of increasing the surface roughness of the counterface as the sliding velocity increased and also changing the surface characteristics of the pins, due to fracture and reattachment of reinforcing B(SiC) fibres. Consequently, the coefficient of friction decreased with sliding speed. With the 32% fibre composite, the friction-reducing action of fibres was a very great, and produced a very low friction at high speed. Again this suggested that more fibre contacting area and fragmentation of fibre fracture particles might be responsible for this trend.

The variation of friction coefficient with sliding speed for the P orientation was shown in Figure 4.38. The friction coefficient was found to be higher than the matrix alloy due to hard fibres and the friction increased up to 1.0 m/s and then decreased in a similar way to

the matrix, but a considerable difference was observed between them. This was due to changing of the surface characteristics of the composite pin, where the ploughing component of friction became more effective up to 1.0 m/s and led to increased friction coefficient in this orientation.

5.6 Wear and Friction Behaviour of PMCs

From the discussion of the results of the preliminary tests for MMCs it was quite clear that the unidirectional reinforced composites had shown excellent wear properties. Among the three main orientations, the N orientation of the fibres appeared to have more wear resistance than the others. On the other hand, the P orientation showed the highest wear rate. In order to clarify the effect of the matrix type on wear behaviour, PMCs were produced by a hot pressing technique using the same unidirectional fibre of B(SiC) and tested under similar conditions to find the predominant mechanisms of wear. The following discussion, therefore, is related with the wear and friction behaviour of the PMCs.

The volumetric wear rate versus sliding speed data for the composites tested in N orientation, as shown in Figure 4.102, indicated that the PMC reduced the volumetric wear rates of unreinforced HDPE matrix considerably, and a transition region was observed for the polymer matrix at a critical speed of 1.0 m/s. The rapid increases in the wear rates for HDPE matrix above this speed were due to extensive softening of the polymer because of frictional heat and as a result of the destruction of its structure due to ease of slippage between the crystalites. This softening resulted in increasing by further deformation the area of contact with increasing sliding speed and load. Under high speed conditions, the decreases in wear rates for the polymer matrix were also due to the generating of orientated molecular chains distributed mainly parallel to the sliding direction.

For the composites no such big transition region could be observed, but only a little variation was evident under low sliding speed and a small increase in volumetric wear rates was observed. In fact, PMCs rubbing on the wear track behaved like an unreinforced polymer matrix but at very different wear levels. It may be however that high interfacial

temperatures were only generated in small local areas due to protective covering of fibres on the sliding surface of the pin and the load was carried by means of these fibres. Consequently, there was a great reduction in the wear rates of the composites in comparison to the matrix. Similarly, the volumetric wear rates of the composites almost remained constant at a speed of 1.6 m/s, but a slight trend to increased wear with speed was evident in the case of the 28% fibre composite. In other words, sliding speed did not affect the wear rates of the composite much while the matrix was significantly affected by speed and fibre volume fraction had little effect as well. Briscoe et al [110] studied the friction and wear behaviour of HDPE matrix and 5% Wt lead-oxide and 30% copper-oxide HDPE composites under low and high sliding speeds (0.01 m/s and 2.1 m/s) and different loads up to 6.0 kgf. They reported no change in the frictional behaviour of the HDPE and its composites at low speed. At high speed, however, the wear behaviour of both the polymer matrix and its composites against smooth steel was markedly affected. For loads over 5.0 kgf, the wear of the unreinforced matrix increased very rapidly with load compared with the reinforced composites. Also the coefficient of friction of the HDPE increased sharply with load due to frictional heating, but the coefficient of friction of the composites remained constant at all loads. This was in contrast to the present case.

For the P orientation, volumetric wear rate versus sliding speed for the composites, as seen in Figure 4.103, showed quite different behaviour in respect to the previous one. It appeared that the volumetric wear rate decreased slightly up to 1.0 m/s and no significant variation was observed, but there was an indication of increasing wear rate with speed over 1.6 m/s. In addition, both volume fraction of the composites showed a similar trend with speed, but the 28% fibre composite had a lower wear rate. This was due to the fact that unidirectional fibres made direct contact with the hardened steel disc and this led to a rise of temperature between the disc and composite pin with repeated sliding, softening of the matrix and hence reducing the fibre/matrix interfacial shear strength. The above factors may be responsible for obtaining a higher wear rate in this orientation of the tested composites.

As for the case of the effect of load on wear rate, very variable behaviour was evident in all orientations shown in Figure 4.104, tested at a speed of 0.6 m/s. It was seen that the wear rate of the matrix increased non-linearly with increasing load. For the composites, the wear rates were low at a load of 12 N and also no big difference was noted between the PMC with different orientations except for the P orientated 28% fibre composite. However, for the tests conducted at 22 N load, the wear of the polymer matrix and composite increased rapidly and slowly respectively. With increasing loads over 22 N, the wear loss of the matrix could be extremely large and lead to complete destruction of the sample, but this was unclear (with some exceptions) for the composites. Among the orientation effects, the AP orientation gave a lower wear rate than the others while the P orientation again showed the highest wear. This might be due to mechanisms of pull-out, as will be discussed in a forthcoming section. Similarly, Figure 4.105 showed the volumetric wear rate as a function of load for B(SiC)/PMC at a speed of 1.0 m/s and quite different features could be observed for the unreinforced matrix while the composites in general formed a group but showing some differences between them. For instance, wear rates of the matrix increased with load up to 22 N load and thereafter, there was an indication of decreasing wear with increasing load. In the case of the composite, the P orientation produced more wear than the others at low and high load conditions. However the AP orientation generated higher wear at a load of 22 N. This suggested that more fibre fractures occurred for the AP orientation with the load.

The effect of fibre volume fraction on composite wear, as shown in Figures 4.106 and 4.107 for the N and P orientations respectively, indicated a considerable reduction in the wear rate of the composites compared with the matrix at a load of 22 N under various sliding speeds. The first figure showed that changing fibre volume fraction had little effect on volumetric wear rates for the N orientated composites due to a similar mechanism of wear, but the 28% fibre composite showed that the higher wear rate was obtained for the test carried out at a speed of 0.6 m/s. Possibly more fibre breakage could have occurred during the initial sliding period. However, in the P orientation, as shown in Figure 4.107,

wear volume seemed to be more dependent on the volume fraction of fibre in particular for the composite with low fibre volume fraction. This might be because of the softening of the matrix material and as a result of this, the high volumetric wear rate appeared for the composite with low volume fraction of fibres. However little additive effect was observed when the volume fraction of fibre was increased to 28%, and both composites showed the similar trend, but the test performed at low sliding speed gave a higher wear rate than that at medium speed. This also confirmed the previous work of MMCs which was tested in the P orientation as shown in Figure 4.78 and this also suggested that the pull-out was more pronounced at low speed and resulted in more wear than the other orientations. This was also related to the fibre orientation, therefore, more detail will be given in the following section.

Variations in the volumetric wear rate for all three orientations with the volume fraction of fibre under 22 N load were shown in Figures 4.108 and 4.109. This figure showed that the wear rate was strongly controlled by the sliding direction in PMCs. The highest wear rate was obtained for the P orientation, while progressives lower wear rates were found for the AP and N orientations respectively. Generally the AP orientation was found to be only slightly different to the N orientation. However, it is interesting to note that there was little effect of fibre orientation on the composite at the highest volume fraction of fibre of 28%. This work was consistent with previous work on the effect of fibre orientation of graphite-polyester based composite.[111] In their work, for a composite with low volume fraction (20%) the longitudinal direction had higher wear rate, whereas for the composite with high volume fraction (greater than 40%), no orientation effect was found. Again there is still some disagreements among the investigators. For instance, Sung and Suh, [112] Cirino, [117] and Tsukizoe and Ohmae, [114] showed that the N orientation exhibited a lower wear than the P orientation. However, Giltrow and Lancaster's later work with a high volume fraction of graphite/epoxy composite showed no observed orientation effect on the wear rate which is opposite to the present results obtained for B(SiC)/HDPE polymer composite. This was probably be because there was more contacting surface area of the

matrix in the case of composites with low volume fractions, and this also led to rapid softening of the matrix for this case. Thus sliding of the fibres out of the surface occurred under the shearing force of the counter disc, in the P orientated samples, and this produced the high observed wear rates for this orientation. The reduction of wear with increased volume fraction of fibre can be attributed to lower surface stress when more fibres were present which reduced pulling out by shear. However, fibre fracture and displacement became more dominant for the N and AP orientated composite samples.

For the N and AP orientations sliding of the fibres out of the surface was not possible, but fibres were broken off and chipped (N) or bent and removed by fracturing of longer length (AP). Thus although the addition of 14% fibres to the matrix greatly reduced the wear rate, the high volume fraction composites resulted in ventrally no improvement in wear resistance, and in some cases an actual deteriation (Figures 4.108 and 4.109). It was observed that fragments of fibres were not embedded in the surface of the polymer composites, in contrast to the metal matrix composites. Thus the fibre fragments were simply lost from the surface and could play no further point in resisting wear. It is considered that this was the principal reason for the poor effect of high volume fraction fibre on the wear rates.

It was noted that B(SiC) fibres reduced very much the wear rate of the polymer matrix. The reductions of the 14% fibre composite at a speed of 0.6 m/s were about 43, 61 and 93% for P, AP and N orientations with respect to the matrix respectively, but it was also dependent on the operational conditions. For example, the reductions of 14% PMC were 56, 91 and 92% for the P, AP and N orientations while the reductions of 28% fibre PMC were 74, 93 and 83% for the P, AP and N orientations respectively at a speed of 1.6 m/s.

It was concluded that the effect of fibre orientation was found to be more pronounced for the PMC with low volume fraction due to softening of the matrix in the composite specimen. In the case of high fibre volume fraction, however, only a little dependency on the orientation was observed because of the different mechanism of wear.

The fibre orientations in increasing order of wear were normal, anti-parallel and parallel. Considering the coefficient of friction, there was almost a reverse trend. The results obtained here were quite different from those observed in studies of in graphite fibre composites, [112] but similar results were reported by others.[114, 117, 118] Figures 4.110 to 4.112 showed the coefficients of friction for both composite and its matrix in N, AP and P orientations respectively, tested at a speed of 0.6 m/s. It could be observed from the figures that the highest coefficients of friction were obtained in the N orientation, but the lowest wear was evident for this composite, while the lowest friction coefficient was attained in the P orientation of the composite. From the first figure, B(SiC) fibres in the N orientation samples reduced the friction coefficient of the matrix slightly as a consequence of changing the nature and properties of the interacting surfaces with increasing the fibre content. For instance, the friction coefficient of the matrix was about 0.52 while it was about 0.39 for the 14% composites under 12 N and 22 N loads. Some indication of increasing coefficient of friction was observed with further increasing volume fraction of fibre. This might be due to increasing fragmentation of fibres on the worn surface. On the other hand, the hard B(SiC) fibres cut the hardened bearing steel counterpart thus increasing the cutting component of friction coefficient. As a result, the ploughing component of friction was higher. This trend was true in the N orientated samples especially under high load test conditions. For the AP orientation under high load, similar trend was observed but the difference in the friction coefficient was found to be great between the AP and N orientations. This might be due to forming of a thin plastic film over the counterface disc and pin sample or possibly the other reason was that the ploughing component of friction was not as effective in this orientation. For the P orientation whereas there was a decreasing trend in both fibre composites due to the domination of fibre sliding.

As for the case of high speed test condition of 1.6 m/s, Figure 4.112 showed the coefficient of friction versus volume fraction of fibre for PMCs, tested at loads of 12 and 22 N. Similar observation was seen at this condition especially for P and AP orientations. This could be because of their having an identical surface. In other words, it was clear that

the coefficient of friction decreased highly with increasing fibre volume fraction for both P and AP sliding direction at this speed. Again the decrease in friction coefficient was due to smooth fibres on the counterface surface, partially lubricated by melted polymer features. However for the N orientation, the friction coefficient increased with increasing fibre volume fraction and a slight increase in the friction was also observed with load due to the ploughing of the exposed fibre ends into the counterface. The reductions in the coefficient of frictions were about 49 and 78% for the 28% fibre PMC in comparison with the polymer matrix.

The effects of sliding speed on the coefficient of friction for the PMCs in three orientations were shown in Figure 4.112. It appeared that the coefficient of friction was higher in the matrix than the composites with different sliding speeds. In other words, the coefficient of friction of the matrix increased from 0.52 up to 0.68 with increasing speed. This might be because of softening of the polymer due to frictional heating and causing an increased area of contact. A little dependency was observed at speeds of 0.6 and 1.0 m/s. Above this speed a little more dependency was obtained in both orientated composites. On the other hands, the coefficient of friction of the composite increased with increasing sliding speed especially over the 1.0 m/s speed, but rate of increase in coefficient of friction was proportional and was in order of AP, P and N, and unreinforced matrix respectively. The increase in friction coefficient of the N orientated sample might be due to progressive fracturing of fibres with increased speed, and ploughing of the debris. Softening of the matrix is considered to be the reason for the high friction coefficient of the matrix. For the P and AP composites increased fracturing of fibres at increased speeds is considered to have formed sharp bodies on the surface, which gave increased ploughing, modified by localised melting of plastic under contact loads.

In summary, among the orientation effects, the highest coefficient of friction was obtained for the N sliding direction due to effectiveness of ploughing component and showing a slightly anistropic behaviour while the P and AP orientations indicated the lowest coefficient of friction and was found very close to each other because of identical surfaces.

5.7 Wear Mechanisms of PMCs

In the previous section, unidirectional B(SiC) fibres were found to be very effective in reducing the wear rates of the composites in comparison to unreinforced matrix. Also the effect of fibre orientation on the wear rates of the PMCs under different experimental conditions revealed that the highest wear rate was obtained in the P orientation while the lowest wear was found in the N orientation. However, the AP orientation in some cases was competitive with the N orientation. In order to understand what happens at the contact surface of the tested materials, metallographic investigations were performed to determine the mechanisms of wear based on the SE microscopy observations.

An SE micrograph of a typical pin surface of HDPE polymer matrix, as shown in Figure 4.115, showed features characteristic of relatively ductile material. The pin was tested at a high sliding speed of 1.6 m/s and 12 N load. It was clearly evident that longitudinal furrows had formed because hard metal asperities had ploughing the softened surface of the polymer. Some layers were also observed on the surface of the composite pin. Wear debris was formed by the subsequent microcutting mechanisms which was necessary to separate the ploughed material from the surface. A magnified view of the same polymer pin was shown in Figure 4.116. It appeared that small particles of polymeric debris had been flattened or melted during wear, and were re-attached to the surface. At the lower speed of 0.6 m/s, these particles were much fewer in number (Figure 4.117) showing that sliding speed had a powerful effect and thus that melting may have been of primary importance. The sliding process appeared to orientate the polymer molecules in the direction of sliding as evidenced in the Figure 4.116. This process also enabled a very highly orientated uniform film of polymer to be transferred onto the counterface which appeared as a yellow layer when viewed with the naked eye. Continuous sliding of the polymer over this film did not cause any further transfer as sliding was between two highly orientated films which moved over each other. The shear strength at the interface may be comparable with the force necessary to pull further orientated polymer out of the pin. This was thought to be reason for low wear of HDPE after critical speed. At low sliding speed,

however, it was observed that the yellow transferred films were thin and transfer of HDPE matrix to the counterface was relatively weak held, and the film was readily detached. As a result of this, a continuous transfer and removal of polymer matrix from the counterface could take place. This might be responsible in producing a high wear rate up to 1.0 m/s speed. On the other hands, at high sliding speed, the surface roughness of the counterface was reduced because the transferred polymer, and sliding occurred between orientated molecular chains of HDPE on both surfaces which could lead to considerable reductions in the wear rates.

Furthermore, some cracks were also observed on the surface layers. This might be thermal cracking due to local heat at the contact spots because of the low thermal conductivity of the polymer. The width of the surface layer was about 100-180 μm while the length of the cracks was approximately 20 μm. The same matrix material was also studied using a similar technique by other researchers, For example, Pooley and Tabor [119] investigated the wear and transfer properties of HDPE and PTFE and found them very different from those of other polymers having bulky side groups in the molecular chain. They observed the extensive transfer of a thin film about 2.5 nm thick, and suggested that the low friction and light transfer of PTFE and HDPE during sliding were essentially due to their smooth molecular profiles. Tanaka and Miyato [120] also observed an extremely thin PTFE transfer film on a glass surface at a speed of 0.18 mm/s. However, they observed that the transfer properties of HDPE were different from those of PTFE and were similar to those other polymers having a spherulite crystal structure. The transfer of polymers other than PTFE contrast markedly with the film-like transfer of PTFE, being generally as small lumps or short streaks. They suggested that the HDPE molecule, having a smooth profile similar to PTFE, also possessed an excellent ability for film formation, provided that easy drawing of molecules from the spherulite structure is possible during sliding. Tanaka et al [121] studied transfer in multiple passes at various sliding speeds. In their work, the thickness of the polymer layer transferred to a steel surface was measured using electron capacity resistance. They reported a great variation in reduced thickness at low and high

speed conditions. With PTFE and HDPE, the reduced thickness after 1000 revolutions at 0.01 m/s was found to be smaller than that at the higher speed at 1.0 m/s. They concluded that the thickness of the transferred layer at 1.0 m/s was greater than that at 0.01 m/s. This was consistent with the results of the present work on HDPE tested under low and high speed conditions.

Considering the effect of fibre orientations on the wear behaviour of PMCs, different forms of wear mechanisms were observed for each of the main orientations, as shown in Figures 4.117 to 4.126. Figure 4.117 showed the worn surface of the composite pin tested in the N orientation under 12 N load and at a speed of 1.0 m/s. The major contribution for material removal was caused by the asperity particles cutting the fibre ends and generated splinters. A few of these splinters were reattached to polymer surface, especially toward the trailing edge of the wear pin where a fibre rich region was formed and transfer films were formed on both smooth surface. A similar observation was made for the anti-parallel orientation. The average length of the fibre pieces was greater than the original fibre diameter. Figure 4.118 taken at high magnification showed that fibre fracture took place from the end in short pieces. The average size of the fracture particles was about 20-30 μm, much bigger than in the MMC samples. Such particles were observed close to the trailing edge of the fibre. Moreover, some cavities were also evident. The cavities on the worn surface must be produced by the detachment of pieces of fibres from the frictional surface of the composite and plucking out of this broken of these splinters.

A similar surface appearance was observed in the case of high sliding speed, as shown in Figure 4.119, but this test was carried out at a load of 22 N. Again, some large fractured fibre particles were evident over the surface of the pin due to bending action of fibres in the direction of sliding against to the steel disc and limited reattached to the pin surface. As a result of this, a fibre rich region was produced near to the trailing edge of the specimen. The size of the particles seemed to be much higher than the former case. The SE image of the same sample of Figure 4.119 was shown in Figure 4.120 under high magnification. In this micrograph, the topography of the worn surface showed fibre ends which were not planar

with HDPE matrix surface, the fibre ends were standing proud of the worn surface. The fibre was debonded from the matrix in the worn surface region especially on the trailing side the weak matrix was unable to restrain the lateral movement of the fibres due to their contact with the counterface material. Therefore the fibres were protruding above the matrix without any matrix support after the release of the load, as shown in Figure 4.120. The length of protrusion was about 30 μm. These observations suggested that the matrix wore faster than the fibres during initial wear and led to the fibre ends being slightly higher than the matrix surface. Moreover, some of the fibres ends were seen to have been broken into a large fragments. There was also evidence of fibre removal through the surface. This also suggested that the wear behaviour for this case was mainly determined by the wear resistance of fibre material itself.

For the P orientation, as shown in Figure 4.121 at low magnification, a distinctly different wear surface appearance was observed when compared to that of the N orientation. The composites were tested at a speed of 0.6 m/s and load of 22 N. This micrograph revealed that continuous grooves were observed in the composite pin surface in the direction of sliding. This suggested that the dominant mechanism had been pulling-out of fibres from their place, leaving long, rounded grooves. As a consequence of this, the highest wear rates was obtained in this orientation. The reason for pulling-out could be explained as follows : The bulk surface temperature of the composite pin increases with normal load and sliding speed as expected. The increase in sliding interface temperature led to thermal penetration and thereby resulted in softening of the HDPE matrix. This induced weakening of the bonds between the reinforcing B(SiC) fibres and the polymer matrix. As a result of this weakening, the fibres worked loose in the matrix and some of the fibres were fractured, and pulled-out due to the lateral frictional force as evidenced by the above figure. A similar composite sample was shown in Figure 4.122 under high magnification, but tested at high sliding speed of 1.6 m/s. This micrograph showed debonding of the fibre due to weakening of the bond as a result of softening of the matrix. This micrograph also demonstrated that fibre fracture occurred directly on the contact region and part of the fractured fibre was

removed from the surface due to the same reason. In addition, a thin matrix layer was evident and this was also an indication of softening of the polymer.

In the case of medium speed of 1.0 m/s test condition, a similar surface appearance was observed in Figure 4.123 when the composite pin was tested at a load of 12 N. This micrograph showed the same continuous long grooves through the specimen in the direction of sliding, besides plastic deformation. This was evidence that fibres were completely pulled away from the surface. Furthermore, fibre removal from the contact region was further influenced by the ploughing and cutting of the matrix in between the exposed fibres. Again the responsible mechanism for materials removal was the pulling-out of fibres and rapid wear of the bare matrix. Thus the wear rate in this orientation was higher than that of the N orientation, regardless of speed and load. Furthermore, the wear debris and matrix between the fibres were easily swept away by the counterface interaction resulting in high wear. For example, the same sample of Figure 4.123 was shown in the SE image of Figure 4.124 at high magnification, and showed grooves due to fibre loss over the composite pin surface. These grooves were then partially filled by plastic flow of the matrix and hardly any of the wear debris was retained during the sliding process. Evidently once the fibres had been lost extensive ploughing of the surface by asperities on the hard steel disc became extensive and rapid wear then took place.

For the AP orientation, an SEM micrograph of the worn surface of a PMC pin was shown in Figure 4.125 at low magnification. Fibres were broken due to an in-plane bending load caused by the hard asperity particles of the counterface. Rarely, large pieces of fibres were then embedded into the surface of the pin and subsequently removed from the worn surface or forced to break the other fibres. The length of broken fibre particles varied greatly from place to place and the layer particles were readily visible on the pin surface. However despite the very extensive damage, many more lengths of fibre were retained on the wear surface compared with the P orientation. Therefore this orientation exhibited a lower wear rate than the P orientation. As with the other samples, a plastic transfer layer was also formed over the sliding surface.

A higher magnification micrograph of the same sample, as shown in Figure 4.126, showed a broken fibre with matrix flowing over the fracture. The fibre was debonded on the trailing side and the debonded region extended to entire length of the fibre although part of it is shown here. As a consequence, fibre pull-out was difficult unless the fibre broke into short pieces. Polymer debris particles are visible over the surface.

Figure 4.127 showed the worn surface of the composite pin, but tested at high speed. The micrograph indicated that a small number of grooves was generated because of pulling-out of fibres. However, it should be noted that fibres were cracked in different length before removal from the surface. It was also evident that a few fractured particles were reattached to the pin surface. The SE image of the same sample of Figure 4.127 is shown in Figure 4.128 under high magnification and revealed some fibre fractures, and that the wear surface of the composite was partially covered with the HDPE polymer due to melting/softening of polymer at this speed. This suggested that once the film formed fibre displacement was reduced and hence giving a lower wear. But such a molten film was not observed under low sliding speed condition in the earlier figure.

Briscoe et al [110] also examined the formation of a transfer film on a steel surface by SE microscopy rubbing against unfilled and filled samples. The transferred film formed when unfilled HDPE was tested at a load of 3.0 kgf and speed of 2.1 m/s. The sliding appeared to deposit a relatively uniform film of polymer as well as extensive lumps of polymer. Under the same conditions, for an unfilled sample a surface film was also formed, but the film was much more coherent than that of the matrix. Moreover, the particles of filler could observed to be protruding out of the surface of the film by up to 0.01 μm. It was concluded that the filler inhibited the removal of the transferred film by the slider. The film also underwent extensive buckling with the result that circular patches were pulled-out of the film when the filled sample was slid over a film of HDPE. These structures did not appear on the films of HDPE. This was in contrast to the our present work.

5.8 Summary of the Wear Mechanisms and Influence of Fibre on the Wear Rate

The discussion presented in the previous section indicated that the sliding wear resistance of the unidirectional reinforced composites and their matrices is complex, structure property which depends not only on the volume fraction, distribution of its components and orientation of fibre, but also on the intrinsic mechanisms of wear and debris formation in each of its components. In any case, several mechanisms may operate in the matrix and composite, and one mechanism can trigger others. Metallographic examination revealed that in both the Al alloy and B(SiC) fibre reinforced composites distinct deformations of the matrix were developed at or below the contact surfaces. It is therefore of value to summarize the wear mechanism in each of the components, namely; Al alloy and HDPE, and the matrix of the corresponding composites reinforced by B(SiC) fibre.

Let us consider the wear mechanism of the Al alloy matrix first. SE micrographs of the worn surfaces revealed a number of important features. One was the continuous and long grooves which was indicative of an abrasive type of the wear process. Another one was severe damage to regions on the surface which showed different form depending on the experimental conditions. High loads resulted in a high level of disruption and extensive plastic deformation while the type of the worn surfaces and severity of damage also changed with increase in sliding speed. In accordance with this view, investigations on the cross-sections parallel and perpendicular to the sliding direction showed the development of a plastically deformed and distorted zone under the sliding contact surface. The deformation zone penetrated to a depth of around 30 μm. Thirdly, fragmented debris or oxide particles compacted into the surface grooves were also observed due to repeated welding and fracturing of debris particles. Furthermore, the SE micrographs revealed the formation and elongation of voids at a certain distance under the wear track. This suggested that the principal wear mode was deformation and failure due to stress associated with both normal and friction forces. Finally, the existence of several subsurface cracks 80-150 μm long in various cross-sections suggested that crack propagation was an important and

possibly rate controlling step of debris formation. These cracks eventually reached the contact surface and caused the detachment of thin plate-type debris particles in a manner similar to delamination. However, the presence of other types of debris particles, although less numerous suggested that wear was not entirely controlled by delamination, and oxidative and adhesion may be partly responsible. The reduction in coefficients of friction with load was result of the frictional heating between the pin and disc. The coefficient of friction also decreased with increasing sliding speed, but this was more significant at a speed of 1.6 m/s.

As a result, the sliding wear of Al alloy matrix, particularly at low pressures and low speeds was characterized by processes such as delamination and abrasion, while at high pressures/speeds was characterized by subsurface and plastic deformation, and formation of an iron-rich adhered layer and oxidation. Since the major wear seemed to be due to delamination as evidenced by a large amount of plate-like debris, the wear resistance can be increased either by suppressing the crack nucleation and propagation process or by reducing the plastic deformation by increasing the flow stress of the matrix.

Regarding the composite materials investigated in this research, the incorporation of B(SiC) fibre improved considerably the wear resistance of the unreinforced matrices. The improvement in the wear resistance is considered here to be due to changes in the wear mechanisms brought about by the presence of the fibre. The presence of B(SiC) fibres changed the stress distribution in the wear pin since the loads were carried mostly by the fibres, instead of purely by the matrix. However the metal matrix being stronger and stiffer than the HDPE matrix, would be expected to contribute significantly to the load-bearing capacity. The fibres also provided protection to the softer matrix during the sliding process and also improved its thermal stability. This gave reduced material adhesion to the counterface disc. Thus smoother wear surfaces were produced in this case and also resulted in a low wear rates, regardless of the type of the matrix and in all three orientations.

The SE micrographs showed that the wear mechanisms appeared to be the similar for the two types of the composites, although the wear behaviour was quite different. The

presence of a number of microcracks on the some of the fibres in both composites provided strong evidence for wear to be taking place through microfracture of fibres. The size of the fractured particles was very small compared to the fibre dimensions for the MMCs, but it was a larger size for case of the PMCs.

The various wear mechanisms coupled with the anistropy of the composites could account for the differences in wear rates among the three orientations. Let us consider the wear mechanisms of MMCs first. SEM investigations showed a fairly smooth surface in the N orientation under low and intermediate loads and speeds. Wear occurred mainly by fracturing of the ends of the fibres on a small scale by the counterface bending the fibres under the frictional force. But fibre ends protruding out of the surface were capable of collecting displaced matrix material. The broken fibre particles were on average about 10-25 μm in length and the fractured fibre ends also were smeared by the matrix which gave a supporting effect. Transverse and longitudinal cross-sections of the subsurfaces of composites in the N orientation revealed that regions of fibre near the surface had been deformed and fractured into small pieces. This must have been accompanied by plastic flow of the matrix in that subsurface region. The length of the fractured particles was about 20-25 μm and the fractured ends of the fibres were also smeared by the base alloy and the thickness of the smeared layer was found to be small. In the case of high sliding speed, however, SE image of the worn surface showed more cracks in the fibres underneath the wear track, the depth of the cracked fibres was also bigger since fibres were loaded as cantilevers under the action of frictional force, which produced large stress and deflection in the fibre. In other words, the combination of compressive stress with shear in the fibres caused a bending action and this was exacerbated by the unsupported length of the fibres as evidenced here. Therefore this facilitated easier crack growth, resulted in a higher wear rate than under the previous conditions. In the case of the bidirectional orientation, the SE micrograph indicated a substantial amount of fibre fracture and fibre pull-out due to debonding and chattering effect. In consequence of this, the microstructure of the composites was greatly distorted in this orientation.

The dominant mechanism for the material removal in this orientation was microfracture of fibres and gouging of the matrix, but the wear rate was reduced by embedded of fibre fragments in the matrix, and matrix smearing over the fractured fibre ends in this orientation.

In the P orientation, fibre cracks occurred in the contact region or subsurface regions. The appearance of the worn surface of the pin was found to be quite different from those of the N orientation. Microscopic examination revealed that the fibres had cracked into short segments, some of which had peeled away along the axis of the fibres. This might be because tensile stress was set up at an angle of 45^{o} to the plane of shear when the fibre was partially embedded in the matrix and subjected to an axial shear stress. As a result of this, the fibres broke up into short segments with angled fracture surfaces. The cracks also might be initiated at the interface region due to loading since the interfacial reaction products were usually brittle or porous. Under low speeds, there was some pull-out which produced grooving and cratering on the surface which resulted in more wear. At high speeds there was more matrix flow and fibre fragmentation, and less pull-out.

The transverse sectional micrographs in the P orientation showed that the subsurface damage zone, where cracks and fibre splinters were generated, deep to the depth of a crack was about 40-60 μm. In other words, the damaged areas were generally larger in the P and AP sliding directions than the N sliding direction. In addition, the surface grooves had been filled with the matrix debris. Moreover, the contribution to the wear of the composite was by ploughing, cutting and cracking removal of the matrix between the exposed fibres. Thus, in addition to fibre fracture and pull-out, abrasion and plastic and subsurface of the matrix deformation were the operative wear mechanisms for this orientation.

In the the case of the AP orientation, it appeared that fibres were broke up into irregular fragments in the contacting surface because of the bending action of the counterface disc. The fragments and debris particles were then embedded into the matrix surface and then were preserved on the wear surface and were thus available to resist counterface interaction. This resulted in a low wear for the AP orientation, assisted by the

formation of iron rich material which was transferred from the steel to the pin. This suggested that the removal of material from the surface of the steel slider was due to abrasive action of the embedded fragments of hard B(SiC) fibres. The surface appearance seemed to be smooth and gentle despite a considerable amount of chopped fibres embedded in the matrix. This suggested that mild wear (oxidative) wear might be predominant. However, transverse sections of the AP orientation showed that catastrophic fibre fracture had taken place close to the wearing surface. Long subsurface deformation cracks were observed below the wear track, similar to those found in the P orientation. The presence of these cracks indicated that fatigue might be an important mode of material removal. It is suggested that adhesive wear was one of the wear mechanisms and adhesion, abrasion, plastic deformation, fatigue and fibre fragmentation are important mechanisms in this orientation.

Fibre orientation was also seemed to have only a little effect on friction coefficient. The lowest friction coefficient was found in the P orientation despite the fact that higher wear rates were obtained for this case. The highest friction coefficient was for the AP orientation. The friction coefficient decreased for all cases when the sliding speed increased, and it is believed that this reduction was due to an increase in temperature due to frictional heat which changed the surface characteristics of the pin and disc. The friction coefficient in the P orientation was relatively low at around 0.53, because the hardened steel made direct contact with the B(SiC) fibre. The friction coefficient in the N orientation was found to be slightly higher than the P orientation because protruding fibres strongly abraded the counterface and giving a higher ploughing component of friction. However the large numbers of fibres meant that the average contact load was small. In the AP case where the fibres were transverse to the sliding direction, few large wear particles were generated. These particles could either be lost from the contact zone or remained there for a period of time, and thus these hard particles ploughed the counterface effectively. Because of the small number of large particles the average contact load was high and as a consequence of this, the friction coefficient was high at bout 0.65 .

The friction coefficient in general decreased with increasing load and fibre content. The reduction in the friction at higher loads is considered to be due to chipping and fragmentation of the fibre ends at higher compressive loads. As for the case of increased fibre content, the average stress on the fibre ends decreased and limited to the depth of penetration of the fibre into the counterface disc. This led to a eventual reduction in friction coefficient with fibre content.

Very similar wear mechanisms were found for the case of PMC materials in spite of the fact that some differences have been pointed out. However, the wear behaviour of the polymer matrix was quite different from that of the metal matrix. In that, wear rate increased initially and then decreased with an increase in sliding speed. This resulted in maximum wear at the intermediate speed. This was due to a change of the mechanism of wear. As speed increased, then the microcutting increased giving a higher wear rate. At the highest speed, the SE micrographs showed that HDPE molecules were orientated in the direction of sliding and there was also greater transfer of polymer to the disc due to melting of polymer. As a result of this, the surface roughness of the counterface was reduced at high speeds, and wear rates decreased. At low speeds, microcutting was the predominant mechanism of wear, and the surface was smooth with a number of lumps and streaks.

Although a similarity existed between the two types of the composite materials, some differences for the PMCs were observed. For the N orientation, the major contribution to material removal was the disc asperity particles cutting the fibre ends in a slicing manner and produced splinters. These particles were much bigger than those of the MMCs, therefore the dominant mechanism for the removal of fibre was fracture. However, SE micrographs also revealed that the fibre ends were protruding above the worn surface and the fibres debonded from the matrix in the worn surface region due to their contact with the counterface. The length of the protrusion was about 30 μm. This suggested that the matrix was removed preferentially from the surface during initial wear and resulted in a fibre ends being slightly larger than the matrix surface. This was not the case for the MMCs although a similar mechanism was operative during sliding. In addition, large fragments of fibres

were broken from the ends suggesting that the wear behaviour was basically determined by the wear resistance of the fibres themselves in a matrix which was much less supportive to them than in MMCs.

In the P orientation, the dominant mechanism was pulling-out of fibres from their places. In this orientation, increases in load or speed increased frictional heat which, because of the low thermal conductivity, resulted in localised heating and softening of the polymer matrix at the surface. The vast different thermal expansion coefficient of boron and HDPE (about $6x10^{-6}$ ^{o}C and $150x10^{-6}$ ^{o}C respectively) would also have contributed significantly to weakening of the bonds at the fibre/matrix interface, as true bonding was probably absent in this system, and the fibres held in the matrix by elastic compressions. Thus the fibres became loose in the matrix of the hot surface and with the continuation of the sliding process, some of them slid away under the axial frictional thrust of the counterface, while other remained in place. However the hard disc asperities as sliding continued gradually slid them out of the matrix until the complete fibre was removed from the surface, leaving long, continuous and rounded grooves on the composite wear surfaces. Therefore, the time to remove the fibre from the surface was much shorter in this orientation than in the cases where fibres must be fractured into many small pieces before eventual removal could occur (N and AP). Hence, the highest wear rates were found to be due to pulling-out mechanisms for the PMCs in the P orientation. Moreover, the wear debris and matrix between the fibres were easily swept away by a counterface interaction, although the grooves were partially filled with the matrix material by plastic flow of the matrix at the edge.

Compared with the MMCs, the fibre/matrix interface of the PMCs was much weaker and cracking along the fibre/matrix interface was absent. In the MMCs the short length of the cracks at the interface meant that as the fibres fractured into short segments, fibre pull-out was difficult. Some fibres in the MMCs showed a little pulling-out but the vast difference between these and the PMCs indicated that pulling-out was very much more difficult.

As for the case of the AP orientation, like the MMCs, fibres were broken due to an in-plane bending load by the hard asperity particles. The SE micrographs showed some broken fibres embedded in the matrix surface, but the length of the broken particles varied greatly from place to place. Furthermore, the worn surface of the composite pin was partially covered with the HDPE polymer matrix because of softening and melting at high speeds. Again the wear debris was trapped between the fibres, and thus was retained to resist counterface interaction. However, most of the long of fibres were retained in the place on the worn surfaces, in spite of the extensive damage in comparison to the P orientation. Because of these two effects a lower wear rate was found in this orientation compared with the P orientation.

As a result, for PMCs, fibre microfracture and matrix microcutting were the main mechanisms of wear in both N and AP orientations, while fibre pull-out was the predominant mechanism of wear for the P orientation. However microcutting and plastic/elastic deformation were the responsible mechanisms for wear in the unreinforced HDPE polymer matrix.

The coefficient of friction of all three orientations increased with increase in sliding speed. The rate of increase in coefficient of friction with speed was proportional to speed and was in order of AP, P and N, and unreinforced matrix respectively. Despite the fact that the lowest wear rates were found in the N orientation, the highest coefficients of friction were measured in this orientation due to the effectiveness of the ploughing component of friction. Also there was a trend to increase in friction coefficient with fibre content because of the increasing fragmentation of fibres on the worn surface. A slight increase in friction coefficient was also observed with load as a result of higher penetration of the exposed fibre ends into the counterface.

Both P and AP orientations showed similar trends and were closed to each other. The coefficient of friction decreased highly with increasing fibre volume fraction due to dominating of fibre/steel contact at the counterface, and the effect of a partially formed

polymer film on the counterface. For the AP orientation, however, a slight trend to increased coefficients of friction with load was also observed.

Let us consider a brief summary of the friction and wear behaviour of B(SiC) reinforced composites. Two categories of such materials have been studied so far, namely, those that used metals and polymers as the matrix materials. In each case, the incorporation of fibres has been observed to improve wear behaviour significantly and increased the friction behaviour of the MMCs, but reduced friction coefficient of the PMCs. The influence of the fibres, however, has been found to be a complex one. Variables such as volume fraction of fibre, fibre orientation, type of matrix, operational variables and whether the matrices were metal or polymer have been found to affect wear and friction to varying extents. The effectiveness of the fibres was dependent on the degree of support provided to them by the matrix. Conditions which decrease this support lead to an increase in wear and friction by allowing the fibres to be uprooted.

The effect of the presence of fibres was to resist the flow of the matrix at wear surface of the tested composite materials. B(SiC) fibres on the surface seemed to carry the load in dry sliding, although they often were broken or fragmented in the composite samples, and thus they contributed a great deal to the wear resistance of the composites. This could be expected from their hardness, strength and modulus. Their contribution to the wear resistance was roughly 3 to 10 fold increases in wear resistance for the MMCs compared to the metal matrix. They decreased the wear rate of the composite by supporting the applied load with less deformation than the Al alloy matrix or HDPE matrix and they retard the wear damage generated in unreinforced matrices. In other words, reduced effective area fraction of the unreinforced matrix in contact with the counterface due to the presence of this fibres in the matrix led to a relatively smaller temperature rise at the mating surface of the composites than for the base alloy.

The another effect of the presence of B(SiC) fibre on the surface was to abrade the disc material preferentially thus promoting the formation of an iron-rich layer on the surface. This was only for the MMCs where presumably mechanical alloying of the pin

materials with the abraded pin caused it to adhere to the pin wear surface. For PMCs the wear debris was lost from the contacting surfaces. Abrasion of the counterface by fibre particles from the pin increased the surface roughness of the pin, but for the N orientation this increased roughness was less than for the P orientation. It was contended here that the better performance of composites was due to both above these reasons. An increase in B(SiC) content here from 16% to 32% did not seem to change the mechanisms qualitatively and only a small quantitive improvement was observed for the MMCs.

Wear of MMCs has shown the lesser dependence on these variables. However, wear of PMCs were influenced to the greatest extent by these test parameters, providing that the composite had a low volume fraction of fibre.

It was interesting to note that the plastic matrix in PMCs, although less supportive than Al alloy, reduced the avearage coefficient of friction, and thus reduced the shear loads at the surface. Differences in behaviour of the composites seemed to be derived from the amount and the nature of the plastic film formed on the counterface, which could decrease the wear and friction coefficient. As a result of this was that the overall wear rates of PMCs were lower than those of MMCs. Global average values of volumetric wear rate were calculated for the composites, and found to be 0.14 mm^3/km for PMCs and 0.36 mm^3/km for MMCs. Thus for low temperature applications the use of a HDPE matrix might be preferred to a metallic matrix.

CHAPTER SIX

6.1 CONCLUSIONS AND SUGGESTIONS FOR FUTURE WORK

The main conclusions that can be drawn from the work described in this thesis concern (1) mechanical tests of metal matrix composites (MMCs), (2) wear tests of the MMCs and PMCs, (3) observations of worn surface and wear mechanisms obtained from the dry wear testing on the both types of the composite materials.

1). The presence of unidirectional B(SiC) fibres in a metallic matrix improved appreciably the tensile strength at room and elevated temperatures. The resulting fracture surfaces showed a mixture of brittle and ductile features, and it was concluded that the interfaces between the fibre and matrix were strong enough to allow the transfer of loads from the matrix to the fibres in MMCs.

2). Room temperature and elevated temperature tensile strength and hardness of MMCs increased linearly with vol% fibres in unidirectional composites, according to the rule of mixtures law. But bidirectionally-reinforced composites had lower properties than the expected values.

3). The wear rate of the unreinforced aluminium matrix increased significantly and approximately linearly with load under medium and high speeds. At low speed, the wear rate appeared to increase exponentially with load because of a change in the mechanism of wear. The wear rate also increased strongly with sliding speed up to 1.2 m/s, then reduced very rapidly at higher speeds. This is considered to be due to heat generated at the contacting surface.

4). The wear rate of the unreinforced HDPE matrix increased with increasing load and sliding speed up to a critical speed of 1.0 m/s, and then decreased rapidly due to formation of orientated polymer molecules.

5). Fibre-reinforced aluminium alloy and HDPE composites showed excellent wear resistance compared with the unreinforced matrices when tested in air against a steel counterface. The improvement in the wear resistance of the composites ranged from 2 to 4 fold and 2-11 fold for MMCs and PMCs respectively, at a speed of 0.6 m/s, but this also strongly depended on the sliding conditions used.

6). The wear rates of MMCs and PMCs increased slightly with load. The minimum fibre contents caused a large decrease in wear rate compared with the respective unreinforced matrix, but further increase in fibre content had little effect. Sliding speed also had little effect on the wear rates.

7). The orientation of the fibres with respect to the sliding direction was found to affect the wear rates and coefficients of friction. Among the MMCs tested, the N orientation displayed the best wear resistance, the AP orientation showed an intermediate resistance, and the P orientation was only very slightly worse than the AP orientation. The orientation effect for PMCs was found to be much clearer, in particular, the P orientation produced more wear due to softening of matrix, which caused the fibre to lose its support.

8). The coefficient of friction of the unreinforced aluminium alloy matrix, which averaged about 0.35 over the range of loads used, decreased with increasing sliding speed and load, both effects being due to temperature increase.

9). The coefficient of friction of the HDPE matrix was nearly twice that of the aluminium alloy and increased with increasing sliding speed. It was almost independent of load at low and medium speeds, but increased slightly with load at a speed of 1.6 m/s.

10). The coefficient of friction of the MMCs varied between the 0.41 to 0.79 and decreased with the sliding speed for all orientations. The friction coefficients increased in order of the P, N and AP orientations. For MMCs in general, the friction coefficient decreased with increasing load and increasing fibre content due to incorporation of fragments of fibres in the pin surface, and limitation of the depth of fibre penetration into the counterface respectively.

11). The coefficient of friction of the PMCs was found to be lower than the matrix in contrast to MMCs, and varied between 0.49 to 0.20 at a speed of 1.0 m/s. It increased with speed in order of AP, P, and N, and the unreinforced matrix, but the P and AP orientations were quite similar.

12). The basic wear mechanisms differed for each orientation in both types of composites and unreinforced matrices. For the unreinforced Al matrix, delamination, abrasion and plastic deformation were found to be significant mechanisms for material removal. However, microcutting was the predominant mechanism of wear for the HDPE matrix. For the MMCs, in the N orientation, angled fracture of the fibre ends and matrix smearing over the fractured part of the fibres was dominant, resulting in a low wear rate. In the P orientation, the fibres cracked into short segments in the contact region due to experiencing tension and shear loads and failure was enhanced by fibre-matrix debonding. In addition, ploughing and cutting of the matrix material between the fibres aided fibre removal from the surface. For the AP orientation, fibres fractured into irregular fragments due to in-plane bending. This resulted in slightly lower wear compared with the P orientation because of reattachment of debris on the matrix and trapping of the wear debris and matrix between the fibres.

13). For the PMCs fibre pull-out was found to be a predominant mechanism of wear in the P orientation of these composites due to softening of the HDPE polymer matrix which relaxed the compressive loads at the fibre/matrix interfacial bonding. Therefore, the highest wear rate was obtained for this case. Fibre fracturing, however, was the same in the N and AP orientations like the MMCs.

14). The XPS analysis showed that there was no significant variation in the amount of oxide over the surface under the test conditions used. At low speed in the N orientation, boron oxide and iron boride were formed. At high speeds, the proportions of these components were different. This suggested that high speed led to mechanically mixed or alloyed material with more iron boride and aluminium, but less boron in total, while

low speed caused a mild form of wear in the N orientation due to less pulling-out of fibre.

15). Differences in wear behaviour between B(SiC)/Al and B(SiC)/HDPE composites were due to the differences in the support given to the fibres by the matrix, and in the coefficient of friction. The global average volumetric wear rate for the HDPE composites was about 0.14 mm^3/km, substantially lower than that for the MMC's, which was around 0.36 mm^3/km. This indicated that the effect of low friction more than compensated for the poor fibre support.

6.2 SUGGESTIONS FOR FUTURE WORK

(1). The present work has been carried out over a load range from 12 to 60 N inclusive, at sliding speeds of 0.6, 1.0 and 1.6 m/s respectively under dry sliding. All the test parameters mentioned above can be applied to the lubricated condition to obtain more information on the composite materials ;

(2). An attempt should be made to describe mathematically the wear behaviour of both MMCs and PMCs ; and for a quantitative understanding of the wear process a finite element analysis should also conducted, where the role of elastic modulus, interfacial shear strength, fibre volume fraction and so on should be considered in the fibre pull-out process.

(3). An attempt should also be made to measure surface temperature so that estimation could be made of the temperature at which the Al matrix underwent plastic deformation and subsurface layer formation, clarifying the temperature rise between the disc and composite pin which is orientated in the N, P and AP direction.

REFERENCES

1. **M. Taya** and **R. J. Arsenault,** (1988), *Metal Matrix Composites-Thermal and Mechanical Behaviour*, Pergamon Press.

2. **G. K. Kreider**, (1974), *Metallic Matrix Composites*, Academic Press, New York.

3. **D. Huda, M. A El Baradie** and **M. S. J. Hashmi**, (1993), Metal Matrix Composites : Material Aspect Part II, *J. Mat. Process. Techn.*, **37**, 529 Elsevier.

4. **T. J. Reinhard et al.**, (1987), Engineered Materials Handbook, **1**, Composites, *ASM Int. Handbook Committee*, Metals Park, Ohio, 44073.

5. **M. Islam** and **W. Wallace**, (1988) *Carbon Fibre Reinforced Aluminium Matrix Composites : A critical review*, Division of Mechanical Engineering, National Research Council, Canada *NRC No 23498*, 2984/4.

6. **D. H. Hughes**, (1986), Fibres for Reinforcement Composite Materials~Part 2, *The J. Institute of Metals, Metals and Materials*, 365-369.

7. **G. Lubin**, (1982), *Handbook of Composites*, Van Nostrand Reinhold Co., 196.

8. **A. Brent Strong**, (1989), *Fundamentals of Composites Manufacturing* : Materials, Methods and Applications, Society of Manufacturing Engineers, Publications Development Dep. Ref. Publ. Divs., Dearborn, Michigan.

9. **D. Hull**, (1985), *An Introduction to Composite Materials*, Cambridge Solid State Science Series, Cambridge University Press, Cambridge.

10. **P. K. Mallick**, (1988), *Fibre Reinforced Composites*, Materials, Manufacturing and Design, Marcel Dekkery Inc. New Yok, USA.

11. **T. W. Clyne, M. G. Bader, G. R. Cappleman** and **P. A. Hubert,** (1985), The Use of δ-alumina fibre for Metal Matrix Composites, *J. Mat. Sci.*, **20**, 85-96.

12. **M. G. Bader**, (1984), Alumina-Fibre Reinforced Aluminium Alloy Castings for Automative Applications, *Int. Association for Vehicle Design Congress*, Geneva, Switzerland, 22-24.

13. **S. T. Mileiko** and **A. Kelly** (Edt.), (1985), Handbook of Composites, **1,** *Strong Fibres*, (Vol. Edt. W. Watt and B.V. Perow), North-Holland/Amsterdam, Elsevier Publishers B.V.

14. **R. J. Arsenault** and **S. B. Wu**, (1988), The Strength of PM vs Melted SiC/Al Composite, 231-236, *Cast Reinforced Metal Composites Conf. Proc., ASM Int. USA.*

15. **B. P. N. Bai,** (1992), Dry Sliding Wear of A356/Al-SiCp Composites, *Wear*, **157**, 295-303.

16. **A. T. Alpas** and **J. D. Embury,** (1990), Sliding and Abrasive Wear Behaviour of an Al(2014)/SiC Particulate Reinforced Composite, *Scripta Metallurgica et. Materialia*, **24**, 931-935, Pergamon Press Plc, USA.

17. **G. R. Cappleman, J. F. Watts** and **T. W. Clyne**, (1985), The Interface Region in Squeeze Infiltrated Composites δ–alumina fibre in an Aluminium Matrix, *J. Mat. Sci.*, **20**, 2159-167.

18. **R. L. Trumper**, (1987), Metal Matrix Composites, Appliccations and Prospects, *J. Institute of Metals, Metals and Materials*, **3** (11), 663-667.

19. **Anon**. *Toka-whisker*, (1980), Tokai Carbon Corp., Shizuoka, Japan.

20. **A. R. Champion, W. H. Krueger, H. S. Hartman** and **A. K. Dhingra**, (1978), *Proc. Int. Conf. on Composite Materials*, AIME, Warrendala, PA, 883.

21. **G. A. Chadwick** and **T. M. Yue**, (1989), The Principles of Squeeze Casting in MMCs, *The* J. *Institute of Metals, Metals and Materials*, **5** (1), 7-13.

22. **H. Matsubara, Y. Nishida, M. Yamada, I. Shirangi** and **T. Imai**, (1987), *J. Mat. Sci. Lett.*, **6**, 1313.

23. **S. Ahmed, V. Gopinattan** and **P. Ramaakrisnan**, (1988), Squeeze Casting and Properties Evaluation of Alumina Fibre Reinforced Al/Si alloy matrix Composites, pp 149-153, In *Proceedings of the Int. Symp.* on *Advances in Cast Reinforced Metal Composites*, edt by S. G. Fishmman and A.K. Dhingra, 1988 World Material Congress, Chiccago, USA.

24. **M. C. Flemings** and **R. Mehrabian**, (1974), *Met. Trans.*, **5**, 1899.

25. **C. Milliere** and **M. Suery**, (1988), Fabrication and Properties of Metal Matrix Composite Based on SiC fibre Reinforced Aluminium Alloys, *Mat. Sci. and Techn.*, **4**, 40-50.

26. **M. M. Farag**, (1989), *Selection of Materials and Manufacturing Processses for Engineering* Design, Prentice Hall, Intern (UK) Ltd., The Cambridge University Press, Cambridge.

27. **T. C. Willis**, (1988), Spray Deposition Process for MMCs Manufacture, *J. Metals, Metals and Materials*, **4** (8), 485-488.

28. **J. R. Vinson** and **T. W. Chou**, (1975), *Composite Materials and Their Use in Structures*, Materials Science Series, Applied Science Publishers, London.

29. **D. Huda, M. A. El. Baradie** and **M. S. J. Hashmi**, (1993), Metal Matrix Composites: Manufacturing Aspect Part I, *J. Mat. Process. Techn.*, **37**, 513.

30. **J. T. Moore, D. V. Wilson** and **W.T. Roberts**, (1981), *Mat. Sci. Engnr.*, **48**, 107.

31. **A. Kelly** and **G. J. Davies**, (1965), The Principles of the Fibre Reinforced of Metals, *Met. Revi.*, **10**(37).

32. **H. Krenchel**, (1964), *Fibre Reinforcement*, Academisk, Forlag, Copenhagen.

33. **S. Harris** and **T. E. Wilks**, (1986), Tensile and Fatigue Behaviour of Alumina Fibre Reinforced Aluminium Alloys at Ambient and Elevated Temperatures, in *Fibre-Reinforced Composites*, **86**, Liverpool, UK. 19-28.

34. **G. Piatti**, (1983), *Advances in Composite Materials*, Applied Science Publishers Ltd., London.

35. **T. C. Willis, J. White, R. M. Jordan** and **I. R. Hughes**, (1987), *3rd Int. Solid Processings* Conf. , Sheffield.

36. **C. T. Herokovich et al.**, (1977), Tensile and Compressive Behaviour of Borsic/Aluminium, *Composite Materials: Testing and Design (Fourth Conference), ASTM STP 617, ASME*, 344-357.

37. **C. T. Lynch et al.**, (1972), *Metal Matrix Composites*, Air Force Materials Laboratory, Wright-Paterson AFB, Ohio, CRC Press, .

38. **K. J. Toth**, (1972), An Exploratory Investigation of the Time Dependent Mechanical Behaviour of Composite Materials, *AFML-TR-69-9.*

39. **W. H. Scheafer** and **J. L. Christian**, (1969), Evaluation of Structural Behaviour of Filament Reinforced MMCs, *AFML-TR-69-36, Vol II.*

40. **K. G. Kreider, L. Dardi** and **K. Prewo,** (1969), MMC Technology, Technical Management Report for *F33615-69-C-1549, AFML*, Wright-Patterson AFB, Ohio.

41. **R. C. Jones**, (1969), Fractography of Aluminium/Boron Composite Materials: *Testing and Design, ASTM STP 460*, 512-527.

42. **N. R. Adsit** and **J. D. Forest**, (1969), Compression Tests of B/Al Composite Materials: *ASTM Special Technical Publication, 460.*

43. **K. C. Antony** and **W. H. Cheng** , (1968), T*rans., ASM* 61, 550.

44. **D. A. Meyn**, (1974), Effect of Temperature and Strain Rate on the effect of Tensile Properties of Boron/Aluminium and Boron/Epoxy Composites, *Composite Materials (Third Conf.), ASTM STP 546, ASME* 225-236.

45. **K. Akechi** and **Z. Hara**, (1979), Preparation of Boron Fibre Reinforced Aluminuim by a Resistance Sintering Process, *Trans., JIM*, **20**, 50-56.

46. **I. J. Toth**, (1974), Comparison of the Mechanical Behaviour of Filamentary Reinforced Aluminium and Titanuium Alloys, *Composite Materials: Testing and Design (Third Conference), ASTM STP 546, ASME*, 542-560.

47. **I. J. Toth**, (1969), Creep and Fatigue Behaviour of Unidirectional and Cross-Plied Composite Materials, *ASTM 460.*

48. **E. M. Breinan** and **K. G. Kreider**, (1970), *Metall. Trans.*, **1**, 93.

49. **W. R. Hoover** and **R. E. Allred**, (1974), The Effect of Crack Length and Bond Strength on the Delamination Process in Borsic/Al Composites, *J. Composite Materials,* **8**, 55-65.

50. **R. E. Allred, W. R. Hoover** and , **J. A. Horak,** (1974), Elastic-Plastic Poisson's Ratio of Borsic/Aluminium, *J. Composite Materials,* **8**, 15-27.

51. **K. Prewo, G. McCarthy**, (1972), Interface Characteristics of Silicon Carbide Coated Boron Reinforced Aluminium Matrix Composites, *J. Mat. Sci.*, **7** , 919-928.

52. **F. S. Galasso**, (1969), *High Modulus Fibres and Composites,* Gordon and Breach Science Publishers, New York NY.

53. **J. H. Young**, (1969), Advanced Composite MMaterials Structural Hardware Development and Testing Programme, *AFML Report TM-69-249*, GE.

54. **K. G. Kreider et al.,** (1968), Plasma Sprayed Metal Matrix Fibre Reinforced Composites, *AFML Report-TR-68-119.*

55. **A. A. Baker, D. M. Braddick** and **P. W. Jackson**, (1972), Fatigue of Boron/Aluminium and Carbon/aluminium Fibre Reinforced Composites, *J. Mat. Sci.*,**7**, 747-762.

56. **W. S. Johnson,** (1982), Mechanism of Fatigue Damage in Boron/Aluminium Composites, *Damage in Composite Materials, ASTM* STP 775, K.L. Reifsnider, Ed, ASTM, 83-102.

57. **M. Gounda, K. M. Prewo** and **A. J. McEvily**, (1981), Mechanism of Fatigue in Boron/Aluminium Composites : *Fatigue of Fibrous Composite Materials, ASTM STP 723, ASME*,101-115.

58. **J. Halling**, (1983), *Principles of Tribology*, The McMillan Press Ltd.

59. **D. A. Rigney,** (1981), *Introduction Fundamentals of Friction and Wear of Materials*, D.A. Rigney (Ed.) 1-12, ASM, Cleveland

60. **T. H. C. Childs** and **D. Tabor**, (1967-68), Basic Principles of Dry Friction Testing, *Proc. Inst. Mech. Engnr.* , **182** (3G), 7-15.

61. **F. P. Bowden** and **D. Tabor**, *The Friction and Lubrication of Solids, Part 2*, Oxford University Press, 1964.

62. **N. P. Suh** and **H. C. Sin**, (1986), *Tribophysics*, Englewood Cliffs, Prentice Hall Inc., USA.

63. **M. B. Peterson**, (1976), Wear Testing Objectives and Approaches, *Selection and Use of Wear for Metals, ASTM* STP 615, (Edt.) R.G. Bayer, 3-11.

64. **J. F. Archard** and **W. Hirst**, (1956), The Wear of Metals under Unlubricated Conditions, *Proceeding of Royal Society of London, Seri* A, **236**, 397-410.

65. **J. F. Archard**, (1953), *J. Appl. Phys.*, **24**, 981-988.

66. **P. N. Suh**, (1977), The Delamination Theory of Wear, *Wear*, **44**, 1-116.

67. **S. Jahanmir,** (1978), On the Wear Mechanisms and the Wear Equations Fundamentals of Tribology, *Proc. Int. Conf. on Tribology*, The MIT Press, 456-467.

68. **J. P. Giltrow** and **J. K. Lancaster**, (1968), Friction and Wear Properties of Carbon Fibre Reinforced Metals, *Wear*, **12**, 91-105.

69. **Z. Eliezer et al.**, (1978), High Speed Tribological Properties of Graphite Fibre/Cu-Sn Matrix Composites, *Wear*, **49**, 119-133.

70. **Z. Eliezer** and **V. D. Khanna**, (1978), Wear Mechanism in Composites: A qualitative Model, *Wear*, **51**, 169-179.

71. **M. F. Amateau, R. H. Flowers** and **Z. Eliezer,** (1979), Tribological Behaviour of Metal Matrix Composites, *Wear,* **54,** 175-185.

72. **M. McKittrick, N. S. Sridharan** and **M. F. Amateau,** (1984), Wear Behaviour of Graphite Fibre Reinforced Glass, *Wear,* **96**, 285-299.

73. **K. J. Pearsall** and **Z. Eliezer,** (1980), The Effect of Sliding Time and Speed on the Wear of Composite Materials, *Wear,* **63**, 121-130.

74. **H. Nayeb-Hashemi, J. T. Blucher** and **J. Mirageas**, (1991), Friction and Wear Behaviour of Aluminum/Graphite Composites as a Function of Interface and Fibre Direction, *Wear*, **150**, 21-39.

75. **S. Das** and **B. K. Prasad**. (1989), Microstructure and Wear of cast Aluminium/silicon alloy Graphite Composites, *Proc, Int. Conf. on Wear of Materials*, ASME.

76. **P. K. Rohatgi, Y. Liu** and **S. Ray**, (1990), Friction and Wear in Metal Matrix Graphite Particle Composites, University of Wisconsin, Milwaukee, 801-812.

77. **A. K. Jha , S. V. Prasad** and **G. S. Upadhyaya**, (1989), Sintered 6061-Aluminium Alloy Solid Lubricant Particle Composites : Sliding Wear and Mechanisms of Lubrication, *Wear*, **133**, 163-172.

78. **Y. B. Liu, S. C. Lim, S. Ray** and **P. K. Rohatgi**, (1992), Friction and Wear of Aluminum/graphite Composites: The Smearing Process of Graphite During Sliding, *Wear,* **159**, 201-205.

79. **B. N. Keshavaram, P. K. Rohatgi, R. Asthanna** and **K. G. Sathyanarayana,** (1989), Friction and Wear Behaviour of Al-glass Particle Composite, *Proc. IMS Fall Meeting*, Indianapolis, 133-145.

80. **K. C. Ludema**, (1976), Wear Debris as an Indicator of Valid Simulation in Wear Tests, Selection and Use of Wear Tests for Metals, *ASTM STP 615,* (Edt. R. G. Bayer), ASTM 102-109.

81. **S. K. Biswas** and **B. N. Pramila Bai**, (1981), Dry Wear of Al-Graphite Particle Composites, *Wear,* **68**, 348-358.

82. **P. R. Gibson, A. J. Clegg** and **A. A. Das**, (1984), Production and Evaluation of Squeeze-Cast Graphitic Al-Si Alloys, *Wear*, **95**, 328-333.

83. **Y. B. Liu, S. C. Lim** and **P. K. Rohatgi,** (1992), *Wear*, **159**, 201-205.

84. **N. Saka** and **N. K. Szeto**, (1992), Friction and Wear of Fibre-Reinforced Metal Matrix Composites, *Wear,* **157**, 339-35.

85. **J. Tao et al.,** (1991), Friction and Wear Behaviour of C/Zn Composite, Wear of Materials, *8th Int. Conf.* April 1991, Orlando, ASME 601-605, Orlando.

86. **Z. Lu** and **K. Friedrich**, (1993), Wear and Friction of a Unidirectional Carbon Fibre Glass Matrix Composite Against Various Counterparts, *Wear*, **162-164** ,1103-1113.

87. **A. T. Alpas** and **J. D. Embury,** (1991), The Role of Subsurface Deformation and Strain Localization on the Sliding Wear Behaviour of Laminated Composites, *Wear*, **146**, 285-300.

88. **A. T. Alpas** and **J. Zhang,** (1992), Effect of SiC Particulate Reinforcement on the Dry Wear of Aluminium-Silicon Alloys (A 356), *Wear*, **155**, 83-104.

89. **B. N. Pramila Bai et al.,** (1992), Dry Sliding Wear of A-356-Al-SiCp Composites, *Wear*, **157**, 295-303.

90. **C. S. Ramesh, S. K. Seshadri** and **K. J. L. Iyer**, (1992), A Model for Wear Rates of Composite Coatings, *Wear*, **156**, 205-209.

91. **F. M. Hosking, F. F. Portillo** and **R. Wundeline** and **R. Mehrabian,** (1982), Composite of Aluminium Alloys: Fabrication and Wear behaviour, *J. Mat. Sci.*, **17**, 477-498.

92. **A. Alahelistan, F. Bergman** and **M. Olson**, (1993), On the Wear of Aluminium and Magnesium Metal Matrix Composites, *Wear*, **165**, 221-226.

93. **R. Arikan** and **S. Murphy,** (1990), Anistropic Wear of Planar-Random Metal Matrix Composites with Zinc Alloy Matrix, *Wear*, **143**, 149-157.

94. **S. Murphy** and **R. Arikan**, (1991), Metallographic Study of Wear in Planar-Random Fibre Reinforced Composites with an Aluminium-Zinc-Copper Alloy Matrix, *Wear*, **143**, 105-115.

95. **H. Fukunaga** and **I. Sakai**, (1984), Wear Behaviour of Alumina Fibre Reinforced Composites, *Proc. 5th Inter. Conf. on Production Engineering*, Tokyo, 673-677.

96. **I. G. Greenfield** and **R. R. Vignaud**, (1985), Dependence of Abrasive and Sliding Wear of Fibre Orientation in a Metal Matrix Composite, *Proc. ASM Conf. on Advanced Comp. ASM, Metals Park, OH*, 213-221.

97. **N. Saka** and **D. P. Karalekas**, (1985), Friction and Wear of Particle-Reinforced Metal Ceramic Composites, *Int. Conf. on the Wear of Materials*, Canada, ASME.

98. **I. M. Hutchings** and **A. Wang,** (1990), Wear of Aluminium-Alumina Metal Matrix Composites by Abrasion and Erosion, *Inst. Phys. Conf. Ser. No 111*, Int. Conf. on New Materials and Their Applications, University of Warwick, Coventry.

99. **A. M. Sherman** and **C. McHugh**, (1979), An evaluation of TiC-Al Matrix Composite Materials for Wear Resistant Surfaces, *2nd Int. Conf. on Wear of Material II, Wear of Materials*, 156-160.

100. **G. A. Chadwick** and **T. M. Yue**, (1989), Principles and Applications of Squeeze Casting, *J. Metals, Metals and Materials*, 6-13.

101. **S. G. Fishman** and **A. K. Dhingra,** (1988), *Int. Symposium on Advanced Cast Reinforced Metal Composites*, Chicago, Ilinois, USA.

102. **K. Kreider** and **M. Marciano,** (1969), *Trans. Met. Soc., AIME*, **245**, 1269.

103. **R. J. Sample et al.,** (1988), High Pressure Squeeze Casting of Unidirectional Graphite Fibre Reinforced Al Matrix Composites, *179-183 in Proceedings of Cast Reinforced MMCs* Edit by S.G. Fishman and A.K. Dhingra.

104. **A. K. Dhingra** and **L. B. Gulbransen**, (1988), Effect of Matrix Strengthening and Fibre Orientation on the Mechanical Behaviour of Cast Boron/Magnesium Composites, *Proc. Cast Reinforced Metal Composites*, Chicago, USA, 271-280.

105. **K. Razavizadeh** and **T. S. Eyre,** (1982), Oxidative wear of Al alloys, *Wear,* **79**, 325-333.

106. **K. Razavizadeh** and **T. S. Eyre**, (1983), *Wear*, **87**, 261-270.

107. **R. Shivanath, P. K. Sengupta** and **T. S. Eyre**, (1978), *Source Book on Wear Control Technology, ASTM,* Compiled by D. Rigney, and W. A. Glaser, 186-192.

108. **Z. Eliezer** and **V. D. Khanna,** (1979), On the Effect of Fibre Orientation on the Wear of Composite Materials, *Wear*, **53** , 387-389.

109. **M. F. Amateau, W. W. French** and **D. M. Goddard**, (1976), Friction and Wear Behaviour of Metal matrix Graphite Fibre Reinforced Composites, *Proc. 1975 Int. Conf. on Composite Materials*, Vol 2, Metallurgical Society of AIME, New York, 623-643.

110. **B. J. Briscoe** and **A. K. Pagosion** and **D. Tabor**, (1974), The Friction and Wear of HDPE: The Action of Lead and Copper Oxide Fillers, *Wear*, **27**, 19-34.

111. **J. K. Lancaster**, (1968), The Effect of Carbon Fibre Reinforcement on the Friction and Wear of Polymers, *J. Physics, D*, **1**, 549.

112. **N. H. Sung** and **N. P. Suh**, (1979), Effect of Fibre Orientation on Friction and Wear of Fibre Reinforced Polymeric Composites, *Wear*, **53**, 129-141.

113. **H. H. Shim and O. K. Kwon** and **J. R. Young**, (1992), Effect of Fibre Orientation and Humidity on Friction and Wear Properties of Graphite Fibre Polymer Composites, *Composites*, 141-149.

114. **T. Tsukizoe** and **N. Ohmae,** (1975), Wear Performance of Unidirectionally Orientated Carbon-Fibre Reinforced Plastics, *Tribology Int.*, 171-175.

115. **J. P. Giltrow** and **J. K. Lancaster**, (1970), The Role of the Counterface in the Friction and Wear of Carbon Fibre Reinforced Thermosetting Resins, *Wear*, **16**, 359 - 374.

116. **T. Tsukizoe** and **N. Ohmae**, (1983), Friction and Wear of Advanced Composite Materials, *Fibre Science and Technology*, Applied Science Publishers Ltd., England, **18** , 265-286.

117. **M. Cirino, R. B. Pipes** and **K. Friedrich,** (1987), The Abrasive Wear Behaviour of Continuous Fibre Polymer Composites, *J. Mat. Sci.*, **22** , 2481-2492.

118. **C. Lhymn** and **R. Light**, (1987), Effect of Sliding Velocity on Wear Rate of Fibrous Polymer Composites, *Wear*, **116**, 343-359.

119. **C. M. Pooley** and **D. Tabor**, (1972), Friction and Molecular Structure : The Behaviour of Some Thermoplastics, *Proc. Roy. Soc.*, London, A 329, 251-274.

120. **K. Tanaka** and **T. Miyata,** (1977), Studies on the Friction and Transfer of Semicrystalline Polymers, *Wear*, **41**, 383-398.

121. **K. Tanaka** and **V. Uchiyama**, (1974), Friction, Wear and Surface Melting of Crystalline Polymers, In L. H. Lee (Ed.), in *Advances in Polymer Friction and Wear*, **5 B**, Plenum Press, 499.

122. **H. Voss** and **K. Friedrich**, (1987), On the Wear Behaviour of Short Fibre Reinforced Peek Composites, *Wear*, **116**, 1-18.

123. **C. Lhymn**, (1988), Tribological Properties of Unidierctional Polyphenylene Sulfide Carbon Fibre Laminate Composites, *Wear*, **118**, 147-159.

124 **K. Friedrich et al.**, (1992), On the Sliding Wear Performance of Polyethernitrile Composites,*Wear*, **158**, 157-170.

125. **H. V. Chang**, (1983), Wear Characteristics of Composites : Effect of Fibre Orientation, *Wear*, **85**, 81-91.

126. **M. Cirino, K. Friedrich** and **R. B. Pipes**, (1988), The Effect of Fibre Orientation on the Abrassive Wear Behaviour of Polymer Composite Materials, *Wear*, **121**, 127-141.

127. **Z. Eliezer, C. J. Schulz** and **H. E. Mecredy**, (1979), A Relation between Wear Volume and Sliding Time for Composite Materials, *Wear*, **52**, 134-139.

128 **B. Vishwanath et al.**, (1991), Effect of Fabric Geometry on Friction and Wear of Glass Fibre Reinforced Composites, *Wear*, **143**, 87-89.

129. **A. L. Ward**, (1974), Wear of Glass Fibre Reinforced Composite Materials, *Composite Materials (Third Conf.), ASTM STP* 546, 477-494.

130. **V. K. Jain and S. Bahadur**, (1977), Material Transfer in Polymer Sliding, *Int. Conf. on Wear of Materials*, ASME, New York (Ed. by Lam V.K.).

131. **S. T. Mileiko** and **A. Kelly (Edt.)**, (1983), *Handbook of Composites*, **4**, Elsevier Science Publishers, B.V, Netherlands.

132. **D. J. Lloyd**, (1988), Metal Matrix Composites, *Proc. Int. on Advanced structural Materials,(Edt. D. S. Wilkinson), 27th Annual Conf. on Mat., Pergamon Press*, 1-21.

133. **M. E. Buck**, (1987), High Strength and Modulus Filaments of Boron and Silicon Carbide, *Mat. and Design.*, **8** (5), 273- 277.

134. **C. G. Levi, G. J. Abbaschian** and **R. Mehrabian**, (1978), Intern. Interactions during Fabrication of Aluminium Alloys Alumina Fibre Composites, *Metall. Transactions* A, **9 A**, 679-710.

135. **R. B. Pipes**, (1986), *Friction and Wear of Polymer Composite, 1*, Composite Materials Series, (Edt. by K. Friedrich), Elsevier, Delaware, USA.

136. **C. Subramanian**, (1992), Some Considerations Towards the Design of a Wear Resistant Aluminium Alloys, *Wear*, **155** , 194- 205.

137. **S. L. Rice**, (1982), The Role of Specimen Stiffness in Sliding and Impact Wear, *Wear*, **77**, 14-28.

138. **H. Fukunaga**, (1988), *Adv. Mater. Manufacturing Process*, **4**, 669.

139. **R. Mehrabian, R. G. Riek** and **M. C. Flemings**, (1974), *Met. Trans.*, **5** (8), 1899.

140. **P. Lui** and **S. Bahadur**, (1993), The Mechanical and Tribological Behaviour of Cu-Nb in Situ Composites, *Wear*, **166**, 133-139.

141. **O. Vingsbo**, (1986), Fundamentals of Friction and Wear Engineered materials for Advanced Friction on Wear Applications *Conf. Proceedings* Edit by F. A. Smidth and P. J. Blau, *ASM Int.*, Mayland, USA.

142. **F. A. Davis** and **T. S. Eyre**, (1993), The Effect of Silicon Content and Morphology on the Wear of Al/Si Alloys Under Dry and Lubricated Conditions, *Tribology Int.*, 171-181.

143. **D. A. Rigney**, (1994), The Role of Hardness in the Sliding Behaviour of Materials, *Wear*, ***175***, 63-69.

144. **B. N. Pramila Bai, S. K. Biswas** and **N. N. Kumtekar**, (1983), *Wear*, ***87***, 237-249.

145. **L. Yingjie, B. Xingui** and **C. Keqiang**, (1993), A Study on the Formation of Wear Debris During Abrasion, *Tribol. Int.*, 107-111.

146. **P. Divakar, B. Kotieerachari** and **B. G. Krishna Reddy**, (1983), A Study of Wear Characteristics of Different Materials, *Wear*, ***85*** , 151-161.

147. **J. H. Byett** and **C. Allen**, (1992), Dry Sliding Wear Behaviour of Polymide 66 and Polycarbonate Composites, *Tribol. Int.*, 237-247.

148. **B. Vishwanath, A. P. Verma** and **C. V. S. K. Rao**, (1990), Friction and Wear of a Glass Woven Roving/Modified Phenolic Composites, *Composites*, **21**, 531-537.

149. **K. Miyoshi**, (1990), Fundamental Considerations in Adhesion, Friction and Wear for Ceramic-Metal Contacts, *Wear*, ***141***, 35-44.

150. **T. S. Eyre**, (1991), Surface Engineering Friction and Wear Control in Industry, J. *Inst. Metals, Metals and Materials*, **7**, 143-149.

151. **D. Khanna**, (1983), *Ph. D. Thesis*, A study of the Tribological Properties of Graphite Fibre-Glass Matrix Composites, The University of Texas at Austin.

152. **S. Das** and **B. K. Prasad**, (1993), Tribological Behaviour of Al-Alloy Composites : A Comparative Study with a Copper-Based Alloy, *Wear*, ***162-164***, 64-74.

153. **O. O. Ajayi** and **K. C. Ludema**, (1990), Mechanism of Transfer Film Formation During Repeated Pass Sliding of Ceramic Materials, *Wear*, ***140***, 191-206.

154. **D. N. Hendrickson, J. M. Hollander** and **W. L. Jolly**, (1970), *Inorg. Chem.*, ***9***, 612.

155. **J. A. Schreifels, P. C. Maybury** and **W. E. Swartz**, (1980), *J. Catal.*, ***65***, 195.

156. **D. J. Joyner, O. Johnson** and **D. M. Hercules**, (1980), *J. Chem. Phys.*, ***72***, 1095.

157. **A. Kapoor** and **S. Bahadur**, (1994), Transfer Film Bonding and Wear Studies on CuS-Nylon Composites Sliding Against Steel, *Tribol. Int.*, 323-329.

158. **S. Bahadur, Q. Fu** and **D. Gong**, (1994), The Effect of Reinforcement and the Synergism Between CuS and Carbon Fibre on the Wear of Nylon, *Wear, **178**,* 123-130.

159. **K. Marcus** and **C. Allen**, (1994), The Sliding Wear of Ultrahigh Molecular Weight Polyethylene in an Aqueous Environment, *Wear, **178**,* 17-28.

160. **Y. Mizutani**, (1978), Structural Changes in the Surface Layer Due to Sliding and Their Effects on Friction and Wear of Materials, *Tribol. Conf.*, 223-235.

161. **O. P. Modia, B. K. Prasad, A. H. Yegneswaran** and **M. L. Vaidya**, (1992), Dry Sliding Wear Behaviour of Squeeze Cast Al Alloy-Silicon Carbide Composites, *Mat. Sci. and Engnr.*, **A 151**, 235-245.

162. **K. Friedrich** and **O. Jacobs**, (1992), On Wear Synergism in Hybrid Composites, *Composites Sci. and Techn.*, **43**, 71-84.

163. **T. F. J. Quinn**, (1983), Review of Oxidational Wear: Part I, The Origins of Oxidational Wear, *Tribol. Int.*, 257-271.

164. **T. F. J. Quinn**, (1983), Review of Oxidational Wear, Part II, Recent Developments and Future Trends in Oxidational Wear Research, *Tribol. Int.*, 305-315.

165. **S. Jahanmir, N. P. Suh** and **E. P. Abrahamson**, (1974), Microscopic Observations of the Wear Sheet Formation by Delamination, *Wear*, **28**, 235-249.

166 **S. Jahanmir, N. P. Suh** and **E. P. Abrahamson**, II, (1975), The Delamination Theory of Wear and the Wear of a Composite Surface, *Wear*, **32**, 33-49.

167 **M. O. A. Mokhtar**, (1982), The Effect of Hardness on the Frictional Behaviour of Metals, *Wear*, **78**, 297-304.

168. **R. A. Higgins**, (1994), *Properties of Engineering Materials*, Second Edition, St Edmunds Press, Bury St. Edmunds, London NW1 3BH.

169. **R. K. Everett** and **R. J. Arsenault**, (1991), *Metal Matrix Composites : Processing and Interfaces*, Academic Press, Harcourt Brace Jonano, Vich Publishers, London NW1 7DX.

170. **P. Pearl Lee, T. Savaskan** and **E. Laufer**, (1987), Wear Resistance and Microstructure of Zn-Al-Si and Zn-Al-Cu Alloys, *Wear*, **117**, 79-89.

171. **D. A. Rigney**, (1978), On the Mechanical Properties of Near Surface Material in Friction and Wear, *Int. Conf. on Tribology*, The MIT Press, 119-125.

172. **A. D. Sarkar**, (1983), The Role of Wear Debris in the Study of Wear, *Wear*, **90**, 39-47.

173. **M. Clerico**, (1978), Sliding Wear Mechanisms of Polymers, *Int. Conf. on Tribology*, The MIT Press, 769-785.

174. **B. K. Prasad, O. P. Modi** and **A. K. Jha**, (1994), The Effect of Alumina Fibres on the Sliding Wear of a Cast Aluminium Alloy, *Tribol. Int.*, 153-159.

175. **A. S. Jayatilaka**, (1979), *Fracture of Engineering Brittle Materials*, Applied Science Publishers Ltd., London.

176. **L. N. Gilbertson** and **R. D. Zipp**, (1979), Fractography and Material Science, *ASTM Special Technical Publication*, 733, Williansbury.

177. **D. Francois**, (1981), Advances in *Fracture Research, Proc. 5th Int. Conf. on Fracture* (IGF5), Cannes, France, Pergamon Press.

178. **M. Cirino**, (1985), *M. Sc. Thesis*, The Friction and Wear Behaviour of Unidirectional Continuous Fibre Reinforced Polymer Composites, University of Delaware.

179. **B. S. Tripathy** and **M. J. Furey**, (1993), Tribological Behaviour of Unidirectional Graphite-Epoxy and Carbon-PEEK Composites, *Wear*, **162-164**, 385-396.

180. **M. H. Stacey**, (1988), Production and Characteristics of Fibres for Metal Matrix Composites, *Mat. Sci. and Tech.*, **4**, 227-231.

181. **B. Roebuck, T. A. E. Gorley** and **L. N. M. Cartney**, (1989), Mechanical Property Test Procedures For Metal Matrix Composites, *Mat. Sci. and Tech.*, **5**, 105-115.

182. **H. R. Shetty** and **T. W. Chou**, (1985), Mechanical Property and Failure Characteristics of FP/Aluminium and W/Aluminium Composites, *Mat. Trans.*, **A**, 853- 865.

183. **N. J. Hurd**, (1988), Fatigue Performance of Alumina Reinforced Metal Matrix Composites, *Mat. Sci. and Tech.*, **4**, 513-517.

184. **G. H. Han, L. Cao, L. Geng** and **C. K. Yao**, (1987), The In Situ SEM Observation of Tensile Fracture Processses in Boron/Al. Composites, *Composites*, **18**, Number 5, 387-405.

185. **K. Purazrang, K. U. Kainer** and **B. L. Mordike**, (1991), Fracture Toughness Behaviour of a Magnesium Alloy Metal Matrix Composite Produced by the Infiltration Technique, *Composite*, **22**, Number 6, 456-461.

186. **K. Schulte** and **K. Minoshima**, (1993), Damage Mechanisms Under Tensile and Fatigue Loading of Continuous Fibre-Reinforced Metal Matrix Composites, *Composites*, **24**, Number 3, 197-208.

187. **A. Mittelman** and **I. Roman**, (1990), Tensile Properties of Real Unidirectional Kevlar/Epoxy Composites, *Composites, Vol.* **21,** Number 1, 63-69.

188. **J. K. Lancaster**, (1980), In *Proc. of Int. Conf. : Tribology in 80s*, Vol. **1**, 333.

189. **B. J. Briscoe** and **P. J. Tweedale**, A view of Polymer Composite Tribology, In P. K. Rohatgi, P. J. Blau and C. S. Yust (Edt.), *Proc.Conf. in Tribol. of Composite Materials*, Oak Ridge, T. N, ASME, Materials Park, Ohio, 15.

189. **B. Vishwanath, A. P. Verma,** and **C. V. S. K, Rao**, (1989), Wear Study of Glass Woven Roving Composites, *Wear*, **131**, 197-205.

191. **J. Bijwe** and **U. S. Tewari**, (1987), Friction and Wear Studies of Short Glass-Fibre Reinforced Polyetheride Composite, *Int. Tribol. Conf. on Wear of Composites, Melbourne.*

192. **J. W. Weeton, D. M. Peters** and **K. L. Thomas**, (1987), Engineer's Guide to *Composite Materials* , *ASME*, Metals Park Ohio 44073, USA.

193. **K. Tanaka**, (1977), Friction and Wear of Glass and Carbon Fibre Filled Thermoplastic Polymers, *J. Lubr. Techn.*, **99**, 409.

194. *ASM Engineered Materials Reference Book,* (1989), ASM International, Metals Park, Ohio 44073, USA.

195. ASTM Standards and Literature *References for Composite Materials,* (1987), *ASTM* First Edit by ASTM, USA.

APPENDICES

Appendix 1 (Table 5, 6, 7 and 8)

Appendix 2 (Table 9, 10, and 11)

TABLE 5

WEAR DATA FOR THE B(SiC) FIBRE-REINFORCED ALUMINIUM COMPOSITE MATERIALS TESTED AT A SPEED OF 1.0 m/s.

Materials tested	Applied Load (N)	Mass Loss (mg)	Gravi. Wear Rate (mg/km)	Volume Loss (mm^3)	Volumetr. Wear Rate (mm^3/km)	Average Coef. of Friction
Al-M	12	31.78	4.413	11.419	1.586	0.40
Al-M	24	52.00	7.222	18.682	2.594	0.36
Al-M	44	91.00	12.638	32.698	4.541	0.31
Al-M	60	112.00	15.555	40.244	5.589	0.33
B16 N	12	8.83	1.226	3.198	0.444	0.52
B16 N	24	14.56	2.022	5.273	0.732	0.55
B16 N	44	20.07	2.787	7.269	1.009	0.57
B16 N	60	21.82	3.030	7.902	1.097	0.41
B16 P	12	6.20	0.861	2.245	0.311	0.50
B16 P	24	12.69	1.762	4.596	0.638	0.52
B16 P	44	18.15	2.52	6.573	0.913	0.56
B16 P	60	33.15	4.604	12.00	1.667	0.44
B16AP	12	5.760	0.80	2.064	0.286	0.72
B16AP	24	10.00	1.388	3.621	0.502	0.63
B16AP	44	16.84	2.338	6.099	0.847	0.60
B16AP	60	21.43	2.976	7.761	1.078	0.58
B21 N	12	6.50	0.902	2.429	0.337	0.55
B21 N	24	10.86	1.508	4.059	0.563	0.64
B21 N	44	12.63	1.754	4.721	0.655	0.52
B21 N	60	15.15	2.104	5.663	0.786	0.56

(Continued)

Materials tested	Applied Load (N)	Mass Loss (mg)	Gravi. Wear Rate (mg/km)	Volume Loss (mm^3)	Volumetr. Wear Rate (mm^3/km)	Average Coef. of Friction
B21 P	12	5.29	0.734	1.977	0.274	0.63
B21 P	24	14.10	1.958	5.271	0.732	0.60
B21 P	44	24.52	3.405	9.166	1.273	0.50
B21 P	60	27.91	3.876	10.433	1.449	0.45
B21AP	12	3.36	0.466	1.256	0.174	0.83
B21AP	24	12.40	1.722	4.635	0.643	0.77
B21AP	44	19.14	2.658	7.155	0.993	0.55
B21AP	60	37.80	5.25	14.13	1.76	0.63
B23 N	12	2.40	0.333	0.876	0.121	0.73
B23 N	24	8.13	1.129	2.967	0.412	0.62
B23 N	44	11.03	1.531	4.025	0.559	0.53
B23 N	60	20.90	2.902	7.627	1.059	0.58
B23 P	12	5.33	0.74	1.945	0.27	0.53
B23 P	24	12.79	1.776	4.667	0.648	0.57
B23 P	44	22.84	3.172	8.335	1.157	0.57
B23 P	60	25.45	3.534	9.288	1.290	0.52
B23AP	12	3.80	0.527	1.386	0.192	0.79
B23AP	24	11.02	1.530	4.021	0.558	0.68
B23AP	44	13.48	1.872	4.919	0.683	0.57
B23AP	60	24.26	3.369	8.854	1.229	0.55
B27 N	12	2.24	0.311	0.823	0.114	0.72
B27 N	24	5.04	0.70	1.848	0.256	0.59

(Continued)

Materials tested	Applied Load (N)	Mass Loss (mg)	Gravi. Wear Rate (mg/km)	Volume Loss (mm^3)	Volumetr. Wear Rate (mm^3/km)	Average Coef. of Friction
B27 N	44	15.95	2.215	5.848	0.812	0.44
B27 N	60	13.95	1.937	4.822	0.669	0.53
B27 P	12	5.22	0.725	1.914	0.265	0.54
B27 P	24	11.00	1.527	4.033	0.560	0.55
B27 P	44	21.62	3.00	7.928	1.101	0.53
B27 P	60	19.96	2.772	7.319	1.016	0.57
B27AP	12	4.40	0.611	1.613	0.224	0.79
B27AP	24	8.00	1.111	2.934	0.407	0.68
B27AP	44	17.15	2.381	6.288	0.873	0.57
B27AP	60	18.00	2.50	6.60	0.916	0.55
B32 N	12	5.34	0.74	1.967	0.273	0.64
B32 N	24	7.65	1.062	2.818	0.391	0.47
B32 N	44	12.50	1.736	4.237	0.588	0.46
B32 N	60	14.69	2.040	5.412	0.751	0.48
B32 P	12	6.29	0.873	2.317	0.321	0.56
B32 P	24	11.95	1.659	4.403	0.611	0.50
B32 P	44	15.96	2.216	5.88	0.816	0.45
B32 P	60	20.78	2.886	7.656	1.063	0.53
B32AP	12	5.84	0.811	2.151	0.298	0.70
B32AP	24	9.42	1.308	3.470	0.482	0.63
B32AP	44	13.86	1.925	5.106	0.709	0.61
B32AP	60	17.49	2.429	6.444	0.895	0.59

TABLE 6

WEAR DATA FOR THE B(SiC) FIBRE-REINFORCED ALUMINIUM COMPOSITE MATERIALS TESTED AT A SPEED OF 0.6 m/s.

Tested Materials	Applied Load (N)	Mass Loss (mg)	Gravi. Wear Rate (mg/km)	Volume Loss (mm^3)	Volumetric W.Rate (mm^3/km)	Average Coef. of Friction
Al/2014	6	3.930	0.909	1.409	0.326	0.40
Al-M	12	8.185	1.894	2.934	0.679	0.43
Al-M	22	17.05	3.946	6.115	1.415	0.50
Al-M	32	38.40	8.888	13.76	3.185	0.47
Al-M	42	54.53	12.622	19.55	4.525	0.45
B16 N	6	0.321	0.074	0.116	0.0269	0.54
B16 N	12	0.725	0.167	0.262	0.060	0.54
B16 N	22	6.125	1.417	2.218	0.640	0.55
B16 N	32	9.125	2.112	3.304	0.764	0.54
B16 N	42	14.12	3.268	5.114	1.183	0.50
B16 P	12	3.180	0.736	1.151	0.266	0.45
B16 P	22	8.630	1.997	3.125	0.733	0.54
B16 P	32	9.420	2.180	3.410	0.789	0.49
B16 P	42	16.600	3.844	6.012	1.391	0.51
B21 N	6	0.730	0.168	0.266	0.061	0.69
B21 N	12	4.534	1.049	1.642	0.380	0.56
B21 N	22	9.420	2.180	3.488	0.807	0.61
B21 N	32	11.56	2.675	4.218	0.976	0.55
B21 N	42	18.45	4.270	6.833	1.581	0.57

(Continued)

Tested Materials	Applied Load (N)	Mass Loss (mg)	Gravi. Wear Rate (mg/km)	Volume Loss (mm^3)	Volumetric W.Rate (mm^3/km)	Average Coef. of Friction
B32 N	6	0.266	0.061	0.097	0.021	0.72
B32 N	12	0.65	0.150	0.238	0.055	0.50
B32 N	22	1.565	0.362	0.575	0.133	0.76
B32 N	32	8.085	1.871	2.972	0.687	0.52
B32 N	42	19.625	4.542	7.215	1.470	0.42
B32 P	12	2.590	0.599	0.950	0.219	0.50
B32 P	22	5.955	1.378	2.189	0.506	0.43
B32 P	32	7.440	1.722	2.735	0.633	0.45
B32 P	42	14.345	3.220	5.273	1.20	0.48

TABLE 7
WEAR DATA FOR THE B(SiC) FIBRE-REINFORCED ALUMINIUM COMPOSITE MATERIALS TESTED AT A SPEED OF 1.6 m/s.

Materials tested	Applied Load (N)	Mass Loss (mg)	Gravi. Wear Rate (mg/km)	Volume loss (mm^3)	Vol.Wear Rate (mm^3/km)	Average Coef. of Friction
Al-M	6	7.56	0.65	2.71	0.235	0.24
Al-M	12	39.00	3.385	13.98	1.25	0.21
Al-M	22	68.44	5.94	24.53	2.129	0.28
Al-M	32	79.40	6.892	28.46	2.47	0.31
Al-M	42	97.02	8.421	34.786	3.019	0.32
B16 N	6	4.20	0.364	1.521	0.132	0.40
B16 N	12	6.96	0.604	2.52	0.218	0.44
B16 N	22	26.65	2.313	9.652	0.95	0.42
B16 N	32	29.605	2.569	10.72	1.187	0.41
B16 N	42	31.505	2.734	11.40	0.989	0.65
B16 P	12	7.10	0.616	2.571	0.223	0.36
B16 P	22	9.16	0.795	3.317	0.287	0.37
B16 P	32	11.45	0.993	4.147	0.359	0.40
B16 P	42	15.80	1.371	5.81	0.504	0.38
B21 N	6	5.106	0.443	1.863	0.161	0.42
B21 N	12	13.23	1.148	4.828	0.419	0.43
B21 N	22	18.94	1.644	6.912	0.60	0.44
B21 N	32	27.40	2.378	10.00	0.93	0.41
B21 N	42	35.05	3.042	12.981	1.126	0.50

TABLE 8
CHEMICAL COMPOSITION OF A WORN SURFACE FORMED DURING DRY SLIDING WEAR.

Level of peak No	Element identific	N orient atomic (%) (1*)	N orient atomic (%) (2*)	P orient atomic (%) (3*)
1	Al 2s	3.44	12.45	14.06
2	Si 2s	1.17	-	-
3	B 1s	21.46	9.38	12.12
4	Cl 2p	0.96	-	-
5	C 1s	29.06	43.00	38.05
6	N 1s	0.54	0.74	0.68
7	O 1s	33.89	32.12	34.09
8	Fe 2p3	9.50	2.20	0.91
9	Sn 3d	-	0.06	0.04
10	In 3d5	-	0.05	0.04

1* Test conducted at a speed of 0.6m/s. (N)

2* Test conducted at a speed of 1.6m/s. (N)

3* Test conducted at a speed of 1.6m/s. (P)

TABLE 9
WEAR DATA FOR THE B(SiC) REINFORCED PLASTIC MATRIX COMPOSITE MATERIALS TESTED AT A SPEED OF 0.6 m/s.

Materials tested	Applied load (N)	Mass Loss (mg)	Gravi. Wear Rate (mg/km)	Volume Loss (mm^3)	Volume Wear Rate (mm^3/km)	Average Coef. of Friction
HDPE	12	0.710	0.328	0.799	0.369	0.52
HDPE	22	2.200	1.028	2.501	0.979	0.51
B!4 N	12	0.170	0.078	0.142	0.065	0.44
B14 N	22	0.195	0.0902	0.163	0.075	0.35
B14 P	12	0.245	0.113	0.205	0.095	0.35
B14 P	22	1.110	0.513	0.923	0.427	0.22
B14 AP	12	0.220	0.101	0.184	0.085	0.20
B14 AP	22	0.230	0.106	0.193	0.089	0.19
B28 N	12	0.320	0.148	0.230	0.106	0.45
B28 N	22	0.525	0.243	0.376	0.174	0.46
B28 P	12	0.793	0.367	0.570	0.263	0.18
B28 P	22	0.775	0.358	0.556	0.254	0.17
B28 AP	12	0.190	0.087	0.136	0.062	0.12
B28 AP	22	0.775	0.358	0.556	0.254	0.17

TABLE 10
WEAR DATA FOR THE B(SiC) REINFORCED PLASTIC MATRIX COMPOSITE MATERIALS TESTED AT A SPEED OF 1.0 m/s.

Materials Tested	Applied Load (N)	Mass Loss (mg)	Gravi. Wear Rate (mg/km)	Volume Loss (mm^3)	Volumet. Wear Rate (mm^3/km)	Average Coef. of Friction
HDPE	12	4.685	1.301	5.278	1.466	0.62
B14 N	12	0.125	0.034	0.105	0.029	0.49
B14 P	12	0.480	0.133	0.403	0.119	0.20
B14 AP	12	0.190	0.052	0.159	0.044	0.26
B28 N	12	0.185	0.0513	0.132	0.036	0.48
B28 P	12	0.960	0.266	0.689	0.191	0.20
B28 AP	12	0.125	0.034	0.089	0.024	0.14
HDPE	22	5.605	1.5556	6.314	1.754	0.60
B14 N	22	0.285	0.0791	0.239	0.066	0.45
B14 P	22	1.525	0.423	1.281	0.355	0.29
B14 AP	22	1.065	0.295	0.894	0.248	0.29
B28 N	22	0.390	0.108	0.279	0.077	0.45
B28 P	22	0.557	0.154	0.399	0.144	0.20
B28 AP	22	0.510	0.141	0.366	0.101	0.21

TABLE 11
WEAR DATA FOR THE B(SiC) REINFORCED PLASTIC MATRIX COMPOSITE MATERIALS TESTED AT A SPEED OF 1.6 m/s.

Materials tested	Applied load (N)	Mass Loss (mg)	Gravi. Wear Rate (mg/km)	Volume Loss (mm^3)	Volumetr. Wear Rate (mm^3/km)	Average Coef. of Friction
HDPE	12	1.625	0.286	1.830	0.317	0.68
B14 N	12	0.160	0.0277	0.134	0.023	0.24
B14 P	12	1.480	0.256	1.243	0.180	0.39
B14 AP	12	0.850	0.147	0.714	0.123	0.30
B28 N	12	0.573	0.099	0.414	0.068	0.51
B28 P	12	0.715	0.124	0.513	0.089	0.23
B28 AP	12	0.885	0.153	0.635	0.110	0.21
HDPE	22	3.730	0.647	4.202	0.729	0.76
B14 N	22	0.385	0.066	0.323	0.056	0.39
B14 P	22	2.820	0.489	2.369	0.371	0.38
B14 AP	22	0.950	0.164	0.798	0.138	0.32
B28 N	22	0.640	0.111	0.459	0.079	0.54
B28 P	22	1.275	0.221	0.915	0.178	0.17
B28 AP	22	o.750	0.130	0.538	0.093	0.20